Precision Scale Setting in Lattice QCD

Dissertation zur Erlangung des Grades

Doktor der Naturwissenschaften

am Fachbereich Physik, Mathematik und Informatik der Johannes Gutenberg-Universität in Mainz

Vorgelegt von

Alexander Michael Segner

Mainz, den 01.04.2026

Alexander Michael Segner: Precision Scale Setting in Lattice QCD
1. Gutachter: Univ-Prof. Dr. Hartmut Wittig
2. Gutachterin: Univ-Prof. Dr. Sonia Bacca
Tag der Promotionsprüfung: 26.03.2026

Abstract

We investigate the prospects of setting the lattice scale via the mass of one of the SU(3)-octet or -decuplet baryons including isospin-breaking effects in Lattice Quantum Chromodynamics and discuss first, but incomplete results on the topic. To determine values for the lattice scale, we compute the correlation functions for SU(3)-octet and -decuplet baryons as well as pseudoscalar octet mesons on ten of the (2+1)-flavor QCD gauge ensembles of the Coordinated Lattice Simulations (CLS) collaboration at five different lattice spacings on a trajectory of constant average quark mass. As these ensembles are simulated in the isospin-symmetric limit, i.e. with two identical light quarks instead of distinct up and down quarks, we also compute corrections to the above mentioned correlation functions to account for a difference in mass of these two light quarks and for electromagnetic interactions of the quarks to leading order following a perturbative approach by the RM123 collaboration. We compute masses and their corrections for the baryons that are stable in isospin-symmetric QCD as well as the pion and kaon from correlation functions using the model averages of single and two-state fits to an effective mass based on the Akaike information criterion. We use the isospin-symmetric masses as well as available values for the Wilson flow scale t_0 to extrapolate the combinations $\sqrt{8t_0}m_B$ for all stable baryons B to the physical point following a procedure by the RQCD collaboration. At the physical point, we match the extrapolated data to modified experimental baryon masses that account for isospin-symmetry in order to determine a physical value $\sqrt{8t_0^{\text{phys}}}$ for the Wilson flow scale. We use this physical value to determine values of the five different lattice spacings at which we have gathered data which we use to compute the isospin-breaking expansion coefficients for each ensembles by matching the differences of squared pion and kaon masses in the isospin-broken theory to experimental data. From these data and the corrections to the baryonic masses in lattice units, we compute masses for the baryons in the isospin-broken theory. We furthermore discuss a method we developed to substantially reduce the computational effort for the computation of electromagnetic corrections of the investigated correlation functions and the generalization of the isospin-symmetric scale-setting procedure to include isospin-breaking corrections. Finally, we discuss the results with with regards to the precision achievable for the lattice scale and the different baryonic candidates to use as intermediate scales.

Publications

Partial and intermediate results of this thesis have been published in the following articles:

- Alexander M. Segner et al. "Isospin-breaking Effects in Octet and Decuplet Baryon Masses". In: *PoS* LATTICE2021 (2022), p. 095. DOI: 10.22323/1.396.0095. arXiv: 2112.08262 [hep-lat]
- Alexander M. Segner et al. "Setting the Scale Using Baryon Masses with Isospin-Breaking Corrections". In: *PoS* LATTICE2022 (2023), p. 084. DOI: 10.22323/1.430.0084. arXiv: 2212.07176 [hep-lat]
- Alexander M. Segner, Andreas Risch, and Hartmut Wittig. "Precision Determination of Baryon Masses including Isospin-breaking". In: *PoS* LATTICE2023 (2024), p. 044. DOI: 10.22323/1.453.0044. arXiv: 2312.09065 [hep-lat]
- Hartmut Wittig et al. "Machine-learning techniques as noise reduction strategies in lattice calculations of the muon $g-2$". In: *PoS* LATTICE2024 (2025), p. 270. DOI: 10.22323/1.466.0270. arXiv: 2502.10237 [hep-lat]

Contents

Chapter 1
Introduction

Modern physics is governed by two major theories. While general relativity describes gravity at large scales through the curvature of spacetime, the standard model of particle physics (SM) accurately describes matter and its interactions at microscopic scales as a relativistic quantum field theory (QFT). Both theories are well tested and established as highly accurate descriptions of reality at their respective scale, however, a unification of the two has as of yet not successfully been established.

The SM describes elementary particles as fields classified into four categories. The first category encompasses the gauge bosons, which mediate the three fundamental forces of electromagnetism, the weak and the strong nuclear force, the first two of which are unified in the electroweak interaction. The second category is comprised of the leptons which can be subdivided into the charged leptons (electron, muon, and tau) and the neutrinos of which one flavor exists for each charged lepton. Thirdly, the only strongly interacting particles called quarks of which there are six flavors; three positively charged (up, charm, top) and three negatively charged (down, strange, bottom) ones. In addition to these spin-1 gauge bosons and spin-$1/2$ leptons and quarks, a single spin-0 Higgs boson completes the standard model, that gives mass to the leptons, quarks and three of the electroweak gauge bosons. Furthermore, every fermion has an antiparticle of the same mass but opposite charge.

Besides gravity, the SM does, however, miss some crucial properties of the universe that were uncovered through experimental evidence. For example, the neutrinos are massless in the standard model which is not true in nature as evidenced by the observation of neutrino oscillations [1]. Another example is dark matter, which solves the mismatch of the observed speed of stars orbiting far from the center of a galaxy to the theoretical speed that would keep them on a circular orbit. Furthermore, the SM has 18 free parameters, which cannot be computed from first principles and have to be determined from experimental measurements. It is unclear if these are truly free parameters or if a more fundamental model would be able to predict some of them.

To improve our understanding of the fundamental laws of nature, it is crucial to understand, which predictive power our best theories still lack. Working towards this goal, various different experiments test the predictions of the standard model in precise measurements of observables derivable from the SM. One such observable is the *anomalous magnetic moment of the muon*, which has recently been measured to a precision of 127 ppb at the Fermi National Accelerator Laboratory

[2] lowering the experimental world average combining different observables to 124 ppb for the central value $a_\mu^{\text{exp}} = 116\,592\,0715(145) \times 10^{-12}$ [2]. The theoretical value estimated in the latest White Paper as $a_\mu^{\text{SM}} = 116\,592\,033(62) \times 10^{-11}$ [3], i.e. 530 ppb, is also known very precisely. These new updates remove a tension between the experimental and theoretical estimates of more than 3σ that has been found before [4]. However, the uncertainty of the theoretical calculation is strongly dominated by *quantum chromodynamics* (QCD), the theory of the strong nuclear force, where a tension is still present between data-driven calculations and those from lattice QCD (LQCD). To finally resolve the question of agreement between the SM and experimental measurements of a_μ and the tension between the different QCD predictions, it is imperative to improve the precision of these computations.

LQCD solves the computational problems of QCD, namely that the standard perturbative approach breaks down at low energies. This problem stems from the running coupling α_S which, for the strong interaction, tends to zero for large momentum transfers and becomes too big for a perturbative expansion for smaller momentum transfers. LQCD avoids the perturbative approach completely by treating spacetime not as an infinite continuum, but as a finite lattice with discrete points. This makes the numeric computation of observables possible from first principles in a stochastic way via Markov chain Monte Carlo simulations.

Due to algorithmic advantages, LQCD calculations are usually performed in the isospin-symmetric limit. Isospin symmetry is a historical concept to explain hadrons (meaning strongly bound states made up of quarks) of similar masses like the proton and neutron, which were interpreted as the spin-up and spin-down states related to a SU(2) symmetry similar to the mathematical description of quantum spin. Today, it is associated with the global SU(2)-symmetry of QCD mixing up and down quarks. This symmetry is broken in the SM by the mass and charge difference of up and down quarks. For a long time, the errors in LQCD calculations introduced by assuming isospin symmetry and vanishing electromagnetic charges of the quarks were negligible compared to the statistical uncertainty. Today, however, algorithmic advancements, as well as improved and more available hardware for large-scale computations, made it possible for LQCD results to achieve sub-1% uncertainty [3, 5], at which the effects of broken isospin symmetry start to become relevant [6, 7]. In the context of high-precision observables like a_μ, it is therefore imperative to compute corrections for the isospin-breaking effects previously neglected in LQCD calculations.

While working from first principles, LQCD introduces an additional free parameter that vanishes when extrapolating data to the continuum theory. That parameter is the lattice scale a which, like the free parameters of the SM, has to be determined using experimental input to match the lattice theory to the continuum one. It enters any computation of dimensionful observables from the lattice, and thus its uncertainty directly influences the uncertainty of observables computed on the lattice. The uncertainty of the hadronic vacuum polarization contribution to a_μ, for example, is proportional to the relative uncertainty of the quantity Λ used to set the lattice scale,[1] $\Delta a_\mu^{\text{hvp}} \propto \frac{\Delta\Lambda}{\Lambda}$ [4, 8]. It is thus crucial to determine the scale to high precision which also requires the inclusion of isospin-breaking corrections.

[1] For example by matching a hadron mass $\Lambda = am_H$ computed on the lattice to its experimental value, i.e. $a = \frac{am_H}{m_H^{\text{exp}}}$

In this thesis, we investigate the prospects of setting the lattice scale via the mass of one of the octet (nucleon, Λ, Σ, Ξ) or decuplet (Δ, Σ^*, Ξ^*, Ω) baryons with isospin-breaking corrections for the gauge $N_f = 2+1$ ensembles of the CLS collaboration [9]. These masses are computed from two-point correlation functions in isospin-symmetric QCD ($\mathrm{QCD}_{\mathrm{iso}}$) and isospin-breaking corrections thereof. The corrections are computed from a perturbative expansion around $\mathrm{QCD}_{\mathrm{iso}}$ at leading order in the action parameters $(\beta, e^2, m_u, m_d, m_s)$ [10, 11], i.e. the inverse strong gauge coupling, the electromagnetic coupling, and the masses of the three lightest quarks (up, down, and strange) present in the isospin-symmetric CLS simulations. We discuss isospin-breaking corrections in the sea-quark sector, but only include corrections in the valence sector in our calculations.
For the computation of the correlation functions and their corrections, we implement and optimize a highly parallel program to run on computing clusters. We make use of baryonic operators based on a Clebsch-Gordan construction [12] defining a set of multiple operators for each octet and decuplet baryon, from which we compute all possible correlators and cross-correlators mixing two different operators. We furthermore compute correlators for the pseudoscalar meson octet that are needed for an extrapolation of the baryon masses to the physical point as well as for matching the isospin-broken theory to experimental data [13, 14].
We present results for the masses of viable candidates for the scale-setting procedure in the isospin-symmetric limit and with isospin-breaking corrections on ten different gauge ensembles at five different lattice spacings. Using the isospin-symmetric masses, we perform an extrapolation to the physical point and determine physical values $\sqrt{8t_0^{\mathrm{phys}}}$ for the Wilson flow scale [15, 16] from the masses of the nucleon, Λ, Σ, Ξ, and Ω baryons. From these results we derive values of the lattice scale for each value of β for which we compute baryon and meson masses. We finally use the lattice spacings we determine from the baryon giving the most precise results to determine the unknown parameters of the isospin-breaking expansion. We then use these parameters to compute the masses of the baryons in the isospin-broken theory.
We do not extrapolate the isospin-corrected masses to the physical point, but we discuss aspects of setting the scale with isospin-breaking correction. Furthermore, we discuss a technique we developed for an efficient estimation of the electromagnetic corrections which are otherwise expensive to compute.

This document is split into two parts. Part I focuses on the background of the project and the underlying theory. Part II is more focused on the project itself, although this separation is not strict such that we discuss some of our own contributions in part I and discuss methods developed by other researchers in part II that we needed to implement ourselves or that we adapted in parts.
Part I starts with an overview of QCD in the continuum theory in chapter 2 and continues with a brief introduction of LQCD in chapter 3. In chapter 4, we discuss the properties of the CLS ensembles and methods used in previous studies to set the lattice scale for these ensembles. Chapter 5 introduces a formulation of QED we use for the computation of isospin-breaking corrections, and how these corrections are computed. Chapter 6 completes part I with an introduction to the statistical methods used for the generation of gauge ensembles as well as the

treatment of observables calculated on them.
In chapter 7, we discuss the computation of hadronic two-point correlation functions as well as the methods we use to derive the masses of baryons and pseudoscalar mesons from them. We continue in chapter 8 with a description of the setup and implementation of our computations of baryonic and mesonic two-point functions as well as code optimizations and tests. Furthermore, we discuss problems of these two-point functions related to the Monte Carlo noise and our strategies to deal with them. In chapter 9 we discuss our results for the isospin-symmetric baryon masses, their extrapolation to the physical point and first results for the lattice scale based on the data we have gathered thus far. Chapter 10 starts with the discussion of a method to reduce the computational effort of computing the QED corrections followed by our results for the isospin-breaking corrections of the baryon masses and the expansion parameters needed to determine these corrections. We finish chapter 10 with a short discussion of a possible adaption of the scale-setting procedure we used to include isospin-breaking corrections before giving a summary of our results and an outlook on the future of the project in chapter 11.

Part I

Foundations

Chapter 2
QCD in Minkowski and Euclidean Spacetime

The standard model of particle physics, in the following abbreviated as SM, is the best description of the laws of nature at microscopic scales to date. The SM describes the matter and its interactions in terms of 18 distinct particle fields, twelve of which (the fermions, i.e. quarks and leptons) come with an additional corresponding anti-particle. Interactions between particles are mediated via gauge bosons related to local symmetries, namely an action of the gauge group $\mathrm{SU}(3)_C \times \mathrm{SU}(2)_L \times \mathrm{U}(1)$. SU(3) is related to the strong force which is the most central part of this thesis. $\mathrm{SU}(2)_L \times \mathrm{U}(1)$ on the other hand gives rise to the electroweak gauge bosons γ, Z, W^+, and W^-, the latter three of which are the only massive gauge bosons whose mass enters the model through the Higgs mechanism, as do the masses of fermions.
This thesis is based on lattice QCD, a model for studying the physics of the strong force at low energies where traditional perturbative approaches cannot be applied. In part II, we compute baryon and meson masses within this framework with corrections stemming from QED, the theory of electromagnetism associated with $U(1)$ (among others). This chapter aims to give a short overview over the main building blocks for the later discussion in the continuum model before translating the framework to the lattice in chapters 3 and 4. We assume, however, that the reader is already familiar with QFT and the SM. This chapter should thus rather serve as a reminder of some topics of the theory relevant to this thesis.
We start the continuum discussion with a short primer on gauge theories in section 2.1 and deal with QCD as a gauge theory specifically in section 2.2. Section 2.3 then introduces the path integral formalism on which lattice QFTs are built upon, followed by a discussion of Wick's theorem which helps with the computation of observables from QFTs in section 2.4. We end this chapter in section 2.6 where we change the metric of the underlying spacetime from Minkowskian to Euclidean which is necessary for for the later formulation of the lattice theory.

2.1. Gauge Theories

Interactions between fermions in the SM are mediated by gauge bosons. Their name comes from the fact that these are necessary additions to the free Dirac-

Lagrangian

$$\mathcal{L} = \bar{\psi}(i\gamma^\mu \partial_\mu - m)\psi \tag{2.1}$$

when invariance is imposed under the action

$$\begin{aligned}\psi(x) &\mapsto \Omega(x)\psi(x),\\ \bar{\psi}(x) &\mapsto \bar{\psi}(x)\Omega^{-1}(x)\end{aligned}$$

of some non-trivial, unitary, local representation $\Omega(x)$ of a Lie-group $\mathcal{G}$ on the fermions ψ; in other words, a gauge transformation. The Lagrangian (2.1) is obviously not invariant under this action, from which it gains an additional term of the form $\mathcal{L} \mapsto \mathcal{L} + i\bar{\psi}\gamma^\mu(\Omega^{-1}\partial_\mu\Omega)\psi$ stemming from the derivative of the transformed field. In order to eliminate this additional term, one can introduce a parallel transport $U(y,x)$ that transforms as

$$U(y,x) \mapsto \Omega(y)U(y,x)\Omega^{-1}(x) \tag{2.2}$$

and must be an element of the Lie-Group $\mathcal{G}$. This allows us to redefine the derivative in a gauge covariant way [17]:

$$n^\mu \partial_\mu \psi(x) \mapsto n^\mu D_\mu \psi(x) = \lim_{a\to 0} \frac{1}{a}[\psi(x+an) - U(x+an,x)\psi(x)] \tag{2.3}$$

where n is a unit four-vector. Observing that $U(x,x)$ has to be the identity in $\mathcal{G}$ for eq. (2.3) to resemble a derivative, and requiring U to be differentiable, $U(y,x)$ can be expressed in terms of the exponential map on the Lie-Algebra $\mathfrak{g}$ of $\mathcal{G}$ [17],

$$U(y,x) = \mathcal{P}\exp\left(ig\int_{\mathcal{C}} \mathrm{d}^4 z^\mu A_\mu(z)\right) = \mathcal{P}\exp\left(ig\int_0^1 \mathrm{d}t \left|\dot{\mathcal{C}}^\mu(t)\right| A_\mu(\mathcal{C}(t))\right) \tag{2.4}$$

for some path $\mathcal{C} : [0,1] \to \mathbb{R}^{1\times 3}$ connecting x and y. For simplicity we treat $\mathcal{C}$ in the following as a straight line from x to y. $\mathcal{P}$ here denotes the path ordering operator meaning that in the series expansion of the exponential products of A_μ are ordered by the curve parameter t in their argument. Thus, infinitesimally, the gauge transporter can be written as

$$U(x+an,x) = \mathbb{1} + igan^\mu A_\mu(x) + \mathcal{O}(a^2) \tag{2.5}$$

such that the covariant derivative is given by

$$D_\mu = \partial_\mu + igA_\mu$$

where A_μ is a $\mathfrak{g}$-valued field. For a complete Lagrangian, we further need a kinetic term for A, which can be constructed by considering the parallel transport along a loop based at x [17]:

$$\begin{aligned}U_{\mu\nu}(x) :=& U(x, x+a\hat{\nu})U(x+a\hat{\nu}, x+a\hat{\mu}+a\hat{\nu})\\ &\cdot U(x+a\hat{\mu}+a\hat{\nu}, x+a\hat{\mu})U(x+a\hat{\mu}, x),\end{aligned} \tag{2.6}$$

where $\hat{\mu}$ and $\hat{\nu}$ are unit basis vectors of spacetime. A visualization of this path is shown in fig. 2.1. Infinitesimally, this $U_{\mu\nu}$ is given by [17]

$$\begin{aligned}U_{\mu\nu}(x) =& \mathbb{1} - a^2 g\big(\partial_\mu A^a_\nu(x)t^a - \partial_\nu A^a_\mu(x)t^a + g f^{abc} A^b_\mu(x) A^c_\nu(x) t^c\big)\\ &+ \mathcal{O}\big(a^3\big)\end{aligned} \tag{2.7}$$

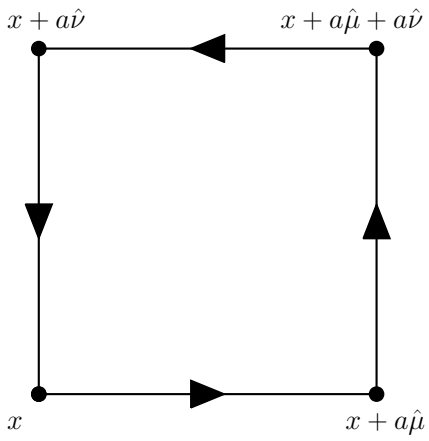

Figure 2.1: A visualization of the path chosen in eq. (2.6) to construct a gauge-invariant object from a parallel transport from point x to itself.

where t^a are the generators of $\mathcal{G}$, i.e. basis vectors of $\mathfrak{g}$ such that the sum $A^a_\mu(x)t^a := \sum_{a=1}^{\dim(\mathfrak{g})} A^a_\mu(x)t^a$ can be any element of $\mathfrak{g}$. f^{abc} are the *structure constants* of $\mathfrak{g}$, defined via

$$\left[t^a, t^b\right] = i\sum_c f^{abc}t^c.$$

The expression in brackets in eq. (2.7) is called the *field strength tensor* $G_{\mu\nu}$ and defines the kinetic term of the gauge fields which, combined with interactions of the gauge bosons with each other, can be condensed in the expression $-\frac{1}{4}\operatorname{tr}_{\mathcal{G}}(G_{\mu\nu}G^{\mu\nu})$. The full so-called *Yang-Mills*-Lagrangian takes the form

$$\mathcal{L}[A,\psi,\bar{\psi}] = \bar{\psi}(x)(i\gamma^\mu D_\mu - m1_{\mathcal{G}\times\mathrm{Spin}})\psi(x) - \frac{1}{4}\operatorname{tr}_{\mathcal{G}}(G_{\mu\nu}G^{\mu\nu})$$

where $1_{\mathcal{G}\times\mathrm{Spin}}$ is the identity element in $\mathcal{G}$ and spinor space, which is usually omitted. This full Lagrangian is then invariant under the local gauge transformation

$$\begin{aligned}\psi(x) &\mapsto \Omega(x)\psi(x),\\ \bar{\psi}(x) &\mapsto \bar{\psi}(x)\Omega^{-1}(x)\\ A_\mu(x) &\mapsto A_\mu(x) + \frac{i}{g}\Omega^{-1}(x)(\partial_\mu\Omega(x)).\end{aligned} \tag{2.8}$$

The terms involving the structure constants in $G_{\mu\nu}G^{\mu\nu}$ define interactions of three or four gauge bosons at a single vertex. In the case of an abelian gauge group, these structure constants vanish and thus, there are no interaction terms involving multiple gauge bosons, but only those arising from the covariant derivative D_μ coupling the gauge bosons to the fields that transform non-trivially under the action of $\mathcal{G}$.

2.2. QCD in the Continuum

Quantum chromodynamics, or QCD, is the theory of the strong nuclear interaction mediated by the gluon fields. It is the gauge theory that is arises from local

gauge invariance under actions of SU(3). The only fields in the SM that transform non-trivially under SU(3) are the quarks u, d, c, s, t, b and the gluons A^a_μ which are QCD's gauge bosons and thus, these are the only strongly interacting fields. The Lagrangian of this theory is given by

$$\mathcal{L}_{\text{QCD}} = \sum_q \bar{q}(i\gamma^\mu D_\mu - m_q)q - \frac{1}{4}G^a_{\mu\nu}G^{\mu\nu}_a \tag{2.9}$$

where the sum runs over all six quark flavors $q \in \{u, d, c, s, t, b\}$. The field strength tensor G here is given by

$$G^a_{\mu\nu} = \partial_\mu A^a_\nu - \partial_\nu A^a_\mu + g f^{abc} A^b_\mu A^c_\nu$$

where A denotes the gluon field, g is the strong coupling constant and f denotes the structure constants of SU(3). A set of generators of the three-dimensional irreducible representation of SU(3) that is commonly used in the literature is given by $t^a = \frac{\lambda_a}{2}$ where λ_a are the *Gell-Mann matrices* [18]

$$\begin{aligned}
\lambda_1 &= \begin{pmatrix} 0 & 1 & 0 \\ 1 & 0 & 0 \\ 0 & 0 & 0 \end{pmatrix} \quad \lambda_2 = \begin{pmatrix} 0 & -i & 0 \\ i & 0 & 0 \\ 0 & 0 & 0 \end{pmatrix} \quad \lambda_3 = \begin{pmatrix} 1 & 0 & 0 \\ 0 & -1 & 0 \\ 0 & 0 & 0 \end{pmatrix} \\
\lambda_4 &= \begin{pmatrix} 0 & 0 & 1 \\ 0 & 0 & 0 \\ 1 & 0 & 0 \end{pmatrix} \quad \lambda_5 = \begin{pmatrix} 0 & 0 & -i \\ 0 & 0 & 0 \\ i & 0 & 0 \end{pmatrix} \quad \lambda_6 = \begin{pmatrix} 0 & 0 & 0 \\ 0 & 0 & 1 \\ 0 & 1 & 0 \end{pmatrix} \\
\lambda_7 &= \begin{pmatrix} 0 & 0 & 0 \\ 0 & 0 & -i \\ 0 & i & 0 \end{pmatrix} \quad \lambda_8 = \frac{1}{\sqrt{3}} \begin{pmatrix} 1 & 0 & 0 \\ 0 & 1 & 0 \\ 0 & 0 & -2 \end{pmatrix}.
\end{aligned} \tag{2.10}$$

Their structure constants are given by [18]

$$f^{123} = 1,\ f^{147} = f^{246} = f^{257} = f^{345} = f^{516} = f^{637} = \frac{1}{2},\ f^{458} = f^{678} = \frac{\sqrt{3}}{2}. \tag{2.11}$$

The remaining structure constants can be deduced from these from the fact that f is antisymmetric under exchange of two indices.

An important property of QCD is the dependence of its coupling constant on the energy or length scale of a given process that occur at non-leading order in perturbative calculations. To take this dependence into account, a scale μ – which might for example be the momentum transfer in a collision – is introduced, allowing for a description of the so-called *running* of the coupling via the β-function, which to one-loop order is given by [19]

$$\beta(g) = \mu\frac{\partial g}{\partial \mu} = -\frac{g^3}{16\pi^2}\left[\frac{11}{3}N_c - \frac{2}{3}N_f\right].$$

In a collision with momentum transfer Q^2, the differentiable equation above can be solved to find the squared coupling constant to be given by [19]

$$g^2(Q^2) = \frac{(4\pi)^2}{\left(\frac{11}{3}N_c - \frac{2}{3}N_f\right)\log\left(\frac{Q^2}{\Lambda^2_{\text{QCD}}}\right)}.$$

The reference scale Λ_{QCD} in this formula depends on the renormalization scheme. This shows, that the strong gauge coupling gets weaker with higher energy transfer and diverges for $Q^2 \to \Lambda_{\text{QCD}}$. This means that at low energies, QCD becomes non-perturbative and has to be tackled by non-perturbative methods like lattice QCD.

2.3. The Path Integral

To get from a Lagrangian or action to a quantum field theory, the fields described by the Lagrangian have to be quantized. One way to do this is by introducing the path integral formalism.
Consider an action $S[\phi]$ describing the dynamics of a field ϕ. Furthermore, consider a correlation function correlating the field ϕ in the state ϕ_a at time $t_a = 0$ with the field in the state ϕ_b at time $t_b = t$, i.e. $\langle\phi_b(t)|\phi_a(0)\rangle = \langle\phi_b|U(t)|\phi_a\rangle$ where $U(t)$ is the time evolution operator $U(t) = e^{-iHt}$ with H being the Hamiltonian corresponding to the action S. The path integral approach to computing this correlation function is to divide this matrix element up into small time increments inserting identities $\mathbb{1} = \int \mathrm{d}\phi_i \, |\phi_i\rangle\langle\phi_i|$:

$$\langle\phi_b(t)|\phi_a(0)\rangle = \int \prod_{k=1}^{N-1} \mathrm{d}\phi_k \, \langle\phi_b|U(t/N)\,|\phi_1\rangle\langle\phi_1|\,U(t/N)\,|\phi_2\rangle\langle\phi_2|\cdots \\ \cdots|\phi_{N-1}\rangle\langle\phi_{N-1}|\,U(t/N)\,|\phi_a\rangle\,.$$

The informal limit taking $N \to \infty$ in this expression defines the path integral which is denoted as

$$Z = \langle\phi_b(t)|\phi_a(0)\rangle = \int_{\phi(0)=\phi_a}^{\phi(t)=\phi_b} \mathcal{D}\phi \exp(iS[\phi])$$

with the path integral measure

$$\mathcal{D}\phi = \lim_{N\to\infty} \prod_{k=1}^{N} \mathrm{d}\phi_k(x_k). \tag{2.12}$$

and $S[\phi] = \int \mathrm{d}^4x \mathcal{L}[\phi](x)$. In this formalism, expectation values of operators $\mathcal{O}[\phi]$ are defined as

$$\langle\mathcal{O}[\phi]\rangle = \frac{\langle\phi_b(t)|\mathcal{O}[\phi]|\phi_a(0)\rangle}{\langle\phi_b(t)|\phi_a(0)\rangle} = \frac{1}{Z}\int_{\phi(0)=\phi_a}^{\phi(t)=\phi_b} \mathcal{D}\phi\mathcal{O}[\phi]\exp(iS[\phi]). \tag{2.13}$$

2.4. Wick's Theorem

Wick's theorem allows for the computation of time ordered n-point correlation functions

$$\mathfrak{W}^{(n)}(x_1, ..., x_n) = \langle\Omega|\mathcal{T}\{\phi_1(x_1)\phi_2(x_2)\cdots\phi_n(x_n)\}|\Omega\rangle$$

by relating the time ordered product of the field operators $\phi_i(x_i)$ to the normal-ordered product $:\phi_1(x_1)\phi_2(x_2)\cdots\phi_n(x_n):$ where $|\Omega\rangle$ is the vacuum state of the theory. The time-ordered product rearranges the operators such that they are sorted from latest time on the left and the earliest time on the right, e.g. for $x_i = (t_i, \mathbf{x}_i)^T$ [17]

$$\mathcal{T}\{\mathcal{O}_1(x_1)\mathcal{O}_2(x_2)\} = \begin{cases} \mathcal{O}_1(x_1)\mathcal{O}_2(x_2) & t_1 > t_2 \\ \pm\mathcal{O}_2(x_2)\mathcal{O}_1(x_1) & t_2 > t_1 \end{cases}$$

where the $\pm$ accounts for possible anti-commutation relations for the operators in the case of fermionic operators. Thus the time ordering lets operators act on

a state in chronological order. The normal ordering, on the other hand, arranges the operators such that all creation operators are on the left and all annihilation operators on the right, i.e.

$$
\begin{aligned}
:a_1^\dagger a_2^\dagger: &= a_1^\dagger a_2^\dagger \\
:a_1 a_2: &= a_1 a_2 \\
:a_1^\dagger a_2: &= a_1^\dagger a_2 \\
:a_1 a_2^\dagger: &= \pm a_2^\dagger a_1
\end{aligned}
$$

where in the last case the sign is "+" if a_1 and a_2 commute and "−" if they anticommute. Wick's theorem relates those two orderings via

$$
\begin{aligned}
\mathcal{T}\{\mathcal{O}_1\cdots\mathcal{O}_n\} = :\mathcal{O}_1\cdots\mathcal{O}_n: &+ \sum_{i<j=1}^{n} :\cdots\overbrace{\mathcal{O}_i\cdots\mathcal{O}_j}\cdots: \\
&+ \sum_{i<j<k<l=1}^{n} \Big(:\cdots\overbrace{\mathcal{O}_i\cdots\mathcal{O}_j}\cdots\overbrace{\mathcal{O}_k\cdots\mathcal{O}_l}\cdots: \\
&\quad + :\cdots\overbrace{\mathcal{O}_i\cdots\mathcal{O}_j\cdots\mathcal{O}_k}\cdots\mathcal{O}_l\cdots: \\
&\quad + :\cdots\overbrace{\mathcal{O}_i\cdots\mathcal{O}_j\cdots\mathcal{O}_k\cdots\mathcal{O}_l}\cdots: \Big) + \cdots
\end{aligned}
\tag{2.14}
$$

i.e. contractions $\overbrace{\mathcal{O}_1\mathcal{O}_2} = \mathcal{T}\{\mathcal{O}_1\mathcal{O}_2\} - :\mathcal{O}_1\mathcal{O}_2:$ of all possible combinations of operators have to be considered to express the time-ordered product in terms of the normal-ordered one. This has the computational advantage that the vacuum-expectation value of the normal-ordered product of any operator vanishes as all annihilation operators act on the vacuum state first. Hence, in the n-point correlation function, $\langle\Omega|\mathcal{T}\{\mathcal{O}_1\cdots\mathcal{O}_n\}|\Omega\rangle$ only those terms in eq. (2.14) remain, in which all operators are contracted. This results in an expression for the correlation function in terms of propagators

$$
i\mathcal{S}_\phi(x-y) = \langle\Omega|\mathcal{T}\{\phi(x)\phi(y)\}|\Omega\rangle = \langle\Omega|\overbrace{\phi(x)\phi(y)}|\Omega\rangle\,. \tag{2.15}
$$

When performing the contractions in eq. (2.14), all operators must be (anti-) commuted such that the operators to be contracted appear right next to each other in the product. This results in some combinatorial factors of equivalent contractions which have to be accounted for. A more systematic approach reducing the statement of Wick's theorem to functional derivatives can be derived in the path-integral formalism. We discuss this in the following.

2.4.1. Wick's Theorem for Bosons

Consider a bosonic field $\phi : \mathbb{R}^{1\times 3} \to \mathbb{R}$ with Lagrangian

$$
\mathcal{L}[\phi] = -\frac{1}{2}\phi\,\Box\,\phi - \frac{1}{2}m^2\phi^2 - V[\phi].
$$

A correlation function in the path integral formalism takes the form

$$
\langle\Omega|T\{\phi_1(x_1)\phi_2(x_2)\cdots\phi_n(x_n)\}|\Omega\rangle = \frac{\int \mathcal{D}\phi\,\phi_1(x_1)\phi_2(x_2)\cdots\phi_n(x_n)e^{iS[\phi]}}{\int \mathcal{D}\phi\, e^{iS[\phi]}}.
$$

Introducing a source field $J : \mathbb{R}^{1,3} \to \mathbb{R}$, we can define a *generating functional*

$$Z[J] = \int \mathcal{D}\phi \, \exp\left(i \int \mathrm{d}^4x (\mathcal{L}[\phi](x) + J(x)\phi(x))\right).$$

Taking the functional derivative of this expression with respect to J, we find

$$\begin{aligned}\left.\frac{\delta Z[J]}{\delta J(x)}\right|_{J=0} &= \int \mathcal{D}\phi \, \frac{\delta}{\delta J(x)} \exp\left(i \int \mathrm{d}^4y (\mathcal{L}[\phi](y) + J(y)\phi(y))\right)\Bigg|_{J=0} \\ &= \int \mathcal{D}\phi \, i\phi(x) \exp\left(i \int \mathrm{d}^4y (\mathcal{L}[\phi](y) + J(y)\phi(y))\right)\Bigg|_{J=0} \\ &= iZ \langle \phi(x) \rangle\end{aligned}$$

where $Z := Z[0]$ and the expectation value is defined as in eq. (2.13). Thus, evaluating the n-th derivative of the above expression with respect to J evaluated at different points, we can compute the n-point correlation function via

$$\begin{aligned}&\langle \Omega | T\{\phi_1(x_1)\phi_2(x_2)\cdots\phi_n(x_n)\} | \Omega \rangle \\ &\qquad = \left[\frac{1}{Z[J]} \left(-i\frac{\delta}{\delta J(x_1)}\right) \cdots \left(-i\frac{\delta}{\delta J(x_n)}\right) Z[J]\right]_{J\equiv 0}.\end{aligned}$$

The propagator is then given by

$$i\mathcal{S}_\phi(x-y) = \langle \Omega | \mathcal{T}\{\phi(x)\phi(y)\} | \Omega \rangle = -\left[\frac{1}{Z[J]} \frac{\delta^2}{\delta J(x)\delta J(y)} Z[J]\right]_{J\equiv 0}.$$

For a free field ϕ (i.e. $V[\phi] \equiv 0$), this formula can be made more explicit via a change of variables $\phi(x) \mapsto \phi(x) - i\int \mathrm{d}^4y \mathcal{S}_\phi(x-y)J(y)$ where $\mathcal{S}_\phi(x-y)$ is the Green's function of the differential operator defining the Klein-Gordon field, i.e. $(\Box_x + m^2)\mathcal{S}_\phi(x) = i\delta^{(4)}(x)$. Then the generating functional is given by

$$Z[J] = Z \exp\left(-\frac{1}{2} \int \mathrm{d}^4x \mathrm{d}^4y J(x)\mathcal{S}_\phi(x-y)J(y)\right)$$

effectively avoiding the computation of the path integral. In this free case, the Green's function can be computed analytically and is given by

$$\mathcal{S}_\phi(x-y) = \frac{1}{(2\pi)^4} \int \mathrm{d}^4p \frac{e^{-ip(x-y)}}{p^2 - m^2 + i\varepsilon}.$$

2.4.2. Wick's Theorem for Fermions

For fermions, the discussion differs from the above in the fact that the anti-commuting nature of the fields has to be accounted for. Taking for example fields described by the Dirac Lagrangian for a free field

$$\mathcal{L}[\psi, \bar{\psi}] = \bar{\psi}(i\gamma^\mu \partial_\mu - m)\psi,$$

the variables used in the path-integral have to be *Graßmann-variables* whose product is anticommutative:

$$\psi_1\psi_2 = -\psi_2\psi_1, \quad \psi_1^2 = 0.$$

Since the fermion action has to independent fields ψ and $\bar{\psi}$, we need two sources $\bar{\eta}$ and η instead of just the one source J in section 2.4.1. The generating functional is then given by

$$Z[\bar{\eta},\eta] = \int \mathcal{D}\psi\mathcal{D}\bar{\psi}\exp\Big(i\int \mathrm{d}^4x\big(\mathcal{L}[\psi,\bar{\psi}](x) + \bar{\eta}(x)\psi(x) + \bar{\psi}(x)\eta(x)\big)\Big)$$

which, analogously to section 2.4.1 can for the free Dirac-field be brought into the form

$$Z[\bar{\eta},\eta] = Z[0,0]\exp\Big(-\int \mathrm{d}^4x\mathrm{d}^4y\,\bar{\eta}(x)\mathcal{S}_\psi(x-y)\eta(y)\Big)$$

where $\mathcal{S}_\psi$ is the Dirac propagator

$$\mathcal{S}_\psi(x-y) = \frac{1}{(2\pi)^4}\int \mathrm{d}^4p\frac{i(\gamma^\mu p_\mu + m)}{p^2 - m^2 + i\varepsilon}e^{-ip(x-y)}.$$

A $(2n)$-point function in this framework can be computed via [17]

$$\begin{aligned}&\langle\Omega|\mathcal{T}\{\bar{\psi}(x_1)\psi(y_1)\cdots\bar{\psi}(x_n)\psi(y_n)\}|\Omega\rangle\\ &\quad= \left[\frac{1}{Z[\bar{\eta},\eta]}\frac{\delta^2}{\delta\bar{\eta}(x_1)\delta\eta(y_1)}\cdots\frac{\delta^2}{\delta\bar{\eta}(x_n)\delta\eta(y_n)}Z[\bar{\eta},\eta]\right]_{\bar{\eta},\eta=0}.\end{aligned}$$

For this derivative, care has to be taken due to the anticommuting nature of all involved fields. This introduces additional minus signs in terms for with an odd permutation of the involved fields.

2.5. Gauge Fields in the Path Integral Formalism

Consider free photon with action [17]

$$\begin{aligned}S[A] =& -\frac{1}{4}\int \mathrm{d}^4xF^{\mu\nu}F_{\mu\nu} = \frac{1}{2}\int \mathrm{d}^4xA_\mu(x)(g^{\mu\nu}\,\Box - \partial^\mu\partial^\nu)A_\nu(x)\\ =&\frac{1}{2}\int \frac{\mathrm{d}^4k}{(2\pi)^4}\tilde{A}_\mu(k)\big(-k^2g^{\mu\nu} + k^\mu k^\nu\big)\tilde{A}_\nu(-k).\end{aligned}$$

This expression does not define a propagator for A which is related to the fact that the functional integral includes a infinitely many different field configurations that are physically equivalent through gauge transformations [17]. One can solve this problem with the Fadeev-Popov procedure by explicitly fixing the gauge in the path integral [17, 20]. This adds an additional *gauge fixing term* $\frac{1}{2\xi}(\partial^\mu A_\mu(x))^2$ in the path integral that for correlation functions can be absorbed into an effective action[1]

$$\begin{aligned}S'[A] =&\frac{1}{2}\int \mathrm{d}^4x\Big[A_\mu(x)(g^{\mu\nu}\,\Box - \partial^\mu\partial^\nu)A_\nu(x) - \frac{1}{\xi}(\partial^\mu A_\mu(x))^2\Big]\\ =&\frac{1}{2}\int \mathrm{d}^4xA_\mu(x)\Big(g^{\mu\nu}\,\Box - \frac{1}{\xi}\overleftarrow{\partial}^\mu\overrightarrow{\partial}^\nu - \partial^\mu\partial^\nu\Big)A_\nu(x)\\ =&\frac{1}{2}\int \frac{\mathrm{d}^4k}{(2\pi)^4}\tilde{A}_\mu(k)\Big(-k^2g^{\mu\nu} + \Big(1-\frac{1}{\xi}\Big)k^\mu k^\nu\Big)\tilde{A}_\nu(-k)\end{aligned}$$

[1] There are additional terms that appear in the path integral during the gauge fixing procedure. However, these cancel in correlation functions $\langle\Omega|\mathcal{T}\mathcal{O}[A]|\Omega\rangle$ as long as $\mathcal{O}[A]$ is gauge-invariant as they appear in the path integral and the partition function [17].

where $\overleftarrow{\partial}$ acts on the left photon while the other derivatives act on the right one. The free photon propagator depending on the gauge fixing parameter ξ is then given by [17]

$$\mathcal{S}_A^{\mu\nu}(x-y) = \frac{1}{(2\pi)^4}\int \mathrm{d}^4k \frac{-i\left(g^{\mu\nu} - (1-\xi)\frac{k^\mu k^\nu}{k^2}\right)}{k^2 + i\varepsilon} e^{-ik(x-y)}.$$

Note, that S' is not gauge invariant, but the correlation functions of gauge-invariant observables do not depend on ξ [17].
For non-abelian gauge fields, there are additional factors in the path integral in the form of *Faddeev-Popov ghosts* c and $\bar{c}$ which act as additional fermionic fields and contribute an additional term to the modified action [17]

$$S'[A,c,\bar{c}] = \frac{1}{2}\int \mathrm{d}^4x \left[A_\mu(x)(g^{\mu\nu}\,\Box - \partial^\mu\partial^\nu)A_\nu(x) - \frac{1}{\xi}(\partial^\mu A_\mu(x))^2 - \bar{c}(\partial^\mu D_\mu)c\right].$$

2.6. Euclidean Quantum Field Theory

The discussion thus far dealt with QFT in Minkowski spacetime. However, discussions of an extension of this theory to Euclidean spacetime in which the time t is replaced by the *imaginary time* $t^{(M)} \mapsto t^{(E)} = it^{(M)}$, date back to the late 1950s [21, 22]. Among other benefits [23], the treatment of QFT in Euclidean spacetime allows for a statistical treatment of QFT on a finite lattice where the action takes on a role similar to that of a Hamiltonian in the treatment of canonical ensembles in statistical physics.
Leaving the spatial vector components equal to their counterparts in Minkowski spacetime, i.e. $x^{k,(E)} = x^{k,(M)}$, the Minkowski scalar product translates to the Euclidean scalar product induced by the metric $g_{\mu\nu}^{(E)} = \delta_{\mu\nu}$. The Euclidean vector and covector components thus have the same sign convention. For derivatives, the relation between Minkowskian and Euclidean spacetime is

$$\partial_0^{(E)} = \frac{\partial}{\partial t^{(E)}} = \frac{\partial}{\partial(it^{(M)})} = -i\partial_0^{(M)}, \quad \partial_k^{(E)} = \frac{\partial}{\partial x^{k,(E)}} = \frac{\partial}{\partial x^{k,(M)}} = \partial_k^{(M)}.$$

However, one has to be careful when going from a Minkowskian QFT to Euclidean one as it is not a priori clear, that the two formulations are equivalent. Different attempts have been made to find conditions for a Euclidean QFT that ensure an equivalence of *Schwinger functions*

$$\mathfrak{S}^{(n)}(x_1^{(E)},...,x_n^{(E)}) = \langle 0|\phi(x_1^{(E)})\cdots\phi(x_n^{(E)})|0\rangle\,,$$

defined in Euclidean spacetime and *Wightman distributions*

$$\mathfrak{W}^{(n)}(x_1^{(M)},...,x_n^{(M)}) = \langle\Omega|\mathcal{T}\{\phi_1(x_1^{(M)})\phi_2(x_2^{(M)})\cdots\phi_n(x_n^{(M)})\}|\Omega\rangle$$

defined via the *Wightman axioms* [24] for Minkowskian QFT. For example, it is possible to construct fields in Minkowski spacetime from Euclidean Markoff fields [25]. The most prominent set of axioms for the Schwinger functions, from which the existence of an analytic continuation to Wightman distributions can be shown, are the Osterwalder-Schrader axioms [26, 27] which can also be applied to lattice QFTs [28].

The following discussion is to be understood to be in Euclidean spacetime. Thus, we omit the superscript (E) when discussing Euclidean coordinates.

Due to the Wick-rotation $t \mapsto it$, the time evolution operator in Euclidean field theory has the form $U(t) = e^{-Ht}$ [19, 28, 29] and the path integral similarly has a negative sign in the exponential [19, 28, 29],

$$\mathfrak{S}^{(n)}(x_1, ..., x_n) = \langle 0|\mathcal{T}\{\phi(x_1)\cdots\phi(x_n)\}|0\rangle = \frac{\int \mathcal{D}\phi\, \phi(x_1)\cdots\phi(x_n)e^{-S[\phi]}}{\int \mathcal{D}\phi\, e^{-S[\phi]}}.$$

As in Minkowski spacetime, the n-point correlation functions can be obtained from a generating functional $Z[J]$. In the case of a free scalar field defined by the action $S[\phi] = \int \mathrm{d}^4x\phi(x)(\Box + m^2)\phi(x)$, for example, the generating functional takes the form

$$Z[J] = \exp\left(\frac{1}{2}\int \mathrm{d}^4x\mathrm{d}^4y J(x)\mathcal{S}_\phi(x,y)J(y)\right)$$

where the propagator is given by

$$\mathcal{S}_\phi(x,y) = \mathfrak{S}^{(2)}(x,y) = \frac{1}{(2\pi)^4}\int \mathrm{d}^4k \frac{e^{ik(x-y)}}{k^2+m^2}.$$

The Dirac matrices in Euclidean spacetime transform slightly different than the coordinates in that the Wick rotation occurs in the spatial Dirac matrices instead of the one related to time, i.e. $\gamma^{0,(E)} = \gamma^{0,(M)}$ and $\gamma^{k,(E)} = i\gamma^{k,(M)}$ [28]. In the contraction of the gamma matrices, with the derivatives, each term therefore picks up a factor of i, such that $i\gamma^{\mu,(M)}\partial_\mu^{(M)} = -\gamma^{\mu,(E)}\partial_\mu^{(E)}$. The free Dirac equation $\left(i\gamma^{\mu,(M)}\partial_\mu^{(M)} - m\right)\psi = 0$ thus becomes

$$(\gamma^\mu\partial_\mu + m)\psi = 0$$

in Euclidean spacetime. The fermion propagator is then given by

$$\mathcal{S}_\psi(x,y) = \frac{1}{(2\pi)^4}\int \mathrm{d}^4p \frac{m-\gamma^\mu p_\mu}{p^2+m^2}e^{ik(x-y)}.$$

Chapter 3
QCD on the Lattice

Lattice QCD (LQCD) is a regularization technique for QCD in which space and time are discretized to a lattice rather than having a continuous spacetime. Furthermore, this theory is defined in Euclidean spacetime compared to the Minkowski spacetime description in the standard model. Making this lattice a finite box, this model has the following advantages over the continuum theory:

- The path integral is well-defined and finite.
- The finite distance a between two lattice points has the effect that the energy is limited by $E \leq \frac{\pi}{a}$ thus introducing an intrinsic ultraviolet-cutoff.
- A description of QFT in Euclidean spacetime together with the finiteness of the path integral allows for a probability-density-interpretation of the path integral such that observables can be estimated using Monte-Carlo techniques.

This chapter aims to give a rough overview of the basic characteristics of a LQCD computation before going into the details of the lattice prescription used for this thesis in chapter 4. This overview starts with some general aspects of a field theory and its constituents in a discretized spacetime in section 3.1 followed by a general discussion of gauge fields in section 3.2 and fermions in section 3.3 in a lattice quantum field theory (LQFT) context. Finally, we discuss how spin, which is related to transformations of particle states under four-dimensional rotations[1], translates to a LQFT with broken $O(4)$ symmetry in section 3.4 and describe the role of the lattice spacing in section 3.5.

3.1. Discretization

When going from a continuum theory to one defined on a lattice, many observables and operations have to be discretized in a way that recovers their continuum counterparts when approaching the limit of an infinitely fine lattice, i.e. in the limit of zero lattice spacing ($a \to 0$). Take for example the action of a free fermion ψ in Euclidean spacetime

$$S[\psi, \bar{\psi}] = \int \mathrm{d}^4x \big(\bar{\psi}(x)\gamma^\mu \partial_\mu \psi(x) + m\bar{\psi}(x)\psi(x)\big).$$

[1] In Minkowski spacetime this would be transformations under the Lorentz group which in Euclidean spacetime translates to $SO(4)$.

Here, positions x at which the fermion fields are evaluated as well as the spacetime integral and the derivatives have to be translated to a lattice description.
On a lattice, the coordinates x are restricted to a finite subset $\Lambda \subset \mathbb{R}^4$ of points at a distance of a to their neighbors, i.e. $\Lambda = \{an | n \in \mathbb{N}_0^4, n_i \leq N_i\}$. Throughout this work, Λ will usually be (anti-)periodically continued in the spatial directions and in some cases also in the time direction. In these cases, Λ is to be understood not as a subset of $\mathbb{R}^4$ but rather of $\mathbb{R} \times \mathbb{T}^3$ or $\mathbb{T}^4$ where $\mathbb{T}^n$ is the n-torus. We then talk of *periodic* or *open boundary conditions*.
The derivatives ∂_μ have to be replaced by finite differences, e.g.

$$\partial_\mu f(x) \mapsto \frac{1}{a}(f(x + a\hat{\mu}) - f(x)). \tag{3.1}$$

This is obviously compatible with the continuum derivative, as it coincides with the definition of a derivative in the limit $a \to 0$. In practice, however, one usually uses a symmetric variant of the above formula, which eliminates leading discretization effects of $\mathcal{O}(a)$:

$$\frac{f(x + a\hat{\mu}) - f(x - a\hat{\mu})}{2a} = \partial_\mu f(x) + \mathcal{O}(a^2). \tag{3.2}$$

The integral can be discretized as $\int\limits_{\mathbb{R}^4} \mathrm{d}^4x \mapsto a^4 \sum\limits_{x \in \Lambda}$ leading to a possible (naive) lattice discretization

$$S[\psi, \bar{\psi}] = a^4 \sum_{x \in \Lambda} \left(\sum_\mu \bar{\psi}(x) \gamma_\mu \frac{\psi(x + a\hat{\mu}) - \psi(x - a\hat{\mu})}{2a} + m\bar{\psi}(x)\psi(x) \right) \tag{3.3}$$

of the fermionic action. However, this action has some unwanted properties which we will discuss in sections 3.3.2 and 3.3.3.

3.1.1. Momentum

Momenta in a lattice theory are located on the reciprocal lattice. For a lattice with periodic boundary conditions, this is given by

$$\tilde{\Lambda} = \left\{ p \in \mathbb{T}^4 \middle| p_\mu = \frac{2\pi k_\mu}{a N_\mu}, k_\mu \in \left\{ -\frac{N_\mu}{2} + 1, ..., \frac{N_\mu}{2} \right\} \right\} \tag{3.4}$$

where N_μ are the number of lattice points in direction μ. Functions on the momentum lattice $\tilde{\Lambda}$ and the spacetime lattice Λ are related via the Fourier transform

$$\begin{aligned} \tilde{f}(p) &= \frac{1}{\sqrt{|\Lambda|}} \sum_{x \in \Lambda} f(x) e^{-ip \cdot x}, \\ f(x) &= \frac{1}{\sqrt{|\Lambda|}} \sum_{p \in \tilde{\Lambda}} f(p) e^{ip \cdot x}. \end{aligned} \tag{3.5}$$

The momenta in eq. (3.4) are bounded by $|p_\mu| \leq \frac{\pi}{a}$ which acts as an intrinsic ultraviolet cutoff.

3.1.2. Discretized Path Integrals

One major benefit of treating QFT on the lattice is the fact that the path-integral is well-defined and can (at least in principle) be computed directly. Coming from the path integral measure in the continuum (2.12), the expression becomes well-defined on the lattice as

$$\mathcal{D}\phi = \prod_{x\in\Lambda} \mathrm{d}\phi(x), \tag{3.6}$$

where the measure $\mathrm{d}\phi$ has to be chosen according to the kind of field ϕ represents. The details of the measure for gauge fields and fermions are discussed in sections 3.2.2 and 3.3.1 respectively.
Similarly to the continuum, expectation values of observables in a lattice theory with action $S[\phi]$ are expressed as

$$\langle \mathcal{O} \rangle = \frac{\int \mathcal{D}\phi\, \mathcal{O}[\phi] e^{-S[\phi]}}{\int \mathcal{D}\phi\, e^{-S[\phi]}}. \tag{3.7}$$

With a real-valued action S, this expression can be interpreted as an expectation value with respect to some probability measure P in field space as

$$\begin{aligned} \langle \mathcal{O} \rangle &= \int \mathcal{O}[\phi] \mathrm{d}P, \\ \mathrm{d}P &= \frac{1}{Z} \mathcal{D}\phi\, e^{-S[\phi]}. \end{aligned}$$

Lattice calculations take advantage of this by estimating the path-integral stochastically via Monte Carlo sampling. A more detailed discussion is provided in section 6.1.

3.2. Gauge Fields on the Lattice

While in the continuum, gauge fields are treated as elements of the Lie-algebra of a given gauge group, we have to take a step back for a lattice description and instead consider a gauge transport as per eq. (2.2). Thus, we introduce *gauge links* $U_\mu : \Lambda \to \mathcal{G}$ for a gauge group $\mathcal{G}$ that connect two neighboring points on the lattice. More specifically, if a field ψ on the lattice transforms via $\psi(x) \mapsto \Omega(x)\psi(x)$ for some local gauge transformation $\Omega : \Lambda \to \mathcal{G}$, then the gauge links transform via

$$U_\mu(x) \mapsto \Omega(x) U_\mu(x) \Omega(x + a\hat{\mu})^{-1}. \tag{3.8}$$

To relate lattice gauge links to the continuum gauge fields, one can interpret the gauge links as Wilson lines (eq. (2.4)), e.g. along a linear path from point $x + a\hat{\mu}$ to point x [30]

$$U_\mu(x) = \mathcal{P} \exp\left(a \int_0^1 \mathrm{d}t A_\mu(x + (1-t)a\hat{\mu}) \right).$$

3.2.1. Gauge Actions

For a successful lattice description of QCD, it is imperative to find an action that, in the limit of $a \to 0$, converges to the continuum gauge action. The most basic

version of such actions is the *Wilson gauge action* [29]

$$S_g[U] = \frac{2}{g^2} \sum_{x\in\Lambda} \sum_{\mu<\nu} \mathrm{Re}\,\mathrm{tr}[\mathbb{1} - U_{\mu\nu}(x)] \tag{3.9}$$

where $U_{\mu\nu}$ is a so-called *plaquette*

$$U_{\mu\nu}(x) = U_\mu(x) U_\nu(x + a\hat{\mu}) U_\mu(x + a\hat{\nu})^\dagger U_\nu(x)^\dagger. \tag{3.10}$$

which is visualized in fig. 2.1 and is in fact a very similar construct (constrained to a finite lattice instead of infinitesimal) to the one used to derive the continuum gauge action in section 2.1. Describing the gauge links $U_\mu \in \mathrm{SU}(3)$ in terms of the continuum gauge fields $A_\mu \in \mathfrak{su}(3)$, it can be shown using the Campbell-Hausdorff formula that [29]

$$U_{\mu\nu}(x) = \exp\big(ia^2 F_{\mu\nu}(x) + \mathcal{O}(a^3)\big)$$

which, when inserted into eq. (3.9) and expanded in powers of a, yields

$$S_g[U] = \frac{1}{2g^2} \sum_{x\in\Lambda} \sum_{\mu,\nu} \big(a^4 \,\mathrm{tr}\big[F_{\mu\nu}(x)^2\big] + \mathcal{O}(a^6)\big).$$

When taking the continuum limit $a \to 0$, the sum $a^4 \sum_{x\in\Lambda}$ turns into a spacetime integral $\int_{\mathbb{R}^4} \mathrm{d}^4x$ and the action converges to its continuum analog.

3.2.2. Haar Measure

To define an overall gauge-invariant theory, the path integral for the gauge links U has to be gauge-invariant as well. Since the action discussed above is already gauge-invariant, this means that a gauge-invariant measure $\mathcal{D}U$ has to be found, meaning a measure that is invariant under gauge transformations as in eq. (3.8). This is satisfied by the *Haar measure* which (for compact Lie groups $\mathcal{G}$) has the properties $\mathrm{d}U = \mathrm{d}(UV) = \mathrm{d}(VU)$ for $V \in \mathcal{G}$ and $\int_{\mathcal{G}} \mathrm{d}U = 1$. For $\mathcal{G} = \mathrm{SU}(N)$ the Haar-measure can be constructed from the group representation in terms of its generators t^a as

$$U(\omega) = \exp\left(i \sum_{a=1}^{N^2-1} \omega_a t^a\right)$$

via [29]

$$\mathrm{d}U(\omega) = c\sqrt{\det(g(\omega))} \prod_k \mathrm{d}\omega_k \tag{3.11}$$

where g is the metric

$$g(\omega)_{ij} = \mathrm{tr}\left[\frac{\partial U(\omega)}{\partial \omega_i} \frac{\partial U(\omega)^\dagger}{\partial \omega_j}\right]$$

on $\mathrm{SU}(N)$ and c is a normalization constant necessary to normalize the integral over the whole group to 1.

3.3. Fermions on the Lattice

Fermions, which have to be taken into account for a complete description of QCD physics, come with a few complications. Multiple ways to deal with these complications have been developed. The following discussion, however, will be restricted to Wilson fermions [31] which are used in this thesis.

3.3.1. Fermions in the Path Integral

To describe fermions, Graßmann variables are commonly introduced that fulfill the usual anti-commutation relations of fermions. These variables are basis elements of the Graßmann algebra, i.e. the Clifford algebra with $Q(v) = 0$ (see section B.1), such that

$$\eta_i \eta_j = -\eta_j \eta_i.$$

On this algebra, derivatives and integrals are defined via [17, 19, 29]

$$\frac{\partial}{\partial \eta} 1 = 0, \qquad \frac{\partial}{\partial \eta_j} \eta_i = \delta_{ij}, \qquad \frac{\partial}{\partial \eta_k} \eta_i \eta_j = \delta_{ik}\eta_j - \delta_{jk}\eta_i,$$

$$\int \mathrm{d}\eta = 0, \qquad \int \mathrm{d}\eta_i \eta_j = \delta_{ij}, \qquad \int \mathrm{d}\eta_k \eta_i \eta_j = \delta_{ik}\eta_j - \delta_{jk}\eta_i.$$

Since the Dirac field ψ and its conjugate $\bar{\psi}$ have to be treated as independent fields in the path-integral, two Graßmann variables are needed for each fermionic degree of freedom. It is customary to label the variables that correspond to the conjugate of η_i as $\bar{\eta}_i$. Note, however, that unlike their field counterparts, η and $\bar{\eta}$ are not related via conjugation with γ^0 ($\bar{\eta} \neq \eta^\dagger \gamma^0$), but are independent variables. Consider a fermionic action like eq. (3.3) which can be written as

$$S[\psi, \bar{\psi}] = a^4 \sum_{x,y \in \Lambda} \bar{\psi}(x) D(x,y) \psi(y). \tag{3.12}$$

Here, D is a matrix in the spaces of lattice sites and spinor components (as well as color components for quark fields) that does not depend on ψ or $\bar{\psi}$. The partition function for this action then takes the form [19, 29]

$$Z = \int \mathrm{d}\eta_N \mathrm{d}\bar{\eta}_N \cdots \mathrm{d}\eta_1 \mathrm{d}\bar{\eta}_1 \exp\left(-a^4 \sum_{i,j=1}^{N} \bar{\eta}_i D_{ij} \eta_j \right) = \det\left(a^4 D\right)^{-1} \tag{3.13}$$

with $N = |\Lambda| N_S (\cdot N_C)$ where N_S is the number of spinor components and N_C is the number of color degrees of freedom. In the following, we abbreviate the path integral measure as

$$\mathcal{D}\psi \mathcal{D}\bar{\psi} = \mathrm{d}\eta_N \mathrm{d}\bar{\eta}_N \cdots \mathrm{d}\eta_1 \mathrm{d}\bar{\eta}_1$$

and treat ψ and $\bar{\psi}$ as N-dimensional Graßmann vectors. If a spacetime-coordinate x is provided, then $\psi(x)$ means those $N_S(\cdot N_C)$ components of ψ that correspond to the specified coordinate. The action in eq. (3.12) can then be written as

$$S[\psi, \bar{\psi}] = a^4 \bar{\psi} D \psi.$$

While in principle, the expectation value of an operator can be computed directly from its definition eq. (3.7), it is in practice quite costly and instead computed via a lattice version of Wick's theorem [29]

$$\begin{aligned} \langle \eta_{i_1} \bar{\eta}_{j_1} \cdots \eta_{i_n} \bar{\eta}_{j_n} \rangle =& \frac{1}{Z} \int \mathcal{D}\psi \mathcal{D}\bar{\psi}\, \eta_{i_1} \bar{\eta}_{j_1} \cdots \eta_{i_n} \bar{\eta}_{j_n} \exp\left(-a^4 \bar{\psi} D \psi\right) \\ =& (-1)^n \sum_{\sigma \in \mathcal{P}_n} \mathrm{sign}(\sigma) \mathcal{S}_{\psi, i_1 j_{\sigma(1)}} \cdots \mathcal{S}_{\psi, i_n j_{\sigma(n)}} \end{aligned} \tag{3.14}$$

where $\mathcal{S}_\psi$ is the propagator of the fermion field. The propagator can be related to the matrix D by introducing source fields $\theta, \bar{\theta}$ for the fermion in analogy to section 2.4.2 and rewriting the two-point function as

$$\begin{aligned}\mathcal{S}_{\psi,ij} &= \langle \eta_i \bar{\eta}_j \rangle = \frac{1}{Z} \int \mathcal{D}\psi \mathcal{D}\bar{\psi}\, \eta_i \bar{\eta}_j \exp\left(-a^4 \bar{\psi} D \psi\right) \\ &= \frac{1}{Z} \frac{1}{a^8} \frac{\delta^2}{\delta\bar{\theta}_i \delta\theta_j} \int \mathcal{D}\psi \mathcal{D}\bar{\psi}\, \exp\left(-a^4 \left[\bar{\psi} D \psi + \bar{\theta}\psi + \bar{\psi}\theta\right]\right)\Big|_{\theta,\bar{\theta}=0}.\end{aligned}$$

Introducing the transformation $\psi \mapsto \psi - D^{-1}\theta$, $\bar{\psi} \mapsto \bar{\psi} - \bar{\theta} D^{-1}$ one finds the commonly known result

$$\mathcal{S}_{\psi,ij} = \frac{1}{a^8} \frac{\delta^2}{\delta\bar{\theta}_i \delta\theta_j} \exp\left(-a^4 \bar{\theta} D^{-1} \theta\right)\Big|_{\theta,\bar{\theta}=0} = \left(D^{-1}\right)_{ij}. \tag{3.15}$$

3.3.2. Fermion Doubling

Comparing the expressions eqs. (3.3) and (3.12), the Dirac operator for the naive fermion action is identified as

$$D(x,y) = \frac{1}{2a} \sum_\mu \gamma_\mu \left(\delta_{x,y-a\hat{\mu}} - \delta_{x,y+a\hat{\mu}}\right) + m\delta_{xy}\mathbb{1}.$$

In momentum space the Dirac operator is then given by

$$\begin{aligned}\tilde{D}(q,p) &= \frac{1}{|\Lambda|} \sum_{x,y\in\Lambda} e^{-iqx} D(x,y) e^{ipy} \\ &= \frac{1}{|\Lambda|} \sum_{x\in\Lambda} e^{-iqx} \left[\frac{1}{2a} \sum_\mu \gamma_\mu \left(e^{ip(x+a\hat{\mu})} - e^{ip(x-a\hat{\mu})}\right) + m e^{ipx}\mathbb{1}\right] \\ &= \underbrace{\frac{1}{|\Lambda|} \sum_{x\in\Lambda} e^{i(p-q)x}}_{=\delta_{pq}} \left[\frac{1}{2a} \sum_\mu \gamma_\mu \left(e^{iap_\mu} - e^{-iap_\mu}\right) + m\mathbb{1}\right] \\ &= \left(\frac{i}{a} \sum_\mu \gamma_\mu \sin(ap_\mu) + m\mathbb{1}\right)\delta_{pq} \\ &=: \tilde{D}(p).\end{aligned} \tag{3.16}$$

In this representation, the Dirac operator is thus site-diagonal[2] and can easily be inverted expanding with unity $\frac{m\mathbb{1} - \frac{i}{a}\sum_\mu \gamma^\mu \sin(ap_\mu)}{m\mathbb{1} - \frac{i}{a}\sum_\mu \gamma^\mu \sin(ap_\mu)}$ and using the identity $\sum_{\mu,\nu} \gamma^\mu \gamma^\nu A_\mu A_\nu = \sum_\mu A^\mu A_\mu$ to give

$$\tilde{\mathcal{S}}_\psi(p) = \frac{m\mathbb{1} - \frac{i}{a}\sum_\mu \gamma^\mu \sin(ap_\mu)}{m^2 + \frac{1}{a^2}\sum_\mu \sin(ap_\mu)^2}.$$

This results in the desired limit for $a \to 0$ matching continuum QFT. However, the massless propagator

$$\tilde{\mathcal{S}}_\psi(p) = -a \frac{\sum_\mu \gamma^\mu \sin(ap_\mu)}{\sum_\mu \sin(ap_\mu)^2}$$

[2] In LQCD, the Dirac operator is usually treated as a matrix in coordinate-, spinor-, and color-space. Site-diagonal in this context means, that the matrix is diagonal in the spatial part, i.e. it only depends on a single coordinate instead of two.

has, 15 additional poles at maximal momenta in different directions,

$$p \in \left\{ \begin{pmatrix} 0 \\ 0 \\ 0 \\ 0 \end{pmatrix}, \begin{pmatrix} 0 \\ 0 \\ 0 \\ \frac{\pi}{a} \end{pmatrix}, \begin{pmatrix} 0 \\ 0 \\ \frac{\pi}{a} \\ 0 \end{pmatrix}, \begin{pmatrix} 0 \\ 0 \\ \frac{\pi}{a} \\ \frac{\pi}{a} \end{pmatrix}, \begin{pmatrix} 0 \\ \frac{\pi}{a} \\ 0 \\ 0 \end{pmatrix}, \begin{pmatrix} 0 \\ \frac{\pi}{a} \\ 0 \\ \frac{\pi}{a} \end{pmatrix}, \begin{pmatrix} 0 \\ \frac{\pi}{a} \\ \frac{\pi}{a} \\ 0 \end{pmatrix}, \begin{pmatrix} 0 \\ \frac{\pi}{a} \\ \frac{\pi}{a} \\ \frac{\pi}{a} \end{pmatrix}, \right.$$
$$\left. \begin{pmatrix} \frac{\pi}{a} \\ 0 \\ 0 \\ 0 \end{pmatrix}, \begin{pmatrix} \frac{\pi}{a} \\ 0 \\ 0 \\ \frac{\pi}{a} \end{pmatrix}, \begin{pmatrix} \frac{\pi}{a} \\ 0 \\ \frac{\pi}{a} \\ 0 \end{pmatrix}, \begin{pmatrix} \frac{\pi}{a} \\ 0 \\ \frac{\pi}{a} \\ \frac{\pi}{a} \end{pmatrix}, \begin{pmatrix} \frac{\pi}{a} \\ \frac{\pi}{a} \\ 0 \\ 0 \end{pmatrix}, \begin{pmatrix} \frac{\pi}{a} \\ \frac{\pi}{a} \\ 0 \\ \frac{\pi}{a} \end{pmatrix}, \begin{pmatrix} \frac{\pi}{a} \\ \frac{\pi}{a} \\ \frac{\pi}{a} \\ 0 \end{pmatrix}, \begin{pmatrix} \frac{\pi}{a} \\ \frac{\pi}{a} \\ \frac{\pi}{a} \\ \frac{\pi}{a} \end{pmatrix} \right\},$$

while the continuum theory only has the first pole at $p = 0$. These additional poles are known as *doublers*. There are different ways to deal with this peculiarity of the lattice. Here we will focus on a modification of the Dirac operator known as the *Wilson-Dirac operator* [31]. The data used in this thesis are based on this approach (see section 4.3). This modification adds a term $\frac{1}{a}\sum_\mu (1 - \cos(ap_\mu))\mathbb{1}$ to the naive Dirac operator in momentum space (3.16) that acts as an additional mass term to all but the physical doublers, effectively removing the unphysical poles in the propagator [29]. The modified operator then takes the form [29]

$$\begin{aligned} D_W(x,y) =& \sum_\mu \left(\gamma^\mu \partial_{y,\mu} - \frac{a}{2}\mathbb{1}\partial_y^{+\mu}\partial_{y,\mu}^{-} \right) + m\mathbb{1} \\ =& \frac{1}{2a}\sum_\mu \left[\gamma^\mu \left(\delta_{x,y-a\hat{\mu}} - \delta_{x,y+a\hat{\mu}} \right) - \left(\delta_{x,y-a\hat{\mu}} - 2\delta_{xy} + \delta_{x,y+a\hat{\mu}} \right)\mathbb{1} \right] \\ & + m\mathbb{1}\delta_{xy} \\ =& \frac{1}{2a}\sum_\mu \left[\gamma^\mu \left(\delta_{x,y-a\hat{\mu}} - \delta_{x,y+a\hat{\mu}} \right) - \left(\delta_{x,y-a\hat{\mu}} + \delta_{x,y+a\hat{\mu}} \right)\mathbb{1} \right] \\ & + \left(m + \frac{4}{a} \right)\mathbb{1}\delta_{xy}. \end{aligned} \tag{3.17}$$

3.3.3. Chiral Symmetry and the Nielson-Ninomiya-Theorem

In the case of vanishing mass, the continuum Dirac action has a chiral symmetry, i.e. it is invariant under the transformation

$$\psi \mapsto e^{i\alpha\gamma_5}\psi, \qquad \bar{\psi} \mapsto \bar{\psi}e^{i\alpha\gamma_5}.$$

This has the effect, that the right- and left-handed parts

$$\psi_{R/L} = \frac{1}{2}(\mathbb{1} \pm \gamma_5)\psi$$

decouple, such that

$$\mathcal{L}[\psi, \bar{\psi}] = \bar{\psi}_L D\psi_L + \bar{\psi}_R D\bar{\psi}_R$$

where D is the continuum Dirac operator $D = i\gamma^\mu\partial_\mu$ for a massless fermion. This symmetry is present in the naive Dirac action (3.3) due to $e^{i\alpha\gamma_5}\gamma^\mu e^{i\alpha\gamma_5} = \gamma^\mu$ which follows from $\{\gamma_5, \gamma^\mu\} = 0$. However, just like the mass term, the additional terms introduced for the Wilson-Dirac operator (3.17) break this symmetry. In fact, the Nielson-Ninomiya theorem [32–36] states that no free Dirac operator on a Euclidean lattice can fulfill the following properties simultaneously [36]:

1. The momentum space Dirac operator $\tilde{D}(p)$ is an analytic function with period $\frac{2\pi}{a}$ in each momentum component.
2. $\tilde{D}(p) = i\gamma^\mu p_\mu + \mathcal{O}(ap^2)$ for $|p| \ll \frac{\pi}{a}$.
3. $\tilde{D}(p)$ has no poles except for the physical one.
4. $D\gamma_5 + \gamma_5 D = 0$.

Any lattice formulation of fermions thus misses at least one of these properties, which are all required for a continuum limit consistent with standard-model fermions [36]. The last of these properties is equivalent to chiral symmetry and thus violated by the Wilson-Dirac operator. However, the Wilson-Dirac operator fulfills a similar property, namely γ_5-hermiticity, i.e.

$$D^\dagger = \gamma_5 D \gamma_5. \tag{3.18}$$

This property ensures that the eigenvalues of the operator are either real or come in complex conjugated pairs [19].

3.4. Spin on the Lattice

In a spacetime $\mathbb{R}^{p+q}$ with a signature $\underbrace{+\cdots+}_{p \text{ times}}\underbrace{-\cdots-}_{q \text{ times}}$ of the metric, particles that transform nontrivially under the $\mathrm{Spin}(p,q)$ (or just $\mathrm{Spin}(n)$ if $p = n, q = 0$) group have an intrinsic spin [37]. In this association, the total spin quantum number $S \in \frac{1}{2}\mathbb{N}$ corresponds to the $2S+1$-dimensional irrep of $\mathrm{Spin}(p,q)$ under which the respective state transforms. An odd dimension or integer spin S then corresponds to bosonic spin states, while even dimensions or half integer spins correspond to fermionic spin states.
The $\mathrm{Spin}(p,q)$ group is the double cover of the rotation group $\mathrm{SO}(p,q)$ and an object that transforms under this group is called a spinor. In the three-dimensional Euclidean space we have $\mathrm{Spin}(3) \cong \mathrm{SU}(2)$, for Minkowski-spacetime it is $\mathrm{Spin}(1,3) \cong \mathrm{SL}(2,\mathbb{C})$, and for four-dimensional Euclidean spacetime the spin group is $\mathrm{Spin}(4) \cong \mathrm{SU}(2) \times \mathrm{SU}(2)$ [37, 38].
Since LQCD is defined on a lattice in four-dimensional Euclidean space, spinors on the lattice are related to irreps of $\mathrm{Spin}(4)$, or $\mathrm{SU}(2) \times \mathrm{SU}(2)$ which can be constructed from irreps of $\mathrm{SU}(2)$ [38]. For $\mathrm{SU}(2)$ it is known that there is exactly one irrep acting on $\mathbb{C}^n$ for each number of dimensions $n \in \mathbb{N}$ with $n = 1$ corresponding to the trivial representation $U \mapsto 1 \forall U \in \mathrm{SU}(2)$ which is the spin-0 irrep. For odd n, $\mathrm{SU}(2)$ irreps $\mathcal{R} : \mathrm{SU}(2) \to \mathrm{GL}(\mathbb{C}^n)$ map the negative identity to the identity in $\mathrm{GL}(\mathbb{C}^n)$ so that these irreps are isomorphic to those of $\mathrm{SO}(3)$. These odd-dimensional irreps correspond to integer spin, i.e. bosons, while the odd-dimensional ones for which for which the corresponding $\mathrm{SU}(2)$-irrep is not isomorphic to $\mathrm{SO}(3)$ correspond to half-integer spin, i.e. fermions.
On the lattice, however, $\mathrm{SO}(3)$ is broken to the octahedral or cubic group O_h, the symmetry group of eight points arranged at the edges of a cube. For a classification of spin on a cubic lattice one thus has to find the decomposition of irreps of $SO(3)$ into those of O_h for integer spin. For half-integer spin, a decomposition of irreps of $SO(3)$'s double cover $\mathrm{Spin}(3) \cong \mathrm{SU}(2)$ into irreps of the double cover O_D of O_h have to be constructed as well.

For finite groups G, irreps are in a one-to-one correspondence to conjugacy classes, i.e. equivalence classes of group elements with two elements $g, h \in G$ being equivalent iff an element $a \in G$ exists s.t. $g = aha^{-1}$. In the case of O_h, the group consists of 24 elements with 5 conjugacy classes listed in table 3.1 while the double cover O_D has 48 elements with 8 conjugacy classes I, J, C_4, C_3, C_6, C_8, C_8', and C_4' [39].

Table 3.1: Conjugacy classes of the octahedral group O_h [39].

#elements	class	description
1	I	The identity element
3	C_2	Rotations about an angle of π about the coordinate axes
8	C_3	Rotations about an angle of $\pm\frac{2\pi}{3}$ about the four diagonals of the cube
6	C_4	Rotations about an angle of $\pm\frac{\pi}{2}$ about the coordinate axes
6	C_2'	Rotations about an angle of π about axes parallel to the cube's faces

The continuum irreps can be mapped to the ones on the lattice using the characters $\chi_\theta^{\mathcal{R}} = \operatorname{tr}\mathcal{R}(\theta)$ of irreps $\mathcal{R}$ of $\mathrm{SU}(2)$ corresponding to a rotation about an angle θ, and the characters $\chi_C^{\mathcal{R}'} = \operatorname{tr}\mathcal{R}'$ of irreps of a conjugacy class C of O_h or O_D of the same dimension as $\mathcal{R}$. The latter are listed in tables C.1 and C.2 while the former can be calculated without loss of generality using a rotation $U(\theta) \in \mathrm{SU}(2)$ about an angle θ about the z-axis which results in the following formula [39]

$$\begin{aligned}\chi_\theta^{(j)} =& \operatorname{tr}[U(\theta)] = \operatorname{tr}\left[e^{is_z\theta}\right] = \sum_{m=-j}^{j} \langle m|e^{is_z\theta}|m\rangle = \sum_{m=-j}^{j} e^{im\theta}\langle m|m\rangle \\ =& e^{-ij\theta}\sum_{m=0}^{2j}\left(e^{i\theta}\right)^m = e^{-ij\theta}\frac{1-e^{i(2j+1)\theta}}{1-e^{i\theta}} = \frac{e^{-i\left(j+\frac{1}{2}\right)\theta} - e^{i\left(j+\frac{1}{2}\right)\theta}}{e^{-i\frac{\theta}{2}} - e^{i\frac{\theta}{2}}} \\ =& \frac{\sin\left(\left(j+\frac{1}{2}\right)\theta\right)}{\sin\left(\frac{\theta}{2}\right)}\end{aligned}$$

for spin j. The decomposition of continuum irreps can then be obtained by computing the multiplicities $m_j^{(r)}$ of each octahedral irrep r w.r.t. the corresponding spin j irrep given by [39]

$$m_j^{(r)} = \frac{1}{g}\sum_k n_k \chi_k^{(r)} \chi_k^{(j)} \tag{3.19}$$

where $g = 24$ for O_h and $g = 48$ for O_D. This decomposition is listed in table 3.2 for the six lowest-dimensional irreps.

These lattice irreps play a role in this thesis for the construction of hadronic operators, which we discuss in more detail in section 7.1. As in the continuum theory, different states can be classified by their spin (among other quantum numbers). For example, pseudo-scalar mesons transform under the A_1 irrep, octet baryons transform under G_1, vector mesons under T_1, and decuplet baryons under H. However, as the mapping between continuum and lattice irreps is not one-to-one, there are always influences from other spin states for a given operator.

Table 3.2: Decomposition of SO(3) and SU(2) irreps into irreps of the octahedral group O_h and its double cover O_D [39]. For an irrep X, we denote $2X := X \oplus X$.

SO(3) Spin	Decomposition into irreps of O_h	SU(2) Spin	Decomposition into irreps of O_D
0	A_1	$1/2$	G_1
1	T_1	$3/2$	H
2	$E \oplus T_2$	$5/2$	$G_2 \oplus H$
3	$A_2 \oplus T_1 \oplus T_2$	$7/2$	$G_1 \oplus G_2 \oplus H$
4	$A_1 \oplus E \oplus T_1 \oplus T_2$	$9/2$	$G_1 \oplus 2H$
5	$E \oplus 2T_1 \oplus T_2$	$11/2$	$G_1 \oplus G_2 \oplus 2H$

For example, an operator defining an octet baryon transforming under G_1 does not only describe states with spin $\frac{1}{2}$, but also such with spin $\frac{7}{2}$, $\frac{9}{2}$, etc. as these continuum irreps have a nontrivial overlap with G_1.

3.5. The Lattice Scale

The discussion thus far usually involved powers of the lattice spacing a which naturally appear when discretizing fields and calculus operations as described in section 3.1. However, a lattice action ultimately becomes dimensionless through these factors involving the lattice scale a which is crucial for the interpretation of $\exp(-S)$ as a likelihood of a field configuration as hinted at in section 3.1.2. As a result, all quantities considered in a lattice simulation are made dimensionless by scaling with an appropriate power of the lattice scale as in table 3.3. This has

Table 3.3: Correspondence of continuum quantities and those intrinsic to a lattice simulation.

Quantity	Continuum version	Lattice version
Scalar field	ϕ	$a\phi$
Fermion field	ψ	$a^{3/2}\psi$
Gauge field	A_μ	$U_\mu = \exp(iaA_\mu)$
Mass	m	am
Length	l	l/a

the effect that a does not enter lattice simulations as a parameter and is thus not known from the simulation alone. Like the free parameters of the standard model, the lattice scale has to be determined from experimental results and cannot be computed from first principles.

Such a matching of the lattice scale is done by comparing the result of a lattice computation for some dimensionful observable to its experimental value. This can in its simplest form be done by simple computing the ratio of both results for the observable in question. If, for example, a hadron mass m is used to determine the lattice scale, it can be computed via $a = \frac{(am)_{\text{lat}}}{m_{\text{exp}}}$. More concrete examples of how this is done in practice are discussed in section 4.4 and chapter 9. Some observables used in practice are the pion and kaon decay constants [40, 41] or the mass of the omega baryon [42–44], usually in combination with a so-called flow

scales (see section 4.4.2 for t_0 which is used later in chapter 9).
A matching can in principle be performed on each simulated lattice, but usually one combines measurements from different simulations into a single value of a. This is possible, as in LQCD simulations the lattice scale is in direct correspondence to the gauge coupling g. In pure gauge theory, the renormalization group equations $\beta(g) = -\frac{\partial g}{\partial \ln a}$ can be solved when expanding

$$\beta(g) = -\beta_0 g^3 - \beta_1 g^5 + \mathcal{O}(g^7)$$

where $\beta_0 = \frac{11}{16\pi^2}$ and $\beta_1 = \frac{51}{128\pi^4}$ for pure QCD. Up to this order, the expansion is independent of the regularization scheme [29] and the result of the above equation is given by [29]

$$a(g) = \frac{1}{\Lambda_L}\left(\beta_0 g^2\right)^{-\frac{\beta_1}{2\beta_0^2}} \exp\left(-\frac{1}{2\beta_0 g^2}\right)\left(1 + \mathcal{O}(g^2)\right).$$

The integration constant Λ_L is a free parameter that can be chosen to set the scale in pure QCD. This allows the use of a single lattice spacing for a set of simulations sharing the same value of the strong gauge coupling g which, contrary to a, is a parameter of the action that directly enters the simulations.
When introducing quarks into the theory, however, the circumstances become more complicated as the lattice spacing does not only depend on the gauge coupling, but also on the sum of all quark masses. This is often accounted for by modelling this additional dependence as [40, 45, 46]

$$\tilde{g}^2 = g^2(1 + b_g a\bar{m}) \tag{3.20}$$

where $\bar{m}$ is the average quark mass. By tuning the simulation parameters such that the average quark mass is kept constant, it is thus still possible, to determine a single lattice spacing for multiple simulations with the same gauge coupling.

In order to derive physical results from a lattice calculation, the data from several computations with different parameters of the lattice action have to be combined in order to extrapolate the data to the continuum. In that regard, there are two distinct limits that have to be taken to reach the continuum theory. The first is the limit to a continuous space time, $a \to 0$ or analogously $\beta \to \infty$, the second is that of infinite volume, i.e. $N_t, N_s \to \infty$ where N_t and N_s are the number of lattice points in the temporal and spatial directions respectively. Note that the limit $a \to 0$ at constant N_t and N_s shrinks the volume to zero and can thus not be taken independently of the second limit [29]. To circumvent this problem, one calculates observables at different lattice spacings a and chooses the number of lattice points such that the physical extent $T = aN_t$, $L = aN_s$ is constant to first perform the $a \to 0$ limit for constant physical volume and then take the infinite volume limit from the extrapolated data at different values of T and L [29].

Chapter 4
Lattice QCD Actions and CLS Ensembles

Lattice discretizations of a continuum theory are not unique. Various choices can be made for the discretization of fields in QFT or algebraic operations and additional terms that vanish in the continuum limit can improve convergence behavior. Different collaborations use different discretizations of QCD. In this chapter we discuss used for the *Coordinated Lattice Simulations* (CLS) ensembles [9].

Before describing the CLS ensembles in section 4.3, we introduce a simple lattice description of fermionic interactions with gauge bosons in section 4.1 and a brief introduction into the role of gauge ensembles in lattice simulations in section 4.2. We end this chapter with a discussion of how the lattice spacing a has been determined for CLS ensembles in previous analyses in contrast to the discussion in chapter 9.

4.1. A Lattice QCD Action for Interacting Fermions

For a lattice description we add a gauge action like eq. (3.9) and a fermion action for each quark flavor entering the model (like eq. (3.12) with the Wilson-Dirac operator (4.2)). As in the continuum, we replace all derivatives in the quark action by gauge-covariant derivatives

$$\begin{aligned}
\nabla^+_\mu\psi(x) =& \frac{1}{a}(U_\mu(x)\psi(x+a\hat{\mu}) - \psi(x)),\\
\nabla^-_\mu\psi(x) =& \frac{1}{a}\big(\psi(x) - U^\dagger_\mu(x-a\hat{\mu})\psi(x-a\hat{\mu})\big),\\
\nabla_\mu\psi(x) =& \frac{1}{2}(\nabla^+_\mu + \nabla^-_\mu)\psi(x)\\
=& \frac{1}{2a}\big(U_\mu(x)\psi(x+a\hat{\mu}) - U^\dagger_\mu(x-a\hat{\mu})\psi(x-a\hat{\mu})\big).
\end{aligned} \tag{4.1}$$

This splits the action into two parts; a gauge part $S_g[U]$ which only depends on the QCD gauge links, and a fermionic part $S_q[\psi,\bar{\psi},U]$ which depends both on the quarks and the gauge links. The Wilson-Dirac operator (3.17) then becomes

[9, 29]

$$\begin{aligned} D_f =& \sum_\mu \left(\gamma^\mu \nabla_\mu - \frac{a}{2} \mathbb{1}_{\text{Spin}} \nabla^{-,\mu} \nabla^+_\mu \right) + m_f \mathbb{1}_{\text{Spin}\otimes\text{SU(3)}} \\ D_f(x,y) =& \frac{1}{2a} \sum_\mu ((\gamma^\mu - \mathbb{1}_{\text{Spin}}) U_\mu(x) \delta_{x,y-a\hat{\mu}} - (\mathbb{1}_{\text{Spin}} + \gamma^\mu) U^\dagger_\mu(x - a\hat{\mu}) \delta_{x,y+a\hat{\mu}}) \\ &+ \left(m_f + \frac{4}{a} \right) \mathbb{1}_{\text{Spin}\otimes\text{SU(3)}} \end{aligned} \tag{4.2}$$

where f denotes the flavor of the quark in question. The total QCD action combining Wilson's gauge and fermion actions for N_f quark flavors for example, is given by

$$\begin{aligned} S[\psi, \bar{\psi}, U] =& S_q[\psi, \bar{\psi}, U] + S_g[U] \\ =& a^4 \sum_{f=1}^{N_f} \sum_{x,y\in\Lambda} \bar{\psi}_f(x) D_f(x,y) \psi_f(y) + \frac{2}{g^2} \sum_{x\in\Lambda} \sum_{\mu<\nu} \text{Re}\,\text{tr}[\mathbb{1} - U_{\mu\nu}(x)]. \end{aligned} \tag{4.3}$$

This is, up to terms improving of the continuum limit, the action used in the project of this thesis. For more details, see section 4.3.

4.2. QCD Gauge Ensembles

Due to the large dimensionality of QCD calculations, direct computations of observables become unfeasible. Thus, the lattice action is treated as a Boltzmann weight defining a probability measure on field space, allowing the computation of observables via expectation values as per eq. (3.7). This is done via Monte-Carlo samples of field configurations which are drawn from the probability distribution $P = \frac{1}{Z} e^{-S}$. However, rewriting the expectation values as

$$\begin{aligned} \langle \mathcal{O} \rangle_S =& \frac{1}{Z} \int \mathcal{D}U \mathcal{D}\psi \mathcal{D}\bar{\psi}\, \mathcal{O}[\psi, \bar{\psi}, U] e^{-S[\psi,\bar{\psi},U]} \\ =& \frac{1}{Z} \int \mathcal{D}U \left(\frac{1}{Z_q[U]} \int \mathcal{D}\psi \mathcal{D}\bar{\psi}\, \mathcal{O}[\psi, \bar{\psi}] e^{-S_q[\psi,\bar{\psi},U]} \right) Z_q[U] e^{-S_g[U]} \\ =& \left\langle \langle \mathcal{O} \rangle_{S_q} \right\rangle_{S_{\text{eff}}} \end{aligned} \tag{4.4}$$

allows the reduction of the fields that have to be sampled to the gauge links U which are drawn from the distribution defined by the effective action

$$S_{\text{eff}}[U] = S_g[U] - \log Z_q[U] = S_g[U] + \sum_f \log\det D_f. \tag{4.5}$$

This effective action corresponds to the QCD action in which all fermionic degrees of freedom are integrated out. In order to draw configurations from its corresponding distribution, the effective action has to be evaluated multiple times (see section 6.1). This is straight-forward for the pure gauge part, S_g, however, the fermion determinant gets very costly at relevant lattice sizes. Some techniques employed in the generation of CLS ensembles [9] that deal with the computational complexity are discussed in section 4.3. However, at this point, a technique for the stochastic estimation of $\det D$ which will become relevant in section 4.3 shall be discussed in the following.

4.2.1. Pseudofermions

Consider two mass-degenerate fermions f_1 and f_2 with Dirac operators D_{f_i}. As for the Wilson-Dirac operator (4.2) we assume that their mass-degeneracy asserts that $D_{f_1} = D_{f_2} = D$ and that the Dirac operators are γ_5-hermitean as in eq. (3.18). Due to the γ_5 hermiticity, one finds

$$\det D = \det \gamma_5 \det D \det \gamma_5 = \det(\gamma_5 D \gamma_5) = \det\left(D^\dagger\right)$$

such that the product of the two determinants can be written as

$$\det D_{f_1} \det D_{f_2} = \det D^2 = \det\left(D^\dagger D\right).$$

Introducing a complex color-triplet, scalar field ϕ, the combined fermion determinant can then be estimated stochastically via [19, 29]

$$\det\left(D^\dagger D\right) = \frac{1}{\pi^N} \int \mathcal{D}\phi^* \mathcal{D}\phi e^{-\phi^\dagger (D^\dagger D)^{-1} \phi} \tag{4.6}$$

where N is the number of degrees of freedom of ϕ, i.e. $N_C|\Lambda|$. The advantage of this way of expressing the determinant is that it can easily be determined stochastically by drawing random vectors $R \in \mathbb{R}^N$ from the normal distribution $P(R) = \frac{1}{\pi^N} e^{-R^\dagger R}$. These independent variables can then be transformed via [19]

$$\phi = D^\dagger R$$

to construct samples distributed according to the multivariate normal distribution (4.6) with covariance matrix $D^\dagger D$. The exponential of the effective action from eq. (4.5) can then be expressed as

$$\exp(-S_{\text{eff}}[U]) = \int \mathcal{D}\phi^* \mathcal{D}\phi \exp\left(-S_g[U] - \phi^\dagger (D^\dagger D)^{-1} \phi\right)$$

where the constant normalization is omitted as it is irrelevant for sampling techniques used in LQCD. This expression can finally be used by sampling N_ϕ fields ϕ_k as described above and adding their contribution to the action as

$$S_{\text{eff}}[U] = S_g[U] + \sum_{k=1}^{N_\phi} \phi^\dagger D[U]^\dagger D[U] \phi$$

and sample U according to this action.[1]

4.3. CLS $N_f = 2 + 1$ Ensembles

The data discussed in this thesis are obtained using the $N_f = 2 + 1$ ensembles of the CLS [9]. These ensembles are generated using the `openQCD` [47] software package. N_f denotes the number of flavors introduced into the simulation and $2 + 1$ is meant to express that two degenerate light-quarks and one additional strange quark at a different mass are used. The ensembles consist of several gauge field configurations on the links of lattices of sizes $N_t \times N_s^3$ where N_t is the number of lattice sites in the time direction and N_s is the number of sites in any of the spatial directions, which is the same for all three directions. The ratios of lattice points in the time and spatial directions are typically $\frac{N_t}{N_s} \in \left\{2, \frac{8}{3}, 3, 4, \frac{16}{3}\right\}$ with $N_t \in \{48, 64, 96, 128, 192, 256\}$. For this thesis, only lattices with $N_t = 2N_s$ and $N_t = \frac{8}{3} N_s$ are used.

[1] Again, the change in normalization due to the sum is irrelevant in the sampling methods used for the CLS ensembles as it is multiplicative in the exponential appearing in the path integral.

4.3.1. Action

For the gauge links, the Lüscher-Weisz action [30] with coefficients determined at tree-level is used. This action has the form [9]

$$S_g[U] = \frac{\beta}{6}\left(c_0 \sum_{x,\mu,\nu} \mathrm{tr}[\mathbb{1} - U_{\mu\nu}(x)] + c_1 \sum_{x',\mu,\nu} \mathrm{tr}\big[\mathbb{1} - R_{\mu\nu}(x')\big]\right) \tag{4.7}$$

with $c_0 = \frac{5}{3}$ and $c_1 = -\frac{1}{12}$, where $U_{\mu\nu}$ are the standard plaquettes as in eq. (3.10) and $R_{\mu\nu}$ are rectangular Wilson loops [30]

$$R_{\mu\nu}(x) = U_\mu(x)U_\mu(x + a\hat{\mu})U_\nu(x + 2a\hat{\mu})U_\mu^\dagger(x + a\hat{\mu} + a\hat{\nu})U_\mu^\dagger(x + a\hat{\nu})U_\nu^\dagger(x).$$

The sums over x and x' run over all lattice sites for which a plaquette or rectangle can be constructed, which excludes some sites on or near an open boundary.
The fermionic part of the action is given by

$$S_q[U, \bar{\psi}, \psi] = a^4 \sum_{f\in\{u,d,s\}} \sum_{x\in\Lambda} \bar{\psi}_f(x) D(m_{0,f}) \psi_f(x) \tag{4.8}$$

with the modified Wilson-Dirac operator

$$D = \sum_\mu \left(\gamma^\mu \nabla_\mu - \frac{a}{2}\nabla^{-,\mu}\nabla_\mu^+\right) + a c_{\mathrm{SW}} \sum_{\mu,\nu} \frac{i}{4}\sigma_{\mu\nu}\hat{F}_{\mu\nu} + m_0. \tag{4.9}$$

The term added to the Wilson-Dirac operator (eq. (4.2)) results in a dimension-5 operator in eq. (4.8), known as the *Sheikholeslami-Wohlert term*, involving the field strength tensor [45]

$$\begin{aligned}\hat{F}_{\mu\nu} =& \frac{1}{8a^2}\{Q_{\mu\nu}(x) - Q_{\nu\mu}(x)\},\\ Q_{\mu\nu}(x) =& U_{\mu\nu}(x) + U_{\nu,-\mu}(x) + U_{-\mu,-\nu}(x) + U_{-\nu,\mu}(x)\end{aligned}$$

and $\sigma_{\mu\nu} = \frac{1}{2i}[\gamma_\mu, \gamma_\nu]$. From five possible dimension-5 operators compatible with all symmetries of the action, two can be eliminated via constraints from the Dirac-equation and another two can be absorbed into redefinitions of the bare mass m_0 and bare coupling strength g, so that only the Sheikholeslami-Wohlert term remains [29, 30, 45, 48]. The addition of this term improves the continuum limit of the gauge action in the same way as taking the symmetric derivative over the forward one does by eliminating the leading terms in the expansion of the action around $a = 0$. This procedure of adding terms improving the continuum limit is generally known as the *Symanzik improvement program.*

4.3.2. Reweighting

Light Wilson quarks in lattice simulations tend to suffer from exceptionally small eigenmodes, making numeric simulations unstable [49], specifically leading to algorithmic instabilities, sampling inefficiencies and ergodicity violations [50]. This is remedied in CLS simulations by introducing a twisted mass term for the mass-degenerate light quarks to the Wilson-Dirac operator, which in its simplest form looks like [49, 50][2]

$$D_{\mathrm{tm}} = D + i\mu\gamma_5. \tag{4.10}$$

[2]This form sometimes includes a third Pauli matrix τ^3 acting in flavor space, i.e. $D_{\mathrm{tm}} = D + i\mu\gamma_5\tau^3$ which thus couples differently to the two light quarks [49].

This modifies the fermion determinant for the pair of degenerate light-quarks as follows [51]:

$$\det\left(D^\dagger D\right) \mapsto \det\left(D^\dagger D + \mu^2\right). \tag{4.11}$$

The eigenvalues appearing in the simulation thus satisfy $\lambda \geq \mu$ resulting in a more numerically stable simulation. The regularization used for CLS ensembles, however, differs from the above prescription by instead modifying the Dirac-Wilson operator as [50]

$$D_{tm}^{\mathrm{CLS}} = (D + i\mu\gamma_5)\frac{\gamma_5 D - i\mu}{\gamma_5 D - i\sqrt{2}\mu} \tag{4.12}$$

which changes the fermion determinant to [51]

$$\det\left(D^\dagger D\right) \mapsto \det\left(\frac{\left(D^\dagger D + \mu^2\right)^2}{D^\dagger D + 2\mu^2}\right) \tag{4.13}$$

to a similar effect as the simpler version. While it is possible to match QCD with a twisted mass to standard QCD in the continuum limit via careful treatment of renormalization and unphysical quantum numbers in correlation functions [49] (see chapter 7), the CLS collaboration instead recovers the non-twisted theory via reweighting [9, 51]. The reweighting factors for the twisted mass are then given by

$$W = \det\left(\frac{D^\dagger D}{D^\dagger D + \mu^2}\right)$$

for the simple version (4.10) and

$$W = \det\left(D^\dagger D\frac{D^\dagger D + 2\mu^2}{\left(D^\dagger D + \mu^2\right)^2}\right) \tag{4.14}$$

for the regularization used in CLS simulations [51].

4.3.3. The Light Quark Action

Instead of computing the fermion determinant in the effective action (4.5) directly, the determinant is instead taken from $Q = \gamma_5 D$ for light quarks, which does not change the action because

$$D^\dagger D = \gamma_5 D \gamma_5 D = Q^2.$$

Given the fact that $\det\gamma_5 = 1$, this does not change the value of the determinant. Furthermore, even-odd-preconditioning [52] is applied which expresses Q in terms of its block LDU decomposition [19, 51, 52]

$$\begin{aligned} Q =& \begin{pmatrix} Q_{ee} & Q_{eo} \\ Q_{oe} & Q_{oo} \end{pmatrix} = \begin{pmatrix} \mathbb{1} & Q_{eo}Q_{oo}^{-1} \\ 0 & \mathbb{1} \end{pmatrix}\begin{pmatrix} \hat{Q} & 0 \\ 0 & Q_{oo} \end{pmatrix}\begin{pmatrix} \mathbb{1} & 0 \\ Q_{oo}^{-1}Q_{oe} & \mathbb{1} \end{pmatrix} \\ \hat{Q} =& Q_{ee} - Q_{eo}Q_{oo}^{-1}Q_{oe} \end{aligned}$$

where Q_{ee} is the subset of Q that contains only those entries $Q(x, y)$ for which $x_0 + x_1 + x_2 + x_3$ as well es $y_0 + y_1 + y_2 + y_3$ are even. Similarly, the sum of the

spatial components in Q_{oo} is odd and Q_{eo} and Q_{oe} mix even and odd lattice sites. This has the advantage, that the determinant of Q is then factorized as

$$\det Q = \det \hat{Q} \det Q_{oo}$$

with Q_{oo} being site-diagonal [19], thus reducing the determinant of Q_{oo} to a product

$$\det Q_{oo} = \prod_{x,y \in \Lambda_{oo}} \det(Q_{oo}(x,y))$$

of determinants of $N_C^2 \times N_S^2 = 144 \times 144$ matrices mixing only color and spin indices.
Finally the twisted-mass regularization (4.13) is applied, but only to the Schur complement $\hat{Q}$. The light quark determinant is then given by

$$\det\left(Q^2\right) = \det(Q_{oo})^2 \det\left(\frac{\hat{Q}^2 + \mu^2}{\hat{Q}^2 + 2\mu^2}\right) \det\left(\hat{Q}^2 + \mu^2\right). \tag{4.15}$$

The reweighting factor for the twisted mass in terms of Q is then given by

$$W_0 = \det \frac{\left(\hat{Q}^2 + 2\mu^2\right)\hat{Q}^2}{\left(\hat{Q}^2 + \mu^2\right)^2}. \tag{4.16}$$

To further reduce fluctuations in the forces, a factorization of the last factor in eq. (4.15) [9, 53, 54]

$$\det\left(\hat{Q}^2 + \mu^2\right) = \det\left(\hat{Q}^2 + \mu_{N_{\mathrm{mf}}}^2\right) \prod_{i=1}^{N_{\mathrm{mf}}} \det\left(\frac{\hat{Q}^2 + \mu_{i-1}^2}{\hat{Q}^2 + \mu_i^2}\right) \tag{4.17}$$

is used, where $\mu = \mu_0 < \mu_1 < \cdots < \mu_{N_{\mathrm{mf}}}$.
Finally, the effective action for the light quarks is computed using pseudofermions (4.6) via [9]

$$\begin{aligned} S_{ud,\mathrm{eff}}[U, \phi_0, ..., \phi_{N_{\mathrm{mf}}}] = &\left(\phi_0, \frac{\hat{Q}^2 + 2\mu^2}{\hat{Q}^2 + \mu^2}\phi_0\right) + \sum_{i=1}^{N_{\mathrm{mf}}} \left(\phi_i, \frac{\hat{Q}^2 + \mu_i^2}{\hat{Q}^2 + \mu_{i-1}^2}\phi_i\right) \\ &+ \left(\phi_{N_{\mathrm{mf}}+1}, \frac{1}{\hat{Q}^2 + \mu_{N_{\mathrm{mf}}}^2}\phi_{N_{\mathrm{mf}}+1}\right) - 2\log\det Q_{oo} \end{aligned} \tag{4.18}$$

where the scalar product including pseudoscalar fields is given by

$$(\phi_1, \phi_2) = \phi_1^\dagger \phi_2 = \sum_{\substack{x \in \Lambda \\ c \in \mathrm{colors}}} (\phi_1^c)^*(x) \phi_2^c(x).$$

4.3.4. The Strange Quark Action

The strange quark determinant, like the one for light quarks, is computed using an even-odd decomposition of the modified Wilson-Dirac matrix $Q_s = \gamma_5 D_s$. This, too does not change the action since $\det \gamma_5 = 1$. However, for the Schur's complement, a rational approximation of $\sqrt{\hat{Q}_s^2}$ is used in a Monte Carlo algorithm known as *Rational Hybrid Monte Carlo* (RHMC) [55]. This procedure has

the advantage that the determinant of $\hat{Q}_s^2$ can be estimated via pseudofermions as is done in eq. (4.18) for the light quark pair. The rational approximation furthermore allows for a much more efficient calculation. However, the approximation comes at the cost of an additional reweighting factor W_1 such that the exact strange quark determinant is given by [9]

$$\det Q_s = \det Q_{s,oo} \operatorname{sign}(\det \hat{Q}_s) \det \sqrt{\hat{Q}_s^2} = W_1 \det Q_{s,oo} \det\left(A^{-1} \prod_{i=1}^{N_p} \frac{\hat{Q}_s^2 + \bar{\mu}_i^2}{\hat{Q}_s^2 + \bar{\nu}_i^2} \right)$$

where the parameters A, $\bar{\mu}_i$, and $\bar{\nu}_i$ are determined using Zolotarev's optimal approximation to the square root in a given interval based on the number of poles N_p [9]. An additional reduction of computational complexity is performed by only computing the N_p' terms with smallest $\bar{\mu}_i$ by individual pseudofermions, while the determinant of the remaining factors is estimated using only one pseudofermion leading to the strange quark effective action [9]

$$\begin{aligned} S_{s,\text{eff}}[U, \phi_0, ..., \phi_{N_p'}] = &\sum_{i=0}^{N_p'-1} \left(\phi_i, \frac{\hat{Q}_s^2 + \bar{\nu}_{N_p-i}}{\hat{Q}_s^2 + \bar{\mu}_{N_p-i}^2} \phi_i \right) \\ &+ \left(\phi_{N_p'}, \prod_{j=1}^{N_p - N_p'} \phi_{N_p'} \frac{\hat{Q}_s^2 + \bar{\nu}_j^2}{\hat{Q}_s^2 + \bar{\mu}_j^2} \phi_{N_p'} \right) - \log \det Q_{s,oo}. \end{aligned}$$

A drawback of this approach is the loss of information about the sign of $\det \hat{Q}_s$ which in some cases turns out to be negative [56]. This sign has to be determined in a separate computation and reintroduced with the reweighting factor W_1.

4.4. Setting the Lattice Scale

For some years, the lattice spacing has been determined in physical units using a combination of the pion and kaon decay constants [40, 41]

$$f_{\pi K} = \frac{2}{3}\left(f_K + \frac{1}{2} f_\pi \right) \tag{4.19}$$

where f_X is the decay constant of the hadron X. These quantities can be determined to high precision in LQCD simulations and thus result in small statistical errors for the lattice spacing. The combination 4.19 is furthermore chosen as its expansion in chiral perturbation theory

$$\begin{aligned} f_{\pi K} \approx f\Big(1 - \frac{7}{6} L_\pi - \frac{4}{3} L_K - \frac{1}{2} L_\eta + \frac{16 B \operatorname{tr} M}{3 f^2} (L_5 + 3 L_4)\Big), \\ L_X = \frac{m_X^2}{(4\pi f)^2} \log\left(\frac{m_X^2}{(4\pi f)^2} \right) \end{aligned} \tag{4.20}$$

suggests it to be constant along a trajectory of ensembles sharing the same average quark mass $\bar{m} = \frac{1}{N_f} \operatorname{tr} M$, where L_4 and L_5 are low energy constants.
In order to combine data from different gauge ensembles at varying physical parameters into a single lattice spacing per choice of the inverse gauge coupling β, $f_{\pi K}$ has to be expressed in terms of the lattice spacing a, the quark masses, and the volume of the lattice. The a dependence is modeled to leading order

as an a^2 correction to the continuum theory, which is justified by the $\mathcal{O}(a)$ improvement of the action used in CLS ensembles. The finite volume effects can be neglected if $f_\pi L \gg 1$ and $m_\pi L \gg 1$ [40], otherwise they have to be modeled depending on the observable.

In the following subsections, we will discuss the experimentally available observables in section 4.4.1, the theory scale t_0 which has no experimentally accessible analog and is ultimately used for the determination of the lattice spacing a in section 4.4.2, and finally the procedure to determine the lattice scale in section 4.4.3.

4.4.1. Physical Observables

The decay constants are obtained from the pseudoscalar density $P = \bar{\psi}_1\gamma_5\psi_2$ and the improved axial vector current $A_\mu = \bar{\psi}_1\gamma_\mu\gamma_5\psi_2 + ac_A\partial_\mu P$ where ψ_1 and ψ_2 are two light quarks for the pion and a light and a strange quark for the kaon. c_A is a non-perturbatively tuned improvement coefficient to eliminate $\mathcal{O}(a)$ cutoff effects [57]. Choosing fixed source positions at $t_y = a$ or $t_y = T - a$, the two-point functions

$$f_P(t_x, t_y) = -\frac{a^6}{L^3}\sum_{\mathbf{x},\mathbf{y}}\langle P(t_x,\mathbf{x})P(t_y,\mathbf{y})\rangle$$
$$f_A(t_x, t_y) = -\frac{a^6}{L^3}\sum_{\mathbf{x},\mathbf{y}}\langle A_0(t_x,\mathbf{x})P(t_y,\mathbf{y})\rangle$$

are combined into a ratio

$$R_{PS}(x_0, y_0) = \sqrt{\frac{f_A(x_0, y_0)f_A(x_0, T - y_0)}{f_P(T - y_0, y_0)}}.$$

This ratio has a plateau of height R which is related to the decay constants via [40]

$$f_X = Z_A(g_0)\big(1 + a\bar{b}_A \operatorname{tr} M + a\tilde{b}_A m_X\big)\sqrt{\frac{2}{m_X}}R$$

where Z_A is a renormalization factor and $\bar{b}_A$ and $\tilde{b}_A$ are constants. The masses m_X for $X \in \{\pi, K\}$ are determined from the asymptotic behaviour of the pseudoscalar two-point function f_P (see chapter 7 and eqs. (7.2) and (7.3) for more details).

4.4.2. The Wilson Flow Scale t_0

The Wilson flow V_t was first introduced in an attempt to improve the sampling of topological sectors in LQCD simulations at small lattice spacings [15] but has later been found to provide a suitable intermediate scale for the scale-setting procedure [16]. It is defined via the equations

$$\dot{V}_{t,\mu}(x) = -g_0^2\{\partial_{x,\mu}S_g[V_t]\}V_{t,\mu}(x), \quad V_{t,\mu}(x)\Big|_{t=0} = U_\mu(x). \tag{4.21}$$

Here, the operator $\partial_{x,\mu}f(U) = \sum_a t^a \frac{\mathrm{d}}{\mathrm{d}s} f\big(e^{st^a}U\big)|_{s=0}$ with the SU(3) generators t^a is acting on the Lüscher-Weisz action 4.7 where g_0 is the bare coupling and $\dot{V}$

stands for the derivative of V_t w.r.t the flow parameter t. The second equation fixes the flow at flow time $t = 0$ to the gauge links on a given lattice.
The Wilson flow has a counterpart defined in terms of the Lie-algebra valued fields of continuum QCD. It is given by the flow $B_\mu : \mathbb{R} \times \mathbb{R}^4 \to \mathfrak{su}(3)$ defined by the differential equation [16]

$$\dot{B}_\mu(t,x) = D^\nu(t,x) G_{\nu\mu}(t,x),$$

where $\dot{B}_\mu(t) = \frac{\mathrm{d}}{\mathrm{d}t} B_\mu(t)$ and

$$D_\mu X = \partial_\mu X + [B_\mu, X], \quad G_{\mu\nu} = \partial_\mu B_\nu - \partial_\nu B_\mu + [B_\mu, B_\nu].$$

As in eq. (4.21), the flow is subject to the constraint $B_\mu(0,x) = A_\mu(x)$ where A_μ is the gluon field. This definition gives rise to the observable

$$E = \frac{1}{4} G^{\mu\nu} G_{\mu\nu}. \tag{4.22}$$

Its next-to-leading-order continuum expectation value in the $\overline{\mathrm{MS}}$ renormalization scheme at the normalization scale μ is given by [16]

$$\begin{aligned}
\langle E \rangle =& \frac{3g^2}{16\pi^2 t^2}\left(1 + \bar{c}_1 g^2 + \mathcal{O}(g^4)\right) \\
\bar{c}_1 =& \frac{1}{16\pi^2}\left(11L + \frac{52}{3} - 9\log 3 - N_f\left(\frac{2}{3}L + \frac{4}{9} - \frac{4}{3}\log 2\right)\right) \\
L =& \log\left(8\mu^2 t\right) + \gamma_E
\end{aligned}$$

making use of the Euler-Mascheroni constant γ_E. In terms of the running coupling $\alpha_S(\mu) = \frac{g^2(\mu)}{4\pi}$ at the scale $\mu = \frac{1}{\sqrt{8t}}$, this then becomes [16]

$$\begin{aligned}
\langle E \rangle =& \frac{3}{4\pi t^2}\alpha_S(\mu)\left(1 + k_1 \alpha_S(\mu) + \mathcal{O}(\alpha_S^2)\right) \\
k_1 =& \frac{1}{4\pi}\left(11\gamma_E + \frac{52}{3} - 9\log 3 - N_f\left(\frac{2}{3}\gamma_E + \frac{4}{9} - \frac{4}{3}\log 2\right)\right) \\
\approx& 1.0978 + 0.0075 N_f.
\end{aligned} \tag{4.23}$$

Thus, up to this order, $t^2 \langle E \rangle$ is a function of the renormalized gauge coupling at the $\overline{\mathrm{MS}}$ scale $\frac{1}{\sqrt{8t}}$ and from eq. (4.23) the renormalized gauge coupling coupling can be matched via [58–61]

$$g^2_{GF}(t; L, T, g_0^2) = \frac{16\pi^2}{3} \frac{1}{(1 + \delta(t, L, T))} t^2 \left\langle E(t, g_0^2) \right\rangle$$

at tree-level, where g_0^2 is the bare coupling going into the simulation and δ introduces a correction for the gauge zero modes on periodic boundary ensembles [58, 59]. δ is a function of the spatial and temporal extent (L and T) and the flow time t.
On the lattice, E can for example be computed via [16]

$$E = 2 \sum_{x \in \Lambda} \sum_{\mu < \nu} \mathrm{Re}\,\mathrm{tr}[\mathbb{1} - V_{t,\mu\nu}(x)] \tag{4.24}$$

where $V_{t,\mu\nu}$ is the plaquette (3.10) built from V_t instead of the gauge links $U = V_0$. Note, however, that this lattice version of E is not unique and a more symmetric version is suggested in [16] that reduces discretization effects.
While the continuum description of the gradient flow is limited to a region of small values of t where the perturbative method is accurate, lattice results of this quantity are valid past that region [16]. In fact, lattice computations show that $t^2 \langle E \rangle$ grows linearly at some point which is not predicted by the continuum description [16, 62].
A useful intermediate scale for the purposes of scale setting can be defined as the flow time t_0 at which $t_0^2 \langle E(t_0) \rangle = c$ with the common choice of $c = 0.3$ which satisfies the condition $a \ll \sqrt{8t_0} \ll aL$ [63] where L is the number of lattice points in the spatial directions. Figure 4.1 shows an example of $t^2 \langle E \rangle$ with the value of t_0 for $c = 0.3$.

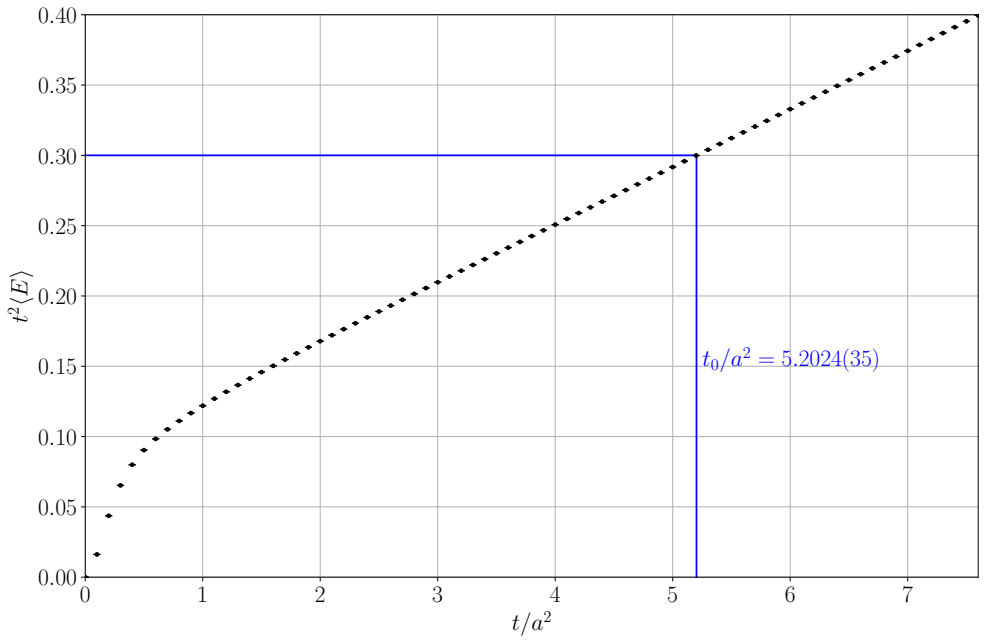

Figure 4.1: Example of the determination of t_0 on the ensemble E250. The two values between which $t^2 \langle E \rangle$ crosses the value 0.3 are linearly interpolated to determine the flow time t_0 at which $t^2 \langle E \rangle = 0.3$.

4.4.3. Chiral Extrapolation and Scale Setting

For the quark mass-dependence, one usually makes use of chiral perturbation theory, which relates the quark masses to the masses of the pseudo-scalar octet mesons via the Gell-Mann-Oakes-Renner (GMOR) relation for SU(3) flavor symmetry [64]

$$\begin{aligned} f_\pi^2 m_\pi^2 &= \frac{1}{2}(m_u + m_d) \langle 0|(\bar{u}u + \bar{d}d)|0\rangle \\ f_K^2 m_K^2 &= \frac{1}{2}(m_u + m_s) \langle 0|(\bar{u}u + \bar{s}s)|0\rangle \\ f_\eta^2 m_\eta^2 &= \frac{1}{6}(m_u + m_d) \langle 0|(\bar{u}u + \bar{d}d)|0\rangle + \frac{4}{3} m_s \langle 0|\bar{s}s|0\rangle \end{aligned} \tag{4.25}$$

which is often reduced to [46]

$$m_\pi^2 = 2B_0 m_l, \quad m_K^2 = B_0(m_s + m_l) \tag{4.26}$$

to relate the light-quark mass m_l and the strange quark mass m_s to the pseudoscalar meson.
All observables are scaled with powers of the flow scale $8t_0$ described in section 4.4.2 such that the scaled quantity is dimensionless. The quark mass dependence is captured in the quantities

$$\phi_2 = 8t_0 m_\pi^2 \quad \text{and} \quad \phi_4 = 8t_0\left(m_K^2 + \frac{1}{2}m_\pi^2\right). \tag{4.27}$$

The ensembles are chosen such that the sum over the quark masses $\operatorname{tr} M$ is constant which suggests that ϕ_4 is a constant along these ensembles assuming eqs. (4.25) and (4.26). In practice, however, slight corrections have to be made because a constant sum of the hopping parameters used in the simulations does not mean a constant sum of renormalized quark masses which to $\mathcal{O}(a)$ are given by [40]

$$\operatorname{tr} M^R = Z_m r_m\big(\big(1 + a\bar{d}_m \operatorname{tr} M\big)\operatorname{tr} M + a d_m \operatorname{tr} M^2\big).$$

This deviation is accounted for by a correction of the quark masses in terms of Taylor expansions of observables w.r.t. the quark masses akin to the treatment of isospin-breaking effects discussed in section 5.2. This shift is performed in a way as to reach a universal value of $\phi_4 = \tilde{\phi}_4$ for all ensembles. For the ϕ_2 dependence of $F = \sqrt{t_0} f_{\pi K}$, two different model are tested. The first is a Taylor expansion

$$F_T^{\text{cont}}(\phi_2) = c_0 + c_1(\phi_2 - \phi_2^{\text{sym}})^2$$

around ϕ_2 at the symmetric point defined by $m_u = m_d = m_s$. The second ansatz comes from eq. (4.20) derived from chiral perturbation theory relating F at different points to F at the symmetric point via

$$\frac{F_\chi^{\text{cont}}(\phi_2)}{F_\chi^{\text{cont}}(\phi_2^{\text{sym}})} = 1 - \frac{7}{6}(L_\pi - L_\pi^{\text{sym}}) - \frac{4}{3}\big(L_K - L_K^{\text{sym}}\big) - \frac{1}{2}\big(L_\eta - L_\eta^{\text{sym}}\big)$$

making use of the fact that at this order t_0 is a constant along the constant ϕ_4 trajectory. The dependence on the lattice spacing in both cases is modeled via

$$\sqrt{t_0} f_{\pi K}(\phi_2, \tilde{\phi}_4) = F_{T/\chi}^{\text{cont}}(\phi_2) + c_{T/\chi}\frac{a^2}{t_0^{\text{sym}}}.$$

For any choice of $\tilde{\phi}_2$, $\tilde{\phi}_4$ a value of t_0 in physical units can be determined by taking the ratio of the experimental value of $f_{\pi K}$ and $\sqrt{t_0} f_{\pi K}(\tilde{\phi}_2, \tilde{\phi}_4)$. This allows for the definition of a physical point at which the choice of $\tilde{\phi}_2 = \phi_2^{\text{phys}}$ and $\tilde{\phi}_4 = \phi_4^{\text{phys}}$ produces the experimental results for the pion and kaon masses as well as $f_{\pi K}$ defining the physical value t_0^{phys} of t_0. Analogously, a value of t_0^{sym} at the symmetric point is defined by taking the quotient of the experimental value of $f_{\pi K}$ and the measured value of $\sqrt{t_0} f_{\pi K}(\phi_2^{\text{sym}}, \phi_4^{\text{phys}})$. This symmetric value is used to set the lattice spacing a at a given $\beta = \frac{2}{g^2}$ from the ratio of t_0^{sym} in physical units and the measured value of $\frac{t_0}{a^2}$ on the lattice [40].

In a later analysis, only the chiral fit was performed, but in a combined fit in ϕ_2 and ϕ_4 via [41]

$$\begin{aligned} F_\chi(\phi_2,\phi_4) =& F_\chi^{\text{cont}}(\phi_2,\phi_4)\left(1 + C\frac{a^2}{t_0}\right) \\ F_\chi^{\text{cont}}(\phi_2,\phi_4) =& \frac{A}{8\pi\sqrt{2}}\left[1 - \frac{7}{6}L\left(\frac{\phi_2}{A^2}\right) - \frac{4}{3}L\left(\frac{\phi_4 - \frac{1}{2}\phi_2}{A^2}\right) - \frac{1}{2}L\left(\frac{\frac{4}{3}\phi_4 - \phi_2}{A^2}\right)\right. \\ & \left. + B\phi_4\right], \\ L(x) =& x\log(x) \end{aligned}$$

In this analysis, the scale is set by extrapolating t_0^{phys} to the symmetric point using the ϕ_2 dependence of t_0 at next-to-leading order in chiral perturbation theory [41]

$$R_{t_0}(\phi_2) = \frac{\sqrt{t_0}}{\sqrt{t_0^{\text{sym}}}} = \sqrt{1 + G(\phi_2 - \phi_2^{\text{sym}})}.$$

In this scheme the lattice spacing for a given β is then given by [41]

$$a = \frac{\sqrt{t_0^{\text{phys}}}}{R_{t_0}(\phi_2^{\text{phys}})\sqrt{\frac{t_0^{\text{sym}}}{a^2}}}.$$

4.4.4. Precision of the Lattice Scale

The main motivation for the project behind this thesis lies in the determination of the anomalous magnetic moment of the muon, $a_\mu = \frac{g_\mu - 2}{2}$. This quantity is very precisely known experimentally (at $\sim 190\,\text{ppb}$ [65] since 2023 and $\sim 124\,\text{ppb}$ [2] since 2025) and from standard model computations. However, while the dominant contributions to the theoretical prediction come from pure QED calculations, hadronic contributions are introduced [3] whose magnitude cannot fully be computed in a perturbative manner like the QED contributions. In fact, the error of the theoretical value of a_μ is at this point dominated by this non-perturbative part, a_μ^{hvp} [3]. Among other contributions, the total uncertainty of a_μ^{hvp} from lattice simulations is proportional to the relative uncertainty of the lattice scale [4, 8]

$$\Delta a_\mu^{\text{hvp}} = \left| M_\mu \frac{\partial a_\mu^{\text{hvp}}}{\partial M_\mu} + M_\pi \frac{\partial a_\mu^{\text{hvp}}}{\partial M_\pi} + M_K \frac{\partial a_\mu^{\text{hvp}}}{\partial M_K} + \cdots \right| \frac{\Delta\Lambda}{\Lambda} \tag{4.28}$$

where Λ is the quantity used to set the scale. It is thus imperative to reduce the error on the lattice scale as much as possible in order to reduce the overall error on a_μ^{hvp}, preferably to the level of a few permil in order to achieve a sub-percent error on a_μ^{hvp} [4].
However, the CLS ensembles are generated with intrinsic isospin-symmetry, meaning that up and down quark have identical properties. This introduces a systematic error for any calculation performed from these ensembles of the order of 1 % [6, 7]. To achieve sub-percent precision on a_μ^{hvp} one thus has to correct for these effects to remove this systematic uncertainty. On one hand, this correction

has to be computed for the direct calculation of the hadronic vacuum polarization itself. On the other hand, the lattice scale too needs to be corrected as otherwise the same 1 % systematic uncertainty of the lattice scale would translate to that of a_μ^{hvp} as per eq. (4.28).
While it is in principle possible to calculate isospin-breaking corrections to the pion and kaon decay constants, it is rather involved [66, 67]. The problem in this case is that contrary to the isospin-symmetric case, the hadronic and leptonic part of the decay process do no factorize in the case where a quark and the charged lepton exchange a photon as illustrated in fig. 4.2. Thus, the lattice calculation cannot be done separately from the perturbative part of the calculation involving non-lattice fields.

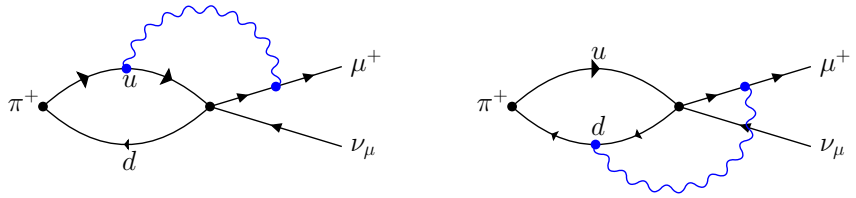

Figure 4.2: Problematic isospin-breaking corrections to the pion decay constant with the W^+ boson integrated out. A photon exchange between a lattice field (u or d) and a non-lattice field (μ^+) cannot be accounted for in a straight-forward way using the methods described in section 5.2.

An alternative, investigated in this thesis, is to replace these quantities in the scale setting procedure by baryonic masses for which it is much more straightforward to calculate isospin-breaking effects on isospin-symmetric ensembles as discussed in section 5.2. However, as these baryon masses suffer from a worse signal-to-noise ratio than the light mesonic decay constants, this is a trade-off that has to be investigated and a suitable candidate for scale setting with sufficient precision has to be found.
Especially the $I(J^P) = 0(3/2)^+$ Ω baryon is a popular candidate for setting the scale [44, 68, 69] as its isospin-breaking corrections are assumed to be very small (which we verify on individual ensembles in table 10.2) and therefore negligible to a higher precision. Furthermore, the computation of this baryon is especially cheap as it only involves strange-quarks which reduces the number of propagators to compute while remaining only the cheaper to compute propagators.

Chapter 5
QED and Isospin-Breaking Effects on the Lattice

Many lattice simulations, such as the ones used for this thesis, make use of an isospin-symmetric action, i.e. up and down quarks are mass-degenerate and of all known forces of the standard model, only the strong SU(3)-force is taken into account. As the weak nuclear force is – as its name suggests – very weak compared to the electromagnetic and strong nuclear force, it can safely be neglected at the current level of precision of hadronic observables in LQCD simulations. Electromagnetic corrections, however, are only suppressed by a factor of the fine structure constant $\alpha_{\mathrm{em}} \approx 0.7\,\%$. So-called *strong isospin-breaking* corrections stemming from the mass-difference of up and down quarks are known to also be of the order of $1\,\%$ of typical energy scales in QCD processes [6, 7]. Thus, one usually finds estimates of $1\,\%$ (depending on the observable) for the combined corrections from strong isospin-breaking and QED effects in the literature [70–72].

5.1. QED on the Lattice

Consider the continuum QED action

$$\mathcal{S}[A,\psi,\bar{\psi}] = \int \mathrm{d}^4x \left(\frac{1}{4} F_{\mu\nu}F^{\mu\nu} + \frac{1}{2\xi}(\partial_\mu A^\mu)^2 + \bar{\psi}(\gamma^\mu \partial_\mu + ie\gamma^\mu A_\mu + m)\psi \right) \tag{5.1}$$

in a periodic box of lengths $\mathcal{L}_\mu$, $\mu \in \{0,1,2,3\}$ with a fermionic field ψ and a photon field A and field strength tensor $F_{\mu\nu} = (\partial_\mu A_\nu - \partial_\nu A_\mu)$. The term $\frac{1}{2\xi}(\partial_\mu A^\mu)^2$ introduces a gauge fixing condition with $\xi = 0$ corresponding to Landau gauge and $\xi = 1$ corresponding to Feynman gauge [17]. Without the gauge fixing term, the above action is invariant under the abelian version of the gauge transformation[1] (see eq. (2.8))

$$\begin{aligned} \psi(x) &\mapsto e^{ie\alpha(x)}\psi(x), \\ \bar{\psi}(x) &\mapsto \bar{\psi}(x)e^{-ie\alpha(x)} \\ A_\mu(x) &\mapsto A_\mu(x) - \partial_\mu \alpha(x). \end{aligned}$$

[1] Note that the gauge fixing term breaks gauge invariance that the expectation value of gauge invariant observables is independent of the choice of ξ [17].

Moreover, due to the periodicity constraint that sets $A_\mu(x) = A_\mu(x + n^\nu \mathcal{L}_\nu)$ for $n \in \mathbb{Z}^4$, there are additional *large gauge transformations* [73]

$$\begin{aligned} A_\mu(x) &\mapsto A_\mu(x) - \frac{2\pi}{e}\left(\frac{n}{\mathcal{L}}\right)_\mu, \\ \psi(x) &\mapsto e^{2\pi i(\mathcal{L}^{-1}n)^\mu x_\mu}\psi(x), \\ \bar{\psi}(x) &\mapsto e^{-2\pi i(\mathcal{L}^{-1}n)^\mu x_\mu}\psi(x). \end{aligned} \tag{5.2}$$

Since these large transformations are not continuously connected to the identity, they are not eliminated by any local gauge fixing procedure [73]. This poses a problem for electrically charged state in such a setup as the propagator of ψ transforms non-trivially under these gauge transformations

$$\left\langle \psi(x)\bar{\psi}(y)\right\rangle \mapsto e^{2\pi i(\mathcal{L}^{-1}n)^\mu (x_\mu - y_\mu)} \left\langle \psi(x)\bar{\psi}(y)\right\rangle$$

and is only invariant for $x = y$. Thus, since eq. (5.2) is a symmetry of the model, the propagator can only be non-zero on the spacetime-diagonal; in other words, an electrically charged fermion cannot propagate in this model. More generally, any observable that does not transform trivially under large gauge transformations has to vanish.
While the above discussion is valid in the continuum, we will continue with a lattice discussion of solutions to the stated problem. However, although it would be possible to treat the photon field with gauge links as we do with QCD, we instead treat QED perturbatively using Lie-algebra valued photons.

5.1.1. Prescriptions

In order to circumvent the above problem of large gauge transformations, several different prescriptions have been proposed and used, for example $\mathrm{QED_m}$ [74], which uses massive photons or $\mathrm{QED_C}$ [75, 76], which imposes boundary conditions of the form $\psi(x + \mathcal{L}\hat{\mu}) = C^{-1}\bar{\psi}^T(x)$ [73]. In the following, we discuss two such prescriptions, which relate to the computations performed for this thesis.

$\mathbf{QED_{TL}}$

The $\mathrm{QED_{TL}}$ prescription [77] avoids large gauge transformations by explicitly setting the zero-momentum-modes of the photon to zero, i.e. the momentum-space photon field $\tilde{A}_\mu(p)$ is restricted to $\tilde{A}_\mu(0) = 0$. To make sense of this restriction, note that the large gauge transformations in eq. (5.2) take the form

$$\begin{aligned} \tilde{A}_\mu(p) &\to \tilde{A}_\mu(p) - \frac{2\pi}{e}\left(\frac{n}{\mathcal{L}}\right)_\mu \sqrt{|\Lambda|}\delta^{(4)}_{p0}, \\ \tilde{\psi}(p_\mu) &\to \tilde{\psi}\left(p_\mu + 2\pi\left(\frac{n}{\mathcal{L}}\right)_\mu\right), \\ \tilde{\bar{\psi}}(p_\mu) &\to \tilde{\bar{\psi}}\left(p_\mu - 2\pi\left(\frac{n}{\mathcal{L}}\right)_\mu\right). \end{aligned} \tag{5.3}$$

The large gauge transformations only contribute to the zero-momentum-mode of the photon field and thus have to vanish when requiring $\tilde{A}_\mu(0) = 0$. However, this prescription does not define a local QFT [73]. Moreover, the effective mass of a charged particle (see section 7.4 for an explanation) diverges in

the limit of infinite time extent [73, 78]. For example, the correlation function $C(t) = \frac{1}{2}\,\mathrm{tr}\big[\frac{1+\gamma_0}{2}\big]\frac{1}{\Lambda}\sum_{x\in\Lambda}\big\langle\psi(t,\mathbf{x})\bar{\psi}(0)\big\rangle_{\mathrm{TL}}{}^2$ on a box with lengths $\mathcal{L} = (T, L, L, L)$ has leading terms of [73]

$$m_{\mathrm{eff}}(t) = -\frac{\mathrm{d}}{\mathrm{d}t}\ln C(t) \approx m + \frac{e^2 T}{16mL^3} + \mathcal{O}\big(e^2T^0\big) + \mathcal{O}\big(e^4\big)$$

for large enough t, where m is the mass of the charged particle. This divergence in the $T \to \infty$ limit implies that if a Hamiltonian exists for $\mathrm{QED}_{\mathrm{TL}}$ it cannot have a regular expansion [73].

$\mathbf{QED_L}$

$\mathrm{QED}_{\mathrm{L}}$ [79] differs from $\mathrm{QED}_{\mathrm{TL}}$ in that only the spatial zero-modes of the photon are set to zero, i.e. $\sum_{x\in\Lambda_3} A_\mu(x) \equiv 0$. This defines a local QFT in time (but not in space) that thus does have a Hamiltonian and thus also a transfer matrix and avoids the divergence in the $T \to \infty$ limit discussed in the $\mathrm{QED}_{\mathrm{TL}}$ paragraph. While this prescription solves the problems discussed above, a calculation with similar constraints to a scalar field in ϕ^4 theory indicates that operators with mass-dimension higher than 4 might not be renormalizable [73] making it impossible to apply Symanzik improvement to $\mathrm{QED}_{\mathrm{L}}$. However, this calculation cannot be trivially adapted to the $\mathrm{QED}_{\mathrm{L}}$ case and it is thus unclear if this is a problem or if it might only appear in higher orders of perturbation theory [73].

In this thesis, we use the $\mathrm{QED}_{\mathrm{L}}$ prescription to compute QED corrections to hadronic masses using a perturbative approach described in the following section.

5.2. Isospin-Breaking Effects

The method to introduce isospin-breaking effects in this project was introduced by the *RM123* collaboration [10, 11], in which electromagnetic and strong isospin-breaking corrections are treated perturbatively. More precisely, the action S of full QCD+QED which is a functional of the lattice gauge links U, the photon field A and the different quark fields ψ,

$$S[U, A, \psi, \bar{\psi}] = S_g[U] + S_\gamma[A] + S_q[U, A, \psi, \bar{\psi}], \tag{5.4}$$

is expanded around its isospin-symmetric counterpart

$$S^{(0)}[U, \psi, \bar{\psi}] = S_g^{(0)}[U] + S_q^{(0)}[U, \psi, \bar{\psi}]. \tag{5.5}$$

Here, S_g is the QCD gauge action, e.g. eq. (4.7), S_γ is the QED gauge action and S_q is the quark action as in eq. (4.8) with non-degenerate quarks, while the actions with superscript (0) have isospin-symmetric parameters and miss the photon field.
In order to derive the perturbative expansion expressing observables in S in terms of observables in $S^{(0)}$, we first need to establish a relation between the

[2] The expectation value of an operator $\mathcal{O}$ in the $\mathrm{QED}_{\mathrm{TL}}$ prescription is defined via [73]

$$\big\langle\mathcal{O}[A,\psi,\bar{\psi}]\big\rangle_{\mathrm{TL}} = \frac{1}{Z_{\mathrm{TL}}}\int \mathcal{D}A\mathcal{D}\psi\mathcal{D}\bar{\psi}\,\delta^{(4)}\Big(\sum_{x\in\Lambda} A(x)\Big)\mathcal{O}[A,\psi,\bar{\psi}]e^{-S[A,\psi,\bar{\psi}]}.$$

two theories. To this end, consider the expectation value of an observable $\mathcal{O}$ in QCD+QED:

$$\begin{aligned}\langle\mathcal{O}\rangle_S &= \frac{1}{Z}\int \mathcal{D}U\mathcal{D}A\mathcal{D}\psi\mathcal{D}\bar{\psi}\,\mathcal{O}[U,A,\psi,\bar{\psi}]e^{-S[U,A,\psi,\bar{\psi}]} \\ &= \frac{1}{Z}\int \mathcal{D}U\left(\frac{1}{Z_{q\gamma}[U]}\int \mathcal{D}A\mathcal{D}\psi\mathcal{D}\bar{\psi}\,\mathcal{O}[U,A,\psi,\bar{\psi}]e^{-S_\gamma[A]-S_q[U,A,\psi,\bar{\psi}]}\right) \\ &\qquad \cdot Z_{q\gamma}[U]e^{-S_g[U]}.\end{aligned} \tag{5.6}$$

The expression in brackets can be interpreted as an expectation value

$$\begin{aligned}\langle\mathcal{O}\rangle_{S_{q\gamma}}[U] &= \frac{1}{Z_{q\gamma}[U]}\int \mathcal{D}A\mathcal{D}\psi\mathcal{D}\bar{\psi}\,\mathcal{O}[U,A,\psi,\bar{\psi}]e^{-S_{q\gamma}[U]} \\ Z_{q\gamma}[U] &= \int \mathcal{D}A\mathcal{D}\psi\mathcal{D}\bar{\psi}\,e^{-S_{q\gamma}[U]}\end{aligned}$$

w.r.t. a QED action $S_{q\gamma}[U,A,\psi,\bar{\psi}] = S_\gamma[A] + S_q[U,A,\psi,\bar{\psi}]$ on a background SU(3) gauge field U. As in eqs. (4.4) and (4.5), we can then define an effective QCD+QED action $S_{\text{eff}}[U] \coloneqq S_g[U] - \log Z_{q\gamma}[U]$[3] to rewrite the expectation value (5.6) in QCD+QED as

$$\langle\mathcal{O}\rangle_S = \frac{1}{Z}\int \mathcal{D}U\,\langle\mathcal{O}\rangle_{S_{q\gamma}}[U]e^{-S_{\text{eff}}[U]} = \left\langle\langle\mathcal{O}\rangle_{S_{q\gamma}}\right\rangle_{S_{\text{eff}}}. \tag{5.7}$$

Note, that the inner expectation value $\langle\mathcal{O}\rangle_{S_{q\gamma}}$ is perturbatively computed in QED using the free photon propagator and Feynman rules to order α_{em} (see section 5.3).
Using the expression (5.7) and an isospin-symmetric version of the effective action $S^{(0)}_{\text{eff}}$ defined via $S^{(0)}_{\text{eff}}[U] \coloneqq S^{(0)}_g[U] - \log Z^{(0)}_q[U]$, one can express the expectation value in full QCD+QED in terms of isospin-symmetric QCD via reweighting [11, 13, 80] as

$$\begin{aligned}\langle\mathcal{O}\rangle_S &= \frac{\frac{1}{Z^{(0)}_{\text{eff}}}\int \mathcal{D}U\,\langle\mathcal{O}\rangle_{S_{q\gamma}}[U]\frac{\exp(-S_{\text{eff}}[U])}{\exp\left(-S^{(0)}_{\text{eff}}[U]\right)}e^{-S^{(0)}_{\text{eff}}[U]}}{\frac{1}{Z^{(0)}_{\text{eff}}}\int \mathcal{D}U\,\frac{\exp(-S_{\text{eff}}[U])}{\exp\left(-S^{(0)}_{\text{eff}}[U]\right)}e^{-S^{(0)}_{\text{eff}}[U]}} \\ &= \frac{\left\langle R\,\langle\mathcal{O}\rangle_{S_{q\gamma}}\right\rangle_{S^{(0)}_{\text{eff}}}}{\langle R\rangle_{S^{(0)}_{\text{eff}}}}, \\ R[U] &= \exp\left(S^{(0)}_{\text{eff}}[U] - S_{\text{eff}}[U]\right) = \frac{Z_{q\gamma}[U]e^{-S_g[U]}}{Z^{(0)}_q[U]e^{-S^{(0)}_g[U]}}.\end{aligned} \tag{5.8}$$

See section 6.2 for an explanation of the concept. The ratio of exponentials $\frac{e^{-S_g[U]}}{e^{-S^{(0)}_g[U]}}$ reflects the change in the strong gauge coupling from $\beta^{(0)}$ to β, while the ratio of the partition functions $Z_{q\gamma}$ and $Z^{(0)}_g$ accounts for the inclusion of QED and the change of the quark masses.

[3] This definition is equivalent to the expression in eq. (5.6) as $Z_{q\gamma}$ and S_g yield a scalar value when applied to a field configuration U and thus, the two summands commute and the exponential function of their sum is the same as a product of the exponential function of each summand. For the same reason, the gluon-action can be separated from the rest of the action in eq. (5.6).

Equation (5.8) provides a connection between expectation values between the two actions which we can now perturbatively expand around the isospin-symmetric action. To do so, we determine the sets of parameters ε and $\varepsilon^{(0)}$ characterizing both actions so we can treat their difference as expansion parameters:

ε	$\varepsilon^{(0)}$	Meaning
β	$\beta^{(0)}$	The inverse (quadratic) strong gauge coupling
e^2	0	The electromagnetic gauge coupling
m_u	m_{ud}	The up-/light-quark mass
m_d	m_{ud}	The down-/light-quark mass
m_s	$m_s^{(0)}$	The strange-quark mass

The expansion is then performed in terms of

$$\begin{aligned}\Delta\varepsilon =&(\Delta\beta, e^2, \Delta m_u, \Delta m_d, \Delta m_s)\\ =&(\beta-\beta^{(0)}, e^2, m_u - m_{ud}, m_d - m_{ud}, m_s - m_s^{(0)}).\end{aligned}$$

Note that the value of $e^2 = 4\pi\alpha_{\text{em}}$ can be taken as the continuum-value as long as the expansion is only performed up to leading order in α_{em} since the running of the electromagnetic coupling comes from its self-energy corrections which first enter at next-to-leading order.
Expanding eq. (5.8) in terms of $\Delta\varepsilon$, we find

$$\begin{aligned}\langle\mathcal{O}\rangle_S &= \langle\mathcal{O}\rangle_{S^{(0)}} + \sum_i \frac{\partial\langle\mathcal{O}\rangle_S}{\partial\Delta\varepsilon_i}\bigg|_{\Delta\varepsilon=0}\Delta\varepsilon_i + \mathcal{O}(\Delta\varepsilon^2)\\ &= \langle\mathcal{O}\rangle_{S^{(0)}} + \sum_i \frac{\partial\langle\mathcal{O}\rangle_S}{\partial\varepsilon_i}\bigg|_{\varepsilon=\varepsilon^{(0)}}\Delta\varepsilon_i + \mathcal{O}(\Delta\varepsilon^2)\end{aligned} \tag{5.9}$$

where

$$\begin{aligned}\frac{\partial\langle\mathcal{O}\rangle_S}{\partial\varepsilon_i}\bigg|_{\varepsilon=\varepsilon^{(0)}} =& \frac{\partial}{\partial\varepsilon_i}\frac{\left\langle R\langle\mathcal{O}\rangle_{S_{q\gamma}}\right\rangle_{S_{\text{eff}}^{(0)}}}{\langle R\rangle_{S_{\text{eff}}^{(0)}}}\bigg|_{\varepsilon=\varepsilon^{(0)}}\\ =& \left\langle\frac{\partial\langle\mathcal{O}\rangle_{S_{q\gamma}}}{\partial\varepsilon_i}\bigg|_{\varepsilon=\varepsilon^{(0)}}\right\rangle_{S_{\text{eff}}^{(0)}} - \left\langle\langle\mathcal{O}\rangle_q\frac{\partial S_{\text{eff}}}{\partial\varepsilon_i}\bigg|_{\varepsilon=\varepsilon^{(0)}}\right\rangle_{S_{\text{eff}}^{(0)}}\\ &+ \langle\mathcal{O}\rangle_{S^{(0)}}\left\langle\frac{\partial S_{\text{eff}}}{\partial\varepsilon_i}\bigg|_{\varepsilon=\varepsilon^{(0)}}\right\rangle_{S_{\text{eff}}^{(0)}}\end{aligned} \tag{5.10}$$

which uses the relations $R|_{\varepsilon=\varepsilon^{(0)}} = 1$ and $\frac{\partial R}{\partial\varepsilon_i} = -\frac{\partial S_{\text{eff}}}{\partial\varepsilon_i}R$.
With the exception of β all derivatives of the effective action can be written as

$$\frac{\partial S_{\text{eff}}}{\partial\varepsilon_i} = -\frac{1}{Z_{q\gamma}}\frac{\partial Z_{q\gamma}}{\partial\varepsilon_i} = \left\langle\frac{\partial S_{q\gamma}}{\partial\varepsilon_i}\right\rangle_{S_{q\gamma}}$$

as only the gluon action depends on β. For the derivative w.r.t β, one finds

$$\frac{\partial S_{\text{eff}}}{\partial\beta} = \frac{\partial S_g}{\partial\beta}.$$

For electromagnetic corrections, it is important to note that, while these corrections are functions of e^2, electromagnetic effects appear at $\mathcal{O}(e)$ in the form

of bremsstrahlung. While these $\mathcal{O}(e)$ effects do not contribute to the mass of a bound state directly, they play a role when one quark emits a photon which is absorbed by another quark, which is an $\mathcal{O}(e^2)$ process that has to be accounted for. In the case of these corrections, we thus have to replace first derivatives $\frac{\partial}{\partial(e^2)}\big|_{\varepsilon=\varepsilon^{(0)}}$ by second derivatives $\frac{1}{2}\frac{\partial^2}{\partial e^2}\big|_{\varepsilon=\varepsilon^{(0)}}$ w.r.t. e [11]. This, however, gets quite lengthy, so for more details refer to section B.2.

5.2.1. IB Corrections To Hadronic Two-Point-Functions

In the scope of this thesis, the main focus lies in the isospin-breaking effects in hadronic two-point-functions, more precisely, baryonic and pseudo-scalar mesonic two-point-functions. The details of these are explained in chapter 7. The important property of these correlation functions at this point is, that they can be written (and are computed as) linear combinations of products of quark propagator components[4]

$$C_{xy} = \left\langle \mathcal{O}_H(x)\overline{\mathcal{O}}_H(y)\right\rangle_S = \left\langle \sum_\alpha \lambda_\alpha \prod_{i=1}^{n_q} \mathcal{S}_{f_i}^{\alpha_i}(x,y)\right\rangle_{S_{\text{eff}}} \tag{5.11}$$

where α is to be understood as a multi-index specifying spin and color structure and $\lambda_\alpha \in \mathbb{C}$. $\mathcal{S}_{f_i}$ is a propagator of the i-th valence quark of the hadron described by $\mathcal{O}_H$ which has flavor f_i. This expression allows for a systematic expansion of correlation functions in terms of corrections to single propagators as per eq. (5.10):

$$\begin{aligned}\frac{\partial C_{xy}}{\partial \varepsilon_i}\bigg|_{\varepsilon=\varepsilon^{(0)}} = \sum_\alpha \lambda_\alpha \Bigg(&\left\langle \sum_{k=1}^{n_q} \frac{\partial \mathcal{S}_{f_k}^{\alpha_k}(x,y)}{\partial \varepsilon_i}\bigg|_{\varepsilon=\varepsilon^{(0)}} \prod_{\substack{j=1\\ j\neq k}}^{n_q} \mathcal{S}_{f_j}^{\alpha_j}(x,y)\right\rangle_{S_{\text{eff}}^{(0)}} \\ &- \left\langle \frac{\partial S_{\text{eff}}}{\partial \varepsilon_i}\bigg|_{\varepsilon=\varepsilon^{(0)}} \prod_{j=1}^{n_q} \mathcal{S}_{f_j}^{\alpha_i}(x,y)\right\rangle_{S_{\text{eff}}^{(0)}} \\ &+ \left\langle \prod_{i=j}^{n_q} \mathcal{S}_{f_j}^{\alpha_j}(x,y)\right\rangle_{S_{\text{eff}}^{(0)}} \left\langle \frac{\partial S_{\text{eff}}}{\partial \varepsilon_i}\bigg|_{\varepsilon=\varepsilon^{(0)}}\right\rangle_{S_{\text{eff}}^{(0)}} \Bigg).\end{aligned} \tag{5.12}$$

To express the derivatives of the propagators, we express them in terms of the Dirac-operator $D_f = {\mathcal{S}_f}^{-1}$ for which the derivative is known. Using matrix calculus, the relevant derivatives can be written as[5]

$$\frac{\partial \mathcal{S}_f(x,y)}{\partial \varepsilon_i} = -\sum_{z,z'\in\Lambda} \mathcal{S}_f(x,z)\frac{\partial D_f(z,z')}{\partial \varepsilon_i}\mathcal{S}_f(z',y). \tag{5.13}$$

[4] In our calculations, we use *smeared sources* (see sections 7.2.2 and 7.2.3) such that the operators $\mathcal{O}_H$ are not located exactly at positions x and y but are smeared out in a certain (spatial) volume around these positions. In that case, the $\mathcal{S}_{f_i}$ are not specific components of the quark propagators.

[5] This identity can be easily seen by applying the product rule $\frac{\partial}{\partial x}(AB) = \frac{\partial A}{\partial x}B + A\frac{\partial B}{\partial x}$ to ${A^{-1}}A$:

$$0 = \frac{\partial \mathbb{1}}{\partial x} = \frac{\partial {A^{-1}}A}{\partial x} = \frac{\partial {A^{-1}}}{\partial x}A + {A^{-1}}\frac{\partial A}{\partial x} \quad \Rightarrow \quad \frac{\partial {A^{-1}}}{\partial x} = -{A^{-1}}\frac{\partial A}{\partial x}{A^{-1}}$$

This describes a so-called *sequential propagator* with an operator insertion. For Wilson-fermions (see sections 3.3 and 4.1, eqs. (3.17), (4.2) and (4.8)), the derivative with respect to the mass of flavor f is given by

$$\frac{\partial \mathcal{S}_f(x,y)}{\partial m_f} = -\sum_{z,z'\in\Lambda} \mathcal{S}_f(x,z)\delta_{zz'}\mathcal{S}_f(z',y) = -\sum_{z\in\Lambda} \mathcal{S}_f(x,z)\mathcal{S}_f(z,y). \tag{5.14}$$

Diagrammatically, this is expressed as a propagator with a vertex indicating the *operator insertion* given by the derivative of D_f:

$$\frac{\partial \mathcal{S}_f}{\partial m_f} = \tag{5.15}$$

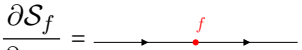

For electromagnetic corrections, we need to expand to second order in e so that instead we find

$$\begin{aligned}\frac{1}{2}\frac{\partial^2 \mathcal{S}_f}{\partial e^2}\bigg|_{\varepsilon=\varepsilon^{(0)}} =& \mathcal{S}_f \frac{\partial D_f}{\partial e}\mathcal{S}_f \frac{\partial D_f}{\partial e}\mathcal{S}_f - \frac{1}{2}\mathcal{S}_f \frac{\partial^2 D_f}{\partial e^2}\mathcal{S}_f \\ =& \end{aligned} \tag{5.16}$$

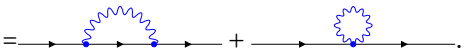

Furthermore, the second derivative of C_{xy} yields additional terms of the form

$$\begin{aligned}&\left\langle \sum_\alpha \lambda_\alpha \sum_{\substack{k,l=1\\k\neq l}}^{n_q} \frac{\partial \mathcal{S}_{f_k}^{\alpha_k}}{\partial e}\bigg|_{e=0} \frac{\partial \mathcal{S}_{f_l}^{\alpha_l}}{\partial e}\bigg|_{e=0} \prod_{\substack{j=1\\j\neq k,l}}^{n_q} \mathcal{S}_{f_j}^{\alpha_j} \right\rangle_{S_{\text{eff}}^{(0)}} \\ =& \left\langle \sum_\alpha \lambda_\alpha \sum_{\substack{k,l=1\\k\neq l}} \left(\mathcal{S}_{f_k}\frac{\partial D_{f_k}}{\partial e}\bigg|_{\varepsilon=\varepsilon^{(0)}}\mathcal{S}_{f_k}\right)^{\alpha_k}\left(\mathcal{S}_{f_l}\frac{\partial D_{f_l}}{\partial e}\bigg|_{\varepsilon=\varepsilon^{(0)}}\mathcal{S}_{f_l}\right)^{\alpha_l} \prod_{\substack{j=1\\j\neq k,l}}^{n_q} \mathcal{S}_{f_j}^{\alpha_j} \right\rangle_{S_{\text{eff}}^{(0)}}\end{aligned}$$

corresponding to the exchange of a photon between different valence quarks. For baryon two-point functions (see section 7.3), these contributions to the expansion can diagrammatically be expressed as follows:

$$\left\langle \overline{B} \; B \right\rangle_S = \tag{5.17}$$

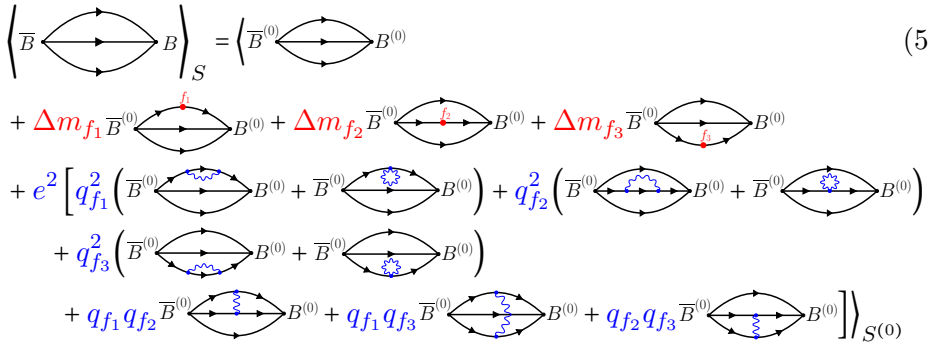

Here, $q_{f_i}e$ is the electric charge of the i-th quark counted from top to bottom of the diagram; Δm_{f_i} is its difference in mass between QCD_{iso} and QCD+QED. The Bs in these diagrams is meant to encode the colour-, spin-, and flavor-structure of the baryons as well as a smearing kernel $B(\mathbf{x},\mathbf{x}')$ (see section 7.2.2) such that the source operator in eq. (5.11) can be written as

$$\begin{aligned}\mathcal{O}_H(x) =& B(x)q_1q_2q_3 \\ =& \sum_{\substack{a,b,c\in\{r,g,b\}\\ f_i\in\{u,d,s\}\\ \mu_j\in\{0,\dots,3\}\\ \mathbf{x}'\in\Lambda_S}} \varepsilon_{abc} B_{f_1f_2f_3}^{\mu_1\mu_2\mu_3}(\mathbf{x},\mathbf{x}') q_{\mu_1}^{f_1,a}(x') q_{\mu_2}^{f_2,b}(x') q_{\mu_3}^{f_3,c}(x')\end{aligned}$$

where $x = (t, \mathbf{x}^T)^T$ and $x' = (t, \mathbf{x}'^T)^T$.
Note, that the terms discussed so far only come from the first term in eq. (5.10) (or its counterpart eq. (B.3) for electromagnetic corrections). The other terms in this expansion, with derivatives of the effective action, are corrections in the sea-quark sector shown in eq. (5.18). An expansion similar to eqs. (5.17) and (5.18) has to be performed for any observable for which isospin-breaking corrections are to be computed. We thus also perform an expansion analogous to eq. (5.17) for mesonic two-point correlation functions.

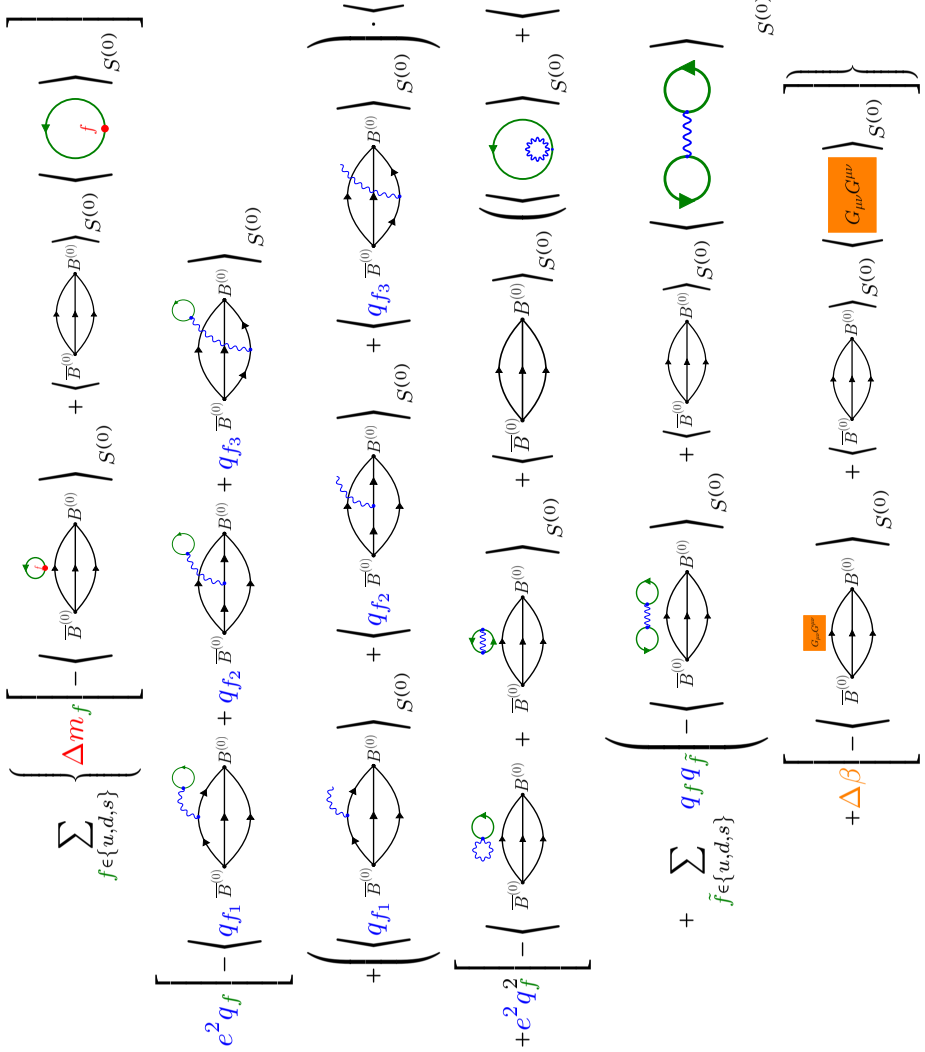

(5.18)

5.3. Implementation of $\mathrm{QED_L}$

This section is based on the thesis of Andreas Risch [81] whose implementation was used for the computation of QED corrections to hadronic observables detailed in part II.
To describe photons in $\mathrm{QED_L}$, a photon action can be defined using a difference operator Δ via [13, 80, 81]

$$\begin{aligned} S_\gamma[A] =& \frac{1}{2}\sum_{x\in\Lambda} A_\mu(x)\Delta^\mu{}_\nu A^\nu(x) \\ =& \frac{1}{2}\sum_{x\in\Lambda}\left([\partial_{+,\mu}A_\nu(x)][\partial_+^\mu A^\nu(x)] - [\partial_{+,\mu}A_\nu(x)][\partial_+^\nu A^\mu(x)]\right) + S_{\gamma\mathrm{gf}}[A] \end{aligned}$$

where ∂_+ is the forward derivative (see section 3.3.2) and $S_{\gamma\mathrm{gf}}$ is a gauge fixing term depending on the gauge fixing condition. For our computation, we use $\mathrm{QED_L}$ in Coulomb gauge which ensures the existence of a transfer matrix [78]. The Coulomb gauge is defined via the condition $\sum_{i=1}^3 \partial_-^i A_i = 0$ where ∂_- is the backward lattice derivative. To achieve this condition, a generalized Coulomb gauge is introduced via the gauge fixing term [13, 81]

$$S_{\gamma\mathrm{gf}}^\xi[A] = \frac{1}{2\xi}\sum_{x\in\Lambda}\left(\sum_{i=1}^3\left(\partial_-^i A_i(x)\right)\right)^2 = \frac{1}{2\xi}\sum_{x\in\Lambda}\sum_{i,j=1}^3 (\partial_{+,i}A_j(x))\left(\partial_+^j A^i(x)\right).$$

whose limit $\xi \to 0$ enforces the Coulomb gauge condition in the path integral in the form of a Dirac distribution. The difference operator for the generalized Coulomb gauge can then be written as [81]

$$\begin{aligned} \Delta^\mu{}_\nu =& \begin{pmatrix} \sum_{i=1}^3 \overleftarrow{\partial}_+^i \overrightarrow{\partial}_{+,i} & -\overleftarrow{\partial}_+^1 \overrightarrow{\partial}_{+,0} & -\overleftarrow{\partial}_+^2 \overrightarrow{\partial}_{+,0} & -\overleftarrow{\partial}_+^3 \overrightarrow{\partial}_{+,0} \\ -\overleftarrow{\partial}_+^0 \overrightarrow{\partial}_{+,1} & \sum_{\rho=0}^3 \overleftarrow{\partial}_+^\rho \overrightarrow{\partial}_{+,\rho} & 0 & 0 \\ -\overleftarrow{\partial}_+^0 \overrightarrow{\partial}_{+,2} & 0 & \sum_{\rho=0}^3 \overleftarrow{\partial}_+^\rho \overrightarrow{\partial}_{+,\rho} & 0 \\ -\overleftarrow{\partial}_+^0 \overrightarrow{\partial}_{+,3} & 0 & 0 & \sum_{\rho=0}^3 \overleftarrow{\partial}_+^\rho \overrightarrow{\partial}_{+,\rho} \end{pmatrix}^\mu_{\ \nu} \\ &+ \left(\frac{1}{\xi}-1\right)\begin{pmatrix} 0 & 0 & 0 & 0 \\ 0 & \overleftarrow{\partial}_+^1 \overrightarrow{\partial}_{+,1} & \overleftarrow{\partial}_+^2 \overrightarrow{\partial}_{+,1} & \overleftarrow{\partial}_+^3 \overrightarrow{\partial}_{+,1} \\ 0 & \overleftarrow{\partial}_+^1 \overrightarrow{\partial}_{+,2} & \overleftarrow{\partial}_+^2 \overrightarrow{\partial}_{+,2} & \overleftarrow{\partial}_+^3 \overrightarrow{\partial}_{+,2} \\ 0 & \overleftarrow{\partial}_+^1 \overrightarrow{\partial}_{+,3} & \overleftarrow{\partial}_+^2 \overrightarrow{\partial}_{+,3} & \overleftarrow{\partial}_+^3 \overrightarrow{\partial}_{+,3} \end{pmatrix}^\mu_{\ \nu}. \end{aligned}$$

where $\overleftarrow{\partial}$ acts on the field to the left of Δ and $\overrightarrow{\partial} = \partial$ acts on the field to the right. Another gauge condition we utilize to test our implementation for hadronic two-point functions (see section 8.1.4) is Feynman gauge which is defined via the gauge fixing term [81]

$$S_{\gamma\mathrm{gf}}^{\mathrm{Feynman}}[A] = \sum_{x\in\Lambda}\left(\sum_{i=1}^3\left(\partial_-^i A_i(x)\right)\right)^2 = \sum_{x\in\Lambda}\sum_{\mu,\nu=0}^3 (\partial_{+,\mu}A_\nu(x))(\partial_+^\nu A^\mu(x)).$$

This gauge is conceptionally simpler as the difference operator takes on the diagonal form

$$\Delta^\mu{}_\nu = \left(\sum_{\rho=0}^3 \overleftarrow{\partial}_+^\rho \overrightarrow{\partial}_{+,\rho}\right)\delta^\mu{}_\nu.$$

The photon propagator, which is given by the inverse of the difference operator, can be computed in momentum space and then translated back to its space-time representation via the discrete Fourier transform. At this stage a distinction has to be made between ensembles with periodic and open temporal boundary conditions:

Periodic BC Using the Fourier transform of the first-order difference operators $\partial_\pm$

$$p_+^\mu = -\frac{i}{a}(\exp(iap^\mu) - 1) \quad \text{and} \quad p_-^\mu = -\frac{i}{a}(1 - \exp(-iap^\mu))$$

the difference operators take the form

$$\tilde{\Delta}(p)^\mu{}_\nu = \begin{pmatrix} \sum_{i=1}^3 p_-^i p_{+,i} & -p_-^1 p_{+,0} & -p_-^2 p_{+,0} & -p_-^3 p_{+,0} \\ -p_-^0 p_{+,1} & \sum_{\rho=0}^3 p_-^\rho p_{+,\rho} & 0 & 0 \\ -p_-^0 p_{+,2} & 0 & \sum_{\rho=0}^3 p_-^\rho p_{+,\rho} & 0 \\ -p_-^0 p_{+,3} & 0 & 0 & \sum_{\rho=0}^3 p_-^\rho p_{+,\rho} \end{pmatrix}^\mu{}_\nu + \left(\frac{1}{\xi} - 1\right) \begin{pmatrix} 0 & 0 & 0 & 0 \\ 0 & p_-^1 p_{+,1} & p_-^2 p_{+,1} & p_-^3 p_{+,1} \\ 0 & p_-^1 p_{+,2} & p_-^2 p_{+,2} & p_-^3 p_{+,2} \\ 0 & p_-^1 p_{+,3} & p_-^2 p_{+,3} & p_-^3 p_{+,3} \end{pmatrix}^\mu{}_\nu .$$

in generalized Coulomb gauge and

$$\tilde{\Delta}(p)^\mu{}_\nu = \sum_{\rho=0}^3 p^\rho p_\rho \delta^\mu{}_\nu$$

in Feynman gauge [81]. These can be inverted in a straight-forward manner leading to the momentum-space propagators

$$\tilde{\Sigma}(p)^\mu{}_\nu = \frac{1}{\left(\sum_{\rho=0}^3 p_-^\rho p_{+,\rho}\right)\left(\sum_{i=1}^3 p_-^i p_{+,i}\right)} \cdot \begin{pmatrix} \sum_{\sigma=0}^3 p_-^\sigma p_{+,\sigma} & 0 & 0 & 0 \\ 0 & p_-^2 p_{+,2} + p_-^3 p_{+,3} & -p_-^2 p_{+,1} & -p_-^3 p_{+,1} \\ 0 & -p_-^1 p_{+,2} & p_-^1 p_{+,1} + p_-^3 p_{+,3} & -p_-^3 p_{+,2} \\ 0 & -p_-^1 p_{+,3} & -p_-^2 p_{+,3} & p_-^1 p_{+,1} + p_-^2 p_{+,2} \end{pmatrix}^\mu{}_\nu$$

in Coulomb gauge [81] (i.e. in the limit $\xi \to 0$) and

$$\tilde{\Sigma}(p)^\mu{}_\nu = \frac{\delta^\mu{}_\nu}{\sum_{\rho=0}^3 p_-^\rho p_{+,\rho}}$$

in Feynman gauge [81].

Open BC CLS ensembles always have periodic boundary conditions in the spatial directions and we thus only treat the temporal direction distinctly for open boundary ensembles. In momentum space, the Fourier transform of the first-order difference operators

$$p_+^k = -\frac{i}{a}\left(\exp\left(iap^k\right) - 1\right) \quad \text{and} \quad p_-^k = -\frac{i}{a}\left(1 - \exp\left(-iap^k\right)\right)$$

is therefore used for the spatial components as for periodic boundary conditions. For the temporal component, however, modified discrete sine- and cosine-transforms are used instead, defining

$$p^0_{+,SC} = \frac{2i}{a}\sin\left(\frac{ap^0}{2}\right) \quad \text{and} \quad p^0_{-,CS} = -\frac{2i}{a}\sin\left(\frac{ap^0}{2}\right).$$

The difference operators and propagators then take on the form [81]

$$\begin{aligned}\hat{\Delta}(p)^\mu{}_\nu =& \left(p^0_{-,CS}p^0_{+,SC} + \sum_{i=1}^3 p^i_- p_{+,i}\right)\delta^\mu{}_\nu,\\ \hat{\Sigma}(p)^\mu{}_\nu =& \frac{\delta^\mu{}_\nu}{p^0_{-,CS}p^0_{+,SC} + \sum_{i=1}^3 p^i_- p_{+,i}}\end{aligned}$$

in Feynman gauge where $\hat{\cdot}$ indicates that the quantity in question is a mix of sine-cosine-transform and Fourier transform of its spacetime analog. For (generalized) Coulomb gauge, the quantities take the form [13, 81]

$$\begin{aligned}\hat{\Delta}(p)^\mu{}_\nu =& \begin{pmatrix} \sum_{i=1}^3 p^i_- p_{+,i} & -p^1_- p^0_{+,SC} & -p^2_- p^0_{+,SC} & -p^3_- p^0_{+,SC} \\ -p^0_{+,SC}p_{+,1} & \mathcal{D}(p) & 0 & 0 \\ -p^0_{+,SC}p_{+,2} & 0 & \mathcal{D}(p) & 0 \\ -p^0_{+,SC}p_{+,3} & 0 & 0 & \mathcal{D}(p) \end{pmatrix}^\mu_\nu \\ &+ \left(\frac{1}{\xi} - 1\right)\begin{pmatrix} 0 & 0 & 0 & 0 \\ 0 & p^1_- p_{+,1} & p^2_- p_{+,1} & p^3_- p_{+,1} \\ 0 & p^1_- p_{+,2} & p^2_- p_{+,2} & p^3_- p_{+,2} \\ 0 & p^1_- p_{+,3} & p^2_- p_{+,3} & p^3_- p_{+,3} \end{pmatrix}^\mu_\nu, \\ \hat{\Sigma}(p)^\mu{}_\nu =& \frac{1}{\mathcal{D}(p)\left(\sum_{i\neq 1}^3 p^i_- p_{+,i}\right)} \\ &\cdot \begin{pmatrix} \sum_{\sigma=0}^3 p^\sigma_- p_{+,\sigma} & 0 & 0 & 0 \\ 0 & p^2_- p_{+,2} + p^3_- p_{+,3} & -p^2_- p_{+,1} & -p^3_- p_{+,1} \\ 0 & -p^1_- p_{+,2} & p^1_- p_{+,1} + p^3_- p_{+,3} & -p^3_- p_{+,2} \\ 0 & -p^1_- p_{+,3} & -p^2_- p_{+,3} & p^1_- p_{+,1} + p^2_- p_{+,2} \end{pmatrix}^\mu_\nu\end{aligned}$$

where $\mathcal{D}(p) = p^0_{-,CS}p^0_{+,SC} + \sum_{i=1}^3 p^i_- p_{+,i}$ and for $\hat{\Sigma}$ the limit $\xi \to 0$ is already taken.

For a more in-depth discussion and derivation of these results, we refer to [81]. As we use the $\mathrm{QED_L}$ prescription, only momenta $p^\mu = (p^0, \mathbf{p})$ with non-vanishing spatial momenta, the support of $\tilde{\Sigma}$ and $\hat{\Sigma}$ is

$$\mathrm{supp}(\tilde{\Sigma}) = \mathrm{supp}(\hat{\Sigma}) = \left\{p \in \tilde{\Lambda} | p_i \neq 0, i \in \{1,2,3\}\right\}.$$

The divergence of the propagators at $p = 0$ is thus not present in this prescription.

While the difference operator defines the photon propagators (at leading order), the QED vertices in eq. (5.16) come from the modified Dirac operator $D_f[U, A]$ for a quark of flavor f, which takes the form of eq. (4.9) with the modification of the gauge links, which are replaced by

$$\begin{aligned}W_\mu(x) =& U_\mu(x)\exp(iaeQA_\mu(x)) \\ \approx& U_\mu(x)\left(\mathbb{1} + iaeQA_\mu(x) - \frac{1}{2}a^2Q^2e^2A_\mu(x)^2 + \mathcal{O}(e^3)\right)\end{aligned}$$

where $Q = \mathrm{diag}(q_u, q_d, q_s)$ is a charge matrix acting in flavor space. Note, that we use the Sheikholeslami-Wohlert term of isospin-symmetric QCD which means that our QCD+QED computation is not $\mathcal{O}(a)$ improved.
Plugging the expanded QCD+QED gauge links back into the Wilson-Dirac action (eqs. (4.3) and (4.8)), one can read off the following vertices [80, 81]:

$$
\begin{aligned}
V_{\bar{q}q\gamma}[U](x,y,z)_\mu =& \frac{\delta}{\delta A_\mu(z)} \frac{\partial D_f[U,A]}{\partial e}\Big|_{\varepsilon=\varepsilon^{(0)},A_\mu=0} \\
=& \frac{iq_f}{2}\Big((\gamma^\rho - \mathbb{1}_{\mathrm{Spin}})U_\sigma(x)\delta_{x,y-a\hat{\mu}}\delta_{xz}g_{\rho\mu}g^\sigma{}_\mu \\
&+(\mathbb{1}_{\mathrm{Spin}} + \gamma^\rho)U_\sigma^\dagger(x-a\hat{\mu})\delta_{x,y+a\hat{\mu}}\delta_{x-a\hat{\mu},z}g_{\rho\mu}g^\sigma{}_\mu\Big) \\
=& x \quad \overset{z}{\sim} \quad y, \\
V_{\bar{q}q\gamma\gamma}[U](x,y,z_1,z_2)_{\mu\nu} =& \frac{\delta^2}{\delta A_\mu(z_1)A_\nu(z_2)^2} \frac{\partial^2 D_f[U,A]}{\partial e^2}\Big|_{\varepsilon=\varepsilon^{(0)},A_\mu=A_\nu=0} \\
=& \frac{aq_f^2}{2}\Big((\mathbb{1}_{\mathrm{Spin}} - \gamma^\rho)U_\sigma(x)\delta_{x,y-a\hat{\mu}}\delta_{xz_1}\delta_{xz_2}\delta_{\mu\nu}g_{\rho\mu}g^\sigma{}_\mu \\
&+(\mathbb{1}_{\mathrm{Spin}}+\gamma^\rho)U_\sigma^\dagger(x-a\hat{\mu})\delta_{x,y+a\hat{\mu}}\delta_{x-a\hat{\mu},z_1}\delta_{x-a\hat{\mu},z_2}\delta_{\mu\nu}g_{\rho\mu}g^\sigma{}_\mu\Big) \\
=& x \quad \overset{z_1}{\sim}\overset{z_2}{\sim} \quad y.
\end{aligned}
\tag{5.19}
$$

We explain how we use the vertices and propagators discussed in this section for the computation of the diagrams in eqs. (5.17) and (5.18) in section 8.1.3.

Chapter 6
Statistical Methods

Although in LQCD it is theoretically possible to perform exact calculations of observables in the path integral formalism, it is computationally infeasible due to the large problem size. However, an observable $\mathcal{O}$ can be estimated stochastically from a probability distribution

$$P[\phi] = \frac{e^{-S[\phi]}}{\int \mathcal{D}\phi\, e^{-S[\phi]}} = \frac{1}{Z} e^{-S[\phi]}, \quad \langle \mathcal{O} \rangle = \int \mathcal{D}\phi\, \mathcal{O}[\phi] P[\phi] = \frac{\int \mathcal{D}\phi\, \mathcal{O}[\phi] e^{-S[\phi]}}{\int \mathcal{D}\phi\, e^{-S[\phi]}} \tag{6.1}$$

dictated by the action S in Euclidean spacetime.
In this chapter, we discuss the statistical methods we use for the computation of such expectation values and their uncertainties and techniques to improve the computational efficiency of these computations. Section 6.1 starts with a discussion of techniques used to sample from eq. (6.1) and to stochastically estimate expectation values. Section 6.2 continues with the reweighting technique already mentioned in chapters 4 and 5 transforming expectation values in one model to functions of those in another model with a similar action. In section 6.3 we describe resampling methods that we use for statistical error estimation followed by a discussion of the effects of autocorrelation in Markov chains in section 6.4. Section 6.5 describes the technique of all mode averaging used to reduce the computational cost of computing observables in LQCD as well as an improvement we use for a cheap estimate of QED corrections to hadronic two-point-functions. Finally, section 6.6 states the assumptions entering our maximum likelihood fits entering the analysis of our data in chapters 8 to 10.

6.1. Monte Carlo Methods

Consider a field (or set of fields) ϕ whose dynamics are described by the action $S[\phi]$. In a QFT setting in Euclidean spacetime, the state of the field(s) ϕ is governed by the probability density eq. (6.1). To avoid computing the involved integrals exactly, which has to be done once for the partition function $Z = \int \mathcal{D}\phi\, e^{-S[\phi]}$ and again for each observable $\mathcal{O}$ of interest, LQCD calculations make use of a technique called *importance sampling*. This technique involves sampling random field configurations ϕ_i, $i \in \{1, ..., N\}$ from the distribution $P[\phi]$ in eq. (6.1) from which the expectation value of an observable $\mathcal{O}$ can be estimated

via

$$\langle \mathcal{O} \rangle \approx \bar{\mathcal{O}} = \frac{1}{N} \sum_{i=1}^{N} \mathcal{O}[\phi_i].$$

However, as this is a stochastic estimate, it comes with an uncertainty, which is usually defined as the standard deviation of the distribution $\bar{\mathcal{O}}$ is drawn from. Depending on the method of sampling, the samples ϕ_i are usually not statistically independent such that the classical central limit theorem is not necessarily applicable. For samples drawn via the Metropolis-Hastings algorithm (see section 6.1.1) a variation of which are used for the generation of the CLS ensembles (see sections 4.3.3, 4.3.4 and 6.1.2) for example, the different samples are correlated in which case there might not be any convergence to a Gaussian distribution for $\bar{\mathcal{O}}$ in the $N \to \infty$ limit, but there are properties of a target distribution P that ensure this convergence [82]. In the case of convergence, the uncertainty of $\bar{\mathcal{O}}$ can be determined via from the variance $\sigma^2_{\mathcal{O}} = \left\langle (\mathcal{O} - \langle \mathcal{O} \rangle)^2 \right\rangle$. For independently sampled ϕ_i, this variance can be estimated via

$$\sigma^2_{\mathcal{O}} \approx \frac{1}{N-1} \sum_{i=1}^{N} \left(\mathcal{O}[\phi_i] - \bar{\mathcal{O}} \right)^2.$$

The factor $\frac{1}{N-1}$ is used as the above sum is a biased estimator in the sense that $\left\langle \frac{1}{N} \sum_{i=1}^{N} \left(\mathcal{O}[\phi_i] - \bar{\mathcal{O}} \right)^2 \right\rangle = \frac{N-1}{N} \sigma^2_{\mathcal{O}}$. The correction of this bias is known as *Bessel's correction*. We discuss the effects of correlated samples on the uncertainty in section 6.4.

The samples ϕ_i can be constructed via a *Markov process*, i.e. a process generating a chain (known as a *Markov chain*) of random values where each value ϕ_k is determined from a transition probability $T(\phi_k | \phi_{k-1})$ that only depends on the previous value ϕ_{k-1} in the chain. In order to sample from a given distribution this way, the Markov chain has to converge to a stationary distribution $\pi(x)$ which has to be equal to the target distribution. In this context, stationary means that the distribution is unchanged by transitions drawn from the transition probability T. To have a stationary distribution, a Markov process must be ergodic, i.e. every possible configuration $\hat{\phi}$ must be reachable in a finite number of iterations of the Markov process and the process must be aperiodic, meaning that there is no state ϕ_p which is periodically visited at fixed intervals in the chain. Furthermore, T and π have to satisfy a balance condition [29]

$$\int \mathrm{d}\phi \, T(\phi' | \phi) P(\phi) = \int \mathrm{d}\phi \, T(\phi | \phi') P(\phi').$$

The CLS ensembles are generated using a *hybrid Monte Carlo algorithm* (HMC, see section 6.1.2) which is a special case of a *Metropolis-Hastings algorithm* (see section 6.1.1). These algorithms ensure the balance condition by constructing a transition probability T with an even stronger *detailed balance condition*

$$T(\phi' | \phi) P(\phi) = T(\phi | \phi') P(\phi'). \tag{6.2}$$

The fact that a probability density defined via the exponential of an action S as in eq. (6.1) is strictly positive allows for a simple construction of a strictly positive transition probability $T(\phi | \phi')$ for all pairs of configurations ϕ and ϕ'. This property is known as *strong ergodicity* [29] and implies ergodicity.

6.1.1. The Metropolis-Hastings Algorithm

The Metropolis-Hastings algorithm for a system with probability distribution P constructs a Markov chain whose stationary distribution is P without requiring any knowledge of the normalization of the distribution. For samples drawn from eq. (6.1), it is therefore not necessary to compute the partition function Z for this algorithm. This is achieved via the following construction of a transition probability [29, 82]

$$T(\phi'|\phi) = \begin{cases} T_0(\phi'|\phi)\min\left(1, \frac{T_0(\phi|\phi')\exp(-S[\phi'])}{T_0(\phi'|\phi)\exp(-S[\phi])}\right) & \text{if } T_0(\phi'|\phi) \neq 0 \\ 0 & \text{if } T_0(\phi'|\phi) = 0 \end{cases} \tag{6.3}$$

where T_0 is a prior transition probability that can be almost arbitrarily chosen as eq. (6.3) ensures detailed balance. The only restriction is that the ergodicity of the Markov chain has to be guaranteed. Since the exponentials are always positive, this can be achieved by choosing T_0 to be nonzero for all combinations of ϕ and ϕ' as such a choice implies a strongly ergodic transition probability.
The Metropolis-Hastings algorithm updates a field by drawing a new candidate from T_0 and accepting or rejecting it with a probability given by the minimum-expression in eq. (6.3). If a candidate is rejected, the last value in the chain is repeated. The full algorithm is listed in algorithm 1.

Algorithm 1: The Metropolis-Hastings Algorithm [29]

Data: Field space $\mathcal{F}$
Data: Prior transition probability $T_0 : \mathcal{F} \times \mathcal{F} \to \mathbb{R}_{\geq 0}$
Data: Action $S : \mathcal{F} \to \mathbb{R}$
Data: Number of iterations N

$\phi_0 \leftarrow$ random configuration in $\mathcal{F}$;
for $n \leftarrow 1$ **to** N **do**
  $\phi' \leftarrow$ random configuration drawn from $T_0(\phi'|\phi_{n-1})$;
  $r \leftarrow$ random number drawn from uniform distribution on $[0, 1)$;
  if $r < \min\left(1, \frac{T_0(\phi_{n-1}|\phi')\exp(-S[\phi'])}{T_0(\phi'|\phi_{n-1})\exp(-S[\phi_{n-1}])}\right)$ **then** ; `// Accept` ϕ'
    $\phi_n \leftarrow \phi'$
  else ; `// Reject` ϕ'
    $\phi_n \leftarrow \phi_{n-1}$

This algorithm is useful for local actions for which a single component of the field(s) ϕ can be updated at a time. This is because the exponentials in eq. (6.3) can be combined such that the acceptance probability can be written in terms of the change in action when going from ϕ to ϕ':

$$\begin{aligned} T_A(\phi'|\phi) &= \min\left(1, \frac{T_0(\phi_{n-1}|\phi')\exp(-S[\phi'])}{T_0(\phi'|\phi_{n-1})\exp(-S[\phi_{n-1}])}\right) \\ &= \min\left(1, \frac{T_0(\phi_{n-1}|\phi')}{T_0(\phi'|\phi_{n-1})}\exp\big(S[\phi_{n-1}] - S[\phi']\big)\right). \end{aligned}$$

Take for example the Wilson gauge action (3.9) for which the change in action $\Delta S_g[U, U'] = S_g[U] - S_g[U']$ when changing U only at spacetime point x and Lorentz-index μ can be computed from just U_μ at x and the points neighboring x (with different Lorentz-indices). In this case, the acceptance probability is cheap to compute and T_0 can be tuned to keep the acceptance probability reasonably high. If, however, fermions are included in the simulations, a very non-local fermion determinant has to be computed (refer to sections 4.3.3 and 4.3.4) such that updating a field at a single point is not a viable solution. When updating all fields at all positions at once, however, the acceptance probabilities are extremely small for large lattices such that the Metropolis-Hastings algorithm alone is too computationally expensive. For these cases, the HMC algorithm can be used to improve the acceptance probabilities, which we discuss in the following.

6.1.2. The Hybrid Monte Carlo Algorithm

The HMC algorithm works by introducing an additional "conjugate momentum" field Π for ϕ which changes the action to $S[\phi] \mapsto S_1[\phi, \Pi] = S[\phi] + \frac{1}{2}\Pi^2$, where Π is to be understood as a vector of all components of the field similar to the notation used in section 3.3.1 and eq. (3.14), i.e. $\Pi^2 := \sum_{x\in\Lambda} \Pi(x)^2$. After drawing a random sample for the field Π from the distribution $P_G[\Pi] = \frac{1}{Z_\Pi} e^{-\frac{1}{2}\Pi^2}$, the fields ϕ and Π are numerically evolved following the classical equations of motion

$$\begin{aligned} \dot{\phi} &= -\frac{\partial S_1}{\partial \Pi} = \Pi, \\ \dot{\Pi} &= -\frac{\partial S_1}{\partial \phi} = -\frac{\partial S}{\partial \phi}, \end{aligned} \tag{6.4}$$

interpreting the action S_1 as a Hamiltonian of a classical microcanonical ensemble [29]. This procedure replaces the step of drawing an update candidate from T_0 in the Metropolis-Hastings algorithm and adds a deterministic step to the random sampling of a field Π which improves the acceptance probability for a global update. The whole procedure can then be interpreted as drawing from a transition probability $T_{\mathrm{md}}(\Pi', \phi'|\Pi, \phi)$ to update the field ϕ as is done in the Metropolis-Hastings algorithm. In order to satisfy the detailed balance condition (6.2), the numeric algorithm to evolve ϕ and Π according to eq. (6.4) has to be chosen such that it is area preserving, i.e. $\mathcal{D}\phi'\mathcal{D}\Pi' = \mathcal{D}\phi\mathcal{D}\Pi$, and reversible, i.e. $T_{\mathrm{md}}(\Pi', \phi'|\Pi, \phi) = T_{\mathrm{md}}(-\Pi, \phi| - \Pi', \phi')$ [29]. Since the Gaussian distribution $P_G[\Pi]$ from which Π is drawn is symmetric in the sense that $P_G[-\Pi] = P_G[\Pi]$, T_{md} is symmetric in the primed and unprimed fields and thus cancels in the acceptance probability of the metropolis update step. The exact algorithm for the update step is listed in algorithm 2.

In the context of LQCD with two mass-degenerate fermion fields $\psi_{1/2} \in \mathbb{R}^{N_C \cdot N_S \cdot |\Lambda|}$ and gauge fields $U \in \Lambda \times \mathrm{SU}(3)$, the fermionic part of the action can be integrated stochastically using pseudofermions (see section 4.2.1) φ drawn from a Gaussian distribution $P_f[\varphi] \propto \exp\left(-\varphi^\dagger \left(D^\dagger D\right)^{-1} \varphi\right)$ where D is the Dirac operator. The gauge links are then drawn using the HMC algorithm with a *leap frog algorithm* for the integration of eq. (6.4) which fulfills the required properties of area preservation and reversibility discussed above. The gauge links are not sampled directly but rather the Lie algebra elements $u \in \mathfrak{su}(3)$ that are related to gauge links via

Algorithm 2: Update step of the general hybrid Monte-Carlo algorithm [29]

Data: Field space $\mathcal{F}$
Data: Action $S : \mathcal{F} \to \mathbb{R}$
Input: Prior field configuration ϕ
Output: The next field configuration ϕ'
$\Pi \leftarrow$ random sample drawn from $P_G[\Pi] \propto \exp\left(-\frac{\Pi^2}{2}\right)$;
Evolve ϕ, Π to ϕ', Π' using eq. (6.4);
$r \leftarrow$ random number drawn from uniform distribution on $[0, 1)$;
if $r < \min\left(1, \frac{\exp(-S[\phi'])}{\exp(-S[\phi])}\right)$ **then**
    return ϕ'
else
    return ϕ

exponentiation,

$$U_\mu(x) = \exp(iu_\mu(x)) = \exp\left(i \sum_{a=1}^{8} u_\mu^a(x) t^a\right).$$

Accordingly, the conjugate momenta Π_μ are also defined in $\mathfrak{su}(3)$,

$$\Pi_\mu(x) = \sum_{a=1}^{8} \Pi_\mu^a(x) t^a.$$

The probability density of Π is then given by [29]

$$P_G[\Pi] \propto \exp\left(-\frac{1}{2}\Pi^2\right) = \exp\left(-\frac{1}{2}\sum_{x,\mu,a}\left(\Pi_\mu^a(x)\right)^2\right) = \exp\left(-\sum_{x,\mu}\mathrm{tr}\left(\Pi_\mu(x)^2\right)\right).$$

Using a "driving force" [29]

$$F[U, \varphi] = \sum_{a=1}^{8} t^a \nabla^a \left(S_g[U] + \varphi^\dagger (DD^\dagger)^{-1} \varphi\right) \text{ where} \tag{6.5}$$
$$\nabla^a f(U) := \frac{\partial f(U)}{\partial u^a} = \frac{\partial}{\partial u} f\left(e^{iut^a} U\right)\Big|_{u=0},$$

the HMC algorithm for LQCD can be implemented as in algorithm 3.
As these sampling algorithms start from a random configuration, the generated Markov chain has to be advanced a number of steps to let it converge to the stationary distribution. These first few steps are known as *thermalization*.
As the HMC algorithm is formulated for two degenerate fermions the algorithm has to be tweaked in order to simulate a single fermion flavor. The method used for the strange quark in the CLS ensembles (see section 4.3.4) is the RHMC algorithm [55] that introduces an operator T to approximate the inverse Dirac operator as $D^{-1} = TT^\dagger$ with T in the form of rational polynomials. Since this is only an approximation, the field configurations sampled by this technique do not exactly follow the distribution described by the action and thus any results obtained via importance sampling from these samples has to be corrected. The method to correct for these inaccuracies is known as *reweighting* which we discuss in the following section.

Algorithm 3: Update step of the HMC algorithm for LQCD with two mass-degenerate fermions [29]

Data: The gluon gauge action $S_g[U]$
Data: The Dirac operator $D[U]$
Input: The prior gauge configuration U_0
Input: The number N_φ of pseudofermion samples to use
Input: The step size for the leapfrog algorithm ε
Input: The number of steps for the leapfrog algorithm N_l
Output: The next field configuration U_n

`// Draw pseudofermion fields`
for $i \leftarrow 1$ **to** N_φ **do**
  $R_i \leftarrow$ random sample drawn from $P_{f,0}[R] \propto \exp\big(-R^\dagger R\big)$;
  $\varphi_i \leftarrow DR_i$;
`// Draw conjugate field`
$\Pi_0 \leftarrow$ random sample drawn from $P_G[\Pi] \propto \exp\big(-\frac{1}{2}\Pi^2\big)$;
`// Initial step of the leapfrog algorithm`
$\Pi_{\frac{1}{2}} \leftarrow \Pi_0 - \frac{\varepsilon}{2} F[U,\varphi]\big|_{U=U_0}$;
`// Intermediate leapfrog steps`
for $k \leftarrow 1$ **to** N_l **do**
  $U_k \leftarrow \exp\Big(i\varepsilon\Pi_{k-\frac{1}{2}}\Big)$;
  $\Pi_{k+\frac{1}{2}} \leftarrow \Pi_{k-\frac{1}{2}} - \varepsilon F[U,\varphi]\big|_{U=U_k}$;
`// Final leapfrog step`
$U_{N_l} \leftarrow \exp\Big(i\varepsilon\Pi_{n-\frac{1}{2}}\Big)U_{n-1}$;
$\Pi_n \leftarrow \Pi_{n-\frac{1}{2}} - \frac{\varepsilon}{2} F[U,\varphi]\big|_{U=U_n}$;
`// Metropolis-Hastings accept-reject step`
$r \leftarrow$ random number drawn from uniform distribution on $[0,1)$;
$\Delta S_f \leftarrow \sum_{i=1}^{N_\varphi} \varphi_i^\dagger \Big(\big(D[U_0]D[U_0]^\dagger\big)^{-1} - \big(D[U_n]D[U_n]^\dagger\big)^{-1}\Big)\varphi_i$;
$T \leftarrow \exp\big(\Pi_0^2 - \Pi_n + S_g[U_0] - S_g[U_n] + \Delta S_f\big)$;
if $r < T$ **then**
  return U_n;
else
  return U_0;

6.2. Reweighting

Reweighting is a technique that is widely used in Lattice simulations with the goal of improving algorithmic stability (see for example sections 4.3.2 and 4.3.3), for improved sampling efficiency (see for example section 4.3.4), or to simulate physics at slightly different physical parameters which is sometimes employed in finite-temperature QCD with non-zero chemical potential [83–85]. The computation of isospin-breaking corrections as discussed in section 5.2 can be interpreted in this way as well.
This technique allows to compute expectation values $\langle\cdot\rangle_S$ in a theory defined by the action S from Monte Carlo samples generated for a theory with action S_0, which is distinct but similar to S. This can be done by rewriting the expectation values (6.1) in the following way:

$$\begin{aligned}\langle\mathcal{O}\rangle_S =& \frac{\int \mathcal{D}\phi\, \mathcal{O}[\phi] e^{-S[\phi]}}{\int \mathcal{D}\phi\, e^{-S[\phi]}} = \frac{\int \mathcal{D}\phi\, \mathcal{O}[\phi] e^{S_0[\phi]-S[\phi]} e^{-S_0[\phi]}}{\int \mathcal{D}\phi\, e^{S_0[\phi]-S[\phi]} e^{-S_0[\phi]}} \\ =& \left(\frac{\int \mathcal{D}\phi\, \mathcal{O}[\phi] e^{S_0[\phi]-S[\phi]} e^{-S_0[\phi]}}{\int \mathcal{D}\phi\, e^{-S_0[\phi]}}\right)\left(\frac{\int \mathcal{D}\phi\, e^{S_0[\phi]-S[\phi]} e^{-S_0[\phi]}}{\int \mathcal{D}\phi\, e^{-S_0[\phi]}}\right)^{-1} \\ =& \frac{\left\langle \mathcal{O} e^{S_0-S}\right\rangle_{S_0}}{\left\langle e^{S_0-S}\right\rangle_{S_0}} =: \frac{\langle R\mathcal{O}\rangle_{S_0}}{\langle R\rangle_{S_0}}.\end{aligned} \tag{6.6}$$

The factor $R[\phi] = e^{S_0[\phi]-S[\phi]}$ is called a *reweighting factor*.
While in the limit of infinite statistics, this method gives the correct result, for a finite set of samples it is crucial that the bulk of the distributions defined by S and S_0 overlap enough so that the sampled data contains enough configurations typical of S [19].

6.3. Resampling

In lattice calculations there are typically two distinct types of observables; *primary observables* that can be computed directly from the path integral as in eq. (6.1), and *secondary observables* that instead are functions of primary observables. The results of this thesis, for example are derived from two-point correlation functions (discussed in detail in chapter 7). The correlation functions themselves are primary observables[1], but all derived quantities are secondary ones.
Secondary observables can be analyzed using resampling methods which qualitatively determine uncertainties and other statistics of expectation values of observables and functions of these expectation values. Consider an experiment yielding N data points for observables $(\mathcal{O}_1, ..., \mathcal{O}_n) \in \mathcal{F}$ where $\mathcal{F}$ is a n-dimensional sample $\mathbb{R}$-vector space. Suppose, one is interested in functions $f(\langle\mathcal{O}_1\rangle, ..., \langle\mathcal{O}_n\rangle)$ of their expectation values. It is straightforward to define an estimator for such a function by simply plugging the averages over the N samples into f. However, due to the finite sample size, the result is shifted due to statistical fluctuations in the sample and thus has an uncertainty attached. Two systematic methods to

[1] Note, that for CLS ensembles even correlation functions are secondary observables since the data obtained from them require reweighting and thus (as per eq. (6.6)) an otherwise primary observable $\mathcal{O}$ is in fact a function of the primary observables $R\mathcal{O}$ and R.

estimate these uncertainties are described in sections 6.3.1 and 6.3.2. For brevity, we will denote the index set $\{1, ..., N\}$ as I_N.

6.3.1. Jackknife

To compute an estimator $\hat{F}$ for the derived quantity $F = f(\langle \mathcal{O}_1 \rangle, ..., \langle \mathcal{O}_n \rangle)$ and its uncertainty σ_F from N samples $\mathcal{O}_1^k, ..., \mathcal{O}_n^k$ where $k \in \{1, ..., N\}$, the jackknife procedure uses N resamplings

$$J_i := \left\{ (\mathcal{O}_1^k, ..., \mathcal{O}_n^k)^T \middle| k \in I_N^i \right\} \tag{6.7}$$

of the original data, where $I_N^i = I_N \backslash \{i\}$. For each of these resamplings, we define sample means

$$\tilde{J}_i := \left(\tilde{\mathcal{O}}_1^i, ..., \tilde{\mathcal{O}}_n^i \right)^T = \left(\frac{1}{N-1} \sum_{k \in I_N^i} \mathcal{O}_1^k, ..., \frac{1}{N-1} \sum_{k \in I_N^i} \mathcal{O}_n^k \right)^T . \tag{6.8}$$

These sample means serve as proxies for samples drawn from the distribution of averages of N measurements of $\mathcal{O}$. We then define the estimator $\hat{F}$ as the result of applying f to the sample mean:

$$\begin{aligned} \hat{F} :=& f(\bar{\mathcal{O}}_1, ..., \bar{\mathcal{O}}_n) \text{ where} \\ \bar{\mathcal{O}}_i :=& \frac{1}{N} \sum_{i \in I_N} \mathcal{O}_i . \end{aligned} \tag{6.9}$$

The uncertainty of $\hat{F}$ is estimated via the jackknife distribution

$$\begin{aligned} \sigma_{F_k}^2 =& \frac{N}{N-1} \sum_{i \in I_N} \left(f_k(\tilde{J}_i) - \tilde{F}_k \right)^2 \text{ where} \\ \tilde{F} =& \frac{1}{N} \sum_{i \in I_N} f(\tilde{J}_i) \end{aligned} \tag{6.10}$$

Analogously, if f maps to a multi-dimensional vector $f : \mathcal{F} \to \mathbb{R}^m$, we define the covariance matrix of the observable vector $F \in \mathbb{R}^m$ via

$$\mathrm{Cov}_F = \frac{N}{N-1} \sum_{i \in I_N} \left(f(\tilde{J}_i) - \tilde{F} \right) \left(f(\tilde{J}_i) - \tilde{F} \right)^T \in \mathbb{R}^{m \times m} . \tag{6.11}$$

6.3.2. Bootstrap

The bootstrap procedure is similar to the jackknife one. The main difference lies in the way the samples are constructed. Contrary to jackknife samples, there can be any number of bootstrap samples, which are randomly chosen. In the following, we denote the number of bootstrap resamplings by N_B. Each of these resamplings are constructed by randomly sampling N times from the original data with replacement, i.e. in analogy to eq. (6.7) the bootstrap resamplings are given by

$$B_i := \left\{ \left(\mathcal{O}_1^k, ..., \mathcal{O}_n^k \right)^T \middle| k \in I_N^{B,i} \right\} \tag{6.12}$$

where $I_N^{B,i}$ is a collection of N samples drawn from I_N with replacement. The indices $I_N^{B,i}$ are sampled once and are then reused for all computations performed on a certain set of measurements. The sample means for the bootstrap are then given by

$$\tilde{B}_i := \left(\tilde{\mathcal{O}}_1^i, ..., \tilde{\mathcal{O}}_n^i\right)^T = \left(\frac{1}{N}\sum_{k\in I_N^{B,i}} \mathcal{O}_1^k, ..., \frac{1}{N}\sum_{k\in I_N^{B,i}} \mathcal{O}_n^k\right)^T. \tag{6.13}$$

The estimator $\hat{F}$ is defined as in eq. (6.9) with N replaced by N_B. The estimates of the squared uncertainty and covariances are then

$$\sigma_{F_k}^2 = \frac{1}{N-1}\sum_{i\in I_N^{B,k}} \left(f_k(\tilde{B}_i) - \tilde{F}_k\right)^2, \tag{6.14}$$

$$\mathrm{Cov}_F = \frac{1}{N-1}\sum_{i\in I_N^{B,k}} \left(f(\tilde{B}_i) - \tilde{F}\right)\left(f(\tilde{B}_i) - \tilde{F}\right)^T \text{ where} \tag{6.15}$$

$$\tilde{F} = \frac{1}{N}\sum_{i\in I_N^{B,k}} f\left(\tilde{B}_k\right).$$

6.4. Autocorrelation

Configurations of lattice ensembles are constructed as Markov chains and thus, observables computed on close configurations of such a chain are generally correlated. When computing the expectation value of such an observable $\langle x\rangle \approx \bar{x} = \frac{1}{N}\sum_{i=1}^N x_i$, the correlations of the different x_i influence the uncertainty of $\bar{x}$ and thus have to be accounted for. The covariances of different measurements depend only on the difference between the configurations in the Markov chain and can thus be described in terms of a *autocovariance function* [86]

$$C_x(t) = \langle x_i x_{i+t}\rangle_i - \langle x\rangle^2 \tag{6.16}$$

or an *autocorrelation function*

$$\rho_x(t) = \frac{C_x(t)}{C_x(0)}. \tag{6.17}$$

Note that C_x and thus also ρ_x are symmetric in t, i.e. $C(-t) = C(t)$, so that [29, 86]

$$\sigma_x^2 = \frac{1}{N^2}\sum_{r,s=1}^N C_x(r-s) = \frac{1}{N}\sum_{t=-(N-1)}^{N-1}\left(1 - \frac{|t|}{N}\right)C_x(t). \tag{6.18}$$

In order to relate this to the naive variance $\tilde{\sigma}_x^2 = C_x(0)$, it is common to introduce the *integrated autocorrelation time* [29, 86, 87]

$$\tau_{\mathrm{int,x}} = \frac{1}{2}\sum_{t=-\infty}^{\infty}\rho_x(t) = \frac{1}{2} + \sum_{t=1}^{\infty}\rho_x(t) \tag{6.19}$$

with which the variance of x can be approximated by

$$\sigma_x^2 \approx \frac{2\tau_{\mathrm{int,x}}}{N}\tilde{\sigma}_x^2. \tag{6.20}$$

In principle, one could simply compute the error of an observable using eq. (6.18). However, this formula is only applicable for primary observables and secondary observables have to be treated differently. Furthermore, $C_x(t)$ has itself an uncertainty that grows with $|t|$ making the application of this formula unreliable in practice. To deal with these problems, there are two methods used in some part of the project described in chapters 8 and 9 to get a reliable estimate of the full variance (6.18). The first is by combining multiple measurements in order to reduce the autocorrelation time of the resulting values described in section 6.4.1, the other being the Γ-method introduced by Ulli Wolff [87] calculating $\tau_{\text{int,x}}$ directly, which is briefly explained in section 6.4.2.

6.4.1. The Binning Method

Binning is the main method used in this thesis' project wherever applicable. This method groups consecutive configurations into chunks of size B and treats the average of each chunk for a primary observable as a single measurement of said observable. That means, for a primary observable x with measurements x_i on N configurations we define the binned measurements

$$x_{B,i} = \frac{1}{B} \sum_{j=Bi}^{B(i+1)} x_j.$$

These binned measurements are less correlated than the original x_i so that for large B the naive variance $N_B \tilde{\sigma}^2_{x_B} = N_B C_{x_B}(0)$ converges to the full variance σ_x^2 in eq. (6.18) up to a correction of order $\frac{\tau_{\text{int,x}}}{B}$ [87], where N_B is the number of bins $N_B = \left\lfloor \frac{N}{B} \right\rfloor$.
In combination with jackknife or bootstrap resampling, one can use the full set of original measurements x_i to compute the mean of an observable and construct the jackknife or bootstrap samples from the binned measurements. Note, that the sampling distribution can be treated as if it were the full distribution for error analysis as the variance of the mean $\bar{x} = \sum_{i=1}^{N} x_i$ is given by

$$\sigma^2_{\bar{x}} = \frac{\sigma_x^2}{N} \approx \frac{B\tilde{\sigma}^2_{x_B}}{N} \approx \frac{\tilde{\sigma}^2_{x_B}}{N_B},$$

i.e. the factor of the binsize is approximately canceled in the normalization if B is large enough. This makes this method suitable for resampling analyses which is why we use it in the analysis of the data gathered for this thesis' project. Secondary observables are treated just as in the limit of vanishing autocorrelations discussed in section 6.3 by using the binned resampling distributions.
Binning has a few drawbacks however, which have to be taken into account. Firstly, one might not be able to use all samples if B does not divide N. One should thus choose B such that the number of unused samples, $B \mod N$, is small if possible. Secondly, binning drastically reduces the number of samples left for error analysis which means that the binsize B cannot be chosen arbitrarily large. Especially for LQCD simulations where the number of configurations per ensemble is already only in the order of ~1000 this can lead to bad estimators if $\frac{N}{\tau_{\text{int}}}$ is too small. With the goal of minimizing the error of $\sigma_{\bar{x}}$ (i.e. the *error of the error*) it can be shown that an "optimal" binsize is given by [87]

$$B_{\text{opt}} \approx \left(2N{\tau_{\text{int,x}}}^2\right)^{\frac{1}{3}} \tag{6.21}$$

for which the relative error of $\sigma_{\bar{x}}$ is given by $\frac{\Delta\sigma_{\bar{x}}}{\sigma_{\bar{x}}} = \frac{3}{2}\sqrt[3]{\frac{\tau_{\mathrm{int,x}}}{2N}}$.

6.4.2. The Gamma Method

A different approach to autocorrelated data is the Γ-method introduced in [87] on which this section is based.
The Γ-method uses eq. (6.20) to compute the error of primary observables $x \in \mathbb{R}^n$ as well as secondary observables $F = f(\langle x \rangle) \in \mathbb{R}$ using error propagation. To this end, an analog

$$\Gamma_F(t) = \sum_{\alpha,\beta=1}^{n} \frac{\partial f(x)}{\partial x_\alpha}\bigg|_{x=\bar{x}} \frac{\partial f(x)}{\partial x_\beta}\bigg|_{x=\bar{x}} C_{x,\alpha\beta}(t)$$

to the autocovariance function C_x in eq. (6.16) is defined. Here, Greek letters enumerate the components of the observable vector x and

$$\begin{aligned} C_{x,\alpha\beta}(t) &= \left\langle (x_{i,\alpha} - \langle x_\alpha \rangle)(x_{i+t,\beta} - \left\langle x_\beta \right\rangle) \right\rangle_i \\ &\approx \frac{1}{N}\sum_{i=1}^{N} (x_{i,\alpha} - \bar{x}_\alpha)(x_{i+t,\beta} - \bar{x}_\beta) \end{aligned}$$

models the covariances of x_α and x_β in addition to the autocovariance. From this, the integrated autocorrelation time is defined for F as

$$\tau_{\mathrm{int,F}} = \frac{1}{2\tilde{\sigma}_F^2} \sum_{t=-\infty}^{\infty} \Gamma_F(t) \tag{6.22}$$

with $\tilde{\sigma}_F^2 = \Gamma_F(0)$ being the naive, uncorrelated variance of $\bar{F} = \sum_{i=1}^{N} f(\bar{x})$. The variance of $\bar{F}$ is then given by

$$\sigma_{\bar{F}}^2 = \frac{2\tau_{\mathrm{int,F}}}{N}\tilde{\sigma}_F^2.$$

As mentioned above, this procedure still has the problem that the uncertainty of Γ_F grows with large t, which is accounted for in [87] by defining a truncated autocorrelation time with a summation cutoff W in eq. (6.22) via

$$2\tilde{\sigma}_F^2 \tau_{\mathrm{int,F}}(W) = \sum_{t=-W}^{W} \Gamma_F(t) = \Gamma_F(0) + 2\sum_{t=1}^{W} \Gamma_F(t).$$

To find a suitable cutoff, the error of the error $\Delta\sigma_{\bar{F}}$ is estimated based on the assumption that $\Gamma_F(t)$ asymptotically decays exponentially as $\exp(-t/\tau)$ for some τ, in which case [87]

$$\frac{\Delta\sigma_{\bar{F}}}{\sigma_{\bar{F}}} \approx \frac{1}{2}\exp\left(-\frac{W}{\tau}\right) + 2\sqrt{\frac{W}{N}}. \tag{6.23}$$

W is then chosen such that the above relative error of the error is minimized. In practice, this is done based on the assumption that there exists a factor S such that

$$2\tau_{\mathrm{int,F}}(W) = \sum_{t=-\infty}^{\infty} \exp\left(-\frac{S|t|}{\tau(W)}\right).$$

Using a guess for the value of S, this equation is solved for $\tau(W)$ which in turn is substituted for τ in eq. (6.23) to find the W that minimizes the error of the error.
While this method is only applicable for $N \gg \tau$ [87], it allows for a more reliable estimation of the autocorrelation time τ_{int} than binning, especially if τ_{int} is large. Nevertheless, it requires a guess of the value of S which may require tuning for each observable and only treats errors of secondary observables up to first order in the Taylor expansion of f and up to the second moment of the probability distribution from which the expectation values $\langle x \rangle$ are sampled.

6.5. All Mode Averaging

All mode averaging (AMA) [88, 89] is a technique to reduce expensive parts of a computation by trading off precision and computational cost using control variates [90]. The general idea is to split an expectation value $\langle e \rangle$ into expectation values of an expensive part and a cheap part:

$$\langle e \rangle = \langle e - s \rangle + \langle s \rangle . \tag{6.24}$$

Here, s is a sloppy estimator that is strongly correlated with the *exact* estimator e and this method reduces the error σ_e if $2\text{Cov}(e, s) > \sigma_s^2$ [90]. The benefit in Lattice simulations comes in terms of saved computational resources: Instead of computing e very often to reduce the error on the stochastic estimate of $\bar{e} = \frac{1}{N}\sum_{i=1}^{N} e_i$ for $\langle e \rangle$, one can compute only a few measurements for the first term in eq. (6.24) and reduce the error by instead computing more values for s to get a more precise result of the second term. In this procedure, s has to be measured on the same data as e to make use of the correlation between the two estimators which reduces the error of the first term. Otherwise, the overall error is dominated by the few measurements of e.
Given a cheap estimator s, the error on the prediction can often be improved by a rescaling of s: Let $b = e - s$ be the bias of the cheap estimator. Then, the variance of the bias is given by

$$\sigma_b^2 = \sigma_e^2 + \sigma_s^2 - 2\text{Cov}(e, s).$$

Introducing a scaled cheap estimator $\hat{s} := rs$ for some $r \in \mathbb{R}$, we find that the error of the bias for the scaled estimator $\hat{b} := e - \hat{s}$ depends on r:

$$\sigma_{\hat{b}}^2 = \sigma_e^2 + r^2\sigma_s^2 - 2r\text{Cov}(e, s).$$

Thus, the error of the bias can be minimized by choosing r such that it minimizes $\sigma_{\hat{b}}^2$, i.e.

$$r = \frac{\text{Cov}(e, s)}{\sigma_s^2},$$

in which case the error of the bias is given by

$$\sigma_{\hat{b}} = \sqrt{1 - \rho_{es}^2}\sigma_e \leq \sigma_b^2$$

where $\rho_{xy} = \frac{\text{Cov}(x,y)}{\sigma_x \sigma_y}$ is the Pearson correlation coefficient. This generally reduces the error of the final estimator $\langle \hat{b} \rangle + \langle \hat{s} \rangle$ for $\langle e \rangle$, however, this error reduction is smaller if positive correlations between $\hat{b}$ and $\hat{s}$ can be leveraged, as the optimal value of r completely de-correlates $\hat{b}$ and $\hat{s}$, i.e. $\text{Cov}(\hat{b}, \hat{s}) = 0$. The correlation between the bias and exact value for optimal r is given by $\rho_{\hat{b}e} = \sqrt{1 - \rho_{es}^2}$.

AMA with multiple control variates

The above procedure can be further improved upon if one has multiple control variates $s_1, ..., s_N$ that are correlated (or anticorrelated) to e. In that case, we can replace the coefficient r above by a set of coefficients $\theta = (\theta_1, ..., \theta_N)^T \in \mathbb{R}^N$ and with $s := (s_1, ..., s_N)^T$ define $\hat{s} = \theta^T s$ and $\hat{b} = e - \hat{s}$. The variance of $\hat{b}$ can then be written as

$$\sigma_{\hat{b}}^2 = \sigma_e^2 + \theta^T \mathrm{Cov}_s \theta - 2\theta^T c_{e,s}$$

where Cov_s is the covariance matrix $(\mathrm{Cov}_s)_{ij} = \langle (s_i - \langle s_i \rangle)(s_j - \langle s_j \rangle) \rangle$ of s and $c_{e,s} = (\mathrm{Cov}(e, s_1), ..., \mathrm{Cov}(e, s_N))^T \in \mathbb{R}^N$ is a vector whose entries are the covariances of e with the individual control variates. This is minimal for

$$\theta = \mathrm{Cov}_s^{-1} c_{e,s} \tag{6.25}$$

in which case the variance of $\hat{b}$ is reduced to

$$\sigma_{\hat{b}}^2 = \sigma_e^2 - c_{e,s}^T \mathrm{Cov}_s^{-1} c_{e,s}.$$

In this approach, different control variates s_i and s_j must not be affine transformations of each other, i.e. there must not exist real numbers α and β s.t. $s_i = \alpha s_j + \beta$ since this leads to a singular covariance matrix.

6.6. Maximum Likelihood Fits

Consider a function $f : \mathbb{R} \times \mathbb{R}^l \to \mathbb{R}$ modeling the dependence of two known quantities x and $y = f(x, \theta)$ dependent on additional unknown quantities $\theta \in \mathbb{R}^l$. To determine the values of the parameters θ from a set of data $(x_D, y_D) \in \mathbb{R}^n \times \mathbb{R}^n$ where y_D is drawn from a distribution $P : \mathbb{R}^n \to \mathbb{R}_{\geq}$, we make the usual assumption that the best guess of the parameters given the data is the vector $\hat{\theta}$ that maximizes the likelihood of producing the observed data if $\langle y \rangle_P = f(x, \hat{\theta})$. In the context of this thesis all data entering fits are averages over data drawn from a distribution defined via the lattice action. We thus assume that by the central limit theorem the probability distribution P is to a good approximation a normal distribution

$$P(y) = \frac{\det V}{\sqrt[n]{2\pi}} \exp\left(-\frac{1}{2}(y - \mu)^T V (y - \mu)\right)$$

where V is the inverse covariance matrix of y which is computed from a jackknife or bootstrap distribution. Thus, under the assumption that $\mu = f(x, \hat{\theta})$, we define $\hat{\theta}$ as the set of parameters that minimize the correlated χ^2,

$$\hat{\theta} = \underset{\theta \in \mathbb{R}^l}{\arg\min} \, (y - f(x, \theta))^T V (y - f(x, \theta)).$$

An overview of fits used for this thesis – as well as closed-form solutions for the minimization if known – can be found in section B.3. We compute the uncertainties and covariances of $\hat{\theta}$ from the bootstrap- or jackknife-distribution of the fit results.

Part II

Project

Chapter 7
Computation of Hadronic 2-Point Functions

The results of this thesis rely heavily on the extraction of hadron masses from LQCD gauge ensembles which are described in more detail in section 4.3. Ground-state masses of hadrons can be computed from hadronic 2-point functions

$$C(t) = \frac{1}{\Lambda_3} \sum_{\mathbf{x}_{\text{sink}} \in \Lambda_3} \operatorname{tr} \left\langle \mathcal{O}(t_{\text{src}} + t, \mathbf{x}_{\text{sink}}) \bar{\mathcal{O}}(t_{\text{src}}, \mathbf{x}_{\text{src}}) \right\rangle_{G, t_{\text{src}}} \tag{7.1}$$

where $\mathcal{O}(t, \mathbf{x})$ is an operator annihilating a hadronic state at spacetime coordinates $(t, \mathbf{x}^T)^T$. The sum over the spatial sink positions projects the respective operator to zero momentum as per section 3.1.1, eq. (3.5).
Rewriting eq. (7.1) in the energy eigenbasis $|n\rangle$ and performing a time evolution, one finds that it is described by a tower of exponentially decaying functions

$$\begin{aligned}
C(t) =& \frac{1}{\Lambda_3} \sum_{\mathbf{x}_{\text{sink}} \in \Lambda_3} \operatorname{tr} \langle 0 | \mathcal{O}(t, \mathbf{x}_{\text{sink}}) \bar{\mathcal{O}}(0, \mathbf{x}_{\text{src}}) | 0 \rangle \\
=& \frac{1}{\Lambda_3} \sum_{\mathbf{x}_{\text{sink}} \in \Lambda_3} \sum_n \operatorname{tr} \big[\langle 0 | \mathcal{O}(t, \mathbf{x}_{\text{sink}}) | n \rangle \langle n | \bar{\mathcal{O}}(0, \mathbf{x}_{\text{src}}) | 0 \rangle \big] \\
=& \frac{1}{\Lambda_3} \sum_{\mathbf{x}_{\text{sink}} \in \Lambda_3} \sum_n \operatorname{tr} \big[\langle 0 | e^{Ht} \mathcal{O}(0, \mathbf{x}_{\text{sink}}) e^{-Ht} | n \rangle \ \langle n | \bar{\mathcal{O}}(0, \mathbf{x}_{\text{src}}) | 0 \rangle \big] \\
=& \sum_n \left(\frac{1}{\Lambda_3} \sum_{\mathbf{x}_{\text{sink}} \in \Lambda_3} \operatorname{tr} [\langle 0 | \mathcal{O}(0, \mathbf{x}_{\text{sink}}) | n \rangle \ \langle n | \mathcal{O}(0, \mathbf{x}_{\text{src}}) | 0 \rangle] \right) e^{-(E'_n - E'_0)t} \\
=& : \sum_n c_n e^{-E_n t}.
\end{aligned} \tag{7.2}$$

Note that the experimentally accessible energies E_n are differences of the actual energy eigenvalues E'_n to the vacuum energy E'_0. Furthermore, $c_0 = 0$ as it corresponds to the vacuum expectation value of an annihilation operator. Thus the constant term in the exponential tower vanishes. In the above expression, there is an implicit dependence of c_n on $\mathbf{x}_{\text{src}}$. However, due to translational symmetry of the underlying theory,[1] this dependence vanishes when taking the average over multiple gauge configurations.

[1] This symmetry is of course not given for open boundary conditions. However, the CLS ensembles used in this project have exclusively periodic boundary conditions in the spatial directions, such that this assumption is justified as long as the temporal boundary conditions are also periodic or the source and sink times are in a region where this translational symmetry is approximately valid.

Due to the zero-momentum projection, the $n = 1$ contribution decays with the ground-state mass $m = E_1$. Since all states with higher energy decay faster than the ground state ($e^{-E_n t} \ll e^{-E_1 t}$ for large enough t and $n > 1$), the correlation function eq. (7.1) asymptotically behaves like

$$C(t) \xrightarrow{t\to\infty} c_1 e^{-mt} \tag{7.3}$$

allowing for the extraction of the ground state mass m. This is explained in more detail in section 7.4.

7.1. Operator Basis

In order to calculate a two-point function as in eq. (7.1), suitable operators $\mathcal{O}$ – also called *interpolators* – have to be found that describe the desired hadron. *Suitable* here means that the operators match all required quantum numbers and properties of the desired hadron. In the scope of this project, this typically means quark content, parity, spin, and color structure. Popular choices of such interpolators for the proton and π^+ for example would be

$$\begin{aligned} \mathcal{O}_p(x) &= \mathcal{P}_+ \sum_{a,b,c} \varepsilon_{abc} u^a(x) \big(u^b(x)^T \mathcal{C}\gamma_5 d^c(x)\big), \\ \mathcal{O}_{\pi^+}(x) &= \sum_a \bar{d}^a(x)\gamma_5 u^a(x), \end{aligned} \tag{7.4}$$

where u and d denote Dirac spinors for the up and down-quark, $\mathcal{C} = \gamma_0\gamma_2$ is the charge-conjugation operator, $\mathcal{P}_+ = \frac{1}{2}(\mathbb{1} + \gamma_0)$ projects onto positive parity, and the sums are over color indices. The Clifford-algebra element $\mathcal{C}\gamma_5$ has the effect that the term in parentheses has spin 0 (a so-called *diquark*) [29] such that, combined with the first up-quark, the total operator $\mathcal{O}_p$ describes a spin-$\frac{1}{2}$ state.

While we use operators of the form given in eq. (7.4) for mesons, the baryonic operators used in this project are based on a different construction by the Lattice Hadron Physics Collaboration [12] using a Clebsch-Gordan based approach. The following discussion makes use of their notation and conventions.
The construction builds operators from Weyl-spinors in the Dirac-Pauli representation in which Dirac-matrices are trivially decomposed into a *ρ-spin* and a *s-spin* component:

$$\gamma = c\rho \otimes \sigma.$$

This decomposition takes the form

$$\begin{aligned} \mathbb{1} &= \rho_0 \otimes \sigma_0 \\ \gamma_0 &= \rho_3 \otimes \sigma_0 \\ \gamma_k &= \rho_2 \otimes \sigma_k \\ \gamma_5 &= \rho_1 \otimes \sigma_0 \\ \mathcal{C} &= -i\rho_1 \otimes \sigma_2 \\ \mathcal{S} &= \rho_0 \otimes \sigma_3 \end{aligned}$$

where ρ_k and σ_k denote the k-th Pauli matrix, $\rho_0 = \sigma_0 = \mathbb{1}_{2\times 2}$, and $\mathcal{S}$ is the spin-operator with eigenvalues $s = \pm 1$ for spin-up and spin-down.

The ρ-spin is linked to the parity transformation $\mathcal{P}$ as it can be written as

$$\mathcal{P}\psi(\mathbf{x},t)\mathcal{P}^{-1} = \gamma_0\psi(-\mathbf{x},t) = (\rho_3 \otimes \sigma_0)\psi(-\mathbf{x},t) =: \rho\psi(-\mathbf{x},t) \tag{7.5}$$

when acting on a Dirac-spinor-field ψ, where $\rho = \pm 1$ is the parity eigenvalue. Since $\rho_3 = \sigma_3 = \begin{pmatrix} 1 & 0 \\ 0 & -1 \end{pmatrix}$ and ρ_0 and σ_0 are the identity, a direct mapping from combinations of s and ρ to the Dirac spinor indices emerges as listed in table 7.1. In the following, we will adopt the notation from that table in which we denote a spin-up quark-state with + and a spin-down state with −.

Table 7.1: Identification of Dirac indices α with spin and parity eigenvalues in the Dirac-Pauli representation. + and − are to be understood as ±1 respectively.

α	ρ	s
1	+	+
2	+	−
3	−	+
4	−	−

For baryonic operators, we now have to consider a product state of three quarks with color, spinor, and flavor components. For the purpose of the operator construction, we ignore the spatial information assuming all three quarks to be at the same position as in eq. (7.1). The operators discussed here are classified based on the symmetries of the three spin, color, and flavor indices. The color indices of the three quarks have to be antisymmetrized in order to construct a gauge-invariant state. Thus, in order to fulfill the spin-statistic theorem, the combined spinor and flavor components have to be either symmetric under the exchange of two quarks or have no symmetry under this exchange so that the overall state is totally antisymmetric under exchange of two quarks.
In the isospin-symmetric limit with a heavier strange quark, the SU(3)-octet and decuplet baryons are classified by their flavor content and flavor symmetry in the sense that the flavor component of the baryonic state can be symmetric under exchange of up- and down-quarks but not under exchange of light- and strange-quarks. In this classification there are 5 baryons with total symmetry under exchange of two flavors (Ω^-, Δ^{++}, Δ^+, Δ^0, and Δ^-) consisting of only strange-quarks or only light-quarks respectively.[2] Next, there are 10 baryons that have flavor symmetry in two of their three quarks (which we call *mixed symmetry*). 6 of these consist of two light-quarks and one strange-quark (Σ^+, Σ^0, Σ^-, as well as their first excited states), the other 4 have one light- and two strange-quarks (Ξ^0, Ξ^-, and their first excited states). Furthermore, the states can be antisymmetric in their flavor content giving rise to 1 mixed antisymmetric baryon with one strange-quark (Λ), and 2 mixed antisymmetric states consisting only of light-quarks (p and n). An additional singlet state which does not correspond to the octet or decuplet can be constructed with totally antisymmetric quark-flavor content, which we denote as Λ^0. For a list of the various states and their quark-flavor symmetrization see table C.3.

[2]The symmetry here only refers to the quark-flavors and the mentioned quark content only refers to the valence quarks.

In order to fulfill the symmetry requirements on the complete baryonic state discussed above, this restricts the symmetry of the Dirac-indices of quark fields to be identical to the flavor symmetry. The Dirac-structure of the baryonic interpolators are constructed from products of three ρ- and three s-spins as shown in table 7.3. The Weyl-spinor states going into the Dirac-spinor construction are listed in table 7.2.

Table 7.2: ρ-/s-spin combinations defining totally symmetric (S), mixed-symmetric (MS), and mixed-antisymmetric (MA) baryonic states [12].

Symmetry	Spin	State construction
S	$3/2$	$\lvert+++\rangle$
	$1/2$	$\frac{1}{\sqrt{3}}(\lvert++-\rangle + \lvert+-+\rangle + \lvert-++\rangle)$
	$-1/2$	$\frac{1}{\sqrt{3}}(\lvert+--\rangle + \lvert-+-\rangle + \lvert--+\rangle)$
	$-3/2$	$\lvert---\rangle$
MS	$1/2$	$\frac{1}{\sqrt{6}}(2\lvert++-\rangle - \lvert+-+\rangle - \lvert-++\rangle)$
	$-1/2$	$\frac{1}{\sqrt{6}}(\lvert-+-\rangle + \lvert+--\rangle - 2\lvert--+\rangle)$
MA	$1/2$	$\frac{1}{\sqrt{2}}(\lvert+-+\rangle - \lvert-++\rangle)$
	$-1/2$	$\frac{1}{\sqrt{2}}(\lvert+--\rangle - \lvert-+-\rangle)$

Table 7.3: Decomposition of Dirac spin symmetries in ρ-/s-spin symmetries for the relevant baryonic spin irreps G_1 and H [12].

Dirac symmetry	Irrep	$\rho \otimes s$
S	G_1	MA $\otimes$ MA + MS $\otimes$ MS
	H	S $\otimes$ S
MS	G_1	S $\otimes$ MS MA $\otimes$ MA – MS $\otimes$ MS
	H	MS $\otimes$ S
MA	G_1	S $\otimes$ MA MA $\otimes$ MS + MS $\otimes$ MA
	H	MA $\otimes$ S
A	G_1	MA $\otimes$ MS – MS $\otimes$ MA

As an example of this construction, consider the proton interpolator with spin-up (i.e. $s_z = +\frac{1}{2}$) and even parity. In the classification above, the proton's flavor content is mixed-antisymmetric, i.e. it is a linear combination of interpolators of the form

$$p_{\mu_1\mu_2\mu_3} = \frac{1}{\sqrt{2}}\varepsilon_{abc}\big(u^a_{\mu_1} d^b_{\mu_2} - d^a_{\mu_1} u^b_{\mu_2}\big)u^c_{\mu_3}$$

with different combinations of Dirac-indices μ_i and implicit sum over the color indices a, b, and c. As a spin-$\frac{1}{2}$ state, its transforms under the G_1 irrep (see section 3.4, especially table 3.2 for more details on the correspondence of continuum- and lattice-irrep of the spin-group). Looking up the decomposition of the mixed-antisymmetric Dirac-structure for G_1 in table 7.3, we find that the first variant is S $\otimes$ MA, i.e. totally symmetric ρ-spin and mixed-antisymmetric s-spin. A state with totally symmetric ρ-spin has even parity for $\rho_3 = \frac{3}{2}$ and $\rho_3 = -\frac{1}{2}$ as these

states have an even number of quarks with negative parity-eigenvalue (to see this, compare the entries in table 7.2 with eq. (7.5)). We thus find, that one option for such an operator has $\rho = |+++\rangle$ and $s = \frac{1}{\sqrt{2}}(|+-+\rangle - |-++\rangle)$ and therefore the Dirac-structure is given by

$$\begin{aligned} p_D =& \rho \otimes s = |+++\rangle \otimes \frac{1}{\sqrt{2}}(|+-+\rangle - |-++\rangle) \\ =& \frac{1}{\sqrt{2}}\left(\left|\begin{matrix}+\\+\\+\end{matrix}\right\rangle - \left|\begin{matrix}+\\-\\+\end{matrix}\right\rangle\right). \end{aligned}$$

Each column in these kets can now be mapped to a Dirac-spinor index via table 7.1, where we find that $\begin{matrix}+\\+\end{matrix}$ corresponds to the index 1 and $\begin{matrix}+\\-\end{matrix}$ corresponds to the index 2. We thus find that the total interpolator for the proton is given by

$$p = \frac{1}{\sqrt{2}}(p_{121} - p_{211}) = \frac{1}{2}\varepsilon_{abc}\left(u_1^a d_2^b - d_1^a u_2^b - u_2^a d_1^b + d_2^a u_1^b\right) u_1^c$$

This operator can further be simplified using the observation that

$$\begin{aligned} p_{\mu_1\mu_2\mu_3} =& \frac{1}{\sqrt{2}}\varepsilon_{abc}\left(u_{\mu_1}^a d_{\mu_2}^b - d_{\mu_1}^a u_{\mu_2}^b\right) u_{\mu_3}^c = \frac{1}{\sqrt{2}}\varepsilon_{abc}\left(-d_{\mu_2}^b u_{\mu_1}^a + u_{\mu_2}^b d_{\mu_1}^a\right) u_{\mu_3}^c \\ =& \frac{1}{\sqrt{2}}\varepsilon_{abc}\left(d_{\mu_2}^a u_{\mu_1}^b - u_{\mu_2}^a d_{\mu_1}^b\right) u_{\mu_3}^c = -p_{\mu_2\mu_1\mu_3} \end{aligned}$$

making use of the Graßmann nature of quark operators and the antisymmetry of the Levi-Civita-symbol. This results in a simplified operator

$$p = \sqrt{2} p_{121} = \varepsilon_{abc}\left(u_1^a d_2^b - d_1^a u_2^b\right) u_1^c.$$

A full list of all operators used can be found in section C.2 in tables C.4 to C.7.

7.2. Sources

Consider a quark propagator $\mathcal{S}$ which is a $(V \times V) \otimes (N_S \times N_S) \otimes (N_C \times N_C)$ component object where V is the lattice volume (i.e. the total number of lattice points), N_S is the number of spinor components and N_C is the number of colors. This notation is to be understood as $\mathcal{S}$ acting like a $V \times V$ matrix in space-time, a $N_S \times N_S$ matrix in spinor space, and a $N_C \times N_C$ matrix in color space. A complete computation of such a propagator is unfeasible with (at the time of writing of this thesis) available hardware. This is mostly due to the immense size of these propagators. For example for the largest box of 192×96^3 lattice sites, this matrix in spacetime, spinor, and color indices would take up 57.7 EiB of storage. Even on the smallest box with 48×24^3 lattice sites, it would still need $\sim$ 1 PiB. However, as the physical theory behind LQCD simulations is translationally invariant, the expectation value of a propagator entry $\langle \mathcal{S}(y,x) \rangle$ is simply a function of the distance between the spacetime points x and y, i.e. $\langle \mathcal{S}(y,x) \rangle \equiv \langle \mathcal{S}(y-x) \rangle$.[3] One could thus also average all the different entries of the propagator with the two positions at the same distance. However, this would still require the computation of $V \cdot N_S \cdot N_C$ objects with $V \cdot N_S \cdot N_C$ components which is still not viable with modern hardware. Instead, one thus approximates this exact average stochastically with *sources* of which we discuss a certain type used in our computations in the following.

[3] The expectation values $\langle \cdot \rangle$ are meant w.r.t. the path integral measure.

7.2.1. Point Sources

The propagator $\langle \mathcal{S}(y-x) \rangle$ can be stochastically approximated at certain distances by only computing a column of the propagator $\mathcal{S}(y,x)$, i.e. we fix the position x and the respective spin and color indices α and a at x_{src}, α_{src}, and a_{src}. This can be written as [29]

$$\mathcal{S}(y, x_{\text{src}})^{ba_{\text{src}}}_{\beta\alpha_{\text{src}}} = \sum_{x,\alpha,a} \mathcal{S}(y,x)^{ba}_{\beta\alpha} \eta(x, x_{\text{src}})^{aa_{\text{src}}}_{\alpha\alpha_{\text{src}}} \tag{7.6}$$

where

$$\eta(x, x_{\text{src}})^{aa_{\text{src}}}_{\alpha\alpha_{\text{src}}} = \delta(x - x_{\text{src}}) \delta_{\alpha\alpha_{\text{src}}} \delta_{aa_{\text{src}}}.$$

In this expression, η is what is known as a *point source* in the context of LQFT. The restricted propagator on the left-hand-side of eq. (7.6) is also called a *one-to-all* propagator since it physically describes a particle at x_{src} which then propagates to any other spacetime point y on the lattice. To get a stochastic estimate of $\langle \mathcal{S}(y-x) \rangle$ one can then compute different $\mathcal{S}(y, x_{\text{src},i})$, $i \in \{1, ..., n\}$ for several source positions and approximate

$$\langle \mathcal{S}(\Delta x) \rangle \approx \frac{1}{n} \sum_{i=1}^{n} \mathcal{S}(x_{\text{src},i} + \Delta x, x_{\text{src},i}).$$

7.2.2. Source Smearing

A problem with simple point-like sources as in eq. (7.6) shows when trying to compute ground state energies using eq. (7.2). One usually finds that the operator $\mathcal{O}$ defined as a point-source has a low overlap with the ground state $|0\rangle$ resulting in a very late ground state domination in the correlation function. This effect is showcased in fig. 7.1. An approach to fix this is to construct sources that resemble more physical wave functions [91]

$$\tilde{\eta}(\mathbf{x}, t) = \sum_{\mathbf{x}' \in \Lambda_S} F(\mathbf{x}, \mathbf{x}') \eta(\mathbf{x}', t) \tag{7.7}$$

where η is a point-like fermion source which results in modified propagators

$$\tilde{\mathcal{S}}(y,x) = \left\langle \sum_{\mathbf{x}', \mathbf{y}' \in \Lambda_S} \eta(t_y, \mathbf{y}') F(\mathbf{y}', \mathbf{y}) F(\mathbf{x}, \mathbf{x}')^* \bar{\eta}(t_x, \mathbf{x}') \right\rangle. \tag{7.8}$$

This procedure is known as *source smearing* as it extends the point-source to a less local object. The procedure used in this work is known as *Wuppertal smearing* and is defined by iteratively applying a gauge-covariant transformation [92, 93]

$$\begin{aligned} \eta(\mathbf{x}, t) &\mapsto \gamma \sum_{\mathbf{x}' \in \Lambda_S} \left(\delta_{\mathbf{x},\mathbf{x}'} + \kappa_G H(\mathbf{x}, \mathbf{x}') \right) \eta(\mathbf{x}, t) \\ H(\mathbf{x}, \mathbf{x}') &= \sum_{\mu=1}^{3} \left(U_\mu(x) \delta_{x', x+\hat{\mu}} + U^\dagger_\mu(x - \hat{\mu}) \delta_{x', x-\hat{\mu}} \right) \end{aligned} \tag{7.9}$$

N times with a free parameter κ_G.
Note, that the smeared sources are still point-like in the time direction. Thus, the time separation of source and sink is still well-defined in the context of Wuppertal-smeared point sources which allows for a rigorous treatment of hadronic correlation functions constructed from smeared operators.
For examples of the effects of Wuppertal smearing on the correlation function and the effective mass, see figs. 7.1 and 7.2.

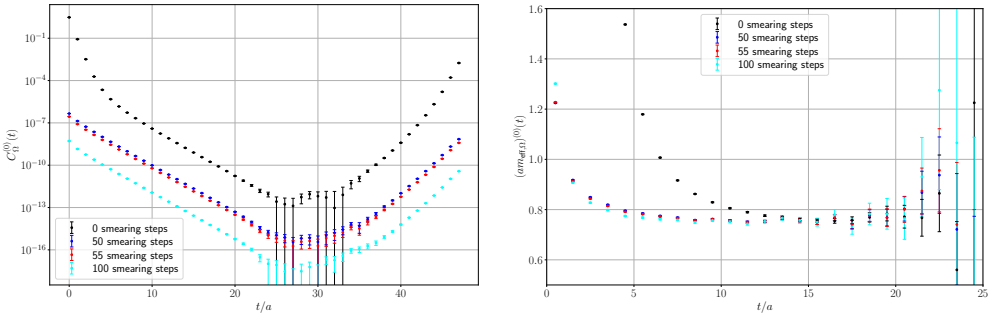

Figure 7.1: Zero-momentum-projected correlation function (left) and effective masses (right, see eq. (7.12)) of the Ω baryon for different number of iterations of Wuppertal smearing with $\kappa_G = 1.1$ on the periodic A654 CLS ensemble. t/a denotes the temporal difference of source and sink.

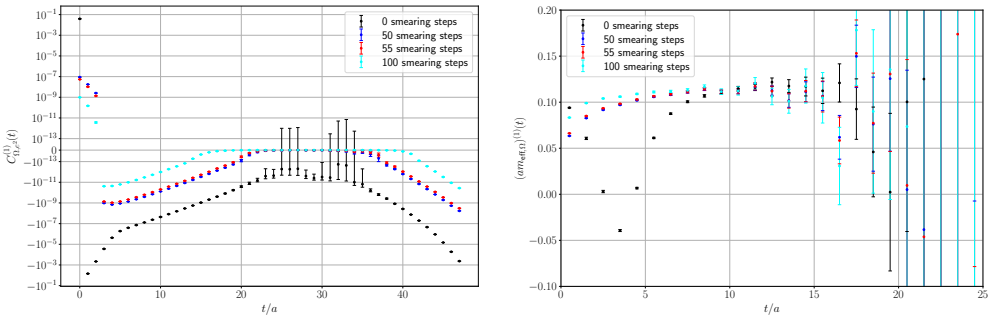

Figure 7.2: Zero-momentum-projected correlation function (left) and effective masses (right, see eq. (7.18)) of the first order QED correction Ω baryon for different number of iterations of Wuppertal smearing with $\kappa_G = 1.1$ on the A654 CLS ensemble. t/a denotes the temporal difference of source and sink.

7.2.3. Link Smearing

A typical problem in gauge theory simulations are strong short-distance fluctuations in the gauge links [94, 95]. These fluctuations negatively impact the uncertainties of observables even at long distances. To reduce these unwanted effects, it is common practice to define operators in terms of smoothed gauge links. In the project of this thesis, *APE smearing* [95] is used which replaces individual gauge links U_μ by a weighted average V_μ of the gauge link itself and the staples $C_{\mu\nu}$ connecting the ends of the link [29]:

$$V_\mu(x) = (1-\alpha)U_\mu + \frac{\alpha}{6}\sum_{\nu\neq\mu} C_{\mu\nu}(x), \text{ where} \tag{7.10}$$

$$C_{\mu\nu}(x) = U_\nu(x)U_\mu(x+\hat{\nu})U_\nu(x+\hat{\mu})^\dagger + U_\nu(x-\hat{\nu})^\dagger U_\mu(x-\hat{\nu})U_\nu(x-\hat{\nu}+\hat{\mu}).$$

For $U_\mu(x) \in \mathrm{SU}(3)$, the smeared link $V_\mu(x)$ is in general not an element of SU(3) and thus has to be projected back onto the gauge group [95]. This can be achieved by scaling the gauge link such that it has determinant 1 [96, 97], i.e. $V_\mu(x) \mapsto \frac{1}{\det V_\mu(x)} V_\mu(x)$. A more commonly used practice, however, is to choose the element $X \in \mathrm{SU}(3)$ that maximizes $\mathrm{Re}\left(\mathrm{tr}\left[XV_\mu^\dagger(x)\right]\right)$ to replace $U_\mu(x)$ [29, 98].

This method of link smearing is usually iteratively applied, replacing the new, smeared gauge link V_μ again using the procedure in eq. (7.10). However, the number of iterations of this algorithm and the parameter α have to be carefully balanced as not to change underlying physical properties of the theory [99].
While link-smearing methods are effective for the treatment of long-distance observables in pure gauge theories where quarks are introduced in a quenched manner, they cannot be used as is in combination with fermionic actions that introduce non-localities in the sea-quark sector [100]. However, as described in [100], one can replace gauge links by smeared links in eq. (7.9) when smearing quark sources in order to further improve the overlap of the smeared operators with the ground state.

7.3. Correlation functions

The calculations performed for this thesis use the operators introduced in section 7.1 for baryons and operators of the form

$$\mathcal{O}_M(x) = \sum_{f_1,f_2\in\{u,d,s\}} c_M^{f_1f_2} \sum_a \bar{q}^a_{f_1}(x)\gamma_5 q^a_{f_2}(x),$$

for pseudo-scalar mesons where $q^a_{f_i}$ denotes a valence quark of M with flavor f_i and color a and $c_M^{f_1f_2}$ are normalization coefficients satisfying $\sum_{f_1,f_2\in\{u,d,s\}} \left|c_M^{f_1f_2}\right|^2 = 1$, e.g. $c_{K^+}^{f_1f_2} = \delta_{f_1s}\delta_{f_2u}$, $c_{\pi^0}^{f_1f_2} = \frac{1}{\sqrt{2}}\left(\delta_{f_1u}\delta_{f_2u} - \delta_{f_1d}\delta_{f_2d}\right)$.
The correlation functions considered in this thesis are hadronic two-point functions for these operators of the form $C_M(y,x) = \mathrm{tr}\left\langle \mathcal{O}_M(y)\bar{\mathcal{O}}_M(x)\right\rangle$. In order to calculate these correlation functions, they first have to be expressed in terms of propagators using Wick's theorem (see eqs. (2.14) and (2.15)). For example, consider the 2-point correlation function for the K^+ meson

$$\begin{aligned} C_M(y,x) &= \mathrm{tr}\left\langle \overbrace{\bar{s}(y)\gamma_5 \overbrace{u(y)\bar{u}(x)}\gamma_5 s(x)}\right\rangle = \mathrm{tr}\left\langle \gamma_5 \overbrace{s(x)\bar{s}}(y)\gamma_5 \overbrace{u(y)\bar{u}}(x)\right\rangle \\ &= \mathrm{tr}\left[\gamma_5 \mathcal{S}_s(x,y)\gamma_5 \mathcal{S}_u(y,x)\right] = \mathrm{tr}\left[\mathcal{S}_s{}^\dagger(y,x)\mathcal{S}_u(y,x)\right] \end{aligned}$$

where in the first row we rearranged the terms using the cyclic symmetry of the trace. In the last step we made use of γ_5-hermiticity (see eq. (3.18)) to rewrite the antiquark propagator in terms of one propagating in the opposite direction. This has the advantage, that each quark propagator only needs to be calculated once per quark source which can then be used for the antiquarks as well. The above correlation function would diagrammatically be denoted as

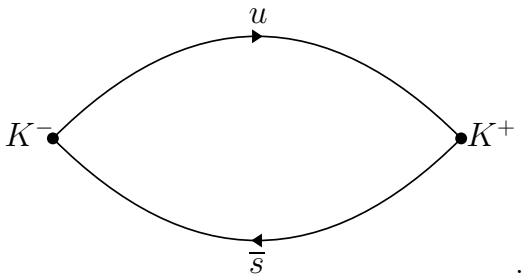

.

For mesons with quark and antiquark of the same flavor, there are additional quark-disconnected contributions:

$$\begin{aligned} C_{ff}(y,x) &= \mathrm{tr}\left\langle \bar{q}_f(y)\gamma_5 q_f(y)\bar{q}_f(x)\gamma_5 q_f(x)\right\rangle \\ &= \underbrace{\mathrm{tr}\left\langle \gamma_5 \overbrace{q_f(x)\bar{q}_f(y)}\gamma_5 \overbrace{q_f(y)\bar{q}_f(x)}\right\rangle}_{=\mathrm{tr}\left[\mathcal{S}_f{}^\dagger(y,x)\mathcal{S}_f(y,x)\right]} + \underbrace{\mathrm{tr}\left\langle \overbrace{\bar{q}_f(y)\gamma_5 q_f(y)}\overbrace{\bar{q}_f(x)\gamma_5 q_f(x)}\right\rangle}_{=:\mathrm{disc.}(y,x)} \end{aligned}$$

The first term is similar to the K^+ correlation function, while the second one corresponds to two quark loops:[4]

$$\begin{aligned} \mathrm{disc.}(y,x) &= \sum_{\substack{\alpha,\beta,\gamma,\delta \\ a,b}} \gamma_{5,\alpha\beta}\gamma_{5,\gamma\delta}\left\langle \overbrace{\bar{q}^a_{f,\alpha}(y)q^a_{f,\beta}}(y)\overbrace{\bar{q}^b_{f,\gamma}(x)q^b_{f,\delta}}(x)\right\rangle \\ &= \sum_{\substack{\alpha,\beta,\gamma,\delta \\ a,b}} \gamma_{5,\alpha\beta}\gamma_{5,\gamma\delta}\mathcal{S}^{aa}_{f,\beta\alpha}(y,y)\mathcal{S}^{bb}_{f,\delta\gamma}(x,x) \\ &= \mathrm{tr}\left[\gamma_5\mathcal{S}_f(y,y)\right]\mathrm{tr}\left[\gamma_5\mathcal{S}_f(x,x)\right] \end{aligned}$$

where the Greek indices are spinor-indices and a, b are color-indices. For the neutral pion $\pi^0 = \frac{1}{\sqrt{2}}\left(\bar{u}\gamma_5 u - \bar{d}\gamma_5 d\right)$, for example, the correlation function is given by

$$\begin{aligned} C_{\pi^0}(y,x) = \frac{1}{2}\Big\langle &\mathrm{tr}\left[\mathcal{S}_u{}^\dagger(y,x)\mathcal{S}_u(y,x)\right] + \mathrm{tr}\left[\mathcal{S}_d{}^\dagger(y,x)\mathcal{S}_d(y,x)\right] \\ &+ \mathrm{tr}[\gamma_5\mathcal{S}_u(y,y)]\,\mathrm{tr}[\gamma_5\mathcal{S}_u(x,x)] + \mathrm{tr}[\gamma_5\mathcal{S}_d(y,y)]\,\mathrm{tr}[\gamma_5\mathcal{S}_d(x,x)] \\ &- \mathrm{tr}[\gamma_5\mathcal{S}_u(y,y)]\,\mathrm{tr}[\gamma_5\mathcal{S}_d(x,x)] - \mathrm{tr}[\gamma_5\mathcal{S}_d(y,y)]\,\mathrm{tr}[\gamma_5\mathcal{S}_u(x,x)]\Big\rangle \end{aligned}$$

or

$$\frac{1}{2}\sum_{f_1,f_2}\Bigg(\mathfrak{c}_{f_1f_2}\,\pi_{f_1f_2} \;\; \underset{\bar{f}_2}{\overset{f_1}{\bigcirc}} \;\; \pi_{f_1f_2} + \mathfrak{d}_{f_1f_2}\,\pi_{f_1} \;\; \bigcirc \;\; \pi_{f_2} \Bigg)$$

in diagrammatic form with $\mathfrak{c}_{f_1f_2} = \delta_{f_1f_2}$, $\mathfrak{d}_{f_1f_2} = \delta_{f_1f_2} - \delta_{f_1u}\delta_{f_2d} - \delta_{f_1d}\delta_{f_2u}$.
For baryonic correlation functions, we use the operators described in section 7.1. As an example, take (one of the) simplest operators,[5] Ω_{111}. These operators use explicit spinor-indices and thus, we write out the spin-indices (all 1 in this case) and color indices (roman letters) explicitly:

$$C_{\Omega^-}(y,x) = \sum_{a,b,c,d,e,f}\varepsilon_{abc}\varepsilon_{def}\left\langle s^a_1(y)s^b_1(y)s^c_1(y)\bar{s}^f_1(x)\bar{s}^e_1(x)\bar{s}^d_1(x)\right\rangle.$$

[4] Each of the contractions comes with a minus sign from anticommuting the q and $\bar{q}$ which cancel to a positive overall sign.

[5] For a complete list of all operators see section C.2, tables C.4 to C.7 in the appendix.

There are six possible contractions of these terms:

$$\left\langle \overbrace{s_1^a(y)\overbrace{s_1^b(y)\overbrace{s_1^c(y)\bar{s}_1^f(x)}\bar{s}_1{}^e(x)}\bar{s}_1^d(x)} \right\rangle = -\left\langle \overbrace{s_1^a(y)\bar{s}_1^f(x)}\overbrace{s_1^b(y)\bar{s}_1^e(x)}\overbrace{s_1^c(y)\bar{s}_1^d(x)} \right\rangle$$
$$= -\mathcal{S}_{s,11}^{af}(y,x)\mathcal{S}_{s,11}^{be}(y,x)\mathcal{S}_{s,11}^{cd}(y,x)$$

$$\left\langle \overbrace{s_1^a(y)\overbrace{s_1^b(y)\overbrace{s_1^c(y)\bar{s}_1^f(x)}\bar{s}_1{}^e(x)\bar{s}_1^d(x)}} \right\rangle = \left\langle \overbrace{s_1^a(y)\bar{s}_1^f(x)}\overbrace{s_1^b(y)\bar{s}_1^d(x)}\overbrace{s_1^c(y)\bar{s}_1^e(x)} \right\rangle$$
$$=\mathcal{S}_{s,11}^{af}(y,x)\mathcal{S}_{s,11}^{bd}(y,x)\mathcal{S}_{s,11}^{ce}(y,x)$$

$$\left\langle \overbrace{s_1^a(y)\overbrace{s_1^b(y)\overbrace{s_1^c(y)\bar{s}_1^f(x)}\bar{s}_1{}^e(x)}\bar{s}_1^d(x)} \right\rangle = \left\langle \overbrace{s_1^a(y)\bar{s}_1^e(x)}\overbrace{s_1^b(y)\bar{s}_1^f(x)}\overbrace{s_1^c(y)\bar{s}_1^d(x)} \right\rangle$$
$$=\mathcal{S}_{s,11}^{ae}(y,x)\mathcal{S}_{s,11}^{bf}(y,x)\mathcal{S}_{s,11}^{cd}(y,x)$$

$$\left\langle \overbrace{s_1^a(y)\overbrace{s_1^b(y)\overbrace{s_1^c(y)\bar{s}_1^f(x)}\bar{s}_1{}^e(x)\bar{s}_1^d(x)}} \right\rangle = -\left\langle \overbrace{s_1^a(y)\bar{s}_1^e(x)}\overbrace{s_1^b(y)\bar{s}_1^d(x)}\overbrace{s_1^c(y)\bar{s}_1^f(x)} \right\rangle$$
$$= -\mathcal{S}_{s,11}^{ae}(y,x)\mathcal{S}_{s,11}^{bd}(y,x)\mathcal{S}_{s,11}^{cf}(y,x)$$

$$\left\langle \overbrace{s_1^a(y)\overbrace{s_1^b(y)\overbrace{s_1^c(y)\bar{s}_1^f(x)}\bar{s}_1{}^e(x)}\bar{s}_1^d(x)} \right\rangle = -\left\langle \overbrace{s_1^a(y)\bar{s}_1^d(x)}\overbrace{s_1^b(y)\bar{s}_1^f(x)}\overbrace{s_1^c(y)\bar{s}_1^e(x)} \right\rangle$$
$$= -\mathcal{S}_{s,11}^{ad}(y,x)\mathcal{S}_{s,11}^{bf}(y,x)\mathcal{S}_{s,11}^{ce}(y,x)$$

$$\left\langle \overbrace{s_1^a(y)\overbrace{s_1^b(y)\overbrace{s_1^c(y)\bar{s}_1^f(x)}\bar{s}_1{}^e(x)\bar{s}_1^d(x)}} \right\rangle = \left\langle \overbrace{s_1^a(y)\bar{s}_1^d(x)}\overbrace{s_1^b(y)\bar{s}_1^e(x)}\overbrace{s_1^c(y)\bar{s}_1^f(x)} \right\rangle$$
$$=\mathcal{S}_{s,11}^{ad}(y,x)\mathcal{S}_{s,11}^{be}(y,x)\mathcal{S}_{s,11}^{cf}(y,x)$$

Using the symmetries of the Levi-Civita-symbol, the correlation function can be simplified to

$$C_{\Omega^-}(y,x) = 6\sum_{a,b,c,d,e,f}\varepsilon_{abc}\varepsilon_{def}\mathcal{S}_{s,11}^{ad}(y,x)\mathcal{S}_{s,11}^{be}(y,x)\mathcal{S}_{s,11}^{cf}(y,x)$$

which diagrammatically would be expressed as

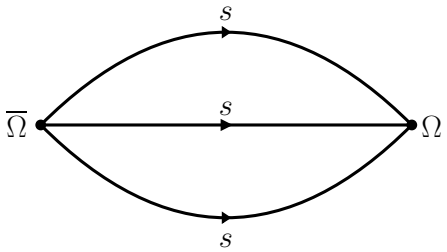

As this kind of calculation gets tedious quite quickly, a `python` program was written at the beginning of the project to compute all these contractions for

isospin-symmetric and isospin-breaking contributions, that algebraically simplifies the results and produces `C++`-code (see section 8.1.5 and listings 8.1 and 8.2) to compute the contraction for a given correlation function.

7.4. Effective Mass

In order to extract the ground state mass from a correlation function as defined in eq. (7.1), one makes use of the asymptotic behaviour (eq. (7.3)) to define an *effective mass*

$$m_{\text{eff}}(t) = -\frac{\mathrm{d}}{\mathrm{d}t} \ln C(t) \xrightarrow{t\to\infty} m. \tag{7.11}$$

For large enough t, the contributions of excited states in the exponential tower eq. (7.2) become subdominant and this function tends to a plateau corresponding to the ground-state mass of the hadron described by the operator used for the correlation function. On the lattice, eq. (7.11) has to be calculated using a discretized version of the derivative. A common choice for this is the forward derivative eq. (3.1) which results in the discretization

$$am_{\text{eff}}^{\text{forward}}(t) = \frac{1}{a} \ln\left(\frac{C(t)}{C(t+a)}\right).$$

However, in the scope of this thesis, we choose to define the effective mass at half-integer multiples of the lattice spacing, i.e.

$$am_{\text{eff}}\left(t+\frac{1}{2}\right) = \frac{1}{a} \ln\left(\frac{C(t)}{C(t+a)}\right), \tag{7.12}$$

which corresponds to the symmetric discretization of the derivative (eq. (3.2)) at half the lattice spacing since this improves the continuum limit.
At finite propagation time t, the effective mass is always influenced by excited states and thus never truly reaches a plateau. However, as we are dealing with noisy data in practice, the excited state effects are subdominant to the uncertainty of the measured effective mass at large enough t. Thus, the large-t behaviour of the effective mass cannot be distinguished from an actual plateau. The asymptotic mass m obtained from a fit to a plateau in the tail of the effective mass can then reasonably be identified with the ground-state mass of the hadron in question.
On lattices with periodic boundary conditions the pseudoscalar mesonic correlation function is symmetric under time reversal such that the exponential tower takes the form

$$\begin{aligned} C(t) &= \sum_n c_n \left(e^{-E_n t} + e^{E_n (t-T)}\right) = \sum_n c_n e^{\frac{T}{2}} \left(e^{-E_n \left(t-\frac{T}{2}\right)} + e^{E_n \left(t-\frac{T}{2}\right)}\right) \\ &= \sum_n \tilde{c}_n \cosh\left(E_n \left(t - \frac{T}{2}\right)\right) \end{aligned} \tag{7.13}$$

This allows for a more robust definition of the effective mass making use of this symmetry via

$$\frac{C(t)}{C(t+a)} = \frac{\cosh\left(m_{\text{eff}}\left(t+\frac{a}{2}\right) \cdot \left(t-\frac{T}{2}\right)\right)}{\cosh\left(m_{\text{eff}}\left(t+\frac{a}{2}\right) \cdot \left(t+a-\frac{T}{2}\right)\right)} \tag{7.14}$$

which has to be solved numerically for $m_{\text{eff}}(t)$ on each (half) timeslice.

While on ensembles with open boundary conditions the mesonic correlation function is not exactly symmetric, the symmetry holds approximately as long as t is far enough away from the boundary. Thus, if the source and sink are close enough to the center of the lattice, one can take the average $\bar{C}(t) = \frac{1}{2}(C(t) + C(-t)) \approx C(t)$ for small enough $|t|$ to effectively increase the number of measurements. For sources close to one of the boundaries, one can instead use only the direction away from the closest boundary in order to avoid boundary effects at early times in $C(t)$. For octet and decuplet baryons, a similar trick can be applied by using the fact that the correlation function of two states $\mathcal{O}_+$ and $\mathcal{O}_-$ differing only in the parity eigenvalue are related via [29]

$$C_{\mathcal{O}_\pm}(t) = -C_{\mathcal{O}_\mp}(-t)$$

on open boundary ensembles or ensembles with antiperiodic temporal boundary conditions for fermionic fields, which is the case for the CLS ensembles. In the construction described in section 7.1, the negative-parity operator $\mathcal{O}_-$ corresponding to a positive-parity operator $\mathcal{O}_+$ can be identified by taking the operator with the same irrep, quark flavor content and s-spin and exchanging ρ with $-\rho$. These pairs can easily be read off the tables C.4 to C.7.

Effective Mass for Isospin-breaking Corrections

In the context of the RM123 approach described in section 5.2, we do not have access to the full correlation functions in QCD+QED with non-degenerate light-quarks. Thus, in order to define an effective mass that helps with the computation of the corrections to the ground-state masses of hadrons, an expansion of the asymptotic correlation function (eq. (7.3)) in terms of isospin-breaking parameters has to be considered and matched to the expansions in (see section 5.2 for the expansion and section 10.2 for an example of matching conditions used in this thesis).
Consider the asymptotic correlation function $C(t) = ce^{-mt}$ in QCD+QED. In this expression, c and m (and thus also C) depend on the values of the quark masses and the electromagnetic coupling and thus have to be expanded, i.e.

$$X = X^{(0)} + \sum_i \Delta\varepsilon_i X_i^{(1)} + \mathcal{O}(\Delta\varepsilon^2)$$

for $X \in \{c, m, C(t)\}$. Performing this expansion up to first order in all these quantities, one finds

$$C^{(0)}(t) + \sum_i \Delta\varepsilon_i C_i^{(1)}(t) = c^{(0)} e^{-m^{(0)}t} + \sum_i \Delta\varepsilon_i \Big(c_i^{(1)} - c^{(0)} m_i^{(1)} t\Big) e^{-m^{(0)}t} \tag{7.15}$$

which leads to the identification

$$\begin{aligned} C^{(0)}(t) =& c^{(0)} e^{-m^{(0)}t}, \\ C_i^{(1)}(t) =& \Big(c_i^{(1)} - c^{(0)} m_i^{(1)} t\Big) e^{-m^{(0)}t}, \end{aligned} \tag{7.16}$$

where $C_i^{(1)}(t)$ are the corrections to the correlation functions computed with the RM123 approach on isospin-symmetric QCD gauge ensembles.

In order to construct an effective mass that, as for the standard version discussed above, asymptotically converges to the mass correction $m_i^{(1)}$ for each contribution, we make use of the observation that

$$C_i^{(1)}(t) = \left(\frac{c_i^{(1)}}{c^{(0)}} - m_i^{(1)} t\right) C^{(0)}(t).$$

Thus, the ratio of first order and zeroth order correlation functions is a linear function in t with the slope equal to the desired quantity $m_i^{(1)}$, leading to the definition of the first-order effective mass

$$m_{\mathrm{eff},i}^{(1)}(t) = -\frac{\mathrm{d}}{\mathrm{d}t}\frac{C_i^{(1)}(t)}{C^{(0)}(t)}. \tag{7.17}$$

In order to calculate this quantity on the lattice, we again need to discretize this expression for which we take the forward derivative, just as for eq. (7.12) to get to the expression

$$a m_{\mathrm{eff},i}^{(1)}\left(t + \frac{a}{2}\right) = \frac{C_i^{(1)}(t)}{C^{(0)}(t)} - \frac{C_i^{(1)}(t+a)}{C^{(0)}(t+a)}. \tag{7.18}$$

As in the isospin-symmetric case, one can utilize the symmetry of the correlation function for pseudoscalar mesonic sates on periodic boundary conditions. Expanding the first term of eq. (7.13) in terms of isospin-breaking parameters, one finds

$$\begin{aligned} C(t) =& \tilde{c}\cosh(m\tau) = C^{(0)}(t) + \sum_i \Delta\varepsilon_i C^{(1)}(t) \\ =& \tilde{c}^{(0)}\cosh(m\tau) + \sum_i \Delta\varepsilon_i \left[\tilde{c}^{(1)}\cosh\left(m^{(0)}\tau\right) + \tilde{c}^{(0)} m^{(1)} \tau \sinh\left(m^{(0)}\tau\right)\right] \end{aligned}$$

where $\tau = t - \frac{T}{2}$. Plugging these definitions into eq. (7.18) results in

$$\frac{C_i^{(1)}(t)}{C^{(0)}(t)} - \frac{C_i^{(1)}(t+a)}{C^{(0)}(t+a)} = m^{(1)}\left[F\left(t - \frac{T}{2}\right) - F\left(t + a - \frac{T}{2}\right)\right]$$

where $F(t) = t\tanh\left(m^{(0)} \cdot t\right)$. This suggests a definition of the first-order effective mass for symmetric correlation functions via

$$m_{\mathrm{eff},i}^{(1)}\left(t + \frac{a}{2}\right) = \frac{\frac{C_i^{(1)}(t)}{C^{(0)}(t)} - \frac{C_i^{(1)}(t+a)}{C^{(0)}(t+a)}}{F\left(t - \frac{T}{2}\right) - F\left(t + a - \frac{T}{2}\right)}. \tag{7.19}$$

Note that this definition requires prior knowledge of the isospin-symmetric asymptotic mass which has to be determined beforehand e.g. via a fit to the isospin-symmetric effective mass.

7.5. Generalized Eigenvalue Problem

Consider a set of N operators $\mathcal{O}_i$ describing the same state. We then define the *cross correlator* of the i-th and j-th operator as the expectation value [101, 102]

$$\begin{aligned} C_{ij}(t) &= \left\langle \mathcal{O}_i(t)\bar{\mathcal{O}}_j(0)\right\rangle = \sum_{n=1}^{\infty} c_{n,ij} e^{-E_n t}, \\ c_{n,ij} &= \langle 0|\mathcal{O}_i|n\rangle\langle n|\bar{\mathcal{O}}_j|0\rangle \in \mathbb{C}. \end{aligned}$$

This defines a Hermitean $N \times N$ matrix $C(t)$ for each time slice t. These matrices can be used to determine excited state energies, i.e. the energies E_n with $n > 1$ using the methods discussed in section 7.4. This can be done via a *generalized eigenvalue problem* (GEVP) defined by [101, 102]

$$C(t)v_n(t,t_0) = \lambda_n(t,t_0)C(t_0)v_n(t,t_0).$$

For the generalized eigenvalues $\lambda(t,t_0)$ it can be shown that [101–103]

$$E_n = \lim_{t\to\infty} \frac{1}{a} \ln \frac{\lambda_n(t,t_0)}{\lambda_n(t+a,t_0)}. \tag{7.20}$$

The expression in Limit here resembles an effective mass as in eq. (7.12), but here, for each n the asymptotic energy is that of the n-th energy level in the exponential tower.
The choice of t_0 is not unique and can for example be chosen such that $t - t_0$ is constant or one could fix t_0 [102]. However, if $C(t_0)$ has large uncertainties, these uncertainties are reflected in $\lambda_n(t,t_0)$. For this reason, it is often useful to fix t_0 at a value large enough to eliminate the influence of higher excited states, but where the uncertainties are still small. It should be chosen such that $t_0 \geq \frac{t}{2}$ as otherwise the effective energies in eq. (7.20) become independent of t_0 [101] and might converge to the ground state energy instead of higher ones.
Beside the application of finding higher energy levels, a GEVP can also improve the convergence to the asymptotic ground state compared to a single correlator. We tested this with correlator matrices from the different embeddings in tables C.4 to C.7. However, we found that the set of operators do not yield an advantage in this case as the $\lambda(t,t_0)$ simply project onto the least noisy correlator as shown in figs. 7.3 and 7.4.
We observed slightly better results using a *generalized pencil of function* (GPOF) in which the GEVP is used on a *Hankel matrix*

$$\mathcal{H}(t) = \begin{pmatrix} C_0(t) & C_0(t+1) & \cdots & C_0(t+N) \\ C_0(t+1) & C_0(t+2) & \cdots & C_0(t+N+1) \\ \vdots & \vdots & \cdots & \vdots \\ C_0(t+N) & C_0(t+N+1) & \cdots & C_0(t+2N) \end{pmatrix}$$

constructed from a single correlation function C_0 [104]. However, we decided to simply use the least noisy correlator for our analysis instead as the benefits of the GPOF were marginal in our tests.

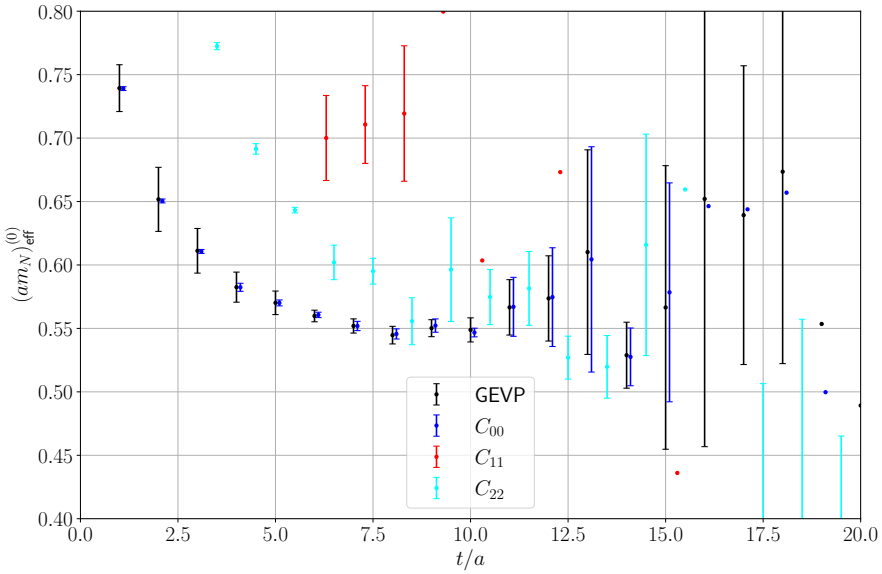

Figure 7.3: Example of a test of the GEVP for the nucleon on the A654 ensemble. The correlation functions C_{00}, C_{11}, and C_{22} are constructed from the embeddings 1, 2, and 3 of the even parity (gerade) G_1 operators in table C.4. Their cross-correlators were used to perform the GEVP. The GEVP here only shows the lowest lying generalized eigenvalue $\lambda_1(t, t_0)$. The timeslice t_0 is fixed at $t_0 = 5$.

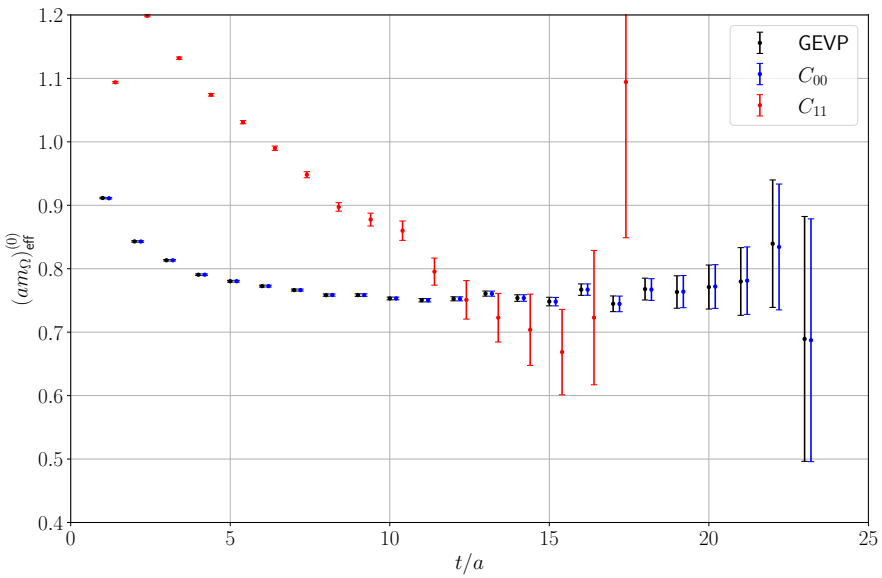

Figure 7.4: Example of a test of the GEVP for the Ω baryon on the A654 ensemble. The correlation functions C_{00} and C_{11} are constructed from the embeddings 1 and 2 of the even parity (gerade) H operators in table C.6. Their cross-correlators were used to perform the GEVP. The GEVP here only shows the lowest lying generalized eigenvalue $\lambda_1(t, t_0)$. The timeslice t_0 is fixed at $t_0 = 5$.

Chapter 8
Analysis

This chapter details the setup for the computation of two-point correlation functions for octet- and decuplet-baryons and pseudoscalar octet-mesons as well as the methodology behind their analysis.
In section 8.1 we describe the algorithmic setup of our computation of two-point-functions starting with the libraries we use and the quantities we compute. In section 8.1.1 we detail the determination of the structure of the hadronic operators we use and their Wick-contractions. Section 8.1.2 outlines the algorithms used to compute propagators from quark sources as well as the algorithmic parameters entering the computation. Finally, sections 8.1.4 and 8.1.5 discuss tests we performed to verify the outputs of our implementation and some optimizations thereof which were necessary to keep the cost of the computations at a reasonable level.
Section 8.2 describes a well-known noise problem typical for baryonic observables in lattice computations and section 8.3 details our methodologies to deal with the noisy data in effective mass fits.

8.1. Simulation Setup

For the project of this thesis, two-point correlation functions of octet and decuplet baryons, as well as pseudoscalar octet mesons, were computed based on a mixture of the `openQCD` [47] and `QDP++` [105] libraries, as well as code written by Andreas Risch in the context of his dissertation [81] for the application of operators for isospin-breaking corrections as described in sections 5.2 and 5.3. The code is written in the `C++` programming language using features from `C++20` and earlier standards. The input files used to specify the setup for a certain ensemble and its individual gauge configurations are written in the YAML format and parsed using `yaml-cpp` [106]. Output data is stored in a single HDF5 file [107] per configuration in newer versions of the code or in one file for exact computations and one file for sloppy computations (see sections 6.5 and 8.1.2) in older versions. The output files contain the content of the respective input file used to produce the data, additional information on the source positions as well as the versions of the `QDP++` library and its dependency `QMP` [105]. The computed correlation functions are stored in individual datasets for each combination of hadron, isospin component I_3, spin-irrep, spin component s_z, parity, isospin-breaking (i.e. QED correction, mass detuning) and isospin-symmetric contributions, and flavor content. For

baryonic correlation functions, a correlator matrix including cross-correlators for the used operators from tables C.4 to C.7 are stored as $N_{\text{src}} \times N_{\text{smear}} \times N_O \times N_O \times N_T$ dimensional arrays of complex values, where N_{src} is the number of available source positions, N_{smear} is the number of different smearing setups, N_O is the number of operators and N_T is the time extent of the lattice. N_{smear} was introduced at an early stage of the project at which experiments were done with different smearing parameters, but was quickly discarded and only a single smearing setup is used for any ensemble. Thus, in newer versions, this axis was removed from the output data.

8.1.1. Determination of Operators and Contractions

To reduce the risk of mistakes in manually copying the operator structure described in section 7.1 and to use a more consistent normalization than in the original publication [12], we wrote a `python` library automating the operator construction outlined in section 7.1 which was also used to generate the tables in section C.2. Based on these operators, we implemented another `python` library computing the contractions for all isospin-symmetric and isospin-breaking correlators with the following simplifications:

- After computing the contraction for a pair of source- and sink-operators, up- and down-quarks are treated as identical particles due to the isospin-symmetric nature of the CLS ensembles used in this project to simplify the contractions. In the following we will refer to these quarks as *light-quarks*. For ensembles with SU(3)-symmetry, the option of also treating the strange-quark as identical to the light-quarks for further optimizations is implemented as well. This identification only affects standard isospin-symmetric propagators and those for the QED-corrections as discussed below; the propagators used for isospin-breaking corrections involving quark-mass-detuning as discussed in section 5.2 are never identified at this stage.

- For QED-corrections to a correlation function, the same identification as above is done after multiplying each isospin-breaking propagator with its respective charge-factor (i.e. its electrical charge in units of e).

The same library includes utilities to generate `C++`-code to compute the contractions using `QDP++` as described in section 8.1.5. The generated code for the contractions was cross-checked with the `LALIBE` implementation [108] which computes a subset of the correlators computed for this thesis.

8.1.2. Computation of Two-Point Functions

For the computation of hadronic two-point functions, one-to-all propagators are sampled on 33 different randomly distributed sources using a DFL+SAP+GCR solver. One-to-all propagator here means that the propagator $\mathcal{S}$ of a quark is obtained by solving the equation $D\mathcal{S} = \eta$ where η is a Wuppertal-smeared point source [91] (see section 7.2.2) with APE-smeared gauge links [95] (see section 7.2.3) and D is the Wilson-Dirac operator (4.9). The position of the source is thus fixed and a value is computed for each sink position. The solver has three main components:

Deflation (DFL) As simulations get close to physical quark masses, the Dirac operator's condition number gets larger, increasing the computational cost of its inversion. This problem is partially mitigated by computing a *deflation subspace* dominated by the low eigenmodes of the Dirac operator and restricting the problem of its inversion to the orthogonal space dominated by high eigenmodes [109], increasing numerical stability and rate of convergence.

Schwarz Alternating Procedure (SAP) The Schwarz alternating method [110] is a method for solving a Dirichlet problem on the union of two overlapping regions iteratively by switching between solving on each of the regions. Each solution on one of the regions then defines the boundary conditions for the next solve on the other region. In the application for the solver however, the lattice is split into an even number (in each direction) of non-overlapping rectangular blocks and then the inversions are solved alternatingly starting with the initial guess $\psi = 0$ [111]. This modification using non-overlapping sets is justified as the SAP is only used to generate an approximate solution $\psi \approx M_{\mathrm{SAP}}\phi$ as a preconditioning. The approximation can then be used to modify the original problem to the better conditioned equation $D(M_{\mathrm{SAP}}\phi) = \eta$ which is then solved via the GCR algorithm [111].

Generalized Conjugate Residual (GCR) Algorithm The generalized conjugate residual algorithm produces a sequence of approximate solutions ψ_k by iteratively minimizing the norm $\|r_{k+1}\|$ of the residual $r_k = \eta - D\psi_k$ [111] over the Krylov subspace $\mathcal{K}_k(D, \eta) = \mathrm{span}\{\eta, D\eta, ..., D^{k-1}\eta\}$.

For improved efficiency, we used the truncated solver method [112] in which all propagators are computed with a fixed cutoff in the number of solver iterations that is lower than what is needed for convergence. This results in slightly incorrect propagators which are then corrected via an additional exact solve on one of the sources on each gauge configuration from which the bias of the solver truncation can be estimated and corrected via all-mode-averaging (see section 6.5). The exact parameters for the solver and the deflation subspace have to be tuned for each ensemble for a good balance between efficiency and precision. This was done by testing different setups on a small subset of gauge configurations and observing the time needed per configuration and the observed uncertainties of correlation functions. While we optimized the solver-efficiency in general, the number of solver iterations for the truncated solver was chosen such that the uncertainty of the inherent bias is subdominant to that of the different correlation functions in regions where a reasonable signal can still be expected (see section 8.2 for more context).

While the action parameters fed into the solver and deflation subspace are faithful to those which entered the generation of a given ensemble, on some individual gauge configurations a small twisted mass was added in the deflation subspace generation when convergence of the exact solves could not be achieved with the general setup.

For link smearing a setup with 15 smearing steps and $\alpha = 0.6$ was used for all ensembles. The parameters chosen for source smearing are listed in table 8.1 and

are chosen such that the smearing radius [92]

$$r_{\mathrm{sm}}^2 = \frac{\sum_x |x-y_0|^2 \|\psi(x)\|^2}{\sum_x \|\psi(x)\|^2}$$

for a smeared source ψ amounts to $\sim 0.5\,\mathrm{fm}$.

Table 8.1: Setup for Wuppertal smearing for different strong gauge couplings. n is the number of smearing iterations while κ_G and C in eq. (7.9) are defined through α via $\gamma = \frac{1}{1+6\alpha}$ and $\kappa_G = \gamma\alpha$.

β	α	n
3.4	1.1	75
3.46	1.1	95
3.55	1.1	125
3.7	1.1	200

The computation of a propagator is finished by smearing the propagator again to effectively achieve a *sink smearing* such that both ends of the propagator are smeared in the same manner.

8.1.3. Sequential Propagators for Isospin-Breaking Corrections

For the isospin-breaking corrections discussed in chapter 5, additional contributions involving operator insertions (see eqs. (5.13) to (5.16) and (5.19)) need to be computed which replace some of the propagators computed as described in section 8.1.2. To this end, we use the method of *sequential propagators* which uses multiple inversions to compute the derivatives in eq. (5.13):

1. We start from a propagator ${\mathcal{S}_f}^{(0)}$ for a quark of flavor f computed in $\mathrm{QCD}_{\mathrm{iso}}$ by solving $D_f {\mathcal{S}_f}^{(0)} = \eta$.

2. We then apply the appropriate operator $V = \frac{\partial D_f}{\partial \varepsilon_i}$ (i.e. $V = -\mathbb{1}_{\mathrm{Spin}\times\mathrm{SU}(3)\times\Lambda}$ for $\varepsilon_i = m_f$ or eq. (5.19) for QED vertices) to ${\mathcal{S}_f}^{(0)}$.

3. Finally, we treat ${\mathcal{S}_f}^{(0)}$ as a source for another inversion $D_f\left(\frac{\partial \mathcal{S}_f}{\partial \varepsilon_i}|_{\varepsilon=\varepsilon^{(0)}}\right) = V{\mathcal{S}_f}^{(0)}$ which is then solved for $\frac{\partial \mathcal{S}_f}{\partial \varepsilon_i}|_{\varepsilon=\varepsilon^{(0)}}$ using the methods in section 8.1.2.

Note, that in this description η is a smeared source, while ${\mathcal{S}_f}^{(0)}$ is not smeared again. Only after the final inversion, sink smearing is applied. Furthermore, for the self energy diagram 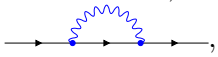 , another operator insertion and inversion are necessary for the second vertex.
Since we also have to incorporate diagrams with two propagators exchanging a single photon (e.g. 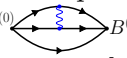), we furthermore need to introduce the *square root* of the photon propagator [81] which we attach to each of the sequential quark propagators. In Feynman gauge, this computation of a square root is trivial as the propagator is diagonal, i.e.

$$\sqrt{\tilde{\Sigma}(p)}^{\mu}_{\ \nu} = \frac{\delta^{\mu}_{\ \nu}}{\sqrt{\sum_\mu p_-^\rho p_{+,\rho}}}$$

for periodic boundary conditions and

$$\sqrt{\hat{\Sigma}(p)}^{\mu}{}_{\nu} = \frac{\delta^{\mu}_{\nu}}{\sqrt{p^0_{-,CS}p^0_{+,SC} + \sum_{\rho\neq 0} p^{\rho}_{-}p_{+,\rho}}}$$

for open temporal boundary conditions. In Coulomb gauge the propagator has to be diagonalized first using a change of basis $U(p)$ before taking the square root (see [81] for the exact form) to find

$$\sqrt{\tilde{\Sigma}(p)} = U(p)\mathrm{diag}\left(\frac{1}{\sum_{i=1}^{3} p^{i}_{-}p_{+,i}}, \frac{1}{\sum_{\mu=0}^{3} p^{\mu}_{-}p_{+,\mu}}, \frac{1}{\sum_{\mu=0}^{3} p^{\mu}_{-}p_{+,\mu}}, 0\right)U(p)^{-1}$$

for periodic boundary conditions and

$$\sqrt{\hat{\Sigma}(p)} = U(p)\mathrm{diag}\left(\frac{1}{\sum_{i=1}^{3} p^{i}_{-}p_{+,i}}, \frac{1}{p^0_{-,CS}p^0_{+,SC} + \sum_{i=1}^{3} p^{i}_{-}p_{+,i}}, \frac{1}{p^0_{-,CS}p^0_{+,SC} + \sum_{i=1}^{3} p^{i}_{-}p_{+,i}}, 0\right)U(p)^{-1}$$

for open boundary conditions.
This application of a *half propagator* allows us to include part of the necessary computation for the inclusion of sea quarks, namely diagrams of the form

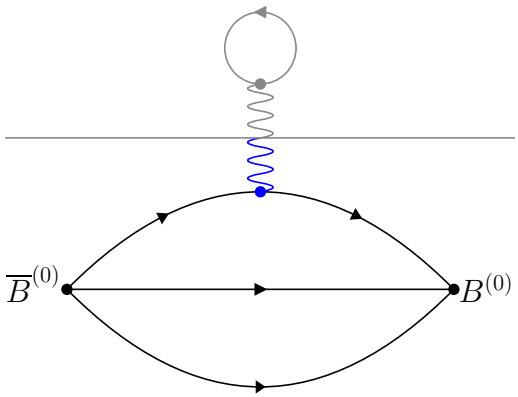

where a valence-quark exchanges a photon with a sea-quark. The lower (valence) part of this diagram involves just another contraction when all the (sequential or non-sequential) propagators are already computed, which is comparatively cheap. We thus include the lower part of this diagram in our computations which can then be multiplied with the upper (sea) part when sea-quark effects are to be included in the calculation at a later stage of the project.
The computation of the sequential propagator with the two-photon-vertex,  , requires the diagonal entries of full photon propagator $\Sigma(x,x)^{\mu}_{\nu}$ which is computed from its known form in momentum-space [81].
The photon half propagators are generated stochastically using sources $J^{\mu}(x)$ drawn such that the expectation value in the limit of infinite sources takes the form $\langle J^{\mu}(x)J^{\nu}(y)\rangle_J = g^{\mu\nu}\delta_{xy}$ [81] for each gauge configuration using a program written by Andreas Risch. From the sources, the half-propagated photon source $A[J]$ is constructed via $A^{\mu}[J](x) = \sum_y \sqrt{\Sigma(x,y)}^{\mu}{}_{\nu} J^{\nu}(y)$ such that the propagator in terms of A is given by $\langle A^{\mu}[J](x)A^{\nu}[J](y)\rangle_J = \Sigma(x,y)^{\mu\nu}$ [81].

8.1.4. Test of Correctness

Before running the code on actual large gauge ensembles, we performed a number of consistency checks to make sure that the code generates physically sound results. For this purpose, two test ensembles with 16×8^3 lattice sites were generated; one with open, one with periodic boundary conditions.
At this stage, the isospin-symmetric contribution could not be tested completely, only that the general shape of the correlation functions was as expected, i.e. a tower of exponential decays in each direction from the source position with different decay rates in the forward time-direction as in the backward one for baryons and a symmetric one for mesons, and zeros on the boundary in the open boundary case. Apart from these tests, invariance w.r.t. SU(3) gauge transformations was tested.
For the mass-detuning contributions, the Ξ baryon-correlation function was computed at varying masses for the light valence-quark. At a single point of these masses the mass-correction (eq. (5.14)) was computed in addition to the isospin-symmetric contribution. As expected, the test depicted in fig. 8.1 showed that the derivative w.r.t. the light-quark mass computed using our implementation of the mass-detuning on the single point is in agreement with that from a numerical derivative gained from multiple simulations around that point.

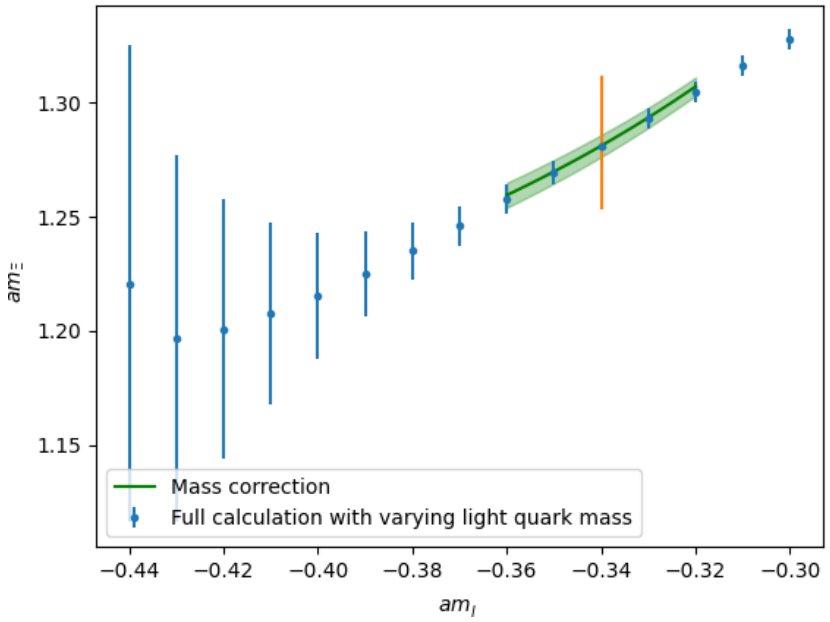

Figure 8.1: Consistency check of the Δm_q correction implementation for the Ξ baryon. The blue data points are isospin-symmetric masses computed at different light-quark masses on the same ensemble. For the light quark mass marked by the orange vertical line, the derivative of the two point function w.r.t. the light quark mass was additionally determined using the methods described in section 5.2 from which the green band is derived which shows the expected (local) dependence of am_Ξ on am_l.

To test the QED-corrections, the same combination of quark sources was processed with 256 photon sources per gauge configuration, once in Coulomb gauge and once in Feynman gauge. For a correct implementation, the results of these computations have to be compatible. The result of this test is shown in fig. 8.2.

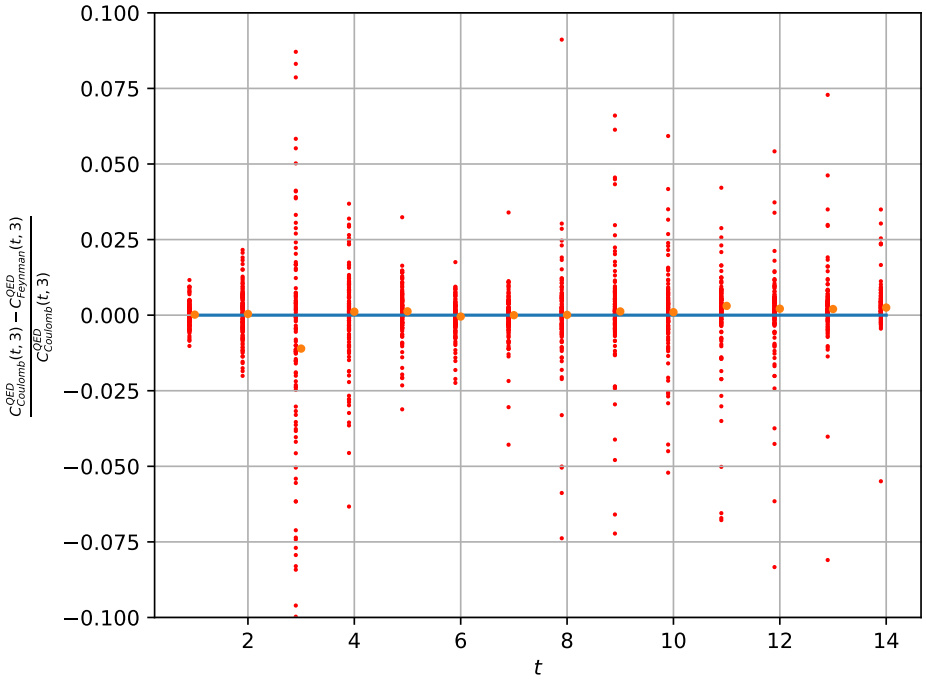

Figure 8.2: Consistency check of the implementation of the QED correction for the pion. The red dots show measurements on individual gauge configurations of the normalized difference between the correlation function with a source positioned at timeslice $\frac{t}{a} = 3$. The orange points show the average of the red dots.

After succeeding in these conceptual cross-checks, the code was used to compute all correlation functions relevant for this project on 563 out of 5068 gauge configurations of the A654 CLS ensemble to compare results to other calculations of the same correlation functions.

8.1.5. Code Optimizations

When testing the code on the A654 ensemble, we found that the run time was dominated by the contractions, which should reasonably be faster than the inversions of the Dirac operator. This was due to the usage of the `QDP++` library, which is optimized for matrix operations for the computation of interpolators based on Dirac-matrices as in eq. (7.4). Indexing spinor- or color-matrices directly, however, is quite slow in this library. To circumvent this problem, we store the propagators as a `std::array<std::array<QDP::LatticeColorMatrix, 4>, 4>` instead of a `QDP::LatticePropagator`[1], which allows for faster indexing of the spinor components. The contractions can then be sped up by performing the color contractions for each possible term needed for the contractions and storing the results for later use. These color-contracted terms are simple `QDP::LatticeComplex`, i.e. one complex number per lattice site and thus take up less memory than a propagator by a factor of 144.
However, with 10104 unique (and 101580 non-unique) terms to be stored this way, this uses a lot more memory than should be afforded. The amount of memory

[1] A `QDP::LatticeColorMatrix` is a matrix in color and coordinate space. A `QDP::LatticePropagator` is a matrix in spinor space on top of that.

needed at once can be reduced by noticing, that the unique terms can further be classified into 25 subsets of different propagator combinations, (l,l,l), (l,l,u_m), (l,l,d_m), (l,l_v,l_v), (l,l,l_s), (l,l,s), (l,s,u_m), (l,s,d_m), (l,l,s_m), (l_v,l_v,s), (l,l_v,s_v), (l,l_s,s), (l,l,s_s), (l,s,s), (s,s,u_m), (l,s,s_m), (l_v,s,s_v), (l,s_v,s_v), (l_s,s,s), (l,s,s_s), (s,s,d_m), (s,s,s), (s,s,s_m), (s,s_v,s_v), (s,s,s_s), where q_m denotes the sequential propagator (5.14) for the mass correction of flavor q, q_v denotes the sequential propagator with a single photon vertex, and q_s denotes the sum of two sequential propagators contributing to the self energy of the quark, i.e. those containing photon loops. We make use of this by only computing all terms for a specific propagator combination, then perform all the contractions containing these terms and writing the results to disk. This reduces the number of `QDP::LatticeComplex` to be held in memory (on top of the required propagators) at a time to at most 640.

Lastly, to speed up the computation of a contraction itself, we cater to the *portable expression template engine* (PETE) that uses operator overloading on templated data types `C++` to optimize expressions involving addition, subtraction, and multiplication [105]. To this end we introduce maps that contain functions computing all the different contractions such that they can be optimized with PETE. A simplified version of this implementation is shown in listing 8.1. A later revision of the implementation used only for isospin-symmetric computations is shown in listing 8.2.

Listing 8.1: A collection of code snippets showcasing the computation of the contractions of the correlator corresponding to the first entry in the nucleon interpolator table, table C.4, including all considered isospin-breaking corrections. The computation itself is performed in a function stored in the `baryonContractionMapG1g` (similar maps exist for the irreps G1u, Hg, and Hu) that is accessed via a `CorrelatorInfo` instance that specifies the state that is computed by the respective function. The tuples used as key for the `cMap`s indicate the spinor indices for each propagator (the first two indices are for the first propagator and so on) with the order being defined by the `baryonCorrKeyType` instance. `cMap`s values correspond to color-contracted terms of the contraction with the specified spinor components for a specific combination of quark flavors.
The states are specified by the octet-/decuplet-state's name, its (doubled) isospin, its irrep, its spin-z component, the embeddings of the sink- and source interpolators (see the tables in section C.2), its contribution type (`"symmetric"`, `"mass"`, or `"qed"`), and the quark content.

```
// This defines the combination of propagators to which a
// contraction corresponds to
typedef std::tuple<std::string, std::string, std::string>
    baryonCorrKeyType;
// A cMap contains all terms needed for a specific propagator
// combination indexed by the spinor-indices
typedef std::map<std:tuple<uint, uint, uint, uint, uint, uint>,
    QDP::LatticeComplex> cMap;
// The type of the functions computing the contractions taking as
// input a map with all potential (color-contracted) terms and a
// reference to the variable to write the result of the contraction
// to
using pfunc = void (*)(const cMap& cm, QDP::LatticeComplex& res);
```

```
// The CorrelatorInfo is used to specify a specific baryonic state
class CorrelatorInfo {
    ...
private:
  std::string flavor; // The name of the state ("nucleon", "xi", ...)
  int two_times_I3; // Denotes the isospin of the state
  std::string irrep; // "G1g", "G1u", "Hg", or "Hu"
  int irrep_row; // Spin-z component counted as rows in interpolator
                 // tables
  int sink_id; // The embedding of the sink interpolator
  int source_id; // The embedding of the source interpolator
  std::string contribution; // IB contribution ("symmetric", "mass",
                            // "qed")
  baryonCorrKeyType tuple_contr; // The combination of propagators to
                                 // be contracted
};

// The `baryonContractionMap`s map state descriptors (i.e.
// CorrelatorInfos) to functions performing the contractions
// for that state
std::map<CorrelatorInfo, pfunc> baryonContractionMapG1g = {
  { CorrelatorInfo("nucleon", 1, "G1g", 1, 1, 1, "symmetric",
    baryonCorrKeyType("l", "l", "l")),
    [](const cMap& cm, LatticeComplex& res) {
      res = 3.0 * cm.at(std::make_tuple(0, 0, 0, 0, 1, 1))
          - 3.0 * cm.at(std::make_tuple(0, 0, 0, 1, 1, 0));
    }
  }, { CorrelatorInfo("nucleon", 1, "G1g", 1, 1, 1, "mass",
    baryonCorrKeyType("l", "l", "u_mass")),
    [](const cMap& cm, LatticeComplex& res) {
      res = 1.0 * cm.at(std::make_tuple(0, 0, 0, 0, 1, 1))
          - 1.0 * cm.at(std::make_tuple(0, 0, 0, 1, 1, 0))
          - 1.0 * cm.at(std::make_tuple(0, 0, 1, 0, 0, 1))
          + 5.0 * cm.at(std::make_tuple(0, 0, 1, 1, 0, 0))
          - 4.0 * cm.at(std::make_tuple(0, 1, 1, 0, 0, 0));
    }
  }, { CorrelatorInfo("nucleon", 1, "G1g", 1, 1, 1, "mass",
    baryonCorrKeyType("l", "l", "d_mass")),
    [](const cMap& cm, LatticeComplex& res) {
      res = 2.0 * cm.at(std::make_tuple(0, 0, 0, 0, 1, 1))
          - 2.0 * cm.at(std::make_tuple(0, 0, 0, 1, 1, 0))
          - 2.0 * cm.at(std::make_tuple(0, 0, 1, 0, 0, 1))
          + 1.0 * cm.at(std::make_tuple(0, 0, 1, 1, 0, 0))
          + 1.0 * cm.at(std::make_tuple(0, 1, 1, 0, 0, 0));
    }
  }, { CorrelatorInfo("nucleon", 1, "G1g", 1, 1, 1, "qed",
    baryonCorrKeyType("l", "l_vertex", "l_vertex")),
    [](const cMap& cm, LatticeComplex& res) {
      res = -0.6666666666666666 *
            cm.at(std::make_tuple(0, 0, 0, 0, 1, 1))
          + 1.3333333333333333 *
            cm.at(std::make_tuple(0, 0, 0, 1, 1, 0))
          - 0.6666666666666666 *
            cm.at(std::make_tuple(0, 1, 0, 0, 1, 0))
          - 0.6666666666666666 *
            cm.at(std::make_tuple(1, 0, 0, 0, 0, 1))
          + 0.6666666666666666 *
            cm.at(std::make_tuple(1, 1, 0, 0, 0, 0));
    }
  }, { CorrelatorInfo("nucleon", 1, "G1g", 1, 1, 1, "qed",
```

```
    baryonCorrKeyType("l", "l", "l_self")),
    [](const cMap& cm, LatticeComplex& res) {
      res = 0.6666666666666666 *
            cm.at(std::make_tuple(0, 0, 0, 0, 1, 1))
          - 0.6666666666666666 *
            cm.at(std::make_tuple(0, 0, 0, 1, 1, 0))
          - 0.6666666666666666 *
            cm.at(std::make_tuple(0, 0, 1, 0, 0, 1))
          + 2.3333333333333335 *
            cm.at(std::make_tuple(0, 0, 1, 1, 0, 0))
          - 1.6666666666666667 *
            cm.at(std::make_tuple(0, 1, 1, 0, 0, 0));
    }
  }, { CorrelatorInfo("nucleon", 1, "G1g", 1, 1, 1, "qed",
    baryonCorrKeyType("l", "l", "l_vertex")),
    [](const cMap& cm, LatticeComplex& res) {
      res = 3.0 * cm.at(std::make_tuple(0, 0, 1, 1, 0, 0))
          - 3.0 * cm.at(std::make_tuple(0, 1, 1, 0, 0, 0));
    }
  },
  ...
};
```

Listing 8.2: A modified and updated version of listing 8.1 used for the computation of baryonic two-point functions on E250 and E300, where we only computed the isospin-symmetric contributions. The main differences are the use of `std::function` instead of `void*` for the contraction functions, `std::array`s instead of tuples as keys for `cMap`, as well as removal of some redundancies that only matter in the case of isospin-breaking corrections: The isospin is not relevant as it is a symmetry and the contributions as well as propagator combinations are unique to a state and are handled before the color contractions. In addition to the interpolator combination showcased in listing 8.1, the first cross-correlator is included which mixes the first and second embedding of the nucleon interpolators.

```
// A cMap contains all terms needed for a specific propagator
// combination indexed by the spinor-indices
typedef std::map<std::array<uint, 6>, QDP::LatticeComplex> cMap;
// The type of the functions computing the contractions taking as
// input a map with all potential (color-contracted) terms and a
// reference to the variable to write the result of the contraction
// to
typedef std::function<void(const cMap &, QDP::LatticeComplex &)>
    pfunc;

// The CorrelatorInfo is used to specify a specific baryonic state
struct CorrelatorInfo {
  std::string hadron; // The name of the state ("nucleon", "xi", ...)
  std::string irrep; // "G1g", "G1u", "Hg", or "Hu"
  int spin_z; // Spin-z component counted as rows in interpolator
              // tables
  int sink_row; // The embedding of the sink interpolator
  int source_row; // The embedding of the source interpolator
};

// The `baryonContractionMap`s map state descriptors (i.e.
// CorrelatorInfos) to functions performing the contractions
// for that state
std::map<CorrelatorInfo, pfunc> baryonContractionMapG1g = {
```

```
  { { "nucleon", "G1g", 1, 1, 1 },
      [](const cMap& cm, QDP::LatticeComplex& res) {
        res = 3.0 * cm.at({0, 0, 0, 0, 1, 1})
            - 3.0 * cm.at({0, 0, 0, 1, 1, 0});
    }
  }, { { "nucleon", "G1g", 1, 1, 2 },
    [](const cMap& cm, QDP::LatticeComplex& res) {
      res = 3.4641016151377544 * cm.at({0, 0, 0, 2, 1, 3})
          - 1.7320508075688772 * cm.at({0, 0, 0, 3, 1, 2})
          - 1.7320508075688772 * cm.at({0, 1, 0, 2, 1, 2})
          + 1.7320508075688772 * cm.at({0, 2, 0, 2, 1, 1})
          - 1.7320508075688772 * cm.at({0, 2, 0, 3, 1, 0});
    }
  },
  ...
};
```

8.2. Baryon Noise Problem

Consider an interpolator $\mathcal{O} = \sum_\alpha \prod_{i=1}^n q_i^{\alpha_i}$ for a hadronic state and its corresponding 2-point correlation function $C(t) = \left\langle \mathcal{O}(t)\bar{\mathcal{O}}(0) \right\rangle$ where α_i are multi-indices for spin and color. According to Wick's theorem, we can rewrite $C(t)$ in terms of quark propagators $\mathcal{S}_{q_i}$ as

$$C_\mathcal{O}(t) = \left\langle \sum_{\alpha,\beta} \prod_{i=1}^n \mathcal{S}_{q_i}^{\alpha_i,\beta_i} \right\rangle.$$

The variance of the correlation function is then given by

$$\sigma^2_\mathcal{O}(t) = \left\langle \left| \sum_{\alpha,\beta} \prod_{i=1}^n \mathcal{S}_{q_i}^{\alpha_i,\beta_i} \right|^2 \right\rangle - |C_\mathcal{O}(t)|^2.$$

The first term of the variance corresponds to a correlation function with all quarks contributing to $\mathcal{O}$ and additionally the same quarks replaced by their antiparticle [113]. For a pion correlation function, this corresponds to two quarks and two antiquarks propagating for which the lightest state with the corresponding quantum numbers is a two-pion-state. Both this term and the $C(t)^2$ term thus asymptotically fall off as $e^{-2m_\pi t}$ thus yielding a standard deviation $\sigma_\pi(t) \sim e^{-m_\pi t}$. As this is the same asymptotic behaviour as that of $C_\pi(t)$, the relative error of a measurement of the correlation function is asymptotically given by [113]

$$\frac{\sigma_\pi(t)}{C_\pi(t)} \sim \frac{\text{const.}}{\sqrt{N}}$$

where N is the number of measurements. This constant results in practice in a clean correlation function for the pion as demonstrated in fig. 8.3.
For a nucleon, on the other hand, the first term in the variance is dominated by a state with three pions [113, 114] which asymptotically decay as $e^{-3m_\pi t}$. The relative error [113, 114]

$$\frac{\sigma_N(t)}{C_N(t)} \sim \frac{1}{\sqrt{N}} e^{(m_N - \frac{3}{2}m_\pi)t}$$

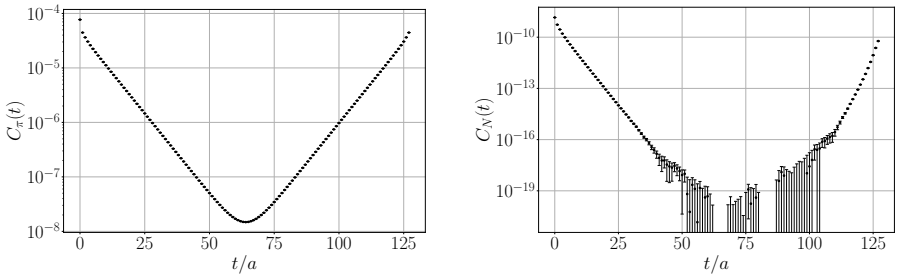

Figure 8.3: Correlation functions of the pion (left) and the nucleon (right) in the isospin-symmetric contribution on the N452 ensemble demonstrating the noise problem for baryons.

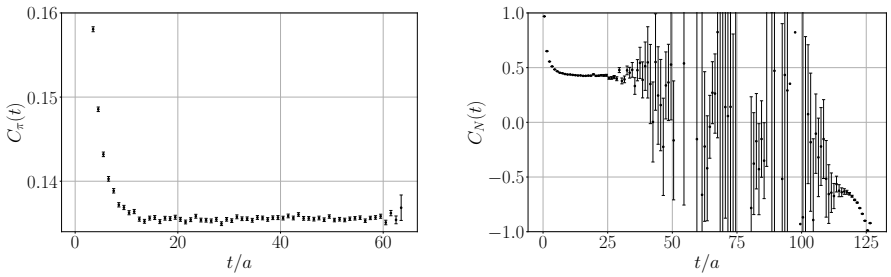

Figure 8.4: Effective mass of the pion (left) and the nucleon (right) in the isospin-symmetric contribution on the N452 ensemble.

of the nucleon thus grows exponentially with t with the result, that the signal is quickly lost as shown in fig. 8.3 for the correlation function and in fig. 8.4 for the effective mass in the isospin-symmetric contribution.
This poses the problem that the noise can in principle grow too large before excited-state effects die off enough to simply fit to an asymptotic exponential in the correlation function or a plateau in the effective to determine the ground state energy.
This problem is even more severe for isospin-breaking corrections as shown in fig. 8.5 where the noise grows much stronger than in the isospin-symmetric contribution. In the data analyzed for this thesis, a plateau can rarely be made out in isospin-breaking corrections.

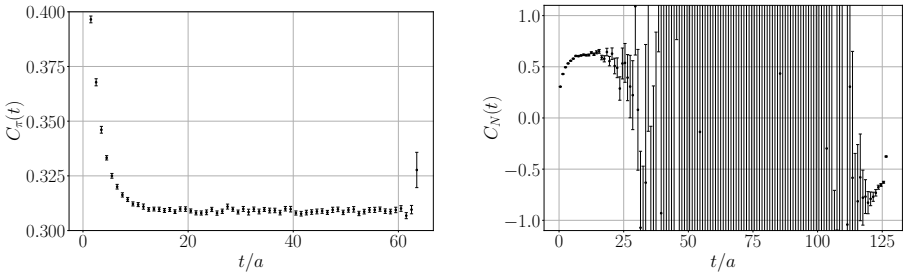

Figure 8.5: Effective mass of the pion (left) and the nucleon (right) of the QED correction on the N452 ensemble.

8.3. Fit Strategies

The simplest strategy to find the asymptotic mass lies in finding a plateau in the effective mass and fitting a constant value to the selected region. Similarly, one could fit a linear function to the analogous region in the correlation function directly. It is not a priori obvious which of the two is preferable, however, early experiments with both fit functions on data gathered in the process of this thesis resulted in a negligible difference between the results of both methods. Thus, we decided to always fit the effective mass as this reduces the number of fit parameters to one.

8.3.1. Two-State Fits for Isospin-Symmetric Contributions

Although fitting a plateau is a viable option for pseudoscalar mesons as can easily be seen from figs. 8.4 and 8.5, the noise of baryonic effective masses can quickly grow too large to allow for a reasonable fit as discussed in section 8.2. This is especially true in the case of isospin-breaking corrections, where it is often not clear whether a plateau has been reached. To compensate for these effects, we decided to include two-state fits as introduced in [115] based on the ansatz that the asymptotic behaviour of the correlation function is governed by two exponentials

$$C(t) = ce^{-mt} + c_* e^{-m_* t}.$$

For this asymptotic model of the correlation function, the effective mass takes the form

$$\begin{aligned}
m_{\text{eff}}(t) &= -\frac{\mathrm{d}}{\mathrm{d}t} C(t) = -\frac{\mathrm{d}}{\mathrm{d}t} \log\left(ce^{-mt} + c_* e^{-m_* t}\right) = \frac{cme^{-mt} + c_* m_* e^{-m_* t}}{ce^{-mt} + c_* e^{-m_* t}} \\
&= \frac{m + \frac{c_*}{c} m_* e^{-\Delta M t}}{1 + \frac{c_*}{c} e^{-\Delta M t}} = \left(m + \frac{c_*}{c} m_* e^{-\Delta M t}\right) \sum_{n=0}^{\infty} \left(-\frac{c_*}{c} e^{-\Delta M t}\right)^n \\
&= m + m \sum_{n=1}^{\infty} \left(-\frac{c_*}{c} e^{-\Delta M t}\right)^n + m_* \sum_{n=0}^{\infty} (-1)^n \left(\frac{c_*}{c} e^{-\Delta M t}\right)^{n+1} \\
&= m + m \sum_{n=1}^{\infty} \left(-\frac{c_*}{c} e^{-\Delta M t}\right)^n + m_* \sum_{n=1}^{\infty} (-1)^{n+1} \left(\frac{c_*}{c} e^{-\Delta M t}\right)^n \\
&= m + \Delta M \sum_{n=1}^{\infty} (-1)^{n+1} \left(\frac{c_*}{c} e^{-\Delta M t}\right)^n \\
&= m + \frac{c_*}{c} \Delta M e^{-\Delta M t} + \mathcal{O}\left(\left(\frac{c_*}{c} e^{-\Delta M t}\right)^2\right).
\end{aligned} \tag{8.1}$$

Combining the factor $\frac{c_*}{c}\Delta M$ into a single fit parameter, the fit function for two-state fits is given by

$$am_{\text{eff}}(t) = am + \gamma e^{-\Delta M t}. \tag{8.2}$$

This is the fit function used in [115] and is what will be used throughout this thesis. It would of course have been possible to fit the exact formula for the effective mass from the two-state fit ansatz, which can be further simplified to

$$m_{\text{eff}}(t) = m_* - \frac{\Delta M}{1 + \frac{c_*}{c} e^{-\Delta M t}} = m + \frac{\Delta M}{1 + \frac{c}{c_*} e^{\Delta M t}}.$$

However, a realistic correlation function still has influences from various different higher energy states in the fit region so that the value of m_* should not be interpreted as the actual mass of the second lowest energy eigenvalue. Moreover, the derived expression up to first order in $\frac{c_*}{c}e^{-\Delta M t}$ does not accurately describe the excited state contributions to the effective mass and is rather a physically motivated ansatz to describe the curvature of the effective mass close to the plateau where the approximation asymptotically converges to the exact expression.

A crucial advantage of using the approximate fit ansatz (8.2) is that it is linear in m and γ, which allows for an exact solution for the maximum likelihood fit for those two parameters as functions of ΔM. Thus, only the parameter ΔM has to be found numerically, which improves the numerical stability of the fit. Details on the exact procedure are given in section B.3.5.

An example of a two-state fit for the Ω baryon on the D450 ensemble is shown in fig. 8.6, where it is compared to a single state (i.e. constant) fit. While the two fits agree well in this example, it is not completely obvious from the data alone that the plateau has been reached in the interval chosen for the constant fit. A comparison of both fit functions is therefore useful to improve confidence in the results.

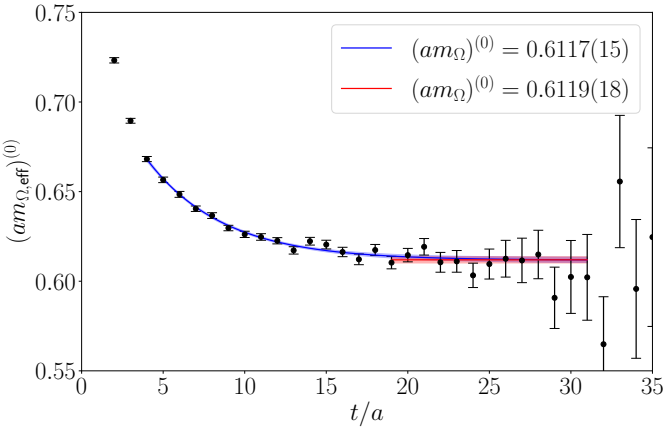

Figure 8.6: A two-state fit (blue) and a single state fit (red) of the isospin-symmetric effective mass of the Ω baryon on the D450 ensemble.

Note that, since the fit ansatz only describes the asymptotic behaviour of the correlation function close to the plateau, a fit should not start at too small times t as the approximation then breaks down, just as that of a plateau from a single exponential does. On the other hand, two-state fits become numerically unstable as one get too close to the plateau, so the fit interval has to be carefully tuned by testing the dependence of the asymptotic mass and stability of the fit depending on the fit interval.

Moreover, note that this discussion explicitly assumes the definition eq. (7.12) for the effective mass and is not applicable to the definition for symmetric correlation functions. Since the signal of pseudoscalar meson correlators is much cleaner than that of baryons with much more defined plateaux, we expect single-state fits to be sufficient in these cases and have thus not derived a two-state fit ansatz.

8.3.2. Two-State Fits for Isospin-Breaking Contributions

For isospin-breaking corrections, where the noise grows quicker than in the isospin-symmetric contribution, compensating for influences from excited states is even more important. For these corrections, we make an analogous ansatz to the one discussed above. To this end, we have to revisit the expansion of the correlation functions in eqs. (7.15) and (7.16) in terms of isospin-breaking parameters and the first-order effective mass in eq. (7.17).
For two states in full QCD+QED expanded around isospin-symmetric QCD, we find

$$\begin{aligned} C(t) =& c^{(0)} e^{-m^{(0)} t} + c_*^{(0)} e^{-m_*^{(0)} t} \\ &+ \sum_i \Delta\varepsilon_i \left[\left(c^{(1)} - c^{(0)} m^{(1)} t \right) e^{-m^{(0)} t} + \left(c_*^{(1)} - c_*^{(0)} m_*^{(1)} t \right) e^{-m_*^{(0)} t} \right] \\ &+ \mathcal{O}(\Delta\varepsilon^2). \end{aligned}$$

To calculate the effective mass, $C^{(0)}$ and $C_i^{(1)}$ in eq. (7.17) have to be set to

$$\begin{aligned} C^{(0)}(t) &= c^{(0)} e^{-m^{(0)} t} + c_*^{(0)} e^{-m_*^{(0)} t}, \\ C_i^{(1)}(t) &= \left(c^{(1)} - c^{(0)} m^{(1)} t \right) e^{-m^{(0)} t} + \left(c_*^{(1)} - c_*^{(0)} m_*^{(1)} t \right) e^{-m_*^{(0)} t}. \end{aligned}$$

In a derivation similar to but more verbose than eq. (8.1), it can be shown, that the effective mass at first order with two states is approximately given by

$$\begin{aligned} m_{\text{eff}}^{(1)}(t) =& -\frac{\mathrm{d}}{\mathrm{d}t} \frac{C^{(1)}(t)}{C^{(0)}(t)} = -\frac{\mathrm{d}}{\mathrm{d}t} \frac{c^{(1)} - c^{(0)} m^{(1)} t + \left(c_*^{(1)} - c_*^{(0)} m_*^{(1)} t \right) e^{-\Delta M^{(0)} t}}{c^{(0)} + c_*^{(0)} e^{-\Delta M^{(0)} t}} \\ =& m^{(1)} - \left(\left(\frac{c^{(1)}}{c^{(0)}} - \frac{c_*^{(1)}}{c_*^{(0)}} \right) \Delta M^{(0)} - \Delta M^{(1)} + \Delta M^{(0)} \Delta M^{(1)} t \right) \frac{c_*^{(0)}}{c^{(0)}} e^{-\Delta M^{(0)} t} \\ &+ \mathcal{O}\left(\left(\frac{c_*^{(0)}}{c^{(0)}} e^{-\Delta M^{(0)} t} \right)^2 \right) \end{aligned}$$

where $\Delta M^{(i)} = m_*^{(i)} - m^{(i)}$. Combining constants into a minimal set of fit parameters, we find

$$a m_{\text{eff}}^{(1)}(t) = a m^{(1)} + (\alpha - \beta t) e^{-\Delta M^{(0)} t}. \tag{8.3}$$

The function turns out to similar to the fit function for isospin-symmetric contributions but the prefactor of the exponential is now a linear function in t. Note that the exponent is the same as for the isospin-symmetric fit function. It is thus not necessary to fit the exponent as it can be taken from the fit to the zeroth order effective mass in eq. (8.2) which comes from less noisy data. This has the additional advantage that the parameters $m^{(1)}$, α, and β maximizing the likelihood of a given set of data for eq. (8.3) can be computed analytically for fixed $\Delta M^{(0)}$ which makes the fit more stable than that of the isospin-symmetric contribution. The exact formula used to compute the optimal fit parameters is listed in eq. (B.9). An example fit comparing the single- and two-state fits for the correction of the effective mass coming from the strange mass detuning for the Ω baryon is shown in fig. 8.7. Here, the two results agree as in the isospin-symmetric example, but the same care has to be taken when fixing the fit interval as discussed above.

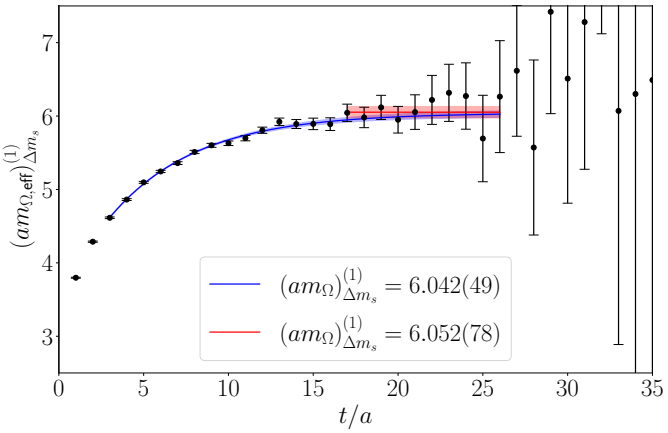

Figure 8.7: A two-state fit (blue) and a single state fit (red) of the isospin-breaking correction to the effective mass of the Ω baryon due to strange mass detuning on the D450 ensemble.

8.3.3. Combining Fits Using Model Averages

While the procedures described in sections 8.3.1 and 8.3.2 allows for a reasonable extraction of the asymptotic mass, the choice of the fit intervals is quite subjective and there is no definitive best choice. In some cases, a small adjustment to the fit intervals may in fact have a significant impact on the fit result, especially when starting the fit interval too early for the asymptotic ansätze to be valid, or, in the case of two-state fits, if the fit interval starts too late such that the fluctuations of the data strongly influence the result of the fit.
We account for these biases by applying a technique known as *model averages* [116, 117] based on the *Akaike information criterion* (AIC) [118]. Given a model M that fits parts of the data D, then the AIC of M and D is given by [116, 117]

$$\mathrm{AIC}(M,D) = \chi^2(M,D) + 2k(M) + 2n(M,D) \tag{8.4}$$

where k is the number of fit parameters defining the model M (i.e. 1 for the single-state ansatz and 3 for the two-state ansätze (8.2) and (8.3)) and n is the number of data points not included in the fit interval. That means for example if the effective mass encompasses $N_t = 40$ timeslices and the fit model fits the interval $\frac{t}{a} \in [23, 35]$, i.e. an interval of 13 timeslices, then $n = 40 - 13 = 27$. χ^2 is the usual measure of fit quality

$$\chi^2 = (y_D - M(x_D))^T \mathrm{Cov}_{y_D}^{-1} (y_D - M(x_D))$$

where in our case y_D is the effective mass and x_D is the set of timeslices included in the fit.
The AIC is roughly speaking a criterion for the reliability of a fit model and is often used for model selection. In that case, one would choose out of a set of different models the one that maximizes the AIC for the given data. However, we take a different approach by Neil et al. [116, 117] in which the AIC is used as a measure to define a probability distribution in the space of models $\mathcal{M}$ via

$$P(M_i|D) = \frac{\exp\left(-\frac{1}{2}\mathrm{AIC}(M_i,D)\right)}{\sum_j \exp\left(-\frac{1}{2}\mathrm{AIC}(M_j,D)\right)}. \tag{8.5}$$

Using this distribution, one can define a model average of a set of observables $a \in \mathbb{R}^l$ described by all the models. To do so, we also need to consider the fact, that the distribution of the data D induces a distribution on a for each model in $\mathcal{M}$. We define $Q_i : \mathbb{R}^l \to \mathbb{R}_{\geq 0}$ to be the resampling distribution of the observables a as obtained from model M_i that is induced by the distribution of D. We then define the model average of a as

$$\langle a \rangle_M = \sum_i \langle a \rangle_{Q_i} P(M_i|D) = \left\langle \langle a \rangle_Q \right\rangle_P . \tag{8.6}$$

The covariance matrix of a is then given by [116, 117, 119]

$$\begin{aligned}
\mathrm{Cov}_a^M &= \left\langle aa^T \right\rangle_M - \langle a \rangle_M \langle a \rangle_M^T \\
&= \left\langle \left\langle aa^T \right\rangle_Q \right\rangle_P - \left\langle \langle a \rangle_Q \right\rangle_P \left\langle \langle a \rangle_Q \right\rangle_P^T \\
&= \left\langle \left\langle aa^T \right\rangle_Q - \langle a \rangle_Q \langle a \rangle_Q^T \right\rangle_P + \left\langle \langle a \rangle_Q \langle a \rangle_Q^T \right\rangle_P - \left\langle \langle a \rangle_Q \right\rangle_P \left\langle \langle a \rangle_Q \right\rangle_P^T \\
&= \sum_i \mathrm{Cov}_a^{M_i} P(M_i|D) + \sum_i \langle a \rangle_{Q_i} \langle a \rangle_{Q_i}^T P(M_i|D) \\
&\quad - \left(\sum_i \langle a \rangle_{Q_i} P(M_i|D) \right) \left(\sum_j \langle a \rangle_{Q_j}^T P(M_j|D) \right).
\end{aligned} \tag{8.7}$$

Examples of the model average procedure are shown in figs. 8.8 and 8.9.
While this procedure helps with subjective bias in the choice of the fit interval, it still has to be used with care. The problem of choosing fit intervals that are expected to accurately describe the data still remains and thus the ranges as shown in figs. 8.8 and 8.9 have to be considered thoroughly. As a general rule, we do not include fit intervals that are longer than that with maximum model probability for the given type of fit and restrict the length further if deemed necessary, e.g. if the longest most probable model according to the AIC gives unreasonable results. Furthermore, fits with smaller fit intervals are not used if they are too noisy, i.e. if the errors of the fit parameters get unreasonably large as this is usually a characteristic of numerical instability. Lastly, all fit intervals end at the same timeslice $t_{\max}$ as shown in figs. 8.8 and 8.9 which is chosen such that it avoids running into the noise problem for baryons. For mesons on open boundary ensembles it might be necessary to restrict the fit intervals such that boundary effects are avoided.
This procedure is of course still subjective but reduces the bias from the model selection and accounts for varying predictions of different models by including the variance stemming from the choice of model in the error of the observables via eq. (8.7).
As the two-state fits have two more fit parameters than the single-state fits, we actually consider two different model distributions for their averages, P_1 where the sum over j in the normalization of eq. (8.5) includes all single- and two-state fits, and a distribution P_2 where the sum only includes the two-state fits. P_1 is used to compute the model average for the asymptotic mass, P_2 is used for the model average of the additional fit parameters in two-state fits.
Since the two-state fits for the isospin-breaking corrections use the results for ΔM from the fits of the isospin-symmetric effective mass, it is not sufficient to simply compute the variance of the model average, but the resampling distribution of ΔM has to have the correct variance as well. This is also the case for the

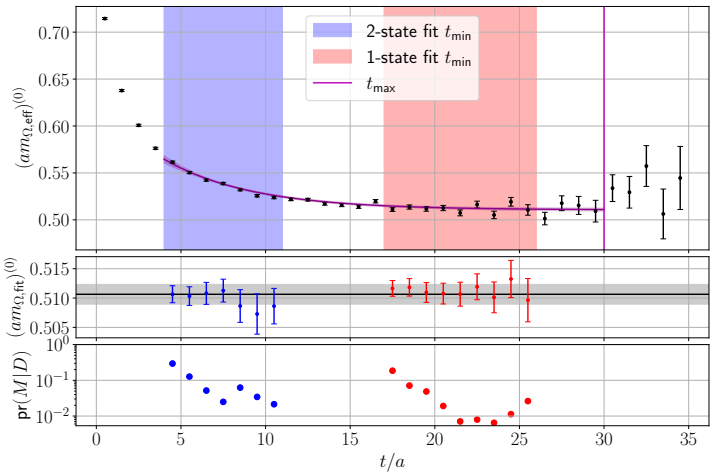

Figure 8.8: An example of an AIC model average for the isospin-symmetric effective mass of the Ω baryon on the N200 ensemble. The upper panel shows the effective mass with a blue region marking the starting points of individual two-state fits and the red region marking the starting points of individual single-state fits. All fit intervals end at the same maximum time $t_{\mathrm{max}} = 30a$ marked with a vertical line. The purple curve and band show the function $f(t) = am + \gamma e^{-\Delta M t}$ with each parameter set to the result of the model average. The center panel shows the individual results for the asymptotic mass for two-state fits in blue and single-state fits in red. The position of each data point indicates the start of the respective fit interval. The black line indicates the model average for the asymptotic mass and the gray band shows the error of the average. The lower panel shows the model probabilities for each of the models with the position of the data point indicating the start of the fit interval.

asymptotic masses obtained from the model average when they are used for the chiral fits in chapter 9.

One possible way to correct the resampling distribution to yield the correct variances and covariances is to add some random Gaussian noise a_0 to a that has mean 0 and whose covariance matrix is given by $\mathrm{Cov}_{a_0} = \mathrm{Cov}_a^M - \mathrm{Cov}_a^R$ where Cov_a^R is the covariance matrix of the resampling distribution of the model average. This works as long as all correlations of entries of a_0 and entries of a vanish[2], which is the case if a_0 is independently generated.

Another option is to apply a transformation

$$a \mapsto A(a - \overline{a^R}) + \overline{a^R} \tag{8.8}$$

to the resampled data, where $\overline{a^R}$ is the average of the resampling distribution and $A \in \mathbb{R}^{l \times l}$ is chosen such that the transformed distribution has the covariance matrix Cov_a^M. Note that the transformation does not change the mean of the distribution. Using the diagonalizations of $\mathrm{Cov}_a^R = ODO^T$ and $\mathrm{Cov}_a^M = U\Sigma U^T$,

[2] In general, $\mathrm{Cov}_a^M = \mathrm{Cov}_a^R + \mathrm{Cov}_{a_0} + 2\left\langle (a - \langle a \rangle)(a_0 - \langle a_0 \rangle)^T \right\rangle$ where the third term vanishes if all entries of a and a_0 are uncorrelated.

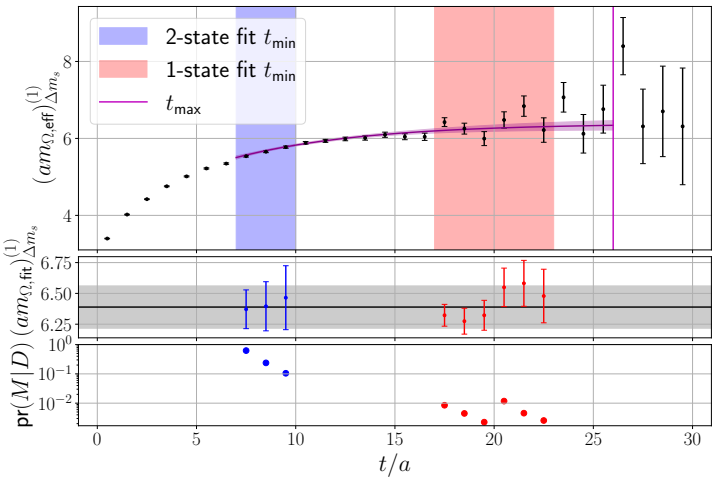

Figure 8.9: An example of an AIC model average for the contribution from strange mass detuning effective mass of the Ω baryon on the N200 ensemble. The upper panel shows the effective mass with a blue region marking the starting points of individual two-state fits and the red region marking the starting points of individual single-state fits. All fit intervals end at the same maximum time $t_{\mathrm{max}} = 27a$ marked with a vertical line. The purple curve and band show the function $f(t) = (am)^{(1)} + (\alpha - \beta t)e^{-\Delta M^{(0)} t}$ with each parameter set to the result of the model average. The center panel shows the individual results for the asymptotic mass for two-state fits in blue and single-state fits in red. The position of each data point indicates the start of the respective fit interval. The black line indicates the model average for the asymptotic mass and the gray band shows the error of the average. The lower panel shows the model probabilities for each of the models with the position of the data point indicating the start of the fit interval.

one choice of such a transformation would be

$$A = U\sqrt{\Sigma}\sqrt{D^{-1}}O^T,$$

which can be easily verified from the transformation of the covariance matrix under eq. (8.8),

$$\mathrm{Cov}_a^R \mapsto A\mathrm{Cov}_a^R A^T,$$

which yields Cov_a^M when using the above choice of A. Note, that this is not a unique choice, as for any $R \in O(l)$, the transformation $A = U\sqrt{\Sigma}R\sqrt{D^{-1}}O^T$ would result in the correct covariance matrix of the transformed distribution. We use this latter option (with $R = \mathbb{1}$) to determine the uncertainties quoted in chapter 9 where applicable.

Chapter 9
Extrapolation and Scale Setting

The extrapolation and scale setting strategy employed in this thesis mostly follows a publication by the RQCD collaboration [46] which uses baryon masses to set the scale of CLS $N_f = 2 + 1$ ensembles in isospin-symmetric QCD. The analysis discussed in this chapter, however, is not to be seen as a full analysis with a final result for the lattice scale. Rather, it is a test of the viability of the data gathered for this project for a high-precision determination of the lattice scale. We use only the marked ensembles in fig. 9.1.

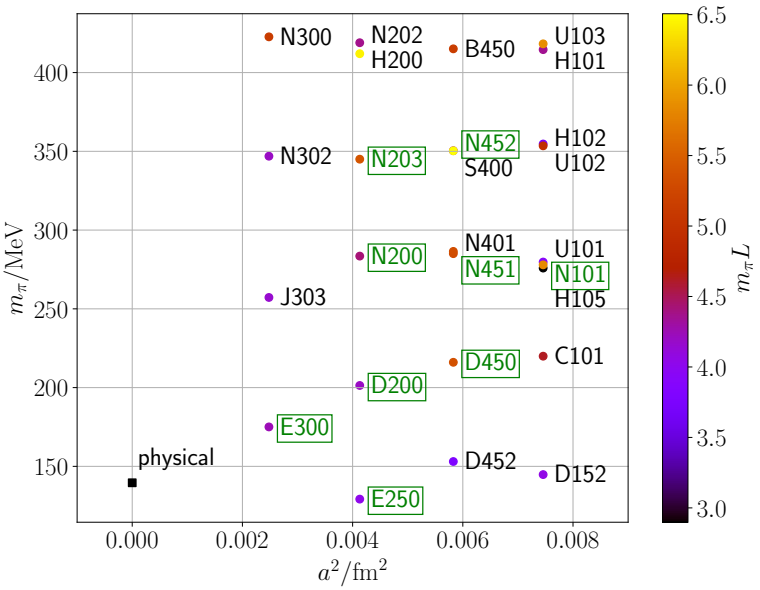

Figure 9.1: The CLS ensemble landscape restricted to the trajectory of constant average quark mass. The ensembles used in the following discussion are marked in green with a border and the black square shows the point of vanishing lattice spacing and physical pion mass. The color of each point indicates the total length of the lattice (in the spatial direction) scaled with the pion mass.

We start this chapter with a short discussion of the values we use for the flow scale t_0 in section 9.1. Section 9.2 continues with a description of the extrapolation strategy for baryon masses following the procedure of the RQCD collaboration

and our results for the extrapolation. Section 9.3 discusses how we determine the lattice scale from the baryon masses and compares our results to those found by other collaborations.

9.1. Determination of t_0

As in the approach to scale setting discussed in section 4.4, the Wilson flow scale t_0 (see section 4.4.2) is used as an intermediate scale in the following discussion. Individual values of the flow scale are measured on each ensemble in order to avoid the necessity to model the chiral dependence of t_0. Measurements of the gradient flow obtained via a program in the `openQCD` software package [47] were available for the Mainz Lattice group and used to determine the ensemble-wise values of $\frac{t_0}{a^2}$. This is done by resampling the available measurements of the gradient flow $a^4E(t)$ to find the two adjacent values t_i, t_{i+1} such that $t_i^2 \langle E(t_i)\rangle < 0.3 < t_{i+1}^2 \langle E(t_{i+1})\rangle$. We then linearly interpolate these points to determine the value $\frac{t_0}{a^2}$ of the flow time for which $t_0^2 \langle E(t_0)\rangle = 0.3$.

We found that the autocorrelation of t_0 is in fact too large to compensate for it via rebinning on the limited number of configurations available per ensemble as detailed in table 9.1. Since on some ensembles only 20 bins remain for the statistical analysis based on an estimate of the optimal binsize [87] (see eq. (6.21)), we decided to treat the uncertainties of t_0 with the Γ-method instead. This is done using the `pyerrors` python-package [120]. To use the measurements of t_0 in our resampling-based analysis, we rescale the bootstrap distribution of t_0 to reflect the uncertainties determined using the Γ-method.

Table 9.1: The autocorrelation time of t_0 for each ensembles measured on the respective subsets of ensembles we used for our analysis. The column B_{opt} lists the optimal binsize for the given replicum as per eq. (6.21) for which N_{bins} bins would be left for the statistical analysis.

Ensemble	τ_{int,t_0}	$\Delta\tau_{\text{int},t_0}$	B_{opt}	N_{bins}
A654	2.1928	0.0086	18	31
N101	2.8901	0.0030	19	21
			16	15
			18	19
			17	18
D450	3.6995	0.0068	24	20
N451	3.6815	0.0090	30	33
N452	3.6687	0.0083	30	33
D200	5.1790	0.0062	47	42
N203	5.1462	0.0073	34	22
			35	22
N200	5.1630	0.0070	36	23
			36	23
E250	5.2017	0.0038	38	26
E300	8.6193	0.0063	44	12

9.2. Extrapolation of Baryon Masses

We adopt an extrapolation procedure by the RQCD collaboration [46] based on chiral perturbation theory. This procedure makes use of the proxies

$$\begin{aligned} \overline{M}^2 &= \frac{2m_K^2 + m_\pi^2}{3} \approx 2B_0\bar{m}, \\ \delta M^2 &= 2\left(m_K^2 - m_\pi^2\right) \approx 2B_0\delta m \end{aligned} \tag{9.1}$$

for the average quark mass $\bar{m} = \frac{2m_l+m_s}{3}$ and the quark mass difference $\delta m = m_s - m_l$ based on the GMOR (see eqs. (4.25) and (4.26)). Furthermore, as in section 4.4.3, all dimensionful quantities are scaled with some appropriate power of t_0. To make the upcoming equations more readable, we thus adapt the notation from [46] for these scaled quantities,[1]

$$\mathrm{m} = \sqrt{8t_0}m, \quad \overline{\mathbb{M}}^2 = 8t_0\overline{M}^2, \quad \delta\mathbb{M}^2 = 8t_0\delta M^2, \quad \mathrm{a} = \frac{a}{\sqrt{8t_0}},$$

where m is a placeholder for various masses and a is the lattice spacing. $\frac{1}{8\mathrm{a}^2}$ thus is the measured value of t_0 in lattice units. The baryon masses are then parameterized as

$$\mathrm{m}_O(\mathrm{m}_\pi, \mathrm{m}_K, \mathrm{a}) = \left(\mathrm{m}_o + \bar{b}\,\overline{\mathbb{M}}^2 + \delta b_O \delta\mathbb{M}^2\right)\left(1 + c_o\mathrm{a}^2\right) \tag{9.2}$$

for an octet baryon $O \in \{N, \Lambda, \Sigma, \Xi\}$ and

$$\mathrm{m}_D(\mathrm{m}_\pi, \mathrm{m}_K, \mathrm{a}) = \left(\mathrm{m}_d + \bar{t}\,\overline{\mathbb{M}}^2 + \delta t_D \delta\mathbb{M}^2\right)\left(1 + c_d\mathrm{a}^2\right) \tag{9.3}$$

for a decuplet baryon $D \in \{\Delta, \Sigma^*, \Xi^*, \Omega\}$. In the above formulae, $m_{o/d}$ is the SU(3) mass of the octet/decuplet baryon. $\bar{b}$, $\bar{t}$, $c_{o/d}$, and $\bar{c}_{o/d}$ are constant for the respective multiplet, while δb_O and δt_D are different for each baryon. This is only the leading order of the parameterization and terms up to $\mathcal{O}\left(\overline{\mathbb{M}}^4, \delta\mathbb{M}^4\right)$ are included in the analysis by the RQCD collaboration [46]. However, due to the limited number of available ensembles at the time of writing, we use the simplest viable fit ansatz.

We determine the free parameters in eqs. (9.2) and (9.3) via a single global fit over various ensembles. The different hadron masses come from fits to the respective effective masses as described in section 8.3. These fits were performed with the `levenberg_marquardt` Rust library [121, 122] using the matrix representation of eqs. (9.2) and (9.3)

$$\begin{pmatrix} \mathrm{m}_{N,1} \\ \mathrm{m}_{\Lambda,1} \\ \mathrm{m}_{\Sigma,1} \\ \mathrm{m}_{\Xi,1} \\ \mathrm{m}_{\Omega,1} \\ \mathrm{m}_{N,2} \\ \vdots \\ \mathrm{m}_{\Omega,n} \end{pmatrix} = (X + c_o X_o + c_d X_d) \begin{pmatrix} \mathrm{m}_o \\ \mathrm{m}_d \\ \bar{b} \\ \bar{t} \\ \delta b_N \\ \delta b_\Lambda \\ \delta b_\Sigma \\ \delta b_\Xi \\ \delta t_\Omega \end{pmatrix}, \tag{9.4}$$

[1] In the referenced paper, a is scaled with $\sqrt{8t_0^*}$ where t_0^* is the value of t_0 at the SU(3) symmetric point. In this project, we instead scale the lattice spacing with the measured value of t_0 on each ensemble.

where the indices 1 through n label the different ensembles included in the fit and the matrices X, X_o, and X_d given by

$$X = \begin{pmatrix} 1 & 0 & \overline{\mathbb{M}}_1^2 & 0 & \delta\mathbb{M}_1^2 & 0 & 0 & 0 & 0 \\ 1 & 0 & \overline{\mathbb{M}}_1^2 & 0 & 0 & \delta\mathbb{M}_1^2 & 0 & 0 & 0 \\ 1 & 0 & \overline{\mathbb{M}}_1^2 & 0 & 0 & 0 & \delta\mathbb{M}_1^2 & 0 & 0 \\ 1 & 0 & \overline{\mathbb{M}}_1^2 & 0 & 0 & 0 & 0 & \delta\mathbb{M}_1^2 & 0 \\ 0 & 1 & 0 & \overline{\mathbb{M}}_1^2 & 0 & 0 & 0 & 0 & \delta\mathbb{M}_1^2 \\ & & & & & & & & \\ 1 & 0 & \overline{\mathbb{M}}_2^2 & 0 & \delta\mathbb{M}_2^2 & 0 & 0 & 0 & 0 \\ & & & \vdots & & & & & \\ 1 & 0 & \overline{\mathbb{M}}_n^2 & 0 & 0 & 0 & 0 & \delta\mathbb{M}_n^2 & 0 \\ 0 & 1 & 0 & \overline{\mathbb{M}}_n^2 & 0 & 0 & 0 & 0 & \delta\mathbb{M}_n^2 \end{pmatrix},$$

$$X_o = \begin{pmatrix} \mathbb{a}_1^2 & 0 & \mathbb{a}_1^2\overline{\mathbb{M}}_1^2 & 0 & \mathbb{a}_1^2\delta\mathbb{M}_1^2 & 0 & 0 & 0 & 0 \\ \mathbb{a}_1^2 & 0 & \mathbb{a}_1^2\overline{\mathbb{M}}_1^2 & 0 & 0 & \mathbb{a}_1^2\delta\mathbb{M}_1^2 & 0 & 0 & 0 \\ \mathbb{a}_1^2 & 0 & \mathbb{a}_1^2\overline{\mathbb{M}}_1^2 & 0 & 0 & 0 & \mathbb{a}_1^2\delta\mathbb{M}_1^2 & 0 & 0 \\ \mathbb{a}_1^2 & 0 & \mathbb{a}_1^2\overline{\mathbb{M}}_1^2 & 0 & 0 & 0 & 0 & \mathbb{a}_1^2\delta\mathbb{M}_1^2 & 0 \\ 0 & 0 & 0 & 0 & 0 & 0 & 0 & 0 & 0 \\ & & & & & & & & \\ \mathbb{a}_2^2 & 0 & \mathbb{a}_2^2\overline{\mathbb{M}}_2^2 & 0 & \mathbb{a}_2^2\delta\mathbb{M}_2^2 & 0 & 0 & 0 & 0 \\ & & & \vdots & & & & & \\ \mathbb{a}_n^2 & 0 & \mathbb{a}_n^2\overline{\mathbb{M}}_n^2 & 0 & 0 & 0 & 0 & \mathbb{a}_n^2\delta\mathbb{M}_n^2 & 0 \\ 0 & 0 & 0 & 0 & 0 & 0 & 0 & 0 & 0 \end{pmatrix},$$

$$X_d = \begin{pmatrix} 0 & 0 & 0 & 0 & 0 & 0 & 0 & 0 & 0 \\ 0 & 0 & 0 & 0 & 0 & 0 & 0 & 0 & 0 \\ 0 & 0 & 0 & 0 & 0 & 0 & 0 & 0 & 0 \\ 0 & 0 & 0 & 0 & 0 & 0 & 0 & 0 & 0 \\ 0 & \mathbb{a}_1^2 & 0 & \mathbb{a}_1^2\overline{\mathbb{M}}_1^2 & 0 & 0 & 0 & 0 & \mathbb{a}_1^2\delta\mathbb{M}_1^2 \\ & & & & & & & & \\ 0 & 0 & 0 & 0 & 0 & 0 & 0 & 0 & 0 \\ & & & \vdots & & & & & \\ 0 & 0 & 0 & 0 & 0 & 0 & 0 & 0 & 0 \\ 0 & \mathbb{a}_n^2 & 0 & \mathbb{a}_n^2\overline{\mathbb{M}}_n^2 & 0 & 0 & 0 & 0 & \mathbb{a}_n^2\delta\mathbb{M}_n^2 \end{pmatrix}.$$

This representation of the fit function makes it simple to construct the residuals

$$r = \sqrt{V}(y - (X + c_o X_o + c_d X_d)\theta),$$

where

$$y = (\mathbb{m}_{N,1}, \mathbb{m}_{\Lambda,1}, \mathbb{m}_{\Sigma,1}, \mathbb{m}_{\Xi,1}, \mathbb{m}_{\Omega,1}, \mathbb{m}_{N,2}, \cdots, \mathbb{m}_{\Omega,n})^T,$$
$$\theta = \left(\mathbb{m}_o, \mathbb{m}_d, \bar{b}, \bar{t}, \delta b_N, \delta b_\Lambda, \delta b_\Sigma, \delta b_\Xi, \delta t_\Omega\right)^T.$$

These residuals and their Jacobians are required for the Levenberg-Marquardt algorithm minimizing

$$\chi^2 = (y - (X + c_o X_o + c_d X_d)\theta)^T V (y - (X + c_o X_o + c_d X_d)\theta), \tag{9.5}$$

where V is the block-diagonal inverse covariance matrix

$$V = \begin{pmatrix} \mathrm{Cov}_{\mathbb{m}_1}^{-1} & 0 & \cdots & 0 \\ 0 & \mathrm{Cov}_{\mathbb{m}_2}^{-1} & \cdots & 0 \\ \vdots & \vdots & \ddots & \vdots \\ 0 & 0 & \cdots & \mathrm{Cov}_{\mathbb{m}_n}^{-1} \end{pmatrix}, \qquad \mathbb{m}_i = \begin{pmatrix} \mathbb{m}_{N,i} \\ \mathbb{m}_{\Lambda,i} \\ \vdots \\ \mathbb{m}_{\Omega,i} \end{pmatrix}$$

of y. Note, that from the decuplet baryons we only include the Ω. We do so because the other decuplet baryons are unstable in QCD and thus need extra care when determining ground state masses.

A problem arises when fitting eq. (9.4) to our current data as the ensembles processed for this project thus far all have very similar average quark mass $\bar{m} \propto \overline{M}^2$. Our fits can thus not sufficiently discern the influences of the average quark mass and the SU(3) octet- or decuplet masses in eqs. (9.2) and (9.3) leading to large uncertainties in the fit results for these quantities. This effect is unfortunately extreme enough to make a determination of the physical point with the available data impossible, as we will explain in more detail in section 9.3. For this reason, we choose to either fit the SU(3) masses or the parameter multiplying the average quark mass for each SU(3) multiplet, setting the other parameter to 0. For the results quoted in this document, we opt to remove $\bar{b}$ and $\bar{t}$ from our fits as these fits turned out to be more stable. The results for the different parameters listed in table 9.2.

Table 9.2: The fit results for the extrapolations in eqs. (9.2) to (9.4) with $\bar{b} = \bar{t} = 0$. m_B and c_B denote the SU(3) octet- or decuplet-masses and the octet's or decuplet's lattice spacing coefficient respectively.

B	$\mathbb{m}_B$	c_B	$\delta b_B/\delta t_B$
N	2.510(27)	−0.25(23)	−0.276(44)
Λ			-0.100(18)
Σ			-0.009(13)
Ξ			0.121(29)
Ω	3.057(57)	-0.71(31)	0.202(33)

The dependence of the baryon masses on $\mathbb{m}_\pi$, $\mathbb{m}_K$, $\mathbb{a}^2$ and δM^2 is shown in fig. 9.2. In these plots (except for the one showing the δM^2-dependence) all but the specified variables are fixed to their physical value. The way these physical values are determined is explained in section 9.3.

Instead of parameterizing our fits in terms of the coefficients in table 9.2, one could also fit the low-energy-constants (LECs) b_0, b_D, b_F, t_{D^0}, and t_D which are related to the other coefficients via [46]

$$\bar{b} = -6b_0 - 4b_D, \quad \bar{t} = 3t_{D^0} + 3t_D,$$
$$\delta b_N = \frac{2}{3}(3b_F - b_D), \quad \delta b_\Lambda = -\frac{4}{3}b_D, \quad \delta b_\Sigma = \frac{4}{3}b_D, \quad \delta b_\Xi = -\frac{2}{3}(3b_F + b_D),$$
$$\delta t_\Delta = -t_D, \quad \delta t_{\Sigma^*} = 0, \quad \delta t_{\Xi^*} = t_D, \quad \delta t_\Omega = 2t_D.$$

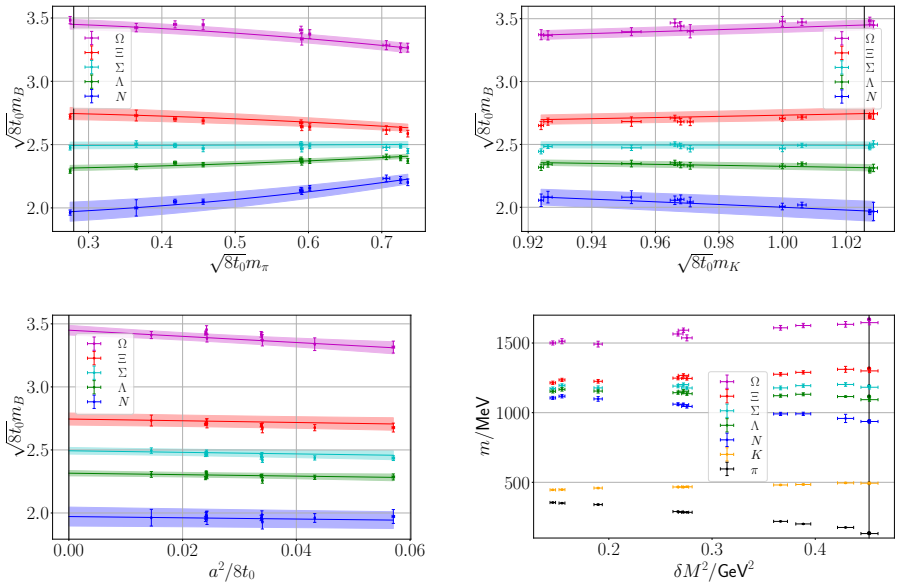

Figure 9.2: The extrapolation of the baryon octet states and the Ω baryon via eqs. (9.2) and (9.3) as a function of the pion mass at physical kaon mass and $a = 0$ (top left), the kaon mass at physical pion mass with $a = 0$ (top right), the squared lattice spacing at physical pion and kaon masses (bottom left), and δM^2 (bottom right). The physical pion and kaon masses here mean the ones listed in table 9.3 scaled with $\sqrt{8t_0^{\text{phys}}}$ from table 9.4 with $\mathfrak{S} = \Lambda$. Each data point corresponds to the respective baryon mass as measured on a single ensemble and the black vertical line corresponds to the physical point determined via eqs. (9.6) and (9.7). In the bottom right panel, the masses are scaled with the respective lattice scale determined with the Λ baryon as reference (see table 9.5).

This fit procedure can simply be implemented by replacing θ in eq. (9.5) by[2]

$$\tilde{\theta} = \begin{pmatrix} 1 & 0 & 0 & 0 & 0 & 0 & 0 \\ 0 & 1 & 0 & 0 & 0 & 0 & 0 \\ 0 & 0 & -6 & -4 & 0 & 0 & 0 \\ 0 & 0 & 0 & 0 & 0 & 3 & 3 \\ 0 & 0 & 0 & -\frac{2}{3} & 2 & 0 & 0 \\ 0 & 0 & 0 & -\frac{4}{3} & 0 & 0 & 0 \\ 0 & 0 & 0 & \frac{4}{3} & 0 & 0 & 0 \\ 0 & 0 & 0 & -\frac{2}{3} & -2 & 0 & 0 \\ 0 & 0 & 0 & 0 & 0 & 0 & 2 \end{pmatrix} \begin{pmatrix} \mathbb{m}_o \\ \mathbb{m}_d \\ b_0 \\ b_D \\ b_F \\ t_{D^0} \\ t_D \end{pmatrix}$$

in which case we can still explicitly set $\bar{b}$ and $\bar{t}$ to 0 in the fit by setting the columns of X, X_o, and X_d in eq. (9.4) corresponding to the specific fit parameter to 0 or removing the respective column from each matrix and the respective row from the parameter vector θ.
We found that this approach generally results in smaller uncertainties on the δb_B and δt_B as well as some derived (extrapolated) quantities such as $\sqrt{8t_0^{\text{phys}}}$

[2]Note that we exclude Δ, Σ*, and Ξ* from our fits. Thus, the corresponding rows are missing.

discussed in section 9.3. However, the baryon masses extrapolated to the physical point with the LEC fit results are less consistent with the experimental values and we still have to leave the $\overline{\mathbb{M}}^2$-dependence out of the fit to be able to determine the physical point. As the latter fact introduces additional systematic errors, we decided to stick to fitting the set of parameters in eq. (9.5) directly which yields less precise but more realistic results.
Note, however, that our fit results in table 9.2 are not compatible with the parameterization via LECs as that would imply that $\delta b_\Lambda = -\delta b_\Sigma$ whereas in our fit δb_Σ seems to be compatible with 0.
In general, there is a quark mass dependence of the strong gauge coupling (see eq. (3.20)) which in its inverse form reads

$$a_0(g^2) = a(\tilde{g}^2(g^2, a\bar{m}))(1 - b_a a\bar{m})$$

with $b_a = 0.315\,83(5)$ for three quark flavors [46]. This leads to $\mathcal{O}(a)$ effects that have to be taken into account. However, as we are only concerned with ensembles lying on a line of (approximately) constant $\bar{m}$ at the time of writing, we neglect this correction for the time being.
Furthermore, note that here and throughout the rest of this thesis we only quote purely statistical uncertainties of our results.

9.3. Setting the Lattice Scale

As in the procedures described in section 4.4.3 and in [46] (on which the rest of this section builds upon), we use the Wilson flow scale t_0 to determine the lattice spacings a for each value of the strong gauge coupling $g^2 = \frac{6}{\beta}$. We do so by matching the lattice measurements $\frac{t_0}{a^2}$ of this scale to a physical value t_0^{phys} that is determined using experimental input. In our case, this experimental input comes from the mass of one of the baryons we extrapolate as discussed in section 9.2 as well as the masses of the π and K mesons in terms of which the baryon masses are extrapolated. As our computation is based on isospin-symmetric data for which no experimental data is available, we use experimental values corrected for isospin-breaking effects [46] listed in table 9.3. These modified experimental values are estimated as [46]

$$\begin{aligned}
m_N &= \frac{1}{2}\left(m_{\Xi^0} + m_{\Xi^-} - \delta m^{\text{QED}}\right),\\
m_\Sigma &= \frac{1}{2}\left(m_{\Sigma^+} + m_{\Sigma^-}\right) - \delta m^{\text{QED}},\\
m_\Xi &= \frac{1}{2}\left(m_\Xi^0 + m_\Xi^- - \delta m^{\text{QED}}\right),\\
m_\Omega &= m_\Omega - 3\,\text{MeV}
\end{aligned}$$

with $\delta m^{\text{QED}} = m_p - m_n - \frac{1}{2}(m_{\Sigma^+} - m_{\Sigma^-}) = 2.75(11)\,\text{MeV}$ assuming that the splittings can be described by two additive parameters δm^{QCD} and δm^{QED} accounting for strong and electromagnetic isospin-breaking respectively. For the pion and kaon, the mass values of the FLAG 2016 Review [123] are used. For the remainder of this chapter, we mark a value taken from table 9.3 with the superscript "exp".

Table 9.3: Physical hadron masses corrected for isospin-breaking effects taken from [46] which we use as input for the determination of $\sqrt{8t_0^{\text{phys}}}$. The authors of [46] note that due to the prescription used to correct for isospin-breaking, "an additional uncertainty of up to 2 MeV may exist".

Hadron H	m_H^{exp} / MeV
π	134.8(3)
K	494.8(3)
N	937.54(6)
Λ	1115.68(1)
Σ	1190.66(12)
Ξ	1316.9(3)
Ω	1669.5(3.0)

For a given scale $\mathfrak{S} \in \{N, \Lambda, \Sigma, \Xi, \Omega\}$, we define the physical point, i.e. the point in the space spanned by m_π, m_K, and a, as the point at which the ratios $\frac{\mathrm{m}_\mathfrak{S}(\mathrm{m}_\pi, \mathrm{m}_K, \mathrm{a})}{\mathrm{m}_\pi}$ and $\frac{\mathrm{m}_\mathfrak{S}(\mathrm{m}_\pi, \mathrm{m}_K, \mathrm{a})}{\mathrm{m}_K}$ take on the *experimental* values $\frac{m_\mathfrak{S}^{\text{exp}}}{m_\pi^{\text{exp}}}$ and $\frac{m_\mathfrak{S}^{\text{exp}}}{m_K^{\text{exp}}}$ where $\mathrm{a} = 0$. We define t_0^{phys} via the ratio of $\mathrm{m}_\mathfrak{S}$ and $m_\mathfrak{S}^{\text{exp}}$ at this point;

$$\sqrt{8t_0^{\text{phys}}} = \frac{\mathrm{m}_\mathfrak{S}\left(\mathrm{m}_\pi = \frac{m_\pi^{\text{exp}}}{m_\mathfrak{S}^{\text{exp}}}\mathrm{m}_\mathfrak{S}, \mathrm{m}_K = \frac{m_K^{\text{exp}}}{m_\mathfrak{S}^{\text{exp}}}\mathrm{m}_\mathfrak{S}, \mathrm{a} = 0\right)}{m_\mathfrak{S}^{\text{exp}}}. \tag{9.6}$$

Plugging the arguments of the numerator of the right-hand side of eq. (9.6) into eq. (9.2) for an octet state $\mathfrak{S}$, we find that the numerator is a solution of

$$\mathrm{m}_\mathfrak{S} = \mathrm{m}_o + \left(\bar{\alpha}\bar{b} + \delta\alpha\delta b_\mathfrak{S}\right)\mathrm{m}_\mathfrak{S}^2,$$

where $\bar{\alpha} = \frac{2m_K^{\text{exp}} + m_\pi^{\text{exp}}}{3m_\mathfrak{S}^{\text{exp}}}$, and $\delta\alpha = 2\left(\frac{m_K^{\text{exp}} - m_\pi^{\text{exp}}}{m_\mathfrak{S}^{\text{exp}}}\right)$. At the physical point, the mass of $\mathfrak{S}$ is thus given by

$$\mathrm{m}_\mathfrak{S} = \frac{1 \pm \sqrt{1 - 4\mathrm{m}_o\left(\bar{\alpha}\bar{b} + \delta\alpha\delta b_\mathfrak{S}\right)}}{2\left(\bar{\alpha}\bar{b} + \delta\alpha\delta b_\mathfrak{S}\right)}. \tag{9.7}$$

For $\mathfrak{S} = \Omega$, replace $\mathrm{m}_o \leftrightarrow \mathrm{m}_d$, $\bar{b} \leftrightarrow \bar{t}$, and $\delta b_\mathfrak{S} \leftrightarrow \delta t_\Omega$.
Note, that eq. (9.7) has two solutions since it solves a quadratic equation. However, one of these solutions results in unphysical, sometimes negative masses for the remaining baryons and can thus be discarded.
A problem we see with our current data arises, when the uncertainties of the fit parameters m_o, $\bar{b}$, and $\delta b_\mathfrak{S}$ (or their counterparts for the decuplet) are too large such that the discriminant $1 - 4\mathrm{m}_o\left(\bar{\alpha}\bar{b} + \delta\alpha\delta b_\mathfrak{S}\right)$ in eq. (9.7) becomes negative on individual bootstrap samples. In that case, the variance of $\mathrm{m}_\mathfrak{S}$ cannot be estimated using the bootstrap procedure due to complex-valued contributions. In our case, this happens, if we try to fit all parameters in eqs. (9.2) to (9.4) of which $\bar{b}$ and $\bar{t}$ cannot be reasonably resolved simultaneously with m_o and m_d on our data for which $\overline{\mathbb{M}}^2$ only varies slightly. This has the effect, that the $\overline{\mathbb{M}}^2$ dependence in our data is almost constant and thus does not give any additional information that cannot be absorbed in $\mathrm{m}_{o/d}$. We thus explicitly set $\bar{b}$ and $\bar{t}$ to

0 as discussed in section 9.2 to circumvent this problem resulting in well-defined variances of $\mathbb{m}_{\mathfrak{S}}$.

Since we extrapolate all baryon masses simultaneously with shared parameters, we can compute physical masses for each baryon via

$$m_B = \frac{\mathbb{m}_B}{\sqrt{8t_0^{\text{phys}}}}$$

using the physical value of t_0 from eq. (9.6) and the extrapolated value of $\mathbb{m}_B$ at the physical point. The results of this computation are shown in table 9.4 and fig. 9.3.

Table 9.4: The hadronic spectrum extrapolated to the physical point and t_0^{phys} determined from the results in table 10.1. For each column a different baryon mass was used as the scale $\mathfrak{S}$ to define $\sqrt{8t_0^{\text{phys}}}$. The masses in MeV are computed via $m_B = \frac{\mathbb{m}_B}{\sqrt{8t_0^{\text{phys}}}}$ where $\mathbb{m}_B$ is extrapolated to the physical point.

Obs. \ $\mathfrak{S}$	N	Λ	Σ	Ξ	Ω
$\sqrt{8t_0^{\text{phys}}}$/fm	0.413(11)	0.4095(37)	0.4131(44)	0.4117(87)	0.4072(60)
m_N/MeV	937.54(50)	950(35)	937(48)	942(40)	958(46)
m_Λ/MeV	1105(31)	1115.68(18)	1104(19)	1109(27)	1123(24)
m_Σ/MeV	1191(39)	1201(17)	1190.66(13)	1195(30)	1208(20)
m_Ξ/MeV	1313(30)	1323(22)	1313(27)	1316.90(38)	1329(30)
m_Ω/MeV	1651(40)	1662(23)	1651(21)	1655(35)	1669.5(3.1)

Note, that in [46] the authors use $t_0^\star$ instead of t_0^{phys} for the computation of physical observables and setting the lattice scale, where $t_0^\star$ is defined as the value of t_0 on the symmetric $m_l = m_s$ line characterized by

$$\phi_4^\star = 8t_0^\star\left(m_K^2 + \frac{1}{2}m_\pi^2\right) = 12t_0^\star m_\pi^2 = 1.110.$$

However, as of the writing of this thesis, we do not have data available at this trajectory. Thus, we use t_0^{phys} instead. Nonetheless, our results can reasonably be compared to such determined using $t_0^\star$ since the two values are related via [46]

$$\sqrt{8t_0^\star} = 0.999\,74(4)\sqrt{8t_0^{\text{phys}}}$$

which is an insignificant difference compared to the uncertainties we find for $\sqrt{8t_0^{\text{phys}}}$ (cf. table 9.4).
To determine the lattice spacing for each value of β, we make use of the fact that the measured values of $\mathbb{a}^2 = \frac{a^2}{8t_0}$ fluctuate at a level much smaller than their uncertainties for a given strong gauge coupling, such that we can assign a lattice spacing for a given beta via

$$a(\beta) = \sqrt{8t_0^{\text{phys}}\overline{\mathbb{a}_\beta^2}} \tag{9.8}$$

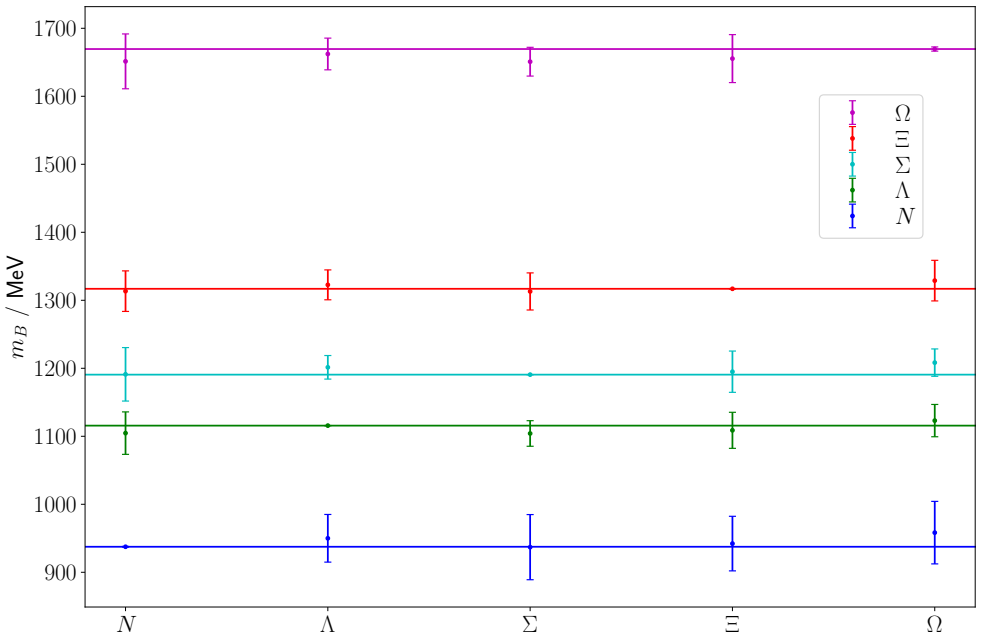

Figure 9.3: A visual representation of the results for the baryon masses at the physical point listed in table 9.4. Each vertical stack of errorbars corresponds to the results using the baryon indicated at the bottom of the plot to determine the physical point. The horizontal lines correspond to the hadron masses used as *experimental input* as listed in table 9.3.

where $\overline{\mathrm{a}^2_\beta}$ is an average value of $\frac{a^2}{8t_0}$ over all ensembles simulated at QCD gauge coupling $g^2 = \frac{6}{\beta}$ which we determine via a constant fit according to eq. (B.4). Table 9.5 lists a set of results for this computation for each β in our set of ensembles and each value of $\sqrt{8t_0^{\mathrm{phys}}}$ listed in table 9.4.

Table 9.5: The lattice spacings $a(m_{\mathfrak{G}})$ determined for each inverse strong gauge coupling β analyzed in this thesis. The values are computed via eq. (9.8) using the results for $\sqrt{8t_0^{\mathrm{phys}}}$ in table 9.4.

β	$a(m_N)$ / fm	$a(m_\Lambda)$ / fm	$a(m_\Sigma)$ / fm	$a(m_\Xi)$ / fm	$a(m_\Omega)$ / fm
3.34	0.0987(26)	0.09787(90)	0.0987(10)	0.0984(21)	0.0973(14)
3.4	0.0859(22)	0.08520(77)	0.08596(91)	0.0856(18)	0.0847(12)
3.46	0.0761(20)	0.07548(69)	0.07615(80)	0.0759(16)	0.0751(11)
3.55	0.0642(17)	0.06369(58)	0.06426(68)	0.0640(13)	0.06333(93)
3.7	0.0498(13)	0.04934(45)	0.04978(52)	0.0496(10)	0.04906(72)

A comparison of our results for $\sqrt{8t_0^{\mathrm{phys}}}$ and the different lattice spacings to different publications is shown in fig. 9.4. Note, that our results using m_Ξ for the determination of the physical point are very similar to those computed by the RQCD collaboration in [46] with the same quantity, albeit with a larger error. However, their computation is expected to be more precise as they include five times the number of ensembles. These additional ensembles especially include ones from trajectories in parameter space which do not lie on the line of constant

average quark mass as our selection does. We thus expect their fits of the parameterization of octet and decuplet quark masses in according to eqs. (9.2) and (9.3) to be more sensitive to the average quark mass proxy $\overline{\mathbb{M}}^2$ making it possible to fit the full set of parameters. This should be investigated in the future by adding ensembles from these additional trajectories of SU(3)-symmetric ensembles and ensembles on a line of constant strange quark mass.

Table 9.6: Isospin-symmetric masses for all considered hadrons and all ensembles. am_H and $\sqrt{8t_0}m_H$ are computed on each ensemble directly, while m_H / MeV is computed by dividing am_H by the lattice spacing listed for the corresponding value of β in table 9.5 with the Λ baryon used to determine the physical point.

β	Ensemble	Obs. \ H	π	K	N	Λ	Σ	Ξ	Ω
3.34	A654	am_H	0.1687(13)	0.22751(100)	0.5447(55)	0.5726(37)	0.5839(36)	0.6074(25)	0.7398(84)
		$\sqrt{8t_0}m_H$	0.7062(47)	0.9525(30)	2.280(22)	2.397(14)	2.445(14)	2.5429(92)	3.097(34)
		m_H / MeV	340.3(3.8)	458.9(4.4)	1099(17)	1155(14)	1178(14)	1225(13)	1492(21)
3.4	N101	am_H	0.12286(41)	0.20189(24)	0.4508(30)	0.4903(26)	0.5080(26)	0.5377(19)	0.6633(67)
		$\sqrt{8t_0}m_H$	0.5909(18)	0.97094(93)	2.168(14)	2.358(12)	2.443(12)	2.5858(88)	3.190(33)
		m_H / MeV	284.7(2.7)	467.8(4.3)	1045(12)	1136(12)	1177(12)	1246(12)	1537(22)
3.46	D450	am_H	0.08392(28)	0.18389(12)	0.3789(26)	0.4289(14)	0.4503(31)	0.48778(94)	0.6152(31)
		$\sqrt{8t_0}m_H$	0.4563(14)	0.99993(86)	2.060(14)	2.3320(73)	2.448(16)	2.6523(52)	3.345(17)
		m_H / MeV	219.5(2.1)	481.0(4.4)	991(11)	1122(11)	1178(13)	1276(12)	1609(17)
	N451	am_H	0.11088(26)	0.17835(16)	0.4056(15)	0.4372(18)	0.4552(22)	0.4771(14)	0.5983(16)
		$\sqrt{8t_0}m_H$	0.6018(12)	0.9680(10)	2.2015(79)	2.3726(96)	2.471(11)	2.5894(76)	3.2473(88)
		m_H / MeV	290.0(2.7)	466.5(4.3)	1061(10)	1143(11)	1191(12)	1248(12)	1565(15)
	N452	am_H	0.13569(17)	0.17047(14)	0.4228(17)	0.4408(18)	0.4485(15)	0.4643(15)	0.5736(20)
		$\sqrt{8t_0}m_H$	0.73551(78)	0.92406(78)	2.2919(89)	2.3894(91)	2.4311(78)	2.5169(80)	3.109(11)
		m_H / MeV	354.9(3.3)	445.9(4.1)	1106(11)	1153(11)	1173(11)	1214(12)	1500(15)

3.55	D200	am_H	0.06494(34)	0.15630(22)	0.3199(23)	0.36524(94)	0.3852(15)	0.41598(77)	0.5245(16)
		$\sqrt{8t_0}m_H$	0.4180(21)	1.0061(13)	2.059(15)	2.3509(61)	2.4795(98)	2.6776(49)	3.376(10)
		m_H / MeV	201.3(2.1)	484.5(4.5)	992(12)	1132(11)	1194(12)	1289(12)	1626(16)
	N203	am_H	0.11309(23)	0.14435(20)	0.3607(25)	0.3767(24)	0.3859(14)	0.3985(11)	0.4880(38)
		$\sqrt{8t_0}m_H$	0.7257(15)	0.9262(13)	2.315(16)	2.417(15)	2.4759(88)	2.5571(67)	3.131(24)
		m_H / MeV	350.5(3.2)	447.4(4.1)	1118(12)	1168(13)	1196(11)	1235(12)	1513(18)
	N200	am_H	0.09179(36)	0.15032(24)	0.3410(26)	0.3723(21)	0.3878(17)	0.4090(16)	0.5136(23)
		$\sqrt{8t_0}m_H$	0.5899(22)	0.9661(15)	2.192(16)	2.393(13)	2.492(11)	2.6284(98)	3.301(15)
		m_H / MeV	284.5(2.8)	465.9(4.3)	1057(11)	1154(11)	1202(11)	1268(12)	1592(16)
	E250	am_H	0.04261(13)	0.159269(42)	0.3022(28)	0.3527(19)	0.3815(21)	0.41936(87)	0.5311(16)
		$\sqrt{8t_0}m_H$	0.27484(81)	1.02741(40)	1.949(18)	2.276(12)	2.461(14)	2.7052(57)	3.426(10)
		m_H / MeV	132.1(1.3)	493.7(4.5)	937(12)	1093(11)	1183(12)	1300(12)	1646(16)
3.7	E300	am_H	0.04396(24)	0.12387(13)	0.2396(78)	0.2788(30)	0.3005(26)	0.3277(48)	0.4084(31)
		$\sqrt{8t_0}m_H$	0.3651(20)	1.0286(12)	1.990(65)	2.315(25)	2.496(22)	2.721(40)	3.391(26)
		m_H / MeV	175.9(2.0)	495.6(4.6)	959(29)	1115.7(4.7)	1202(13)	1311(21)	1634(20)

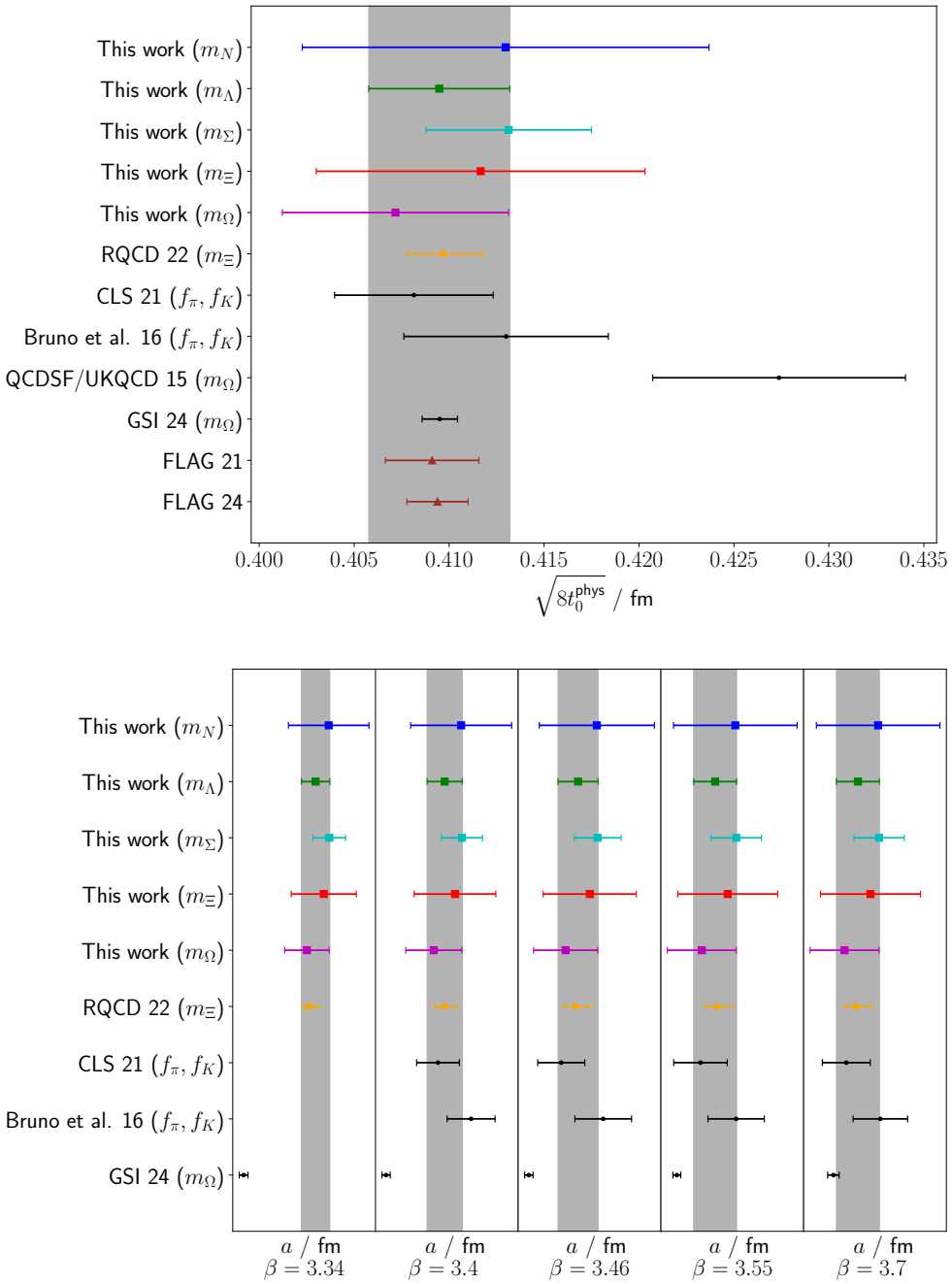

Figure 9.4: Comparison of our results for the physical value of $\sqrt{8t_0}$ (top panel) with different other works (RQCD [46],CLS 21 [41], Bruno et al. 16 [40], QCDSF/UKQCD 15 [124], GSI 24 [68]) as well as the flag averages of the 2021 and 2024 publications (FLAG 21 [70], FLAG 24 [71]). The bottom panel shows the analogous comparison of our results for the lattice spacings at different values of β for which we have data available at the time of writing. The gray band band corresponds to our result using m_Λ to define the physical point. The five topmost values in each plot are our results and the observables in brackets in each line indicate the quantity used to compute the respective value of $\sqrt{8t_0^{\text{phys}}}$.

Chapter 10
Isospin-Breaking Corrections to Hadronic Masses

While in chapter 9 we only discussed isospin-symmetric calculations, this chapter covers our results for the isospin-breaking corrections. As these corrections are expensive to compute, we start in section 10.1 with a discussion of a method we developed to reduce the computational cost for the most expensive part of the computation with stochastical inference of the corrections stemming from photon interactions. We continue in section 10.2 by addressing the method we use to determine the coefficients $\Delta\varepsilon$ necessary to perform the isospin-breaking expansion described in section 5.2. Finally, in section 10.3 we propose a method for setting the scale in the presence of isospin-breaking corrections.

10.1. Improvement of Computation Time of QED Corrections

The computation of isospin-breaking corrections to hadronic masses is more involved than a simple isospin-symmetric computation and thus takes up more computational resources. Figure 10.1 shows how the time spent in the computation described in section 8.1 is split up between the different parts of the calculation for three of our ensembles. As can be seen from these pie charts, the QED part of the calculation takes up roughly half of the total computational time.
We found, however, that part of the QED calculation can be replaced by an inference of its results from the other contributions via linear regression, i.e.

$$\begin{aligned} C^{(1)}_{H,e^2}(t) \approx & c_{H,0}(t)C^{(0)}_H(t) + c_{H,u}(t)C^{(1)}_{H,\Delta m_u}(t) + c_{H,d}(t)C^{(1)}_{H,\Delta m_d}(t) \\ & + c_{H,s}(t)C^{(1)}_{H,\Delta m_s}(t) + d_H(t), \end{aligned} \tag{10.1}$$

which has to be done for any hadron H individually. Note, that we choose to describe each timeslice of the correlation function with a different set of coefficients instead of trying to infer the correlation function as a whole.
To determine the coefficients $c_{H,x}(t)$ and $d_H(t)$ for a hadron H, we compute the full QCD correction on all sources on a subset of the configurations of a given ensemble, of which we treat the different correlation functions for each individual source as different measurements. For a subset of N_c gauge configurations with

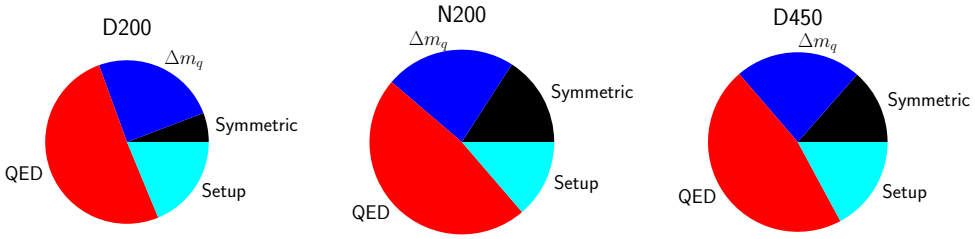

Figure 10.1: Distribution of computing time onto different parts of the calculation on three ensembles. Δm_q means the computation of the mass-shift corrections and *QED* denotes the computations of corrections to correlation functions involving photons. *Setup* includes all parts that are shared between all computations, including loading gauge configurations, constructing the deflation subspace, source smearing and the first inversions (i.e. solving $D_f \mathcal{S}_f^{(0)} = \eta$ as described in section 8.1.3) for the $\mathrm{QCD}_{\mathrm{iso}}$ propagators. *Symmetric* is thus mostly sink smearing and contractions. The timings were taken from a random selection of log files from the respective ensembles.

N_s sources each, we thus have $N_c \cdot N_s$ data points to infer the coefficients $c_{H,x}(t)$ for each timeslice t. We call this subsection of N_c configurations *training set* as is common in machine learning contexts. The complement of the training set we call *evaluation set* in the following, on which we infer the QED contribution from eq. (10.1).

Since this is of course not an exact procedure, we have to correct for an inherent bias this procedure introduces on all configurations of the evaluation set. We do so analogously to the truncated solver method with all mode averaging as explained in section 6.5. The sloppy observables s in this setup are the approximations as per eq. (10.1). For the exact observable e, we use one or more sources on each configuration of the evaluation set for which we compute the complete QED contribution and the prediction from eq. (10.1) so that we can compute the bias correction as per eq. (6.24). Additionally, we compute the complete QED contribution on all exact sources of the truncated solver method in order to be able to correct both biases independently.

While we found that a simple linear regression works reasonably well to determine the coefficients in the above procedure, we instead use a slightly different method. We use the AMA method with multiple control variates we derived at the end in section 6.5 where we absorb the coefficients $c_{H,x}(t)$ in eq. (10.1) into the coefficient vector θ in eq. (6.25) and identify the inputs $C_H^{(0)}(t)$ and $C_{H,\Delta m_q}(t)$ with the control variates s on the training set. The target (exact) value of the QED contribution is then identified as e. This is still a linear prediction as discussed above but with different coefficients compared to a simple linear regression and without a constant term. However, this procedure is more tailored to a precise bias correction taking the covariances of the input data into account. Note, that the sloppy values $\hat{s}$ computed this way are not necessarily compatible with the exact QED corrections. However, they minimize the uncertainty of the bias correction $\hat{b}$ with which the prediction is compatible with the exact calculation.

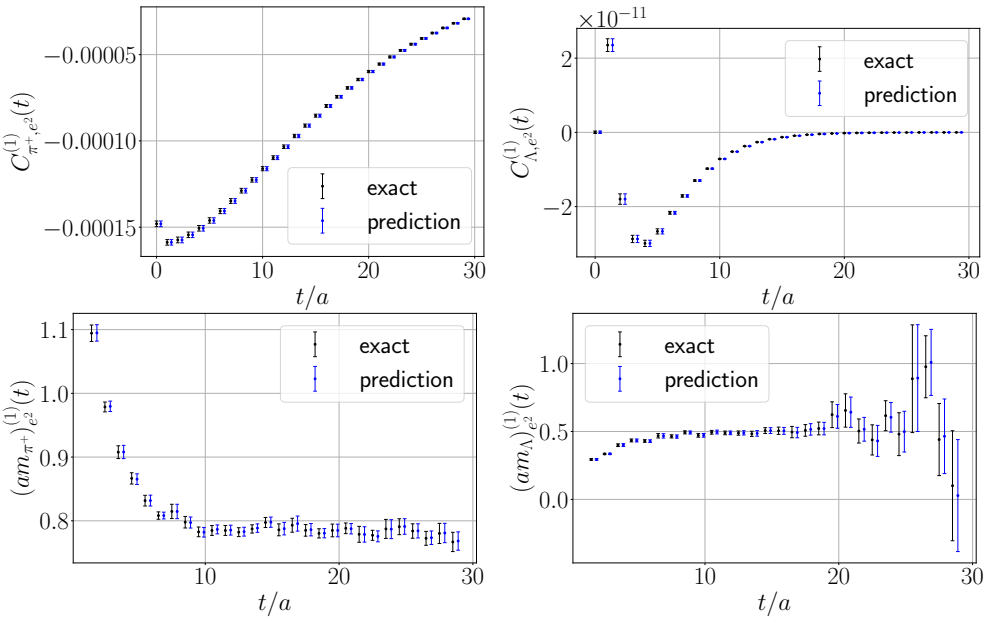

Figure 10.2: The QED correction to the correlation function (top) of the pion (left) and the lambda baryon (right) as well as the first order effective masses (bottom) on the evaluation set of N451. The prediction is computed with the method of multiple control variates in section 6.5. The training set consists of 20 configurations with 33 sources each. The evaluation set spans 988 configurations 1 source per configuration to correct for the bias of the QED prediction and 1 source per configuration to correct for the bias of the truncated solver, leaving 31 sources per configuration for the prediction. The exact data comes from a complete computation of the QED contribution on all sources. The prediction is shifted to the right to make it possible to distinguish the data.

We have tested this method on several ensembles with both open and periodic boundary conditions. An example of such a test is shown in fig. 10.2 for the π^+ and Λ showing a complete computation and the prediction side-by-side. This test using only 20 out of 1008 configurations for the determination of the linear coefficients and only a single source for the bias correction shows, that this procedure produces very accurate results with minimal computational effort. As the prediction and determination of the linear coefficients is negligible in terms of computer time compared to the full computation, we can save approximately 50% of the total runtime based on fig. 10.1.
We used this method in production for the N101 and D200 ensembles, with a more conservative setup than the one in our tests using two sources per gauge configuration for bias correction (on top of those needed for the truncated solver) and using every fourth configuration on D200 and every 25th configuration on N101 for the training set.

10.2. Hadronic Renormalization Scheme

As all lattice ensembles considered for this thesis are simulated in the isospin-symmetric limit, there is no handle on the magnitude of the mass difference

between up- and down-quark as well as the electromagnetic coupling. Like the lattice scale in $\mathrm{QCD}_{\mathrm{iso}}$, these quantities have to be determined using experimental data as they do not arise from the theory but are intrinsic parameters thereof. There are multiple ways such a matching can be achieved. The method used in this thesis is based on a matching of charged meson masses to relate QCD+QED and $\mathrm{QCD}_{\mathrm{iso}}$ based on chiral perturbation theory with QED [14]. The electromagnetic coupling is set to its physical value in the low-energy-limit of $e^2 = 4\pi\alpha_{\mathrm{em}} = 0.091701237$ as this coupling strength does not renormalize at leading order in α_{em} [11, 14]. The shifts of the masses of up, down, and strange quark are then determined via the matching conditions [14]

$$\begin{aligned}
\left(m_{\pi^0}^2\right)^{\mathrm{QCD+QED}} &= \left(m_{\pi^0}^2\right)^{\mathrm{exp}} \\
\left(m_{K^+}^2 + m_{K^0}^2 - m_{\pi^+}^2\right)^{\mathrm{QCD+QED}} &= \left(m_{K^+}^2 + m_{K^0}^2 - m_{\pi^+}^2\right)^{\mathrm{exp}} \\
\left(m_{K^+}^2 - m_{K^0}^2 - m_{\pi^+}^2 + m_{\pi^0}^2\right)^{\mathrm{QCD+QED}} &= \left(m_{K^+}^2 - m_{K^0}^2 - m_{\pi^+}^2 + m_{\pi^0}^2\right)^{\mathrm{exp}} \\
\left(m_{\pi^0}\right)^{\mathrm{QCD_{iso}}} &= \left(m_{\pi^0}\right)^{\mathrm{exp}} \\
\left(m_{K^+}^2 + m_{K^0}^2 - m_{\pi^+}^2\right)^{\mathrm{QCD_{iso}}} &= \left(m_{K^+}^2 + m_{K^0}^2 - m_{\pi^+}^2\right)^{\mathrm{exp}}.
\end{aligned} \tag{10.2}$$

The superscript "exp" here refers to the experimentally determined value. In this scheme, the first three equations match the three quark masses in the full theory, while the latter two fix the isospin-symmetric quark masses in relation to the experimental ones. Plugging the expansion eq. (5.9) into the first three conditions of eq. (10.2) and replacing the isospin-symmetric quark masses by the experimental ones using the last two conditions, eq. (10.2) reduces to [14]

$$\begin{aligned}
\sum_i \Delta\varepsilon_i M_{\pi^0}^i &= 0, \\
\sum_i \Delta\varepsilon_i \left(M_{K^+}^i + M_{K^0}^i - M_{\pi^+}\right) &= 0, \\
\sum_i \Delta\varepsilon_i \left(M_{K^+}^i - M_{K^0}^i - M_{\pi^+}^i + M_{\pi^0}^i\right) &= \frac{a^2}{2}\left(m_{K^+}^2 - m_{K^0}^2 - m_{\pi^+}^2 + m_{\pi^0}^2\right)^{\mathrm{exp}},
\end{aligned} \tag{10.3}$$

where $M_X^i = (am_X)^{(0)}(am_X)_i^{(1)}$ and a is the lattice spacing. a is itself a quantity that has to be expanded in $\Delta\varepsilon_i$, which we discuss in section 10.3. For the following discussion, however, we assume a to be the isospin-symmetric lattice spacing. The above system of equations can easily be solved by rewriting it as a matrix equation[1]

$$\begin{aligned}
&\begin{pmatrix} M_{\pi^0}^u & M_{\pi^0}^d & 0 \\ M_{K^+}^u - M_{\pi^+}^u & M_{K^0}^d - M_{\pi^+}^d & M_{K^+}^s + M_{K^0}^s \\ M_{K^+}^u - M_{\pi^+}^u + M_{\pi^0}^u & -M_{K^0}^d - M_{\pi^+}^d + M_{\pi^0}^d & M_{K^+}^s - M_{K^0}^s \end{pmatrix} \begin{pmatrix} a\Delta m_u \\ a\Delta m_d \\ a\Delta m_s \end{pmatrix} \\
&\quad + e^2 \begin{pmatrix} M_{\pi^0}^{e^2} \\ M_{K^+}^{e^2} + M_{K^0}^{e^2} - M_{\pi^+}^{e^2} \\ M_{K^+}^{e^2} - M_{K^0}^{e^2} - M_{\pi^+}^{e^2} + M_{\pi^0}^{e^2} \end{pmatrix} \\
&\quad = \frac{a^2}{2} \begin{pmatrix} 0 \\ 0 \\ \left(m_{K^+}^2\right)^{\mathrm{exp}} - \left(m_{K^0}^2\right)^{\mathrm{exp}} - \left(m_{\pi^+}^2\right)^{\mathrm{exp}} + \left(m_{\pi^0}^2\right)^{\mathrm{exp}} \end{pmatrix}.
\end{aligned}$$

[1] This assumes only valence-quark contributions. If one were to include sea-quark contributions, all meson masses depend on all quark masses.

Using the symmetries $M^u_{\pi^0} = M^u_{\pi^+} = M^d_{\pi^0} = M^d_{\pi^+} =: M^l_\pi$ and $M^d_{K^0} = M^u_{K^+} =: M^l_K$,[2] this can be reduced to

$$\begin{pmatrix} M^l_\pi & M^l_\pi & 0 \\ M^l_K - M^l_\pi & M^l_K - M^l_\pi & 2M^s_K \\ M^l_K & -M^l_K & 0 \end{pmatrix} \begin{pmatrix} a\Delta m_u \\ a\Delta m_d \\ a\Delta m_s \end{pmatrix} + e^2 \begin{pmatrix} M^{e^2}_{\pi^0} \\ M^{e^2}_{K^+} + M^{e^2}_{K^0} - M_{\pi^+} \\ M^{e^2}_{K^+} - M^{e^2}_{K^0} - M^{e^2}_{\pi^+} + M^{e^2}_{\pi^0} \end{pmatrix}$$
$$= \frac{a^2}{2} \begin{pmatrix} 0 \\ 0 \\ \left(m^2_{K^+}\right)^{\text{exp}} - \left(m^2_{K^0}\right)^{\text{exp}} - \left(m^2_{\pi^+}\right)^{\text{exp}} + \left(m^2_{\pi^0}\right)^{\text{exp}} \end{pmatrix}$$

which is solved by

$$\begin{pmatrix} a\Delta m_u \\ a\Delta m_d \\ a\Delta m_s \end{pmatrix} = \frac{1}{2} \begin{pmatrix} \frac{1}{M^l_\pi} & 0 & \frac{1}{M^l_K} \\ \frac{1}{M^l_\pi} & 0 & -\frac{1}{M^l_K} \\ \frac{M^l_\pi - M^l_K}{M^l_\pi M^s_K} & \frac{1}{M^s_K} & 0 \end{pmatrix} \begin{pmatrix} -e^2 M^{e^2}_{\pi^0} \\ e^2\left(M_{\pi^+} - M^{e^2}_{K^+} - M^{e^2}_{K^0}\right) \\ \frac{a^2}{2} m^2_{KK\pi\pi} - e^2 M^{e^2}_{KK\pi\pi} \end{pmatrix} \tag{10.4}$$

where $m^2_{KK\pi\pi} = \left(m^2_{K^+}\right)^{\text{exp}} - \left(m^2_{K^0}\right)^{\text{exp}} - \left(m^2_{\pi^+}\right)^{\text{exp}} + \left(m^2_{\pi^0}\right)^{\text{exp}}$ and $M_{KK\pi\pi} = M^{e^2}_{K^+} - M^{e^2}_{K^0} - M^{e^2}_{\pi^+} + M^{e^2}_{\pi^0}$.

Note, that in addition to the mentioned contributions to the hadron masses there is an additional shift of the strong gauge coupling which is useful to counter a renormalization of the strong coupling due to the addition of electromagnetism into the theory [81]. This shift would in turn affect the lattice spacing. However, as mentioned above, we only consider quark-connected contributions at this stage of the project and thus do not yet account for this shift.

Using the lattice scales determined using the mass of the Λ baryon as reference in table 9.5, the above matching yields the mass shifts in table 10.1.

Table 10.1: The expansion parameters determined on each ensemble using the scheme in eq. (10.3) and the lattice spacings given in table 9.5 using the mass of the Λ baryon as reference scale.

Ensemble	$a\Delta m_u$	$a\Delta m_d$	$a\Delta m_s$
A654	-0.0084007(83)	-0.0016997(69)	-0.0020553(86)
N101	-0.008604(22)	-0.0018089(78)	-0.0021431(62)
D450	-0.008757(20)	-0.001909(19)	-0.002181(30)
N451	-0.0087815(41)	-0.0019118(39)	-0.0021790(16)
N452	-0.0087889(39)	-0.0019259(38)	-0.0021672(17)
D200	-0.0090279(98)	-0.0020154(100)	-0.002263(13)
N203	-0.0090239(32)	-0.0020385(31)	-0.0022394(38)
N200	-0.0090148(46)	-0.0020329(45)	-0.0022507(44)

Using these results, we find the masses for the different isospin-multiplet listed in table 10.4. tables 10.2 and 10.6 show the correction for the isospin-singlet states Λ and Ω and the splitting of the isospin-multiplet masses respectively. For each of these tables we have one version in lattice units and one in physical units.

Note, that we perform the matching on a per-ensemble basis. If an extrapolation as in section 9.2 were performed in QCD+QED, this could also be done once for

[2] These symmetries are valid in our calculations due to the isospin-symmetric nature of the theory we expand around and because we only consider the quark-connected contributions to the π^0 correlation function.

each value of the inverse strong gauge coupling β. Although the uncertainties of the masses in table 10.4 are larger than the mass splittings due to isospin-breaking, these splittings can be resolved to much better precision since the data for different multiplet-states are highly correlated due to reuse of intermediate results, thus strongly reducing the overall uncertainty of their difference.
Our data in table 10.2 verifies the assumption underlying various other efforts towards precision scale-setting [44, 68, 69] that the Ω^--mass is insensitive to isospin-breaking corrections ($\leq 0.051(29)\,\%$) of the total mass on all our ensembles), making it a suitable reference scale for which isospin-breaking effects can be ignored to much higher precision than for other observables. Going from our data alone, it looks to be similar for the Λ (although the relative correction is larger with at most $0.116(32)\,\%$ in this case) which could be beneficial given our results from section 9.3 which favor the Λ in terms of overall precision of the lattice scale. However, these results have to be taken with a grain of salt as in QCD+QED, Σ^0 and Λ mix so that the state we call Λ in our analysis does not exactly correspond to an experimentally observable mass eigenstate [125]. To achieve accurate results for the Λ baryon in QCD+QED, this mixing has to be explored and taken into account. Cross-correlators for Σ^0 and Λ (as well as the SU(3) singlet Λ^0 corresponding to a totally antisymmetric flavor state) have been collected together with all data necessary for our results so far and can be used to find the actual mass-eigenstates in QCD+QED. However, these data have not been analyzed for the sake of this thesis, so we cannot report the results at this stage.

Table 10.2: The shift in the masses of the Λ and Ω^- baryon when correcting for isospin-breaking effects, $\delta m_X = m_X^{\mathrm{QCD+QED}} - m_X^{\mathrm{QCD_{iso}}}$.

β	Ensemble	$am_\Lambda^{\mathrm{QCD_{iso}}}$	δam_Λ	$am_\Omega^{\mathrm{QCD_{iso}}}$	δam_Ω
3.34	A654	0.5726(37)	0.00062(36)	0.7398(84)	0.00026(11)
3.4	N101	0.4903(26)	0.00057(15)	0.6633(67)	0.00032(12)
3.46	D450	0.4289(14)	0.00031(15)	0.6152(31)	0.00032(19)
	N451	0.4372(18)	0.000159(48)	0.5983(16)	0.00012(20)
	N452	0.4408(18)	0.000282(43)	0.5736(20)	0.000276(15)
3.55	D200	0.36524(94)	-0.00018(17)	0.5245(16)	0.000156(94)
	N200	0.3723(21)	-0.00029(77)	0.5136(23)	0.000128(32)
	N203	0.3767(24)	0.000077(39)	0.4880(38)	0.000162(24)

Table 10.3: The shift in the masses of the Λ and Ω^- baryon when correcting for isospin-breaking effects, $\delta m_X = m_X^{\mathrm{QCD+QED}} - m_X^{\mathrm{QCD_{iso}}}$. The isospin-symmetric lattice spacings $a(m_\Lambda)$ in table 9.5 are used to convert the lattice results to physical units.

β	Ensemble	$m_\Lambda^{\mathrm{QCD_{iso}}}$ / MeV	δm_Λ / MeV	$m_\Omega^{\mathrm{QCD_{iso}}}$ / MeV	δm_Ω / MeV
3.34	A654	1155(14)	1.25(72)	1492(21)	0.53(23)
3.4	N101	1136(12)	1.31(36)	1537(22)	0.73(29)
3.46	D450	1122(11)	0.81(39)	1609(17)	0.82(49)
	N451	1143(11)	0.41(13)	1565(15)	0.31(52)
	N452	1153(11)	0.74(11)	1500(15)	0.722(39)
3.55	D200	1132(11)	-0.56(51)	1626(16)	0.48(29)
	N200	1154(11)	-0.9(2.4)	1592(16)	0.396(100)
	N203	1168(13)	0.24(12)	1513(18)	0.503(74)

Table 10.4: The masses of all available $\mathrm{QCD}_{\mathrm{iso}}$-stable hadrons in QCD+QED determined to first order in isospin-breaking effects.

β	Ensemble	I_3	am_π	am_{K^+/K^0}	am_N	am_Λ	am_Σ	am_Ξ	am_Ω
3.34	A654	1	0.1698(13)				0.5832(37)		
		1/2		0.2273(10)	0.5444(59)			0.6070(25)	
		0	0.1687(13)			0.5733(38)	0.5843(37)		0.7400(84)
		−1/2		0.22857(100)	0.5460(55)			0.6089(25)	
		−1	0.1698(13)				0.5856(36)		
3.4	N101	1	0.12406(42)				0.5072(28)		
		1/2		0.20172(25)	0.4513(30)			0.5370(19)	
		0	0.12286(41)			0.4909(26)	0.5081(28)		0.6636(67)
		−1/2		0.20279(24)	0.4517(30)			0.5387(19)	
		−1	0.12406(42)				0.5096(27)		
3.46	D450	1	0.08516(28)				0.4497(31)		
		1/2		0.18368(12)	0.3796(26)			0.4873(10)	
		0	0.08392(28)			0.4292(14)	0.4506(31)		0.6155(31)
		−1/2		0.18467(12)	0.3800(26)			0.48881(96)	
		−1	0.08516(28)				0.4517(31)		
	N451	1	0.11184(25)				0.4544(22)		
		1/2		0.17814(16)	0.4057(15)			0.4766(14)	
		0	0.11088(26)			0.4373(17)	0.4553(22)		0.5984(17)
		−1/2		0.17915(16)	0.4060(15)			0.4782(14)	
		−1	0.11184(25)				0.4565(22)		

	N452	1	0.13653(17)				0.4479(15)		
		$1/2$		0.17030(14)	0.4231(17)			0.4636(15)	
		0	0.13569(17)			0.4411(18)	0.4487(15)		0.5739(20)
		$-1/2$		0.17130(14)	0.4234(17)			0.4653(15)	
		-1	0.13653(17)				0.4498(15)		
3.55	D200	1	0.06590(34)				0.3848(15)		
		$1/2$		0.15605(22)	0.3195(27)			0.41548(76)	
		0	0.06494(34)			0.36506(92)	0.3854(15)		0.5246(16)
		$-1/2$		0.15695(22)	0.3197(26)			0.41690(76)	
		-1	0.06590(34)				0.3862(15)		
	N200	1	0.09254(37)				0.3871(17)		
		$1/2$		0.15010(25)	0.3411(25)			0.4085(15)	
		0	0.09179(36)			0.3720(23)	0.3880(17)		0.5138(23)
		$-1/2$		0.15100(24)	0.3408(25)			0.4098(15)	
		-1	0.09254(37)				0.3891(16)		
	N203	1	0.11374(23)				0.3855(14)		
		$1/2$		0.14415(20)	0.3608(24)			0.3979(11)	
		0	0.11309(23)			0.3768(24)	0.3863(14)		0.4882(38)
		$-1/2$		0.14505(20)	0.3612(24)			0.3994(11)	
		-1	0.11374(23)				0.3872(14)		

Table 10.5: The masses of all available $\mathrm{QCD}_{\mathrm{iso}}$-stable hadrons in QCD+QED determined to first order in isospin-breaking effects using the isospin-symmetric lattice spacings $a(m_\Lambda)$ in table 9.5 to convert the lattice results to physical units.

β	Ensemble	I_3	m_π / MeV	m_{K^+/K^0} / MeV	m_N / MeV	m_Λ / MeV	m_Σ / MeV	m_Ξ / MeV	m_Ω / MeV
3.34	A654	1	342.5(3.8)				1176(14)		
		$1/2$		458.5(4.5)	1098(17)			1224(13)	
		0	340.3(3.8)			1156(14)	1179(14)		1493(21)
		$-1/2$		461.1(4.4)	1101(17)			1228(13)	
		-1	342.5(3.8)				1181(14)		
3.4	N101	1	287.5(2.8)				1175(13)		
		$1/2$		467.4(4.3)	1046(12)			1244(12)	
		0	284.7(2.7)			1138(12)	1177(13)		1538(22)
		$-1/2$		469.9(4.3)	1047(12)			1248(12)	
		-1	287.5(2.8)				1181(12)		
3.46	D450	1	222.8(2.2)				1176(14)		
		$1/2$		480.5(4.4)	993(11)			1275(12)	
		0	219.5(2.1)			1123(11)	1178(14)		1610(17)
		$-1/2$		483.0(4.4)	994(11)			1279(12)	
		-1	222.8(2.2)				1182(13)		
	N451	1	292.5(2.7)				1188(12)		
		$1/2$		466.0(4.3)	1061(10)			1247(12)	
		0	290.0(2.7)			1144(11)	1191(12)		1565(15)
		$-1/2$		468.6(4.2)	1062(10)			1251(12)	
		-1	292.5(2.7)				1194(12)		

	N452	1	357.1(3.3)				1172(11)		
		1/2		445.5(4.1)	1107(11)			1213(12)	
		0	354.9(3.3)			1154(11)	1174(11)		1501(15)
		−1/2		448.1(4.1)	1108(11)			1217(12)	
		−1	357.1(3.3)				1177(11)		
3.55	D200	1	204.3(2.1)				1193(12)		
		1/2		483.7(4.5)	990(12)			1288(12)	
		0	201.3(2.1)			1132(11)	1194(12)		1626(16)
		−1/2		486.5(4.5)	991(12)			1292(12)	
		−1	204.3(2.1)				1197(12)		
	N200	1	286.8(2.8)				1200(11)		
		1/2		465.2(4.3)	1057(11)			1266(12)	
		0	284.5(2.8)			1153(12)	1203(11)		1592(16)
		−1/2		468.0(4.3)	1056(11)			1270(12)	
		−1	286.8(2.8)				1206(11)		
	N203	1	352.5(3.3)				1195(11)		
		1/2		446.8(4.1)	1118(12)			1233(12)	
		0	350.5(3.2)			1168(13)	1197(11)		1513(18)
		−1/2		449.6(4.1)	1119(12)			1238(11)	
		−1	352.5(3.3)				1200(11)		

Table 10.6: The mass-splitting of each isospin-multiplet for all available ensembles.

β	Ensemble	$am_{\pi^+} - am_{\pi^0}$	$am_{K^0} - am_{K^+}$	$am_n - am_p$	$am_{\Sigma^0} - am_{\Sigma^+}$	$am_{\Sigma^-} - am_{\Sigma^0}$	$am_{\Xi^-} - am_{\Xi^0}$
3.34	A654	0.001109(27)	0.001289(44)	0.0016(14)	0.001133(85)	0.00130(12)	0.00184(11)
3.4	N101	0.00120(12)	0.001070(82)	0.00038(13)	0.00096(19)	0.00147(20)	0.00169(15)
3.46	D450	0.001244(20)	0.000986(31)	0.00034(30)	0.00082(12)	0.00116(11)	0.00151(18)
	N451	0.000959(10)	0.001006(30)	0.000297(92)	0.00091(16)	0.00123(16)	0.00157(10)
	N452	0.0008472(43)	0.001002(31)	0.00036(21)	0.000807(34)	0.001147(60)	0.001684(64)
3.55	D200	0.000965(56)	0.000901(34)	0.00023(70)	0.00060(11)	0.00086(11)	0.001419(77)
	N200	0.000744(20)	0.000899(28)	-0.00028(88)	0.000890(59)	0.001073(57)	0.001299(59)
	N203	0.0006500(50)	0.000900(26)	0.000362(62)	0.000746(49)	0.000960(49)	0.00150(21)

Table 10.7: The mass-splitting of each isospin-multiplet for all available ensembles. The isospin-symmetric lattice spacings $a(m_\Lambda)$ in table 9.5 are used to convert the lattice results to physical units.

β	Ensemble	$m_{\pi^+} - m_{\pi^0}$	$m_{K^0} - m_{K^+}$	$m_n - m_p$	$m_{\Sigma^0} - m_{\Sigma^+}$	$m_{\Sigma^-} - m_{\Sigma^0}$	$m_{\Xi^-} - m_{\Xi^0}$
3.34	A654	2.237(56) MeV	2.601(70) MeV	3.2(28) MeV	2.29(16) MeV	2.61(24) MeV	3.71(21) MeV
3.4	N101	2.79(28) MeV	2.48(18) MeV	0.88(31) MeV	2.22(43) MeV	3.40(47) MeV	3.91(34) MeV
3.46	D450	3.255(61) MeV	2.579(59) MeV	0.89(79) MeV	2.15(30) MeV	3.03(28) MeV	3.95(47) MeV
	N451	2.510(36) MeV	2.630(58) MeV	0.78(24) MeV	2.38(42) MeV	3.22(42) MeV	4.11(27) MeV
	N452	2.216(23) MeV	2.620(60) MeV	0.94(55) MeV	2.111(80) MeV	3.00(15) MeV	4.41(16) MeV
3.55	D200	2.99(18) MeV	2.793(89) MeV	0.7(22) MeV	1.85(34) MeV	2.65(35) MeV	4.40(23) MeV
	N200	2.306(66) MeV	2.787(68) MeV	–0.9(27) MeV	2.76(18) MeV	3.33(17) MeV	4.03(17) MeV
	N203	2.015(24) MeV	2.791(58) MeV	1.12(19) MeV	2.31(15) MeV	2.97(15) MeV	4.64(64) MeV

10.3. Scale Setting Including Isospin-Breaking Effects

As the ultimate goal of this project is to be able to determine a lattice scale that includes isospin-breaking effects, we need to tweak a procedure as the one used in chapter 9 to incorporate isospin-breaking effects. In this section, we want to propose such a procedure that could be utilized in future calculations. To this end, we want to discuss a method setting the scale on a per-ensemble basis in section 10.3.1 and another version using t_0 in section 10.3.2 which would allow a definition of a single lattice scale per value of β.
Before we dive into these proposals, let us first introduce some notation to clean up the calculations: For an observable $\mathcal{O}$, we denote the value determined in isospin-symmetric QCD as $\mathcal{O}^{(0)}$ and the value including isospin-breaking corrections as $\mathcal{O}^{\text{QCD+QED}}$. These two quantities are related via the expansion (see section 5.2)

$$\mathcal{O}^{\text{QCD+QED}} = \mathcal{O}^{(0)} + \mathcal{O}^{(1)}$$

where the correction $\mathcal{O}^{(1)}$ is given by

$$\mathcal{O}^{(1)} = \sum_i \Delta\varepsilon_i \mathcal{O}_i^{(1)} = \sum_i \Delta\varepsilon_i \frac{\partial \mathcal{O}^{\text{QCD+QED}}}{\partial \varepsilon_i}\bigg|_{\varepsilon=\varepsilon^{(0)}}.$$

Note, that if $\mathcal{O}$ is a primary observable (i.e. an observable that can be computed on a single gauge configuration), we refer to its ensemble average in this section. For (differentiable) functions of observables $\mathcal{O}$ and $\mathcal{P}$, we then find

$$\begin{aligned}(f(\mathcal{O}))^{\text{QCD+QED}} &= (f(\mathcal{O}))^{(0)} + \big(f'(\mathcal{O})\big)^{(0)}\mathcal{O}^{(1)},\\ (\mathcal{O}\mathcal{P})^{\text{QCD+QED}} &= (\mathcal{O}\mathcal{P})^{(0)} + \mathcal{O}^{(1)}\mathcal{P}^{(0)} + \mathcal{O}^{(0)}\mathcal{P}^{(1)}.\end{aligned}$$

10.3.1. Setting the Scale on Individual Ensembles

For an individual ensemble, we can define the lattice scale using the mass $m_{\mathfrak{S}}$ of a reference Baryon $\mathfrak{S}$ via

$$a^{\text{QCD+QED}} = \frac{(am_{\mathfrak{S}})^{\text{QCD+QED}}}{m_{\mathfrak{S}}^{\text{exp}}}, \qquad a^{(0)} = \frac{(am_{\mathfrak{S}})^{(0)}}{m_{\mathfrak{S}}^{\text{exp},0}} \tag{10.5}$$

for QCD+QED and QCD_{iso} respectively. Here, $m_{\mathfrak{S}}^{\text{exp}}$ is an input from experimental measurements of $\mathfrak{S}$'s mass and $m_{\mathfrak{S}}^{\text{exp},0}$ is an adapted value reflecting an isospin-symmetric world as we used them in section 9.3 (see table 9.3). Those two lattice spacings are related via

$$\begin{aligned}a^{\text{QCD+QED}} &= \frac{(am_{\mathfrak{S}})^{(0)} + (am_{\mathfrak{S}})^{(1)}}{m_{\mathfrak{S}}^{\text{exp}}} = \frac{m_{\mathfrak{S}}^{\text{exp},0}}{m_{\mathfrak{S}}^{\text{exp}}}\left(\frac{(am_{\mathfrak{S}})^{(0)}}{m_{\mathfrak{S}}^{\text{exp},0}} + \frac{(am_{\mathfrak{S}})^{(1)}}{m_{\mathfrak{S}}^{\text{exp},0}}\right)\\ &= \frac{m_{\mathfrak{S}}^{\text{exp},0}}{m_{\mathfrak{S}}^{\text{exp}}}\left(1 + \frac{(am_{\mathfrak{S}})^{(1)}}{(am_{\mathfrak{S}})^{(0)}}\right)a^{(0)}.\end{aligned} \tag{10.6}$$

Identifying the correction to a in the above expression with $a^{(1)}$ in $a^{\text{QCD+QED}} = a^{(0)} + a^{(1)}$ we find

$$a^{(1)} = \left(\frac{m_{\mathfrak{S}}^{\text{exp},0}}{m_{\mathfrak{S}}^{\text{exp}}}\left(1 + \frac{(am_{\mathfrak{S}})^{(1)}}{(am_{\mathfrak{S}})^{(0)}}\right) - 1\right)a^{(0)}$$

When determining the QCD+QED-value of an observable $\mathcal{O}$ with mass-dimension n, the expression at the end of the first line of eq. (10.6) can be used as follows:

$$\begin{aligned}\mathcal{O}^{\text{QCD+QED}} =& \left(\frac{(a^n\mathcal{O})}{a^n}\right)^{\text{QCD+QED}} = \left(\frac{(a^n\mathcal{O})}{a^n}\right)^{(0)} + \frac{(a^n\mathcal{O})^{(1)}}{(a^n)^{(0)}} - n\frac{(a^n\mathcal{O})^{(0)}}{(a^{n+1})^{(0)}}a^{(1)} \\ =& \left(1 - n\frac{a^{(1)}}{a^{(0)}}\right)\left(\frac{(a^n\mathcal{O})}{a^n}\right)^{(0)} + \frac{(a^n\mathcal{O})^{(1)}}{(a^n)^{(0)}}.\end{aligned}$$

Each term in this last expression can be determined directly using the RM123 method (see section 5.2).

A complication arises when setting the scale in QCD+QED via eq. (10.5) as the isospin-breaking corrections $(am_{\mathfrak{S}})^{(1)}$ of the baryon-mass used to set the scale depend on the parameters $\Delta\varepsilon_i$, which (as outlined in section 10.2) themselves depend on the lattice scale. To circumvent this problem, we propose an iterative scheme to alternatingly set the lattice scale and $\Delta\varepsilon_i$. More precisely, we define two sequences a_n and $\Delta\varepsilon_{i,n}$ with $a_0 = a^{(0)}$ and $\Delta\varepsilon_{i,0}$ determined via eq. (10.4) using $a = a_0$. The next values of these sequences are then given by first computing

$$a_{n+1} = \frac{(am_{\mathfrak{S}})^{(0)} + \sum_i \Delta\varepsilon_{i,n}(am_{\mathfrak{S}})_i^{(1)}}{m_{\mathfrak{S}}^{\text{exp}}} \tag{10.7}$$

and then using a_{n+1} in eq. (10.4) to determine $\Delta\varepsilon_{i,n+1}$. Finally, we define $a^{\text{QCD+QED}} := \lim_{n\to\infty} a_n$ and $\Delta\varepsilon_i := \lim_{n\to\infty} \Delta\varepsilon_{i,n}$ (provided the sequences converge).

We tested this procedure for all baryons used for isospin-symmetric scale setting in section 9.3 as $\mathfrak{S}$ with $m_{\mathfrak{S}}^{\text{exp},0}$ taken from table 9.3 and $m_{\mathfrak{S}}^{\text{exp}}$ taken from the particle data group [126]. We generally found, that the procedure converges within three iterations to a precision of less than 1% of the statistical uncertainty of the results. An example of the intermediate results this procedure produces is shown in table 10.8 for $\mathfrak{S} = \Lambda$ on D200.

Table 10.8: Test of the procedure described in section 10.3.1 using the Λ baryon on D200. n is the iteration step as in eq. (10.7).

n	a_n / fm	$(a\Delta m_u)_n$	$(a\Delta m_d)_n$	$(a\Delta m_s)_n$
0	0.06458(16)	-0.0090296(83)	-0.0020076(74)	-0.002266(11)
1	0.06456(16)	-0.0090295(83)	-0.0020077(73)	-0.002266(11)
2	0.06456(16)	-0.0090295(83)	-0.0020077(73)	-0.002266(11)

10.3.2. Setting the Scale using t_0

While it would in principle be possible to set the scale ensemble-wise as detailed above, the preferred way would be to use a scheme similar to that in section 9.3 allowing for a combined lattice spacing for each value of the strong gauge coupling. To achieve this, we propose a similar prescription as in chapter 9 based on [46].

To define such a scheme, we first note that the expansion of any dimensionless combination of observables does not depend on the lattice spacing. For observ-

ables $\mathcal{O}$ with mass dimension n we then find

$$\begin{aligned}
\left((8t_0)^{n/2}\mathcal{O}\right)^{\text{QCD+QED}} =& \left((8t_0)^{n/2}\mathcal{O}\right)^{(0)} && + \left((8t_0)^{n/2}\right)^{(0)}\mathcal{O}^{(1)} + \left((8t_0)^{n/2}\right)^{(1)}\mathcal{O}^{(0)} \\
=& \left((8t_0)^{n/2}\mathcal{O}\right)^{(0)} && + \left(\left(\frac{8t_0}{a^2}\right)^{n/2}\right)^{(0)}(a^n\mathcal{O})^{(1)} \\
& && + \left(\left(\frac{8t_0}{a^2}\right)^{n/2}\right)^{(1)}(a^n\mathcal{O})^{(0)} \\
=& \left((8t_0)^{n/2}\mathcal{O}\right)^{(0)} && + \left(\left(\frac{8t_0}{a^2}\right)^{n/2}\right)^{(0)}(a^n\mathcal{O})^{(1)} \\
& && + \frac{n}{2}\left(\left(\frac{8t_0}{a^2}\right)^{n/2-1}\right)^{(0)}\left(\frac{8t_0}{a^2}\right)^{(1)}(a^n\mathcal{O})^{(0)}
\end{aligned}$$

Since all isospin-breaking corrections of t_0 come purely from the sea, i.e.

$$\begin{aligned}
\left(\frac{t_0}{a^2}\right)^{(1)} =& \sum_{f\in\{u,d,s\}} \Delta m_f \left(\left\langle\frac{t_0}{a^2}\right\rangle_{S_0}\left\langle\frac{\partial S}{\partial m_f}\Big|_{\varepsilon=\varepsilon^{(0)}}\right\rangle_{S_0} - \left\langle\frac{t_0}{a^2}\frac{\partial S}{\partial m_f}\Big|_{\varepsilon=\varepsilon^{(0)}}\right\rangle_{S_0}\right) \\
& + e^2\Bigg[\left\langle\frac{t_0}{a^2}\right\rangle_{S_0}\left\langle\frac{\partial^2 S}{\partial e^2}\Big|_{\varepsilon=\varepsilon^{(0)}}\right\rangle_{S_0} - \left\langle\frac{t_0}{a^2}\frac{\partial^2 S}{\partial e^2}\Big|_{\varepsilon=\varepsilon^{(0)}}\right\rangle_{S_0} \\
& \quad + \left\langle\frac{t_0}{a^2}\left(\frac{\partial S}{\partial e}\Big|_{\varepsilon=\varepsilon^{(0)}}\right)^2\right\rangle_{S_0} - \left\langle\frac{t_0}{a^2}\right\rangle_{S_0}\left\langle\left(\frac{\partial S}{\partial e}\Big|_{\varepsilon=\varepsilon^{(0)}}\right)^2\right\rangle \\
& \quad + \left(\langle\mathcal{O}\rangle_{S_0}\left\langle\frac{\partial S}{\partial e}\Big|_{\varepsilon=\varepsilon^{(0)}}\right\rangle^2 - \left\langle\mathcal{O}\frac{\partial S}{\partial e}\Big|_{\varepsilon=\varepsilon^{(0)}}\right\rangle_{S_0}\right)\left\langle\frac{\partial S}{\partial e}\Big|_{\varepsilon=\varepsilon^{(0)}}\right\rangle_{S_0}\Bigg] \\
& + \Delta\beta\left(\left\langle\frac{t_0}{a^2}\right\rangle_{S_0}\left\langle\frac{\partial S}{\partial \beta}\Big|_{\varepsilon=\varepsilon^{(0)}}\right\rangle_{S_0} - \left\langle\frac{t_0}{a^2}\frac{\partial S}{\partial \beta}\Big|_{\varepsilon=\varepsilon^{(0)}}\right\rangle_{S_0}\right)
\end{aligned}$$

where S is to be understood as the QCD+QED action and $\langle\cdot\rangle_{S_0}$ means that the expectation values are defined via the path integral in QCD_{iso} (with the QCD_{iso}-action S_0). As long as only corrections in the valence quark sector are taken into account as we have done in our calculations so far, the corrections to $\frac{t_0}{a^2}$ vanish. In this approximation, the value in QCD+QED is identical to that in QCD_{iso}.

We could then define the physical value of $8t_0$ analogously to eq. (9.7) by defining

$$\left(\sqrt{8t_0^{\text{phys}}}\right)^{\text{QCD+QED}} = \frac{\left(\sqrt{8t_0}m_{\mathfrak{S}}\big|_{\text{phys}}\right)^{\text{QCD+QED}}}{m_{\mathfrak{S}}^{\text{exp}}} \tag{10.8}$$

$$\left(\sqrt{8t_0^{\text{phys}}}\right)^{(0)} = \frac{\left(\sqrt{8t_0}m_{\mathfrak{S}}\big|_{\text{phys}}\right)^{(0)}}{m_{\mathfrak{S}}^{\text{exp},0}} \tag{10.9}$$

in order to set the scale for a given β via

$$a_\beta^{\text{QCD+QED}} = \left(\sqrt{\frac{a_\beta^2}{8t_0}}\right)^{\text{QCD+QED}} \left(\sqrt{8t_0^{\text{phys}}}\right)^{\text{QCD+QED}} \tag{10.10}$$

$$= \left(\sqrt{\frac{a_\beta^2}{8t_0}}\right)^{(0)} \left(\sqrt{8t_0^{\text{phys}}}\right)^{\text{QCD+QED}} \tag{10.11}$$

$$a_\beta^{(0)} = \left(\sqrt{\frac{a_\beta^2}{8t_0}}\right)^{(0)} \left(\sqrt{8t_0^{\text{phys}}}\right)^{(0)}. \tag{10.12}$$

$$\tag{10.13}$$

The notation $\cdot|_{\text{phys}}$ above is to be understood such that the part on the left of the bar is to be evaluated at the physical point, whose definition should vary between QCD_{iso} and QCD+QED.
As in section 10.3.1 we propose to alternatingly set the lattice spacing and the isospin-breaking coefficients $\Delta\varepsilon_i$ until the sequences converge to the desired precision. However, unlike in eq. (10.7) one cannot simply expand $a_{\beta,n}$ using $\Delta\varepsilon_n$ in the n-th iteration. Instead $(\sqrt{8t_0}m_{\mathfrak{S}})_n$ has to be extrapolated again each iteration to determine a new physical point. Then, a new value $\sqrt{8t_0^{\text{phys}}}_{n+1}$ has to be determined at the new physical point to finally set $a_{\beta,n+1}$ from the new values.

Chapter 11
Conclusion and Outlook

We calculated octet and decuplet baryon masses as well as those of pseudoscalar octet mesons in QCD including isospin-breaking corrections with the goal of setting the scale to high precision for the QCD gauge ensembles by the Coordinated Lattice Simulations (CLS) [9]. The precision of the lattice scale influences the uncertainties of any dimensionful observables computed in LQCD, and thus plays a major role in the computation of high-precision observables. An example for such a high-precision observable that motivated this project is the anomalous magnetic moment a_μ of the muon, which is known experimentally to a precision of ~ 124 ppb [2]. As lattice computations of the hadronic contribution to this observable surpass the $\mathcal{O}(1\%)$ precision mark [3, 5], isospin-breaking effects, which are estimated to be of that order, have to be incorporated into each part of the calculation. This includes the lattice scale, whose relative uncertainty contributes proportionally to the overall uncertainty of a_μ^{hvp} [4, 8].
We wrote a program to compute the correlation functions from which we could derive the masses of the mentioned hadrons in isospin-symmetric QCD (QCD_{iso}) and corrections accounting for the difference of up- and down-quarks as well as QED effects. To this end, we implemented an operator construction for the baryons based on Weyl spinor decompositions of Dirac spinors which was published by the Lattice Hadron Physics Collaboration [12]. Based on these operators, we wrote another program to determine the symbolic contractions for the two-point functions constructed from these operators. This includes cross-correlators mixing different source and sink operators for the same states and for different states that mix in the mass eigenbasis. These contractions had to be determined for isospin-symmetric QCD and for isospin-breaking corrections.
For the isospin-breaking corrections we employed a perturbative approach by the RM123 collaboration [10, 11]. This method expands expectation values in QCD+QED around QCD_{iso} to leading order in the quantities $(\beta, e^2, m_u, m_d, m_s)$ which parameterize the QCD+QED action. For the QED corrections we used the QED_{L} [79] prescription removing the spatial zero-momentum modes of the photon to avoid problems related to compact QED for which we use an implementation by Andreas Risch [13, 80, 81] operating in Coulomb gauge.
The program computing the correlation functions was written in `C++` with MPI based on the `QDP++` library [105] using the solver of the `openQCD` library [47]. To make the program viable for large scale computations, we performed several cross checks to ensure correctness of the implementation and optimized the code multiple times while working on this project. For a more efficient determination

of the QED corrections we developed a method to cheaply infer them from the isospin-symmetric correlation function and the other corrections.
We computed masses for the various baryons as well as for the pion and kaon using model averages [116, 117] based on the Akaike information criterion (AIC) [118] combining single- and two-state fits for most of which we derived closed form solutions for the χ^2 minimization allowing for a more robust analysis using bootstrap resampling.
We performed an extrapolation of the isospin-symmetric masses of baryons that are stable in $\mathrm{QCD}_{\mathrm{iso}}$ to the physical point following a procedure by the RQCD collaboration [46]. The extrapolation uses observables scaled with powers of the Wilson flow scale [15, 16] for which we could determine a physical value $\sqrt{8t_0^{\mathrm{phys}}}$ by matching one of the baryon masses to a modified experimental value accounting for isospin-symmetry [46]. At the physical point, we were able to deduce masses for the baryons that were not used to determine $\sqrt{8t_0^{\mathrm{phys}}}$ that are mostly compatible with the modified experimental values. Using $\sqrt{8t_0^{\mathrm{phys}}}$, we determined lattice spacings for each value of the strong gauge coupling for which we had data available.
The lattice spacings then allowed us to compute the expansion coefficients for the isospin-breaking corrections for each ensemble. Combining all results mentioned so far, we were able to compute masses of all octet baryons and the Omega baryon in QCD+QED to first order in isospin-breaking effects.
Finally, we proposed a modified version of the procedure used in this thesis for setting the scale including isospin-breaking corrections given an extrapolation scheme in QCD+QED.

While we were able to determine most baryonic masses to better than 1% precision on most ensembles (or on all for some baryons, see table 11.1), the extrapolated masses have significantly larger uncertainties. Consequently, the uncertainties of $\sqrt{8t_0^{\mathrm{phys}}}$ and the lattice spacings which are derived from these extrapolated masses also have larger uncertainties than one could expect from single lattice measurements. A large contribution to these uncertainties comes from the precision of the extrapolated masses at the physical point, which, as we are unable to resolve their dependence on the average quark mass, might not lie exactly on the plane spanned by the accessible extrapolation parameters $\mathbb{a}^2 = \frac{a^2}{8t_0}$ and $\delta\mathbb{M}^2 = 16t_0\left(m_K^2 - m_\pi^2\right)$.
Especially using the Ξ baryon, which is used to determine $\sqrt{8t_0^{\mathrm{phys}}}$ in the paper by the RQCD collaboration [46], the uncertainty of our value for $\sqrt{8t_0^{\mathrm{phys}}}$ is larger by a factor of 3.92 than in the reference calculation. This is a larger discrepancy than one would expect from a factor of 5 more ensembles in their analysis. However, using ensembles with much larger variation in the average quark mass makes their analysis more susceptible to the parameter we could not resolve. For future progress on this project, we thus propose to add ensembles from other trajectories than that of average quark mass to the analysis to be able to properly resolve all fit parameters of our extrapolation. Adding more ensembles in general would also enable fits including higher order chiral perturbation theory and other fit procedures used in [46].
Another option to avoid the above mentioned problem could be to use the already

Table 11.1: Relative uncertainty $\delta am = \frac{\Delta am}{am}$ of the isospin-symmetric masses determined on each ensemble in lattice units as listed in table 9.6.

Ensemble	δam_π	δam_K	δam_N	δam_Λ	δam_Σ	δam_Ξ	δam_Ω
A654	0.77%	0.44%	1.01%	0.65%	0.62%	0.41%	1.14%
N101	0.33%	0.12%	0.67%	0.53%	0.51%	0.35%	1.01%
D450	0.34%	0.06%	0.68%	0.32%	0.69%	0.19%	0.50%
N451	0.23%	0.09%	0.36%	0.40%	0.48%	0.29%	0.26%
N452	0.13%	0.08%	0.40%	0.40%	0.34%	0.32%	0.35%
D200	0.52%	0.14%	0.72%	0.26%	0.39%	0.18%	0.30%
N203	0.20%	0.14%	0.68%	0.64%	0.37%	0.27%	0.77%
N200	0.40%	0.16%	0.76%	0.56%	0.43%	0.38%	0.46%
E250	0.30%	0.03%	0.93%	0.54%	0.56%	0.21%	0.29%
E300	0.54%	0.10%	3.24%	1.08%	0.86%	1.47%	0.77%

computed mass derivatives of the correlation functions, which we computed for the isospin-breaking corrections, to correct for the mismatch of the average quark mass observed on individual ensembles as was done for example in [40].

For the inclusion of isospin-breaking corrections to the lattice scale, a parameterization of the baryon masses that does not assume isospin-symmetry has to be chosen in order to perform an extrapolation to the physical point in QCD+QED and ultimately set the lattice scale in this theory. As the uncertainty of the baryon masses is only marginally affected by the inclusion of isospin-breaking corrections, we expect the uncertainty of the QCD+QED lattice scale to be dominated by the $\mathrm{QCD}_{\mathrm{iso}}$ contributions as well. If our hypothesis is correct that we can improve the precision of the extrapolated masses significantly by adding ensembles from different trajectories, we expect that it is possible to achieve an uncertainty of the lattice scale well below 1 % using one of the baryons discussed in this study.

Based on our results for $\sqrt{8t_0^{\mathrm{phys}}}$ and the lattice scales determined using different baryons, we see the Λ baryon as a suitable candidate for scale setting from a precision-based perspective. However, in QCD+QED, Σ-Λ mixing has to be taken into account, which is not an issue in $\mathrm{QCD}_{\mathrm{iso}}$, the influence of which on the overall precision we cannot estimate at this point. Furthermore, as table 11.1 shows, we find better overall precision on individual ensembles for the Ξ baryon as suggested in [46]. It therefore stands to reason, that our data also favors this baryon if we had a better handle on the average quark mass dependence of the baryon masses.

Another aspect to consider is the fact that the Ω baryon is barely affected by isospin-breaking corrections at shifts of 0.020(23)-0.051(29) % of its mass when going from $\mathrm{QCD}_{\mathrm{iso}}$ to QCD+QED in our calculations. This is subdominant to the uncertainty of the Ω baryon while this uncertainty is well below 1 % on most ensembles. Due to this small correction, it would then be possible to only compute the isospin-breaking corrections on a small set of ensembles and extrapolate the corrections independently from the isospin-symmetric masses, as even a 100 % uncertainty of the isospin-breaking corrections would not noticeably influence the overall uncertainty. This would save a lot of computer time which could be invested in more data points for the isospin-symmetric mass to further improve the

final results. Furthermore, as the Ω baryon consists of only strange quarks in the valence sector, one could avoid the more costly computation of light quark propagators when focusing efforts on a precise determination of the Ω mass. Doing so would thus be the most efficient way to gather data for a precise determination of the lattice scale.

Bibliography

[1] Y. Fukuda et al. "Neutrino induced upward stopping muons in Super-Kamiokande". In: *Phys. Lett. B* 467 (1999), pp. 185–193. DOI: 10.1016/S0370-2693(99)01188-0. arXiv: hep-ex/9908049.

[2] D. P. Aguillard et al. "Measurement of the Positive Muon Anomalous Magnetic Moment to 127 ppb". In: *Phys. Rev. Lett.* 135.10 (2025), p. 101802. DOI: 10.1103/7clf-sm2v. arXiv: 2506.03069 [hep-ex].

[3] R. Aliberti et al. "The anomalous magnetic moment of the muon in the Standard Model: an update". In: (May 2025). arXiv: 2505.21476 [hep-ph].

[4] T. Aoyama et al. "The anomalous magnetic moment of the muon in the Standard Model". In: *Phys. Rept.* 887 (2020), pp. 1–166. DOI: 10.1016/j.physrep.2020.07.006. arXiv: 2006.04822 [hep-ph].

[5] Simon Kuberski et al. "Hadronic vacuum polarization in the muon g − 2: the short-distance contribution from lattice QCD". In: *JHEP* 03 (2024), p. 172. DOI: 10.1007/JHEP03(2024)172. arXiv: 2401.11895 [hep-lat].

[6] Antonin Portelli. "Review on the inclusion of isospin breaking effects in lattice calculations". In: *PoS* KAON13 (2013), p. 023. DOI: 10.22323/1.181.0023. arXiv: 1307.6056 [hep-lat].

[7] Antonin Portelli. "Inclusion of isospin breaking effects in lattice simulations". In: *PoS* LATTICE2014 (2015), p. 013. DOI: 10.22323/1.214.0013. arXiv: 1505.07057 [hep-lat].

[8] Harvey B. Meyer and Hartmut Wittig. "Lattice QCD and the anomalous magnetic moment of the muon". In: *Prog. Part. Nucl. Phys.* 104 (2019), pp. 46–96. DOI: 10.1016/j.ppnp.2018.09.001. arXiv: 1807.09370 [hep-lat].

[9] Mattia Bruno et al. "Simulation of QCD with $N_f = 2 + 1$ flavors of non-perturbatively improved Wilson fermions". In: *JHEP* 02 (2015), p. 043. DOI: 10.1007/JHEP02(2015)043. arXiv: 1411.3982 [hep-lat].

[10] G. M. de Divitiis et al. "Isospin-breaking effects due to the up-down mass difference in Lattice QCD". In: *JHEP* 04 (2012), p. 124. DOI: 10.1007/JHEP04(2012)124. arXiv: 1110.6294 [hep-lat].

[11] G. M. de Divitiis et al. "Leading isospin-breaking effects on the lattice". In: *Phys. Rev. D* 87.11 (2013), p. 114505. DOI: 10.1103/PhysRevD.87.114505. arXiv: 1303.4896 [hep-lat].

[12] Subhasish Basak et al. "Clebsch-Gordan construction of lattice interpolating fields for excited baryons". In: *Phys. Rev. D* 72 (2005), p. 074501. DOI: 10.1103/PhysRevD.72.074501. arXiv: hep-lat/0508018.

[13] Andreas Risch and Hartmut Wittig. "Towards leading isospin-breaking effects in mesonic masses with open boundaries". In: *PoS* LATTICE2018 (2018), p. 059. DOI: 10.22323/1.334.0059. arXiv: 1811.00895 [hep-lat].

[14] Andreas Risch and Hartmut Wittig. "Leading isospin breaking effects in the HVP contribution to a_μ and to the running of α". In: *PoS* LATTICE2021 (2022), p. 106. DOI: 10.22323/1.396.0106. arXiv: 2112.00878 [hep-lat].

[15] Martin Lüscher. "Trivializing maps, the Wilson flow and the HMC algorithm". In: *Commun. Math. Phys.* 293 (2010), pp. 899–919. DOI: 10.1007/s00220-009-0953-7. arXiv: 0907.5491 [hep-lat].

[16] Martin Lüscher. "Properties and uses of the Wilson flow in lattice QCD". In: *JHEP* 08 (2010). [Erratum: JHEP 03, 092 (2014)], p. 071. DOI: 10.1007/JHEP08(2010)071. arXiv: 1006.4518 [hep-lat].

[17] Michael E. Peskin and Daniel V. Schroeder. *An Introduction to quantum field theory*. Reading, USA: Addison-Wesley, 1995. ISBN: 978-0-201-50397-5, 978-0-429-50355-9, 978-0-429-49417-8. DOI: 10.1201/9780429503559.

[18] Murray Gell-Mann. "Symmetries of baryons and mesons". In: *Phys. Rev.* 125 (1962), pp. 1067–1084. DOI: 10.1103/PhysRev.125.1067.

[19] Thomas DeGrand and Carleton E. Detar. *Lattice methods for quantum chromodynamics*. 2006.

[20] L. D. Faddeev and V. N. Popov. "Feynman Diagrams for the Yang-Mills Field". In: *Phys. Lett. B* 25 (1967). Ed. by Jong-Ping Hsu and D. Fine, pp. 29–30. DOI: 10.1016/0370-2693(67)90067-6.

[21] J. Schwinger. "On the Euclidean Structure of Relativistic Field Theory". In: *Proc. Nat. Acad. Sci.* 44.9 (1958), pp. 956–965. DOI: 10.1073/pnas.44.9.956.

[22] Tadao Nakano. "Quantum Field Theory in Terms of Euclidean Parameters". In: *Progress of Theoretical Physics* 21.2 (Feb. 1959), pp. 241–259. ISSN: 0033-068X. DOI: 10.1143/PTP.21.241. eprint: https://academic.oup.com/ptp/article-pdf/21/2/241/5456644/21-2-241.pdf. URL: https://doi.org/10.1143/PTP.21.241.

[23] Francesco Guerra. "Euclidean field theory". In: (Oct. 2005). arXiv: math-ph/0510087.

[24] R. F. Streater and A. S. Wightman. *PCT, spin and statistics, and all that*. 1989. ISBN: 978-0-691-07062-9.

[25] Edward Nelson. "Construction of quantum fields from Markoff fields". In: *Journal of Functional Analysis* 12.1 (1973), pp. 97–112. ISSN: 0022-1236. DOI: https://doi.org/10.1016/0022-1236(73)90091-8. URL: https://www.sciencedirect.com/science/article/pii/0022123673900918.

[26] Konrad Osterwalder and Robert Schrader. "Axioms for Euclidean Green's Functions". In: *Commun. Math. Phys.* 31 (1973), pp. 83–112. DOI: 10.1007/BF01645738.

[27] Konrad Osterwalder and Robert Schrader. "Axioms for Euclidean Green's Functions II". In: *Commun. Math. Phys.* 42 (1975), p. 281. DOI: 10.1007/BF01608978.

[28] I. Montvay and G. Münster. *Quantum fields on a lattice*. Cambridge Monographs on Mathematical Physics. Cambridge University Press, Mar. 1997. ISBN: 978-0-521-59917-7, 978-0-511-87919-7. DOI: 10.1017/CBO9780511470783.

[29] Christof Gattringer and Christian B. Lang. *Quantum chromodynamics on the lattice*. Vol. 788. Berlin: Springer, 2010. ISBN: 978-3-642-01849-7, 978-3-642-01850-3. DOI: 10.1007/978-3-642-01850-3.

[30] M. Lüscher and P. Weisz. "On-shell improved lattice gauge theories". In: *Commun. Math. Phys.* 98.3 (1985). [Erratum: Commun.Math.Phys. 98, 433 (1985)], p. 433. DOI: 10.1007/BF01205792.

[31] Kenneth G. Wilson. "Confinement of Quarks". In: *Phys. Rev. D* 10 (1974). Ed. by J. C. Taylor, pp. 2445–2459. DOI: 10.1103/PhysRevD.10.2445.

[32] Holger Bech Nielsen and M. Ninomiya. "No Go Theorem for Regularizing Chiral Fermions". In: *Phys. Lett. B* 105 (1981), pp. 219–223. DOI: 10.1016/0370-2693(81)91026-1.

[33] H.B. Nielsen and M. Ninomiya. "Absence of neutrinos on a lattice: (I). Proof by homotopy theory". In: *Nuclear Physics B* 185.1 (1981), pp. 20–40. ISSN: 0550-3213. DOI: https://doi.org/10.1016/0550-3213(81)90361-8. URL: https://www.sciencedirect.com/science/article/pii/0550321381903618.

[34] Holger Bech Nielsen and M. Ninomiya. "Absence of Neutrinos on a Lattice. 2. Intuitive Topological Proof". In: *Nucl. Phys. B* 193 (1981), pp. 173–194. DOI: 10.1016/0550-3213(81)90524-1.

[35] Luuk H. Karsten. "Lattice Fermions in Euclidean Space-time". In: *Phys. Lett. B* 104 (1981), pp. 315–319. DOI: 10.1016/0370-2693(81)90133-7.

[36] Martin Lüscher. "Exact chiral symmetry on the lattice and the Ginsparg-Wilson relation". In: *Phys. Lett. B* 428 (1998), pp. 342–345. DOI: 10.1016/S0370-2693(98)00423-7. arXiv: hep-lat/9802011.

[37] Mark Hamilton J. D. *Mathematical Gauge Theory: With Applications to the Standard Model of Particle Physics*. Universitext. Cham: Springer International Publishing, 2017. ISBN: 978-3-319-68438-3, 978-3-319-68439-0. DOI: 10.1007/978-3-319-68439-0.

[38] John D Moore. *Lectures on Seiberg-Witten invariants*. Springer, 2009.

[39] R. C. Johnson. "ANGULAR MOMENTUM ON A LATTICE". In: *Phys. Lett. B* 114 (1982), pp. 147–151. DOI: 10.1016/0370-2693(82)90134-4.

[40] Mattia Bruno, Tomasz Korzec, and Stefan Schaefer. "Setting the scale for the CLS $2+1$ flavor ensembles". In: *Phys. Rev. D* 95.7 (2017), p. 074504. DOI: 10.1103/PhysRevD.95.074504. arXiv: 1608.08900 [hep-lat].

[41] Ben Straßberger et al. "Scale setting for CLS 2+1 simulations". In: *PoS* LATTICE2021 (2022), p. 135. DOI: 10.22323/1.396.0135. arXiv: 2112.06696 [hep-lat].

[42] C. Allton et al. "Physical Results from 2+1 Flavor Domain Wall QCD and SU(2) Chiral Perturbation Theory". In: *Phys. Rev. D* 78 (2008), p. 114509. DOI: 10.1103/PhysRevD.78.114509. arXiv: 0804.0473 [hep-lat].

[43] Sz. Borsányi et al. “Leading hadronic contribution to the muon magnetic moment from lattice QCD”. In: *Nature* 593.7857 (2021), pp. 51–55. DOI: 10.1038/s41586-021-03418-1. arXiv: 2002.12347 [hep-lat].

[44] Nolan Miller et al. “Scale setting the Möbius domain wall fermion on gradient-flowed HISQ action using the omega baryon mass and the gradient-flow scales t_0 and w_0”. In: *Phys. Rev. D* 103.5 (2021), p. 054511. DOI: 10.1103/PhysRevD.103.054511. arXiv: 2011.12166 [hep-lat].

[45] Martin Lüscher et al. “Chiral symmetry and O(a) improvement in lattice QCD”. In: *Nucl. Phys. B* 478 (1996), pp. 365–400. DOI: 10.1016/0550-3213(96)00378-1. arXiv: hep-lat/9605038.

[46] Gunnar S. Bali et al. “Scale setting and the light baryon spectrum in $N_f = 2 + 1$ QCD with Wilson fermions”. In: *JHEP* 05 (2023), p. 035. DOI: 10.1007/JHEP05(2023)035. arXiv: 2211.03744 [hep-lat].

[47] Martin Lüscher and Stefan Schaefer. *openQCD*. Version 1.4. URL: https://luscher.web.cern.ch/luscher/openQCD/.

[48] B. Sheikholeslami and R. Wohlert. “Improved Continuum Limit Lattice Action for QCD with Wilson Fermions”. In: *Nucl. Phys. B* 259 (1985), p. 572. DOI: 10.1016/0550-3213(85)90002-1.

[49] Roberto Frezzotti et al. “Lattice QCD with a chirally twisted mass term”. In: *JHEP* 08 (2001), p. 058. DOI: 10.1088/1126-6708/2001/08/058. arXiv: hep-lat/0101001.

[50] Martin Lüscher and Filippo Palombi. “Fluctuations and reweighting of the quark determinant on large lattices”. In: *PoS* LATTICE2008 (2008). Ed. by Christopher Aubin et al., p. 049. DOI: 10.22323/1.066.0049. arXiv: 0810.0946 [hep-lat].

[51] Martin Lüscher and Stefan Schaefer. “Lattice QCD with open boundary conditions and twisted-mass reweighting”. In: *Comput. Phys. Commun.* 184 (2013), pp. 519–528. DOI: 10.1016/j.cpc.2012.10.003. arXiv: 1206.2809 [hep-lat].

[52] Thomas A. DeGrand. “A Conditioning Technique for Matrix Inversion for Wilson Fermions”. In: *Comput. Phys. Commun.* 52 (1988), pp. 161–164. DOI: 10.1016/0010-4655(88)90180-4.

[53] Martin Hasenbusch. “Speeding up the hybrid Monte Carlo algorithm for dynamical fermions”. In: *Phys. Lett. B* 519 (2001), pp. 177–182. DOI: 10.1016/S0370-2693(01)01102-9. arXiv: hep-lat/0107019.

[54] M. Hasenbusch and K. Jansen. “Speeding up lattice QCD simulations with clover improved Wilson fermions”. In: *Nucl. Phys. B* 659 (2003), pp. 299–320. DOI: 10.1016/S0550-3213(03)00227-X. arXiv: hep-lat/0211042.

[55] A. D. Kennedy, Ivan Horvath, and Stefan Sint. “A New exact method for dynamical fermion computations with nonlocal actions”. In: *Nucl. Phys. B Proc. Suppl.* 73 (1999). Ed. by Thomas A. DeGrand et al., pp. 834–836. DOI: 10.1016/S0920-5632(99)85217-7. arXiv: hep-lat/9809092.

[56] Daniel Mohler and Stefan Schaefer. “Remarks on strange-quark simulations with Wilson fermions”. In: *Phys. Rev. D* 102.7 (2020), p. 074506. DOI: 10.1103/PhysRevD.102.074506. arXiv: 2003.13359 [hep-lat].

[57] John Bulava et al. "Non-perturbative improvement of the axial current in N_f=3 lattice QCD with Wilson fermions and tree-level improved gauge action". In: *Nucl. Phys. B* 896 (2015), pp. 555–568. DOI: 10.1016/j.nuclphysb.2015.05.003. arXiv: 1502.04999 [hep-lat].

[58] Zoltan Fodor et al. "The Yang-Mills gradient flow in finite volume". In: *JHEP* 11 (2012), p. 007. DOI: 10.1007/JHEP11(2012)007. arXiv: 1208.1051 [hep-lat].

[59] Anna Hasenfratz and Oliver Witzel. "Continuous renormalization group β function from lattice simulations". In: *Phys. Rev. D* 101.3 (2020), p. 034514. DOI: 10.1103/PhysRevD.101.034514. arXiv: 1910.06408 [hep-lat].

[60] Anna Hasenfratz and Oliver Witzel. "Continuous β function for the SU(3) gauge systems with two and twelve fundamental flavors". In: *PoS* LATTICE2019 (2019), p. 094. DOI: 10.22323/1.363.0094. arXiv: 1911.11531 [hep-lat].

[61] Christian Schneider, Anna Hasenfratz, and Oliver Witzel. "Gradient flow scale setting with tree-level improvement". In: *PoS* LATTICE2022 (2023), p. 288. DOI: 10.22323/1.430.0288. arXiv: 2211.12406 [hep-lat].

[62] Rainer Sommer. "Scale setting in lattice QCD". In: *PoS* LATTICE2013 (2014), p. 015. DOI: 10.22323/1.187.0015. arXiv: 1401.3270 [hep-lat].

[63] V. G. Bornyakov et al. "Wilson flow and scale setting from lattice QCD". In: (Aug. 2015). arXiv: 1508.05916 [hep-lat].

[64] Ta-Pei Cheng and Ling-Fong Li. *Gauge Theory of Elementary Particle Physics*. Oxford, UK: Oxford University Press, 1984. ISBN: 978-0-19-851961-4, 978-0-19-851961-4.

[65] D. P. Aguillard et al. "Measurement of the Positive Muon Anomalous Magnetic Moment to 0.20 ppm". In: *Phys. Rev. Lett.* 131.16 (2023), p. 161802. DOI: 10.1103/PhysRevLett.131.161802. arXiv: 2308.06230 [hep-ex].

[66] N. Carrasco et al. "QED Corrections to Hadronic Processes in Lattice QCD". In: *Phys. Rev. D* 91.7 (2015), p. 074506. DOI: 10.1103/PhysRevD.91.074506. arXiv: 1502.00257 [hep-lat].

[67] M. Di Carlo et al. "Light-meson leptonic decay rates in lattice QCD+QED". In: *Phys. Rev. D* 100.3 (2019), p. 034514. DOI: 10.1103/PhysRevD.100.034514. arXiv: 1904.08731 [hep-lat].

[68] Renwick J. Hudspith, Matthias F. M. Lutz, and Daniel Mohler. "Precise Omega baryons from lattice QCD". In: (Apr. 2024). arXiv: 2404.02769 [hep-lat].

[69] Alexei Bazavov et al. "High-Precision Scale Setting with the Omega-Baryon Mass and Gradient Flow". In: (Sept. 2025). arXiv: 2509.14367 [hep-lat].

[70] Y. Aoki et al. "FLAG Review 2021". In: *Eur. Phys. J. C* 82.10 (2022), p. 869. DOI: 10.1140/epjc/s10052-022-10536-1. arXiv: 2111.09849 [hep-lat].

[71] Y. Aoki et al. "FLAG Review 2024". In: (Nov. 2024). arXiv: 2411.04268 [hep-lat].

[72] Sz. Borsanyi et al. "Isospin splittings in the light baryon octet from lattice QCD and QED". In: *Phys. Rev. Lett.* 111.25 (2013), p. 252001. DOI: 10.1103/PhysRevLett.111.252001. arXiv: 1306.2287 [hep-lat].

[73] Agostino Patella. "QED Corrections to Hadronic Observables". In: *PoS* LATTICE2016 (2017), p. 020. DOI: 10.22323/1.256.0020. arXiv: 1702.03857 [hep-lat].

[74] Michael G. Endres et al. "Massive photons: an infrared regularization scheme for lattice QCD+QED". In: *Phys. Rev. Lett.* 117.7 (2016), p. 072002. DOI: 10.1103/PhysRevLett.117.072002. arXiv: 1507.08916 [hep-lat].

[75] L. Polley and U. J. Wiese. "Monopole condensate and monopole mass in U(1) lattice gauge theory". In: *Nucl. Phys. B* 356 (1991), pp. 629–654. DOI: 10.1016/0550-3213(91)90380-G.

[76] Biagio Lucini et al. "Charged hadrons in local finite-volume QED+QCD with C * boundary conditions". In: *JHEP* 02 (2016), p. 076. DOI: 10.1007/JHEP02(2016)076. arXiv: 1509.01636 [hep-th].

[77] A. Duncan, E. Eichten, and H. Thacker. "Electromagnetic splittings and light quark masses in lattice QCD". In: *Phys. Rev. Lett.* 76 (1996), pp. 3894–3897. DOI: 10.1103/PhysRevLett.76.3894. arXiv: hep-lat/9602005.

[78] Sz. Borsanyi et al. "Ab initio calculation of the neutron-proton mass difference". In: *Science* 347 (2015), pp. 1452–1455. DOI: 10.1126/science.1257050. arXiv: 1406.4088 [hep-lat].

[79] Masashi Hayakawa and Shunpei Uno. "QED in finite volume and finite size scaling effect on electromagnetic properties of hadrons". In: *Prog. Theor. Phys.* 120 (2008), pp. 413–441. DOI: 10.1143/PTP.120.413. arXiv: 0804.2044 [hep-ph].

[80] Andreas Risch and Hartmut Wittig. "Towards leading isospin breaking effects in mesonic masses with $O(a)$ improved Wilson fermions". In: *EPJ Web Conf.* 175 (2018). Ed. by M. Della Morte et al., p. 14019. DOI: 10.1051/epjconf/201817514019. arXiv: 1710.06801 [hep-lat].

[81] Andreas Risch. "Isospin breaking effects in hadronic matrix elements on the lattice". PhD thesis. Mainz U., 2021. DOI: 10.25358/openscience-6314.

[82] G. O. Roberts and R. L. Tweedie. "Geometric Convergence and Central Limit Theorems for Multidimensional Hastings and Metropolis Algorithms". In: *Biometrika* 83.1 (1996), pp. 95–110. ISSN: 00063444, 14643510. URL: http://www.jstor.org/stable/2337435 (visited on 11/11/2025).

[83] Ian M. Barbour et al. "Results on finite density QCD". In: *Nucl. Phys. B Proc. Suppl.* 60 (1998). Ed. by Y. Iwasaki and A. Ukawa, pp. 220–234. DOI: 10.1016/S0920-5632(97)00484-2. arXiv: hep-lat/9705042.

[84] Z. Fodor and S. D. Katz. "A New method to study lattice QCD at finite temperature and chemical potential". In: *Phys. Lett. B* 534 (2002), pp. 87–92. DOI: 10.1016/S0370-2693(02)01583-6. arXiv: hep-lat/0104001.

[85] Z. Fodor and S. D. Katz. "Critical point of QCD at finite T and mu, lattice results for physical quark masses". In: *JHEP* 04 (2004), p. 050. DOI: 10.1088/1126-6708/2004/04/050. arXiv: hep-lat/0402006.

[86] Neal Madras and Alan D. Sokal. "The Pivot algorithm: a highly efficient Monte Carlo method for selfavoiding walk". In: *J. Statist. Phys.* 50 (1988), pp. 109–186. DOI: 10.1007/BF01022990.

[87] Ulli Wolff. "Monte Carlo errors with less errors". In: *Comput. Phys. Commun.* 156 (2004). [Erratum: Comput.Phys.Commun. 176, 383 (2007)], pp. 143–153. DOI: 10.1016/S0010-4655(03)00467-3. arXiv: hep-lat/0306017.

[88] Thomas Blum, Taku Izubuchi, and Eigo Shintani. "New class of variance-reduction techniques using lattice symmetries". In: *Phys. Rev. D* 88.9 (2013), p. 094503. DOI: 10.1103/PhysRevD.88.094503. arXiv: 1208.4349 [hep-lat].

[89] Thomas Blum, Taku Izubuchi, and Eigo Shintani. "Error reduction technique using covariant approximation and application to nucleon form factor". In: *PoS* LATTICE2012 (2012). Ed. by Derek Leinweber et al., p. 262. DOI: 10.22323/1.164.0262. arXiv: 1212.5542 [hep-lat].

[90] John Hammersley. *Monte carlo methods*. Springer Science & Business Media, 2013.

[91] S. Güsken. "A Study of smearing techniques for hadron correlation functions". In: *Nucl. Phys. B Proc. Suppl.* 17 (1990). Ed. by N. Cabibbo et al., pp. 361–364. DOI: 10.1016/0920-5632(90)90273-W.

[92] Georg M. von Hippel et al. "The Shape of Covariantly Smeared Sources in Lattice QCD". In: *JHEP* 09 (2013), p. 014. DOI: 10.1007/JHEP09(2013)014. arXiv: 1306.1440 [hep-lat].

[93] Gunnar S. Bali et al. "Novel quark smearing for hadrons with high momenta in lattice QCD". In: *Phys. Rev. D* 93.9 (2016), p. 094515. DOI: 10.1103/PhysRevD.93.094515. arXiv: 1602.05525 [hep-lat].

[94] M. Falcioni et al. "AGAIN ON SU(3) GLUEBALL MASS". In: *Nucl. Phys. B* 251 (1985), pp. 624–632. DOI: 10.1016/0550-3213(85)90280-9.

[95] M. Albanese et al. "Glueball Masses and String Tension in Lattice QCD". In: *Phys. Lett. B* 192 (1987), pp. 163–169. DOI: 10.1016/0370-2693(87)91160-9.

[96] M. Falcioni et al. "Large-distance correlation functions for an SU(2) lattice gauge theory". In: *Nuclear Physics B* 215.2 (1983), pp. 265–277. ISSN: 0550-3213. DOI: https://doi.org/10.1016/0550-3213(83)90215-8. URL: https://www.sciencedirect.com/science/article/pii/0550321383902158.

[97] Y. Liang et al. "Lattice calculation of glueball matrix elements". In: *Phys. Lett. B* 307 (1993), pp. 375–382. DOI: 10.1016/0370-2693(93)90236-B. arXiv: hep-lat/9304011.

[98] Colin Morningstar and Mike J. Peardon. "Analytic smearing of SU(3) link variables in lattice QCD". In: *Phys. Rev. D* 69 (2004), p. 054501. DOI: 10.1103/PhysRevD.69.054501. arXiv: hep-lat/0311018.

[99] J. B. Zhang et al. "Stout-link smearing in lattice fermion actions". In: *Phys. Rev. D* 80 (2009), p. 074503. DOI: 10.1103/PhysRevD.80.074503. arXiv: 0908.3726 [hep-lat].

[100] Gunnar S. Bali et al. "Observation of string breaking in QCD". In: *Phys. Rev. D* 71 (2005), p. 114513. DOI: 10.1103/PhysRevD.71.114513. arXiv: hep-lat/0505012.

[101] B. Blossier et al. "Efficient use of the Generalized Eigenvalue Problem". In: *PoS* LATTICE2008 (2008). Ed. by Christopher Aubin et al., p. 135. DOI: 10.22323/1.066.0135. arXiv: 0808.1017 [hep-lat].

[102] Benoit Blossier et al. "On the generalized eigenvalue method for energies and matrix elements in lattice field theory". In: *JHEP* 04 (2009), p. 094. DOI: 10.1088/1126-6708/2009/04/094. arXiv: 0902.1265 [hep-lat].

[103] Martin Lüscher and Ulli Wolff. "How to Calculate the Elastic Scattering Matrix in Two-dimensional Quantum Field Theories by Numerical Simulation". In: *Nucl. Phys. B* 339 (1990), pp. 222–252. DOI: 10.1016/0550-3213(90)90540-T.

[104] Matthias Fischer et al. "On the generalised eigenvalue method and its relation to Prony and generalised pencil of function methods". In: *Eur. Phys. J. A* 56.8 (2020), p. 206. DOI: 10.1140/epja/s10050-020-00205-w. arXiv: 2004.10472 [hep-lat].

[105] Robert G. Edwards and Balint Joo. "The Chroma software system for lattice QCD". In: *Nucl. Phys. B Proc. Suppl.* 140 (2005). Ed. by Geoffrey T. Bodwin et al., p. 832. DOI: 10.1016/j.nuclphysbps.2004.11.254. arXiv: hep-lat/0409003.

[106] Jesse Beder. *yaml-cpp*. https://github.com/jbeder/yaml-cpp/.

[107] The HDF Group. *Hierarchical Data Format, version 5*. URL: https://github.com/HDFGroup/hdf5.

[108] Arjun Gambhir, David Brantley, Jason Chang, Ben Hörz, Henry Monge-Camacho, Pavlos Vranas, André Walker-Loud. *LALIBE*. URL: https://github.com/callat-qcd/lalibe.

[109] Martin Lüscher. "Local coherence and deflation of the low quark modes in lattice QCD". In: *JHEP* 07 (2007), p. 081. DOI: 10.1088/1126-6708/2007/07/081. arXiv: 0706.2298 [hep-lat].

[110] H. A. Schwarz. "Über einen grenzübergang durch alternierendes verfahren". In: *Vierteljahrsschrift der Naturforschenden Gesellschaft in Zürich. v15* (), pp. 272–286.

[111] Martin Lüscher. "Solution of the Dirac equation in lattice QCD using a domain decomposition method". In: *Comput. Phys. Commun.* 156 (2004), pp. 209–220. DOI: 10.1016/S0010-4655(03)00486-7. arXiv: hep-lat/0310048.

[112] Sara Collins, Gunnar Bali, and Andreas Schafer. "Disconnected contributions to hadronic structure: a new method for stochastic noise reduction". In: *PoS* LATTICE2007 (2007). Ed. by Gunnar Bali et al., p. 141. DOI: 10.22323/1.042.0141. arXiv: 0709.3217 [hep-lat].

[113] G. Peter Lepage. "The Analysis of Algorithms for Lattice Field Theory". In: *Theoretical Advanced Study Institute in Elementary Particle Physics*. June 1989.

[114] Michael L. Wagman and Martin J. Savage. "Statistics of baryon correlation functions in lattice QCD". In: *Phys. Rev. D* 96.11 (2017), p. 114508. DOI: 10.1103/PhysRevD.96.114508. arXiv: 1611.07643 [hep-lat].

[115] L. Del Debbio et al. "QCD with light Wilson quarks on fine lattices (I): First experiences and physics results". In: *JHEP* 02 (2007), p. 056. DOI: 10.1088/1126-6708/2007/02/056. arXiv: hep-lat/0610059.

[116] William I. Jay and Ethan T. Neil. "Bayesian model averaging for analysis of lattice field theory results". In: *Phys. Rev. D* 103 (2021), p. 114502. DOI: 10.1103/PhysRevD.103.114502. arXiv: 2008.01069 [stat.ME].

[117] Ethan T. Neil and Jacob W. Sitison. "Improved information criteria for Bayesian model averaging in lattice field theory". In: *Phys. Rev. D* 109.1 (2024), p. 014510. DOI: 10.1103/PhysRevD.109.014510. arXiv: 2208.14983 [stat.ME].

[118] Hirotogu Akaike. "Information Theory and an Extension of the Maximum Likelihood Principle". In: New York: Springer Science+Business Media, 1998. DOI: 10.1007/978-1-4612-1694-0_15.

[119] Alexei Bazavov et al. "Hadronic vacuum polarization for the muon $g-2$ from lattice QCD: Complete short and intermediate windows". In: (Nov. 2024). arXiv: 2411.09656 [hep-lat].

[120] Fabian Joswig et al. "pyerrors: A python framework for error analysis of Monte Carlo data". In: *Comput. Phys. Commun.* 288 (2023), p. 108750. DOI: 10.1016/j.cpc.2023.108750. arXiv: 2209.14371 [hep-lat].

[121] Jannik Schürg and Geordon Worley. *levenberg-marquardt: Levenberg-Marquardt algorithm built on top of nalgebra*. Aug. 2024. URL: %7Bhttps://github.com/rust-cv/levenberg-marquardt%7D.

[122] Jorge J Moré. "The Levenberg-Marquardt algorithm: implementation and theory". In: *Numerical analysis: proceedings of the biennial Conference held at Dundee, June 28–July 1, 1977*. Springer. 2006, pp. 105–116.

[123] S. Aoki et al. "Review of lattice results concerning low-energy particle physics". In: *Eur. Phys. J. C* 77.2 (2017), p. 112. DOI: 10.1140/epjc/s10052-016-4509-7. arXiv: 1607.00299 [hep-lat].

[124] R. J. Dowdall et al. "Vus from pi and K decay constants in full lattice QCD with physical u, d, s and c quarks". In: *Phys. Rev. D* 88 (2013), p. 074504. DOI: 10.1103/PhysRevD.88.074504. arXiv: 1303.1670 [hep-lat].

[125] R. Horsley et al. "Lattice determination of Sigma-Lambda mixing". In: *Phys. Rev. D* 91.7 (2015), p. 074512. DOI: 10.1103/PhysRevD.91.074512. arXiv: 1411.7665 [hep-lat].

[126] S. Navas et al. "Review of particle physics". In: *Phys. Rev. D* 110.3 (2024), p. 030001. DOI: 10.1103/PhysRevD.110.030001.

[127] M. F. Atiyah, R. Bott, and A. Shapiro. "Clifford modules". In: *Topology* 3 (1964), S3–S38. DOI: 10.1016/0040-9383(64)90003-5.

[128] Kenneth Levenberg. “A method for the solution of certain non-linear problems in least squares”. In: *Quarterly of applied mathematics* 2.2 (1944), pp. 164–168.

[129] Donald W Marquardt. “An algorithm for least-squares estimation of nonlinear parameters”. In: *Journal of the society for Industrial and Applied Mathematics* 11.2 (1963), pp. 431–441.

Acknowledgements

I want to thank Prof. Dr. Hartmut Wittig for the chance of working on this project and writing this thesis. Furthermore, I want to thank Andreas Risch for his continued help with the project and I want to thank him and Andrew Hanlon for helping me to get started with the project. I am also grateful for my office mates Miguel Salg, Arnau Beltran Martìnez, Sebastian Lahrtz, and Cornelia Tölle for many fruitful discussions. For many further discussions and help with a side project, I want to thank Kyra Klos. Andreas Risch, Sebastian Lahrtz, Cornelia Tölle, Luiz Frederic Wagner, Niklas Tausendpfund and Florian Stuhlmann gave me comments on parts of this document, helping me with the process of writing.
Furthermore, I want to thank my fiancé Mara Kunz and my family as well as my friends for supporting me throughout the whole process.

I am, at the time of writing, part of the Helmholtz Graduate School for Hadron and Ion Research, HGS-HIRe, who supported me through funding of the first months of my research and several training events.

Parts of this research were conducted using the supercomputer MOGON 2 and/or advisory services offered by Johannes Gutenberg University Mainz (hpc.uni-mainz.de), which is a member of the AHRP (Alliance for High Performance Computing in Rhineland Palatinate, www.ahrp.info) and the Gauss Alliance e.V. The authors gratefully acknowledge the computing time granted on the supercomputer MOGON 2 at Johannes Gutenberg University Mainz (hpc.uni-mainz.de).

The authors gratefully acknowledge the Gauss Centre for Supercomputing e.V. (www.gauss-centre.eu) for funding this project by providing computing time through the John von Neumann Institute for Computing (NIC) on the GCS Supercomputer JUWELS at Jülich Supercomputing Centre (JSC).

Chapter A
Conventions and Notation

In the following, a brief introduction to the notation and conventions in the different contexts of this thesis are introduced.

A.1. Indices

If not specified otherwise, upper and lower indices may mean one of the following:

- **Lorentz indices**

  Greek letters (most commonly starting with μ, ν, ρ, σ) or explicit values (0, 1, 2, or 3) denoting directions in 4D spacetime. In case multiple occurrences of the same indices as super- and subscript these indices are to be understood as a Lorentz-contraction, e.g. in the expression $j^\nu = \partial_\mu F^{\mu\nu}$ an implicit sum over μ is assumed, i.e. $j^\nu = \sum_{\mu=0}^{3} \partial_\mu F^{\mu\nu}$.

- **Spinor indices**

  Indices denoting spinor components for example in the context of a spinor or propagator are denoted with Greek letters (usually starting with α, β) or explicit values (1, 2, 3, or 4). In expressions containing spinor and Lorentz indices it should be mentioned explicitly which indices correspond to which class.

- **Color indices**

  Latin letters (usually a, b, c) are used to denote color indices in the contexts of quark fields or propagators.

- **Spacetime coordinates**

  Spacetime coordinates are denoted by Latin letters and appear in brackets after a field which is restricted to the given coordinates. For example, the value of a quark field at position x might be denoted as $\Psi(x)$ where $x \in \mathbb{R}^4$.

Indices which are not relevant for a specific argument may be omitted for readability.

A.2. Calculus

For discretized derivatives, the following notations are used for the different discretizations:

$$\begin{aligned}\partial_\mu^+ f(x) =& \frac{1}{a}(f(x+a\hat{\mu}) - f(x)),\\ \partial_\mu^- f(x) =& \frac{1}{a}(f(x) - f(x-a\hat{\mu})),\\ \partial_\mu f(x) =& \frac{1}{2a}(f(x+a\hat{\mu}) - f(x-a\hat{\mu})).\end{aligned}$$

The corresponding covariant derivatives for a gauge group with gauge links U are written as

$$\begin{aligned}\nabla_\mu^+ \psi(x) =& \frac{1}{a}(U_\mu(x)\psi(x+a\hat{\mu}) - \psi(x)),\\ \nabla_\mu^- \psi(x) =& \frac{1}{a}\big(\psi(x) - U_\mu^\dagger(x-a\hat{\mu})\psi(x-a\hat{\mu})\big),\\ \nabla_\mu \psi(x) =& \frac{1}{2}(\nabla_\mu^+ + \nabla_\mu^-)\psi(x)\\ =& \frac{1}{2a}\big(U_\mu(x)\psi(x+a\hat{\mu}) - U_\mu^\dagger(x-a\hat{\mu})\psi(x-a\hat{\mu})\big).\end{aligned}$$

A.3. Expectation Values

Expectation values are denoted by angle brackets, $\langle\cdot\rangle$ with a subscript indicating the quantities with respect to which the expectation value is taken. In the context of path integral expectation values, the subscript is the action that appears in the path integral. In general, this subscript should be clear from the context of the equation/formula making use of this notation, or it might be one of the following which are used frequently and thus have a common meaning:

$S_{\text{eff}}^{(0)}$ – Expectation value in isospin-symmetric QCD where the quark fields are integrated out. This corresponds to the average over all gauge configurations.

S_{eff} – Expectation value in QCD+QED where the photon and quark fields are integrated out.

$S_q^{(0)}$ – Expectation value w.r.t. the isospin-symmetric quark action. This corresponds to the Wick contractions of the quark fields on an SU(3) background field. The result is a function of the QCD gauge field.

$S_{q\gamma}$ – Expectation value w.r.t. the combined photon and quark action. This corresponds to the Wick contractions of the quark fields with $\mathcal{O}(\alpha_{\text{em}})$ QED corrections. The result is a function of the QCD gauge field.

The covariance $\langle(x - \langle x\rangle)(y - \langle y\rangle)\rangle$ of two scalar observables $x, y \in \mathbb{R}$ is denoted as $\text{Cov}(x, y)$. For a vector of observables $x \in \mathbb{R}^n$, its covariance matrix is written as

$$\text{Cov}_x = \left\langle (x - \langle x\rangle)(x - \langle x\rangle)^T \right\rangle.$$

Chapter B
Additional Details

B.1. Clifford Algebras

Consider the tensor algebra $T(V) = \bigoplus_{k=0}^{\infty} V^k = \mathbb{K} \oplus V \oplus (V \otimes V) \oplus \cdots$ of a vector space V over a commutative field $\mathbb{K}$ and a quadratic form $Q : V \to \mathbb{K}$. Then, elements $v \otimes v - Q(v)1 \in T(V)$ generate a two-sided ideal [37, 127][1]

$$I(Q) = \{t \otimes (v \otimes v - Q(v)1) \otimes s | v \in V, t, s \in T(V)\}.$$

The Clifford algebra $Cl(Q)$ is then defined as the quotient algebra $T(V)/I(Q)$, i.e. the algebra that results from identifying the tensor product $v \otimes v$ of a vector with itself with $Q(v)$. In the following, we write the product of two elements of the Clifford algebra x and y as xy.
In physics, the most relevant cases arise from $\mathbb{K} \in \{\mathbb{R}, \mathbb{C}\}$ and Q defined by the (pseudo-)metric defined in the respective physical space or spacetime, which in the following is called η which can be either the Euclidean metric or the Minkowski-pseudometric. In these cases, one finds for the Clifford product that $v^2 := vv = \eta(v, v)$, i.e. the Clifford product of a vector with itself is the scalar product of the vector with itself that is induced by η. for $v \in V$ and for $v, w \in V$

$$\begin{aligned} \eta(v,v) + \eta(w,w) + 2\eta(v,w) &= \eta(v+w, v+w) = Q(v+w) = (v+w)^2 \\ &= v^2 + w^2 + vw + wv \\ &= \eta(v,v) + \eta(w,w) + vw + wv \\ \Rightarrow vw &= 2\eta(v,w) - wv. \end{aligned} \tag{B.1}$$

Thus, orthogonal vectors anticommute, while the product of two parallel vectors is equivalent to their scalar product. If Q is the Euclidean norm in $\mathbb{R}^n$, one often writes $Cl(Q) =: Cl(n)$ and $Cl(Q) =: Cl(n, \mathbb{C})$ if $V = \mathbb{C}^n$. If Q is a pseudo-metric with signature $\underbrace{+\cdots+}_{p \text{ times}}\underbrace{-\cdots-}_{q \text{ times}}$, one writes $Cl(p, q)$ or $Cl(p, q, \mathbb{C})$, respectively. For an orthonormal basis $\gamma_\mu, \mu \in \{1, ..., p+q\}$ of V, eq. (B.1) reduces to the well-known anti-commutation relation of the Dirac matrices,

$$\{\gamma_\mu, \gamma_\nu\} = 2\eta_{\mu\nu}.$$

[1] In the literature, Q is often chosen with the opposite sign, as for example in [37].

Since these basis vectors square to scalars, the Clifford algebra is spanned by products of up to n or $p+q$ pairwise distinct basis vectors.
Clifford algebras naturally give rise to the double cover of $\mathrm{SO}(p,q)$, the Spin-group which is the subgroup of invertible elements of $Cl(p,q)$ formed by a product of even numbers of vectors [37]

$$\mathrm{Spin}(p,q) = \{v_1 \cdots v_{2p} w_1 \cdots w_{2q} | \eta(v_i, v_i) = 1, \eta(w_i, w_i) = -1\}.$$

B.2. Expansion of Observables in Isospin-Breaking Parameters

This section details further the expansions in section 5.2.
Assume X to be an observable defined in QCD+QED. In order to expand expectation values of eq. (5.8), we need derivatives of expectation values of X in the isospin-symmetric theory:

$$\begin{aligned}\frac{\partial \langle X \rangle_{S_{\mathrm{eff}}^{(0)}}}{\partial \varepsilon_i} &= \frac{\partial}{\partial \varepsilon_i} \frac{1}{Z_{\mathrm{eff}}^{(0)}} \int \mathcal{D}U X[U] e^{-S_{\mathrm{eff}}^{(0)}[U]} = \frac{1}{Z_{\mathrm{eff}}^{(0)}} \int \mathcal{D}U \frac{\partial X[U]}{\partial \varepsilon_i} e^{-S_{\mathrm{eff}}^{(0)}[U]} \\ &= \left\langle \frac{\partial X}{\partial \varepsilon_i} \right\rangle_{S_{\mathrm{eff}}^{(0)}}\end{aligned}$$

where we use that the isospin-symmetric theory is fixed and thus constant w.r.t. the expansion parameters. Making use of the identity

$$\frac{\partial R}{\partial \varepsilon_i} = \frac{\partial}{\partial \varepsilon_i} \frac{e^{-S_{\mathrm{eff}}}}{e^{-S_{\mathrm{eff}}^{(0)}}} = -R \frac{\partial S_{\mathrm{eff}}}{\partial \varepsilon_i},$$

we can compute the derivative of an expectation value in QCD+QED w.r.t. an action parameter as

$$\begin{aligned}\frac{\partial \langle O \rangle_S}{\partial \varepsilon_i} &= \frac{\partial}{\partial \varepsilon_i} \frac{\left\langle R \langle \mathcal{O} \rangle_{S_{q\gamma}} \right\rangle_{S_{\mathrm{eff}}^{(0)}}}{\langle R \rangle_{S_{\mathrm{eff}}^{(0)}}} \\ &= \frac{\left\langle R \frac{\partial \langle \mathcal{O} \rangle_{S_{q\gamma}}}{\partial \varepsilon_i} \right\rangle_{S_{\mathrm{eff}}^{(0)}} - \left\langle R \langle \mathcal{O} \rangle_{S_{q\gamma}} \frac{\partial S_{\mathrm{eff}}}{\partial \varepsilon_i} \right\rangle_{S_{\mathrm{eff}}^{(0)}}}{\langle R \rangle_{S_{\mathrm{eff}}^{(0)}}} + \frac{\left\langle R \langle \mathcal{O} \rangle_{S_{q\gamma}} \right\rangle_{S_{\mathrm{eff}}^{(0)}}}{\langle R \rangle^2_{S_{\mathrm{eff}}^{(0)}}} \left\langle R \frac{\partial S_{\mathrm{eff}}}{\partial \varepsilon_i} \right\rangle_{S_{\mathrm{eff}}^{(0)}}.\end{aligned} \tag{B.2}$$

Using that $R|_{\varepsilon=\varepsilon^{(0)}} = 1$, the above yields eq. (5.10).
The derivative of $\langle \mathcal{O} \rangle_{S_{q\gamma}}$ can be further expanded by

$$\begin{aligned}\frac{\partial \langle \mathcal{O} \rangle_{S_{q\gamma}}}{\partial \varepsilon_i} &= \frac{\partial}{\partial \varepsilon_i} \left(\frac{1}{Z_{q\gamma}} \int \mathcal{D}A \mathcal{D}\psi \mathcal{D}\bar{\psi}\, \mathcal{O} e^{-S_{q\gamma}} \right) \\ &= \frac{1}{Z_{q\gamma}} \int \mathcal{D}A \mathcal{D}\psi \mathcal{D}\bar{\psi} \left(\frac{\partial \mathcal{O}}{\partial \varepsilon_i} - \mathcal{O} \frac{\partial S_{q\gamma}}{\partial \varepsilon_i} \right) e^{-S_{q\gamma}} \\ &\quad - \frac{1}{Z_{q\gamma}} \frac{\partial Z_{q\gamma}}{\partial \varepsilon_i} \frac{1}{Z_{q\gamma}} \int \mathcal{D}A \mathcal{D}\psi \mathcal{D}\bar{\psi}\, \mathcal{O} e^{-S_{q\gamma}} \\ &= \left\langle \frac{\partial \mathcal{O}}{\partial \varepsilon_i} \right\rangle_{S_{q\gamma}} - \left\langle \mathcal{O} \frac{\partial S_{q\gamma}}{\partial \varepsilon_i} \right\rangle_{S_{q\gamma}} - \langle \mathcal{O} \rangle_{S_{q\gamma}} \frac{\partial \log Z_{q\gamma}}{\partial \varepsilon_i}\end{aligned}$$

where the last derivative of the logarithm of the partition function is given by

$$\begin{aligned}\frac{\partial \log Z_{q\gamma}}{\partial \varepsilon_i} =& \frac{1}{Z_{q\gamma}} \frac{\partial Z_{q\gamma}}{\partial \varepsilon_i} = \frac{1}{Z_{q\gamma}} \frac{\partial}{\partial \varepsilon_i} \int \mathcal{D}A\mathcal{D}\psi\mathcal{D}\bar{\psi}\, e^{-S_{q\gamma}} \\ =& \frac{1}{Z_{q\gamma}} \int \mathcal{D}A\mathcal{D}\psi\mathcal{D}\bar{\psi} \left(-\frac{\partial S_{q\gamma}}{\partial \varepsilon_i}\right) e^{-S_{q\gamma}} = -\left\langle \frac{\partial S_{q\gamma}}{\partial \varepsilon_i} \right\rangle_{S_{q\gamma}}\end{aligned}$$

eq. (5.10) can be written as

$$\begin{aligned}\frac{\partial \langle \mathcal{O} \rangle_S}{\partial \varepsilon_i}\bigg|_{\varepsilon=\varepsilon^{(0)}} =& \left\langle \left\langle \frac{\partial \mathcal{O}}{\partial \varepsilon_i}\bigg|_{\varepsilon=\varepsilon^{(0)}} \right\rangle_{S_q^{(0)}} \right\rangle_{S_{\text{eff}}^{(0)}} - \left\langle \left\langle \mathcal{O} \frac{\partial S_{q\gamma}}{\partial \varepsilon_i}\bigg|_{\varepsilon=\varepsilon^{(0)}} \right\rangle_{S_q^{(0)}} \right\rangle_{S_{\text{eff}}^{(0)}} \\ & - \left\langle \langle \mathcal{O} \rangle_{S_q^{(0)}} \left\langle \frac{\partial S_{q\gamma}}{\partial \varepsilon_i}\bigg|_{\varepsilon=\varepsilon^{(0)}} \right\rangle \right\rangle_{S_{\text{eff}}^{(0)}} \\ & - \left\langle \langle \mathcal{O} \rangle_{S_q^{(0)}} \frac{\partial S_{\text{eff}}}{\partial \varepsilon_i}\bigg|_{\varepsilon=\varepsilon^{(0)}} \right\rangle_{S_{\text{eff}}^{(0)}} + \langle \mathcal{O} \rangle_{S^{(0)}} \left\langle \frac{\partial S_{\text{eff}}}{\partial \varepsilon_i}\bigg|_{\varepsilon=\varepsilon^{(0)}} \right\rangle_{S_{\text{eff}}^{(0)}}.\end{aligned}$$

For the expansion in terms of the electromagnetic charge, we write the expansion as

$$\langle \mathcal{O} \rangle_S \approx \langle \mathcal{O} \rangle_{S^{(0)}} + \sum_f \Delta m_f \left\langle \mathcal{O}^{(1)}_{\Delta m_f} \right\rangle_{S^{(0)}} + e^2 \left\langle \mathcal{O}^{(1)}_{e^2} \right\rangle_{S^{(0)}}$$

where $\left\langle \mathcal{O}^{(1)}_{\Delta m_f} \right\rangle_{S^{(0)}}$ is computed as the first derivative of the left hand side w.r.t. m_f, $\frac{\partial \langle \mathcal{O} \rangle_S}{\partial \varepsilon_i}|_{\varepsilon=\varepsilon^{(0)}}$, as discussed above. For the electromagnetic corrections, however, the expansion has to be performed in e rather than e^2 to accommodate for corrections in which different quarks (valence and/or sea) interact with each other via photon exchange, as a single photon vertex comes at this order. Thus, $\left\langle \mathcal{O}^{(1)}_{e^2} \right\rangle_{S^{(0)}}$ is in fact not the first derivative, but the second w.r.t. e with an additional factor of $\frac{1}{2}$ as this is the second order in e. The above expansion thus can be written as

$$\langle \mathcal{O} \rangle_S \approx \langle \mathcal{O} \rangle_{S^{(0)}} + \sum_f \Delta m_f \frac{\partial \langle \mathcal{O} \rangle_S}{\partial m_f}\bigg|_{\varepsilon=\varepsilon^{(0)}} + e^2 \cdot \frac{1}{2} \frac{\partial^2 \langle \mathcal{O} \rangle_S}{\partial e^2}\bigg|_{\varepsilon=\varepsilon^{(0)}}.$$

We therefore also need to consider the second derivative as in eq. (B.2):

$$\begin{aligned}\frac{\partial^2 \langle \mathcal{O} \rangle_S}{\partial e^2} =& \frac{1}{\langle R \rangle_{S_{\text{eff}}^{(0)}}} \left[\left\langle R \frac{\partial^2 \langle \mathcal{O} \rangle_{S_{q\gamma}}}{\partial e^2} \right\rangle_{S_{\text{eff}}^{(0)}} - 2 \left\langle R \frac{\partial \langle \mathcal{O} \rangle_{S_{q\gamma}}}{\partial e} \frac{\partial S_{\text{eff}}}{\partial e} \right\rangle_{S_{\text{eff}}^{(0)}} \right. \\ & \left. + \left\langle R \langle \mathcal{O} \rangle_{S_{q\gamma}} \left(\frac{\partial S_{\text{eff}}}{\partial e} \right)^2 \right\rangle_{S_{\text{eff}}^{(0)}} - \left\langle R \langle \mathcal{O} \rangle_{S_{q\gamma}} \frac{\partial^2 S_{\text{eff}}}{\partial e^2} \right\rangle_{S_{\text{eff}}^{(0)}} \right] \\ & + 2 \frac{\left\langle R \frac{\partial S_{\text{eff}}}{\partial e} \right\rangle_{S_{\text{eff}}^{(0)}}}{\langle R \rangle^2_{S_{\text{eff}}^{(0)}}} \left(\left\langle R \frac{\partial \langle \mathcal{O} \rangle_{S_{q\gamma}}}{\partial e} \right\rangle_{S_{\text{eff}}^{(0)}} - \left\langle R \langle \mathcal{O} \rangle_{S_{q\gamma}} \frac{\partial S_{\text{eff}}}{\partial e} \right\rangle_{S_{\text{eff}}^{(0)}} \right) \\ & - 2 \frac{\left\langle R \langle \mathcal{O} \rangle_{S_{q\gamma}} \right\rangle_{S_{\text{eff}}^{(0)}}}{\langle R \rangle^3_{S_{\text{eff}}^{(0)}}} \left\langle R \frac{\partial S_{\text{eff}}}{\partial e} \right\rangle^2_{S_{\text{eff}}^{(0)}} \\ & + \frac{\left\langle R \langle \mathcal{O} \rangle_{S_{q\gamma}} \right\rangle_{S_{\text{eff}}^{(0)}}}{\langle R \rangle^2_{S_{\text{eff}}^{(0)}}} \left(\left\langle R \frac{\partial^2 S_{\text{eff}}}{\partial e^2} \right\rangle_{S_{\text{eff}}^{(0)}} - \left\langle R \left(\frac{\partial S_{\text{eff}}}{\partial e} \right)^2 \right\rangle_{S_{\text{eff}}^{(0)}} \right)\end{aligned}$$

Evaluated at vanishing electromagnetic coupling, this yields

$$\begin{aligned}
\frac{\partial^2 \langle \mathcal{O} \rangle_S}{\partial e^2}\bigg|_{e=0} &= \left\langle \frac{\partial^2 \langle \mathcal{O} \rangle_{S_{q\gamma}}}{\partial e^2}\bigg|_{\varepsilon=\varepsilon^{(0)}} \right\rangle_{S_{\text{eff}}^{(0)}} \\
&\quad - 2\left\langle \frac{\partial \langle \mathcal{O} \rangle_{S_{q\gamma}}}{\partial e}\bigg|_{\varepsilon=\varepsilon^{(0)}} \frac{\partial S_{\text{eff}}}{\partial e}\bigg|_{\varepsilon=\varepsilon^{(0)}} \right\rangle_{S_{\text{eff}}^{(0)}} + 2\left\langle \frac{\partial \langle \mathcal{O} \rangle_{S_{q\gamma}}}{\partial e}\bigg|_{\varepsilon=\varepsilon^{(0)}} \right\rangle_{S_{\text{eff}}^{(0)}} \left\langle \frac{\partial S_{\text{eff}}}{\partial e}\bigg|_{\varepsilon=\varepsilon^{(0)}} \right\rangle_{S_{\text{eff}}^{(0)}} \\
&\quad - \left\langle \langle \mathcal{O} \rangle_{S_q^{(0)}} \left(\frac{\partial^2 S_{\text{eff}}}{\partial e^2}\bigg|_{\varepsilon=\varepsilon^{(0)}} - \left(\frac{\partial S_{\text{eff}}}{\partial e}\bigg|_{\varepsilon=\varepsilon^{(0)}} \right)^2 \right) \right\rangle_{S_{\text{eff}}^{(0)}} \\
&\quad + \langle \mathcal{O} \rangle_{S^{(0)}} \left\langle \frac{\partial^2 S_{\text{eff}}}{\partial e^2}\bigg|_{\varepsilon=\varepsilon^{(0)}} - \left(\frac{\partial S_{\text{eff}}}{\partial e}\bigg|_{\varepsilon=\varepsilon^{(0)}} \right)^2 \right\rangle_{S_{\text{eff}}^{(0)}} \\
&\quad + 2\left\langle \frac{\partial \langle \mathcal{O} \rangle_{S_{q\gamma}}}{\partial e}\bigg|_{\varepsilon=\varepsilon^{(0)}} \right\rangle_{S_{\text{eff}}^{(0)}} \left\langle \frac{\partial S_{\text{eff}}}{\partial e}\bigg|_{\varepsilon=\varepsilon^{(0)}} \right\rangle_{S_{\text{eff}}^{(0)}} - 2\langle \mathcal{O} \rangle_{S^{(0)}} \left\langle \frac{\partial S_{\text{eff}}}{\partial e}\bigg|_{\varepsilon=\varepsilon^{(0)}} \right\rangle_{S_{\text{eff}}^{(0)}}^2 .
\end{aligned} \tag{B.3}$$

The derivatives of the effective action in the above formulae can be expressed in terms of derivatives of $S_{q\gamma}$ as follows:

$$\begin{aligned}
\frac{\partial S_{\text{eff}}}{\partial e} &= \frac{\partial}{\partial e}(S_g - \ln Z_{q\gamma}) = -\frac{1}{Z_{q\gamma}} \frac{\partial Z_{q\gamma}}{\partial e} = -\frac{\partial}{\partial e} \frac{\int \mathcal{D}A\mathcal{D}\psi\mathcal{D}\bar{\psi}\, \frac{\partial}{\partial e} e^{-S_{q\gamma}}}{\int \mathcal{D}A\mathcal{D}\psi\mathcal{D}\bar{\psi}\, e^{-S_{q\gamma}}} \\
&= \left\langle \frac{\partial S_{q\gamma}}{\partial e} \right\rangle_{S_{q\gamma}} \\
\frac{\partial^2 S_{\text{eff}}}{\partial e^2} &= -\frac{\partial}{\partial e}\left(\frac{1}{Z_{q\gamma}} \frac{\partial Z_{q\gamma}}{\partial e} \right) = \frac{1}{{Z_{q\gamma}}^2}\left(\frac{\partial Z_{q\gamma}}{\partial e} \right)^2 - \frac{1}{Z_{q\gamma}} \frac{\partial^2 Z_{q\gamma}}{\partial e^2} \\
&= \left\langle \frac{\partial S_{q\gamma}}{\partial e} \right\rangle_{S_{q\gamma}}^2 - \frac{1}{Z_{q\gamma}} \int \mathcal{D}A\mathcal{D}\psi\mathcal{D}\bar{\psi}\, \frac{\partial}{\partial e}\left(-\frac{\partial S_{q\gamma}}{\partial e} e^{-S_{q\gamma}} \right) \\
&= \left\langle \frac{\partial S_{q\gamma}}{\partial e} \right\rangle_{S_{q\gamma}}^2 - \frac{1}{Z_{q\gamma}} \int \mathcal{D}A\mathcal{D}\psi\mathcal{D}\bar{\psi} \left(\left(\frac{\partial S_{q\gamma}}{\partial e} \right)^2 - \frac{\partial^2 S_{q\gamma}}{\partial e^2} \right) e^{-S_{q\gamma}} \\
&= \left\langle \frac{\partial S_{q\gamma}}{\partial e} \right\rangle_{S_{q\gamma}}^2 + \left\langle \frac{\partial^2 S_{q\gamma}}{\partial e^2} - \left(\frac{\partial S_{q\gamma}}{\partial e} \right)^2 \right\rangle_{S_{q\gamma}} .
\end{aligned}$$

B.3. Fit Procedures

This section deals with methods to find the fit parameters θ that minimize

$$\chi^2 = (y - f(t,\theta))^T V (y - f(t,\theta))$$

for a given fit function f and data y with covariance matrix V^{-1}.

B.3.1. Conventions

In the following, these symbols share their meaning across the different paragraphs:

Variable	Type	Meaning
$\mathbb{1}$	$\mathbb{R}^n$	$(1,...,1)^T$
t	$\mathbb{R}^n$	Time slices
y	$\mathbb{R}^n$	The values described by the fit function (e.g. effective masses)
V	$\mathbb{R}^{n\times n}$	The inverse covariance matrix of y
Λ	$\mathbb{R}$	$\frac{1}{\mathbb{1}^T V \mathbb{1}} = \frac{1}{\sum_{i,j=1}^n V_{ij}}$
$f(t,\theta)$	$\mathbb{R}^{n+m} \to \mathbb{R}$	The fit function

$\odot$ means elementwise multiplication, i.e. for $a, b \in \mathbb{R}^n$

$$a \odot b = \begin{pmatrix} a_1 b_1 \\ a_2 b_2 \\ \vdots \\ a_n b_n \end{pmatrix}.$$

B.3.2. Constant Fit

A fit to a constant with correlated data, $f(t,m) = m$ is solved by

$$m = \Lambda \mathbb{1}^T V y. \tag{B.4}$$

The error of m can in this case be calculated analytically and is given by

$$\Delta m = \sqrt{\Lambda}.$$

B.3.3. Linear Fit

For a linear function $f(t,m,b) = mt + b$ the slope and offset are given by

$$\begin{aligned} m &= \frac{t^T V Y_0}{t^T V T_0} \\ b &= \Lambda \mathbb{1}^T V (y - mx) \\ Y_0 &= y - \Lambda(\mathbb{1}^T V y)\mathbb{1} \\ T_0 &= t - \Lambda(\mathbb{1}^T V t)\mathbb{1}. \end{aligned} \tag{B.5}$$

The covariance matrix of m and b is then given by

$$\mathrm{Cov}_{mb} = \frac{1}{t^T V T_0} \begin{pmatrix} 1 & -\Lambda \mathbb{1}^T V t \\ -\Lambda \mathbb{1}^T V t & \Lambda t^T V t \end{pmatrix}$$

B.3.4. General Linear Fit

For a linear function $f : \mathbb{R}^{n\times k} \times \mathbb{R}^k \to \mathbb{R}^n$, $y = f(X, \theta) = X\theta$ the parameter vector θ minimizing the correlated χ^2 is given by

$$\theta = \left(X^T V X\right)^{-1} X^T V y \tag{B.6}$$

with covariance matrix

$$\mathrm{Cov}_\theta = \left(X^T V X\right)^{-1}.$$

Note that the constant fit in section B.3.2 and the simple linear fit in section B.3.3 are special cases of this scenario for

$$\begin{aligned} X &= \mathbb{1}, \qquad \theta = m \text{ and} \\ X &= \begin{pmatrix} t_1 & 1 \\ t_2 & 1 \\ \vdots & \vdots \\ t_n & 1 \end{pmatrix} = \begin{pmatrix} t & \mathbb{1} \end{pmatrix}, \qquad \theta = \begin{pmatrix} m \\ b \end{pmatrix} \end{aligned}$$

respectively.

B.3.5. 2-State Fit for Isospin-Symmetric Mass Contributions

The χ^2-minimization for the fit function $f(t, m, \Delta M, \gamma) = m + \gamma e^{-\Delta M t}$ can be simplified by reducing the number of variables that have to be found numerically by solving for m and γ in terms of ΔM analytically:

$$\begin{aligned} m &= \Lambda \mathbb{1}^T V (y - \gamma E) \\ \gamma &= \frac{E_0^T V Y_0}{E_0^T V E_0} \\ Y_0 &= y - \Lambda (\mathbb{1}^T V y) \mathbb{1} \\ E_0 &= E - \Lambda (\mathbb{1}^T V E) \mathbb{1} \\ E_i &= e^{-\Delta M t_i}. \end{aligned} \tag{B.7}$$

This reduces the χ^2 to be minimized to the expression

$$\chi^2 = (Y_0 - \gamma E_0)^T V (Y_0 - \gamma E_0) \tag{B.8}$$

which only depends on ΔM, thus simplifying the minimization. Results obtained within the scope of this thesis for the fit function above were obtained using the Levenberg-Marquardt algorithm [128, 129] using the `levenberg_marquardt` Rust library [121, 122].

B.3.6. 2-State Fit in First Order Isospin-Breaking

The χ^2 minimization of the fit function $f(t, m, \alpha, \beta) = m + (\alpha - \beta t) e^{-\Delta M t}$ where ΔM is fixed can be solved analytically resulting in the following fit results for the parameters m, α, and β:

$$
\begin{aligned}
m &= \Lambda \mathbb{1}^T V (y + \beta F - \alpha E) \\
\alpha &= \frac{\beta B + C}{A} \\
\beta &= \frac{C\tilde{A} - A\tilde{C}}{A\tilde{B} - B\tilde{A}} \\
X &= E^T V X_0 \text{ for } X \in \{A, B, C\} \\
\tilde{X} &= F^T V X_0 \text{ for } X \in \{A, B, C\} \\
A_0 &= E - \Lambda(\mathbb{1}^T V E)\mathbb{1} \\
B_0 &= F - \Lambda(\mathbb{1}^T V F)\mathbb{1} \\
C_0 &= y - \Lambda(\mathbb{1}^T V y)\mathbb{1} \\
E_i &= e^{-\Delta M t_i} \\
F &= t \odot E
\end{aligned}
\tag{B.9}
$$

Chapter C
Tables

C.1. Characters of O_h and O_D

Tables C.1 and C.2 can be used to compute the decomposition of continuum spin-irreps in table 3.2 into irreps of the octahedral group and its double cover via eq. (3.19).

Table C.1: Characters of the irreps of the octahedral group O_h [39]. The top rows lists the conjugacy classes and their mutliplicities, while the bottom row are the angles of rotation corresponding to the respective conjugacy class.

n_C	1	3	8	6	6
C	I	C_2	C_3	C_4	C_2'
A_1	1	1	1	1	1
A_2	1	1	1	-1	-1
E	2	2	-1	0	0
T_1	3	-1	0	-1	1
T_2	3	-1	0	-1	1
θ	2π	π	$\frac{2\pi}{3}$	$\frac{\pi}{2}$	π

Table C.2: Characters of the irreps of the double cover of the octahedral group O_D [39]. The top row lists the conjugacy classes and their multiplicities, while the bottom row are the angles of rotation corresponding to the respective conjugacy class.

n_C	1	1	6	8	8	6	6	12
C	I	J	C_4	C_3	C_6	C_8	C_8'	C_4'
G_1	2	-2	0	-1	1	$-\sqrt{2}$	$\sqrt{2}$	0
G_2	2	-2	0	-1	1	$\sqrt{2}$	$-\sqrt{2}$	0
H	4	-4	0	1	-1	0	0	0
θ	4π	2π	π	$\frac{4\pi}{3}$	$\frac{2\pi}{3}$	$\frac{3\pi}{2}$	$\frac{\pi}{2}$	π

C.2. Baryonic Operators

Tables C.4 to C.7 list the baryonic operators used to compute the two-point correlation functions discussed in this thesis. Each table (except for table C.5) corresponds to two different baryons which have the same flavor- and spinor symmetry. The embedding (short *Emb.* in the tables' captions) is a convention from the original publication [12] listed here for reference. The indices noted on the operators (e.g. 121 in N_{121} in the first row of table C.4) are to be understood as Dirac-spinor indices and each index corresponds to one of the valence quarks. Color indices and flavor are implicit and the flavor structure is assumed to simplify the operators. Details on the construction are discussed in section 7.1.

Table C.3: The definition of the various baryonic operators used in tables C.4 to C.7 based on the flavor symmetry of the different baryons.

Operator	Symmetry	I_3	Definition
$N_{\mu_1\mu_2\mu_3}$	MA	$1/2$	$\frac{1}{\sqrt{2}}\varepsilon_{abc}\big(u^a_{\mu_1}d^b_{\mu_2} - d^a_{\mu_1}u^b_{\mu_2}\big)u^c_{\mu_3}$
		$-1/2$	$\frac{1}{\sqrt{2}}\varepsilon_{abc}\big(u^a_{\mu_1}d^b_{\mu_2} - d^a_{\mu_1}u^b_{\mu_2}\big)d^c_{\mu_3}$
$\Lambda_{\mu_1\mu_2\mu_3}$	MA	0	$\frac{1}{\sqrt{2}}\varepsilon_{abc}\big(u^a_{\mu_1}d^b_{\mu_2} - d^a_{\mu_1}u^b_{\mu_2}\big)s^c_{\mu_3}$
$\Lambda^0_{\mu_1\mu_2\mu_3}$	A	0	$\frac{1}{\sqrt{6}}\varepsilon_{abc}\big(u^a_{\mu_1}d^b_{\mu_2}s^c_{\mu_3} + d^a_{\mu_1}s^b_{\mu_2}u^c_{\mu_3} + s^a_{\mu_1}u^b_{\mu_2}d^c_{\mu_3}$ $-u^a_{\mu_1}s^b_{\mu_2}d^c_{\mu_3} - d^a_{\mu_1}u^b_{\mu_2}s^c_{\mu_3} - s^a_{\mu_1}d^b_{\mu_2}u^c_{\mu_3}\big)$
$\Sigma_{\mu_1\mu_2\mu_3}$	MS	1	$\varepsilon_{abc}u^a_{\mu_1}u^b_{\mu_2}s^c_{\mu_3}$
		0	$\frac{1}{\sqrt{2}}\varepsilon_{abc}\big(u^a_{\mu_1}d^b_{\mu_2} + d^a_{\mu_1}u^b_{\mu_2}\big)s^c_{\mu_3}$
		-1	$\varepsilon_{abc}d^a_{\mu_1}d^b_{\mu_2}s^c_{\mu_3}$
$\Xi_{\mu_1\mu_2\mu_3}$	MS	$1/2$	$\varepsilon_{abc}s^a_{\mu_1}s^b_{\mu_2}u^c_{\mu_3}$
		$-1/2$	$\varepsilon_{abc}s^a_{\mu_1}s^b_{\mu_2}d^c_{\mu_3}$
$\Delta_{\mu_1\mu_2\mu_3}$	S	$3/2$	$\varepsilon_{abc}u^a_{\mu_1}u^b_{\mu_2}u^c_{\mu_3}$
		$1/2$	$\frac{1}{\sqrt{3}}\varepsilon_{abc}\big(u^a_{\mu_1}u^b_{\mu_2}d^c_{\mu_3} + u^a_{\mu_1}d^b_{\mu_2}u^c_{\mu_3} + d^a_{\mu_1}u^b_{\mu_2}u^c_{\mu_3}\big)$
		$-1/2$	$\frac{1}{\sqrt{3}}\varepsilon_{abc}\big(d^a_{\mu_1}d^b_{\mu_2}u^c_{\mu_3} + d^a_{\mu_1}u^b_{\mu_2}d^c_{\mu_3} + u^a_{\mu_1}d^b_{\mu_2}d^c_{\mu_3}\big)$
		$-3/2$	$\varepsilon_{abc}d^a_{\mu_1}d^b_{\mu_2}d^c_{\mu_3}$
$\Sigma^*_{\mu_1\mu_2\mu_3}$	MS	1	$\varepsilon_{abc}u^a_{\mu_1}u^b_{\mu_2}s^c_{\mu_3}$
		0	$\frac{1}{\sqrt{2}}\varepsilon_{abc}\big(u^a_{\mu_1}d^b_{\mu_2} + d^a_{\mu_1}u^b_{\mu_2}\big)s^c_{\mu_3}$
		-1	$\varepsilon_{abc}d^a_{\mu_1}d^b_{\mu_2}s^c_{\mu_3}$
$\Xi^*_{\mu_1\mu_2\mu_3}$	MS	$1/2$	$\varepsilon_{abc}s^a_{\mu_1}s^b_{\mu_2}u^c_{\mu_3}$
		$-1/2$	$\varepsilon_{abc}s^a_{\mu_1}s^b_{\mu_2}d^c_{\mu_3}$
$\Omega_{\mu_1\mu_2\mu_3}$	S	0	$\varepsilon_{abc}s^a_{\mu_1}s^b_{\mu_2}s^c_{\mu_3}$

Table C.4: Operators used for the N/Λ baryons assuming a mixed antisymmetric flavor state. The value for ρ left of the slash indicates the corresponding ρ-spin for the *gerade* states, the right one corresponds to the *ungerade* states. Red entries were not used in this project.

Irrep	Emb.	ρ	s	gerade	ungerade
G_1	1	$\frac{3}{2}/\frac{1}{2}$	$1/2$	$\sqrt{2}N_{121}$	$\frac{\sqrt{6}(N_{123}+N_{141}-N_{231})}{3}$
			$-1/2$	$\sqrt{2}N_{122}$	$\frac{\sqrt{6}(N_{124}+N_{142}-N_{232})}{3}$
	2	$-\frac{1}{2}/-\frac{3}{2}$	$1/2$	$\frac{\sqrt{6}(N_{143}-N_{233}+N_{341})}{3}$	$\sqrt{2}N_{343}$
			$-1/2$	$\frac{\sqrt{6}(N_{144}-N_{234}+N_{342})}{3}$	$\sqrt{2}N_{344}$
	3	$-\frac{1}{2}/\frac{1}{2}$	$1/2$	$\frac{2\sqrt{3}(N_{134}-N_{233}-N_{341})}{3}$	$\frac{2\sqrt{3}(N_{123}+N_{132}-N_{141})}{3}$
			$-1/2$	$\frac{2\sqrt{3}(N_{144}-N_{243}-N_{342})}{3}$	$\frac{2\sqrt{3}(N_{124}+N_{232}-N_{241})}{3}$
H	1	$-\frac{1}{2}/\frac{1}{2}$	$3/2$	$\sqrt{2}N_{133}$	$\sqrt{2}N_{131}$
			$1/2$	$\frac{\sqrt{6}(N_{134}+N_{143}+N_{233})}{3}$	$\frac{\sqrt{6}(N_{132}+N_{141}+N_{231})}{3}$
			$-1/2$	$\frac{\sqrt{6}(N_{144}+N_{234}+N_{243})}{3}$	$\frac{\sqrt{6}(N_{142}+N_{232}+N_{241})}{3}$
			$-3/2$	$\sqrt{2}N_{244}$	$\sqrt{2}N_{242}$

Table C.5: Operators used for the Λ^0 baryons assuming a totally antisymmetric flavor state. The value for ρ left of the slash indicates the corresponding ρ-spin for the *gerade* states, the right one corresponds to the *ungerade* states.

Irrep	Emb.	ρ	s	gerade	ungerade
G_1	1	$-\frac{1}{2}/\frac{1}{2}$	$1/2$	$2\sqrt{3}\Lambda^0_{134}$	$-2\sqrt{3}\Lambda^0_{123}$
			$-1/2$	$2\sqrt{3}\Lambda^0_{234}$	$-2\sqrt{3}\Lambda^0_{124}$

Table C.6: Operators used for the Ω/Δ baryons assuming a totally symmetric flavor state. The value for ρ left of the slash indicates the corresponding ρ-spin for the *gerade* states, the right one corresponds to the *ungerade* states. Red entries were not used in this project.

Irrep	Emb.	ρ	s	gerade	ungerade
G_1	1	$-\frac{1}{2}/\frac{1}{2}$	$1/2$	$2\,(\Omega_{134}-\Omega_{233})$	$2\,(\Omega_{114}-\Omega_{123})$
			$-1/2$	$2\,(\Omega_{144}-\Omega_{234})$	$2\,(\Omega_{124}-\Omega_{223})$
H	1	$\frac{3}{2}/\frac{1}{2}$	$3/2$	Ω_{111}	$\sqrt{3}\Omega_{113}$
			$1/2$	$\sqrt{3}\Omega_{112}$	$\Omega_{114}+2\Omega_{123}$
			$-1/2$	$\sqrt{3}\Omega_{122}$	$2\Omega_{124}+\Omega_{223}$
			$-3/2$	Ω_{222}	$\sqrt{3}\Omega_{224}$
	2	$-\frac{1}{2}/-\frac{3}{2}$	$3/2$	$\sqrt{3}\Omega_{133}$	Ω_{333}
			$1/2$	$2\Omega_{134}+\Omega_{233}$	$\sqrt{3}\Omega_{334}$
			$-1/2$	$\Omega_{144}+2\Omega_{234}$	$\sqrt{3}\Omega_{344}$
			$-3/2$	$\sqrt{3}\Omega_{244}$	Ω_{444}

Table C.7: Operators used for the Ξ/Σ baryons assuming a mixed symmetric flavor state. The value for ρ left of the slash indicates the corresponding ρ-spin for the *gerade* states, the right one corresponds to the *ungerade* states.

Irrep	Emb.	ρ	s	gerade
G_1	1	$\frac{3}{2}/\frac{1}{2}$	$1/2$	$\frac{\sqrt{6}(\Xi_{112}-\Xi_{121})}{3}$
			$-1/2$	$\frac{\sqrt{6}(\Xi_{122}-\Xi_{221})}{3}$
	2	$-\frac{1}{2}/-\frac{3}{2}$	$1/2$	$\frac{\sqrt{2}(2\Xi_{134}-\Xi_{143}-\Xi_{233}+\Xi_{332}-\Xi_{341})}{3}$
			$-1/2$	$\frac{\sqrt{2}(\Xi_{144}+\Xi_{234}-2\Xi_{243}+\Xi_{342}-\Xi_{441})}{3}$
	3	$-\frac{1}{2}/\frac{1}{2}$	$1/2$	$-\frac{2(\Xi_{134}-2\Xi_{143}+\Xi_{233}-\Xi_{332}+\Xi_{341})}{3}$
			$-1/2$	$\frac{2(\Xi_{144}-2\Xi_{234}+\Xi_{243}+\Xi_{342}-\Xi_{441})}{3}$
H	1	$-\frac{1}{2}/\frac{1}{2}$	$3/2$	$\frac{\sqrt{6}(\Xi_{133}-\Xi_{331})}{3}$
			$1/2$	$\frac{\sqrt{2}(\Xi_{134}+\Xi_{143}+\Xi_{233}-\Xi_{332}-2\Xi_{341})}{3}$
			$-1/2$	$\frac{\sqrt{2}(\Xi_{144}+\Xi_{234}+\Xi_{243}-2\Xi_{342}-\Xi_{441})}{3}$
			$-3/2$	$\frac{\sqrt{6}(\Xi_{244}-\Xi_{442})}{3}$

Irrep	Emb.	ρ	s	ungerade
G_1	1	$\frac{3}{2}/\frac{1}{2}$	$1/2$	$\frac{\sqrt{2}(\Xi_{114}-\Xi_{123}+2\Xi_{132}-\Xi_{141}-\Xi_{231})}{3}$
			$-1/2$	$\frac{\sqrt{2}(\Xi_{124}+\Xi_{142}-\Xi_{223}+\Xi_{232}-2\Xi_{241})}{3}$
	2	$-\frac{1}{2}/-\frac{3}{2}$	$1/2$	$\frac{\sqrt{6}(\Xi_{334}-\Xi_{343})}{3}$
			$-1/2$	$\frac{\sqrt{6}(\Xi_{344}-\Xi_{443})}{3}$
	3	$-\frac{1}{2}/\frac{1}{2}$	$1/2$	$-\frac{2(\Xi_{114}-\Xi_{123}-\Xi_{132}-\Xi_{141}+2\Xi_{231})}{3}$
			$-1/2$	$-\frac{2(\Xi_{124}-2\Xi_{142}-\Xi_{223}+\Xi_{232}+\Xi_{241})}{3}$
H	1	$-\frac{1}{2}/\frac{1}{2}$	$3/2$	$\frac{\sqrt{6}(\Xi_{113}-\Xi_{131})}{3}$
			$1/2$	$\frac{\sqrt{2}(\Xi_{114}+2\Xi_{123}-\Xi_{132}-\Xi_{141}-\Xi_{231})}{3}$
			$-1/2$	$\frac{\sqrt{2}(2\Xi_{124}-\Xi_{142}+\Xi_{223}-\Xi_{232}-\Xi_{241})}{3}$
			$-3/2$	$\frac{\sqrt{6}(\Xi_{224}-\Xi_{242})}{3}$